School of Biomedical Sciences

Expression, Purification and Characterisation of the Recombinant Soluble Receptor for Advanced Glycosylation End Products (sRAGE)

David J Chandler

This thesis is presented for the Degree of Doctor of Philosophy

of

Curtin University

September, 2014

DECLARATION

To the best of my knowledge and belief this thesis contains no material previously published by any other person except where due acknowledgement has been made.

This thesis contains no material which has been accepted for the award of any other degree or diploma in any university.

Signature: 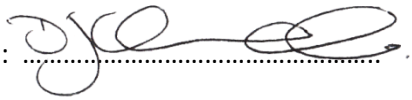

Date: 03/May/2015

ACKNOWLEDGEMENTS

It's difficult to know how to really describe the journey that this project has been. It has been the toughest personal and professional challenge of my life that was only made possible by the wonderful people in my life. I think it's worth pointing out that at the beginning of this project, our lab had never done insect cell culture or bacterial recombinant protein expression before. The Bio-Rad Biologic FPLC used was actually recovered from a dumpster and rebuilt by myself, ultimately purifying over a 100mg of eight different proteins, and it was my pride and joy and I loved to hear it whirring away. This project has run over a substantial proportion of my life and has incorporated the birth of my two sons, and a number of career changes that were required to help pay the bills. Ultimately I think it has been sheer grit and determination that has led to the final completion and submission of this thesis. Without a doubt, the perseverance, support and motivation of my supervisor Erik was a significant driving force that got me over the line. His selflessness in giving his time, knowledge and understanding has been unwavering and a true testament to the wonderful person and amazing scientist he is. I will always be grateful that our lives have crossed paths and hope they will continue to do so for the rest of our days. Thank you also to Ricardo for his unwavering support, guidance and encouragement over the life of this project. My parents and friends Mark, Paul, Wolfgang, Alex and Wresti have endured the many ups and downs of this project and always been there to support and motivate me. To all of them, I can't thank you enough but I can shout you many, many beers – I promise I won't make you read this!

My rock in life is my wife. Through the many, many challenges, ups and downs of this project, she has been there to encourage, support and pick me up. Her belief in me has never wavered and I can never thank her enough for sticking by me all these years. And to my two beautiful boys who were born over the last four years of this project. Their cheeky faces and beautiful laughs always make the most difficult of life's challenges melt away. They are the light in my life along with my wife, and this thesis is for them.

TABLE OF CONTENTS

LIST OF FIGURES

LIST OF TABLES

LIST OF ABBREVIATIONS

Abbreviation	Full name
AA	Amyloid associated protein
Aβ	Beta amyloid
AβA	Aggregated beta amyloid
AβF	Insoluble fibrillary beta amyloid
AβO	Soluble fibrillary beta amyloid
AD	Alzheimer's disease
ADAM	A Disintegrin and Metalloprotease
AGE	Advanced Glycation End-product
AL	Amyloid light chain protein
AOPP	Advanced oxidation protein products
APP	Amyloid precursor protein
Arp 2/3	Actin related protein 2/3
BAD	Bcl-2 associated death promoter protein
BAP	Bio-Rad aurum plasmid purification kit
Bcl-2	B-cell Leukemia/Lymphoma 2
BSA	Bovine serum albumin
BSA-AGE	Bovine Serum Albumin Based Advanced Glycation End-product
C Domain	Constant domain
CD	Cluster of Differentiation
Cdc42	Cell division cycle 42
CML-AGE	Carboxymethyl-Lysine Advanced Glycation End-product
COX-2	Cyclooxygenase-2
CREB	Camp Response Element Binding
CT	Cytosolic tail
DAPK	Death associated protein kinase
Dia1	Diaphanous-1

Abbreviation	Full name
DMSO	Dimethyl sulfoxide
DN-RAGE	Dominant Negative Receptor for Advanced Glycation End-products
DTH	Delayed type hypersensitivity
DTT	Dithiothreitol
E. coli	*Escherichia coli*
EDC	N-ethyl-N'-(3-dimethylaminopropyl) carbodimide hydrochloride
EGFR	Epidermal growth factor receptor
ERK 1/2	Extracellular Signal-regulated Protein Kinase -1 and 2
esRAGE	Endogenous Secretory Receptor for Advanced Glycation End-products
FAK	Focal adhesion kinase
FAP	Familial amyloid polyneuropathy
f-actin	Filamentous actin
FCS	Foetal calf serum
FH1	Formin homology domain-1
FPRL1	Formyl-peptide receptor-like 1
GAP	GTPase-Activating Proteins
GEF	Guanine nucleotide exchange factors
GOLD	Glyoxal-lysine dimer
GTP	Guanosine triphosphate
GTPase	Guanosine triphosphate hydrolase
HBS-EP	HEPES buffered saline - EDTA/p20
HEK293	Human Embryonic Kidney cells 293
HGNC	Human gene nomenclature committee
HMGB1	High mobility group box 1 chromosomal protein
hRAGE	Human Receptor for Advanced Glycation End-products
hRAGEsec	Human Receptor for Advanced Glycation End-products secretory form
ICAM	Inter-cellular adhesion molecule 1
Ig	Immunoglobulin

Abbreviation	Full name
IκB	Inhibitor of kappa B
IL	Interleukin
JAK	Janus kinase
JNK	C-Jun N-terminal Kinases
LDL	Low density lipoprotein
LF-L	Lactoferrin-like Polypeptide
LPC	Lysophosphatidylcholine
LPS	Lipopolysaccharide
LRP	Leukocyte common antigen-related phosphatase
MAP kinase	Mitogen activated protein kinase
MCP-1	Monocyte chemo attractant protein 1
M-CSF	Macrophage colony stimulating factor
MEK	MAP Kinase or ERK
MHC	Major histocompatibility complex
MLCK	Myosin light chain kinase
MMP	Matrix metalloproteinase
MOLD	Methylglyoxal-lysine dimer
MP	Mononuclear phagocyte
MS-AGE	Methylglyoxal modified BSA
NADPH oxidase	Nicotinamide adenine dinucleotide phosphate-oxidase
NCAM	Neuronal cell adhesion molecule
NF-κB	Nuclear Factor - kb
NHS	N-hydroxysuccinimide
NMD	Nonsense-mediated mRNA decay pathway
NMDA-R	N-methyl D-aspartate receptor
NMR	Nuclear magnetic resonance
OSCC	Oral square cell carcinoma
OST	Oligosaccharyl transferase

Abbreviation	Full name
oxLDL	Oxidatively modified low density lipoprotein
P20	polysorbate 20
PAK	P21-Activated Kinase
PDGF	Platelet derived growth factor
PI3K	Phosphoinositide 3-kinase
PKB	Protein kinase B
PKC	Protein kinase C
PMA	Phorbol myristoyl acetate
PMSF	Phenylmethanesulphonylfluoride
PNGaseF	Peptide-N-Glycosidase F
PVDF	Polyvinylidene fluoride
RA	Rheumatoid arthritis
Rac1	Ras-related C3 Botulinum Toxin Substrate-1
RAGE	Receptor for Advanced Glycation End-products
RhoA	Ras homolog gene family, member A
RIP	Regulated intramembrane proteolysis
ROI	Reactive oxygen intermediates
ROS	Reactive oxygen Species
SAA	Serum amyloid A
SAPK	Stress activated protein kinase
SDS	Sodium dodecyl sulfate
SE	Standard Error
Sf	Spodoptera friguperda
SFK	Src family of kinases
SMC	Smooth muscle cells
SNP	Single nucleotide polymorphism
SPR	Surface plasmon resonance
sRAGE	Soluble receptor for advanced glycation end-products

Abbreviation	Full name
STAT	Signal transducer and activator of transcription
TBARS	Thiobarbituric acid reactive substances
TBE	Tris-borate EDTA buffer
TCA	Trichloroacetic acid
TL	Toll-like receptor
TMB	3,5,3',5' - tetramethylbenzidine
TNFα	Tumour necrosis factor - alpha
TTR	Transthyretin
V domain	Variable domain
VCAM	Vascular cell adhesion molecule
VMD	Visual molecular dynamics
WASP	Wiskott-aldrich syndrome protein
WAVE	Wasp family verproline-homologous protein

ABSTRACT

The receptor for advanced glycation end products (RAGE) is a human cell surface receptor that defies simple structural and functional classification. Since its discovery in 1992, a diverse repertoire of RAGE ligands have been identified that progress a myriad of pathophysiological outcomes and disease states.

The promiscuity of this pluripotent pattern receptor has been identified through a number of studies investigating the different molecular characteristics of RAGE and their relationship with its many ligands. Interestingly, there has been a mix and match approach to the source of RAGE used in these studies over the last 20 years, employing both endogenous and recombinant forms expressed in insect and prokaryotic hosts. Verification as to whether these recombinant forms are analogous to their endogenous counterparts has been done sporadically and using a variety of different methodologies and isoforms of the receptor.

Here we set about to evaluate prokaryotic and insect expression systems for the production of three extracellular domain constructs of soluble RAGE (sRAGE). Additionally, this project aimed to produce a number of RAGE ligands using a common expression vector and host, with the intention of simplifying the production of a catalogue of molecules for use in studying the RAGE-ligand paradigm.

This study found that the use of expression vectors for the stable production of RAGE in insect cells that utilise modern recombinant technologies such as single-step topoisomerase cloning (TOPO®) enabled the production of constructs in a matter of days. Transfection of Lepidoptera cell lines was simple with high survival rates following optimisation of a lipid transfection methodology. The *Tn5* insect cell line was found to produce soluble RAGE (VC_1C_2) at levels 7-fold greater than the *Sf9 insect* cell line traditionally used for RAGE baculoviral expression. Heterogeneity of glycosylation of RAGE was observed in both *Sf9* and *Sf21* cell lines, with the *Tn5* cell line producing homogeneously glycosylated forms of the receptor. Optimisation of culturing conditions for the *Tn5* cell line increased the yield of soluble RAGE by about 20%, however, the quantity of protein produced per litre of culture were well short of the mg/L range normally produced by baculoviral systems, or required for structural studies.

Bacterial expression of RAGE has traditionally utilised strains such as BL21 (DE3) and more recently, Origami™ strains. This study utilised five bacterial strains optimised for

protein expression that included BL21 (DE3), Origami™ B, Rosetta-gami™ B, T7 Shuffle® B and T7 Shuffle® K12. It was found that heterologous gene features impacted on the ability of Origami™ B strains to translate RAGE mRNA. Indeed, optimisation of the canonical human RAGE gene led to a 4-fold improvement in the levels of expression in Origami™ B. Additionally, the correct formation of disulphide bonds was found to be a rate limiting step. T7 Shuffle® K12 engineered to express the disulphide bond isomerase C (DsbC) foldase in the cytosolic compartment expressed recombinant soluble RAGE at levels nearly 4-fold higher than Origami™ B. Collectively, this study found that the optimisation of the native sequence, and an enhancement in disulphide bond formation improved yields 27, 10 and 14-fold respectively for RAGE V, VC_1 and VC_1C_2 in comparison to the use of the canonical RAGE sequence in Origami strains in this study and as previously reported in the literature. Importantly, with the exception of the isolated V-domain, mg/L yields of both VC_1 and VC_1C_2 RAGE were obtained using the T7 Shuffle® K12 cells, making this cell line most suitable for future functional and structural studies. Moreover, this cell line also expressed S100A6, S100B, S100P and two HMGB1 constructs with similar mg/L yields.

The isolated V-domain of RAGE was very poorly expressed (μg/L) in all bacterial and eukaryotic hosts tested in this study. This was strongly correlated with the successive removal of the two C-type lectin domains of RAGE. Indeed, in bacterial hosts, the VC_1 and V domains were expressed at levels 4 to 12-fold and 40 to 100-fold lower, respectively than VC_1C_2 sRAGE. The predicted minimum free energy structure of mRNA encoding the V domain suggests a tendency to form matched stem loop structures in the absence of the C_1 domain. Interestingly, the V domain demonstrated a tendency to clone into the TOPO vector in the reverse orientation 93% of the time, suggesting that the 5' end was obscured or unavailable for ligation. Additionally, there was no increase in aggregation of recombinant RAGE with the removal of the C-type domains. In this study, it is speculated that the declining levels of expression with the removal of the C-type domains is due to the formation of mRNA structures that impede translation.

Each of the three RAGE constructs and the various S100 and HMGB1 ligands were purified following optimisation of their expression. Because every protein is different, different technologies and purification strategies were investigated for each type of protein with careful consideration given to the intended use of each protein. The objective in each case was to minimise the number of steps needed to achieve an appropriate level of purity whilst considering the speed, cost and versatility of each

method. The RAGE proteins were purified utilising a hexa-histidine tag attached to its C-terminus and the known affinity of RAGE for heparin. Full length HMGB1 was purified based on its remarkable solubility under acidic conditions and with the aid of a molecular sieve polishing step. Truncated HMGB1 was purified by utilising a GST tag attached to its C-terminus and an on-column cleavage protocol. Each of the S100 proteins were purified by phenyl Sepharose® chromatography, utilising the intrinsic calcium binding characteristics of S100s that leads to the exposure of a hydrophobic cleft able to bind the phenyl side chains. Given the oligomeric propensity of many of the ligands and the likely multivalent nature of their interactions with RAGE, a molecular sieve step immediately prior to the use of any of the proteins expressed and purified in this study is strongly recommended to ensure they are aggregate free prior to commencing functional and structural studies.

The RAGE and HMGB1 proteins expressed and purified in this study had circular dichroism spectra consistent with other published studies and, in general, in accordance with their known secondary structures. Moreover, the functionality of each of the proteins expressed and purified was demonstrated in several assay formats. A novel plate-based assay was developed that was simple to use and did not require expensive equipment or enzyme-conjugated forms of RAGE. This assay demonstrated that there was no discernible difference in the strength of binding between *Tn5* insect and T7 Shuffle® K12 expressed soluble RAGE with a number of its ligands. Although the complex mammalian glycosylation of RAGE has been shown to affect its ability to bind HMGB1 2-fold, no such difference was observed between insect expressed RAGE containing simple N-linked glycans and bacterial expressed RAGE with no glycans. As such, this study concluded that the post translational modifications offered by insect cell systems, such as glycosylation, do not provide a compelling justification for the use of insect over prokaryotic hosts. These observations using a novel plate-based binding assay developed in this study were also confirmed for several ligands by surface plasmon resonance studies.

In conclusion, this study reports the development of a common vector and host capable of the cytosolic expression of soluble RAGE at levels 13-fold higher than those previously reported. This same host and vector also yielded milligram quantities of the RAGE ligands HMGB1, truncated HMGB1, S100B, S100P and S100A6. The development of a novel plate based binding assay demonstrated that recombinant RAGE expressed in both insect cells *Tn5* and T7 Shuffle® K12 *E. coli* is synonymous in function, with

estimates of affinity correlating closely with those determined by surface plasmon resonance. Applications of the proteins produced using this common 'toolbox' methodology is already revealing significant insights into HMGB1 oligomerisation and its binding and activation of RAGE.

1.0 LITERATURE REVIEW

1.1 Discovery of the Receptor for Advanced Glycation End Products

During the 1980's and early 90's, considerable effort went towards identifying cell surface molecules believed to bind protein-aldose adducts commonly known as advanced glycation end products (AGEs). It was thought that AGE molecules initiated or progressed a number of pathologies associated with diabetes and aging through binding a cell surface receptor (Vlassara, 1990; Takata *et al.,* 1989). In 1992, two polypeptides were identified in bovine endothelial cell and lung extract that demonstrated specific AGE binding (Neeper *et al.,* 1992). These were named receptor for advanced glycation end product (RAGE), and lactoferrin-like polypeptide (LF-L) (Neeper *et al.,* 1992; Schmidt *et al.,* 1992).

RAGE has since been classified as a member of the immunoglobulin super family and implicated in a variety of pathologies such as diabetes, amyloidoses, tumour metastasis and inflammation (Matrone *et al.*, 2014; Schmidt and Stern, 2000; Singh *et al.*, 2014; Lee and Park, 2013). It is a multi-ligand receptor that binds a variety of seemingly unrelated ligands including HMGB1, calgranulins, AGE's and β-sheet fibrils characteristic of amyloids (Lee and Park, 2013; Donato, 2007; Manigrasso *et al.*, 2014).

1.2 Expression and Structure of the Receptor for Advanced Glycation End Products

1.2.1 Genetic characterisation and expression of RAGE

RAGE is highly conserved across a number of mammalian species with greater than 80% sequence identity observed between the human, mouse, canine, sheep and bovine forms of the gene (Neeper *et al.,* 1992).

The human gene for RAGE is located on chromosome 6p21.3, near the junction of the major histocompatibility complex (MHC) classes II and III locus. Gene ontology assessment identifies numerous roles for RAGE including protein binding, trans membranous cell signalling and inflammatory responses (Sugaya *et al.,* 1994). This region of chromosome 6 is a highly polymorphic, gene-rich region. A broad array of cell surface receptors and adhesion molecules, consistent with the many roles of RAGE, are located within this region (Figure 1) (Neeper *et al.,* 1992). This locus has been associated with the etiology of numerous chronic diseases such as diabetes and auto-immune responses (Traherne, 2008). The location of RAGE within this locus may explain

some of these associations between this region and pathologies such as diabetic complications, excessive inflammatory responses, and innate immunity.

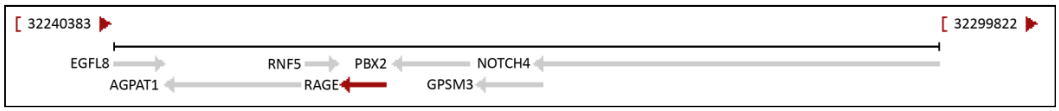

Figure 1. Chromosomal organisation of RAGE and contiguous MHC class genes in *Homo sapiens*.

The RAGE gene consists of a relatively small 5'-promoter region containing binding sites for nuclear factor-κ B (NF-κB) and Sp1 (Yan *et al.,* 1994). The 11 coding regions (~1300 bp) are interlaced with 10 introns, and a 3'-untranslated region (Yan *et al.,* 1994; Hudson *et al.,* 2008). Conserved domain analysis of the RAGE sequence identifies a number of regions correlating with various immunoglobulin-type domains found in cell adhesion molecules such as neuronal cell adhesion molecule (NCAM), CD2, CD4 and CD8.

Early studies into RAGE frequently identified polypeptides ranging in size from 30-50 kDa (Neeper *et al.,* 1992; Schmidt, Vianna *et al.,* 1992; Brett *et al.,* 1993). These isoforms were attributed to possible proteolytic cleavage of RAGE from the cell surface, alternate splicing of the gene or post-translational modification (Neeper *et al.,* 1992; Schmidt *et al.,* 1992; Schmidt *et al.,* 2001). Regulated intramembrane proteolysis (RIP) results in soluble forms of type 1 trans membranous receptors such as NOTCH and LRP (Kopan and Ilagan 2004; Galichet *et al.,* 2008). Similarly, RAGE expressed in HEK293 cells undergoes RIP mediated by ADAM (a disintegrin and metalloprotease) metalloproteases and γ-secretase to produce soluble RAGE (sRAGE) (Galichet *et al.,* 2008). The administration of sRAGE to animal models of tumorigenesis and atherosclerosis, dramatically curtails progression of these diseases by acting as a ligand decoy (Hofmann *et al.,* 1999; Taguchi *et al.,* 2000). Whether RAGE-RIP occurs *in vivo* to produce biologically significant levels of sRAGE has not been fully explored. Development of a method to quantify this particular proteolytic form of RAGE in plasma would provide an excellent means of clarifying this observation.

A large body of research on RAGE alternate splice variants supports this as the predominant mechanism by which receptor isoforms occur (Park *et al.,* 2004; Hudson *et al.,* 2008; Kalea *et al.,* 2009). Alternative splicing is a key mechanism in expanding the

repertoire and activity of biologically significant molecules, with an estimated 35% of all genes predicted to result in alternatively spliced variants (Hanke *et al.,* 1999). To date, 23 mRNA RAGE isoforms in mouse and human tissues have been identified and described in accordance with the human gene nomenclature (HGNC) (Hudson *et al.,* 2008; Kalea *et al.,* 2009; Sterenczak *et al.,* 2009). These variants are generally considered to be grouped according to whether they are N-terminally or C-terminally truncated/modified forms of RAGE.

N-terminus RAGE isoforms are those where introns 1-5 undergo alteration such as occurs in RAGE_v5. In normal lung and aortic smooth muscle cells, RAGE_v5 accounts for approximately 5% of total RAGE mRNA and is distinguished by the presence of two juxtaposed in-frame intron 4 inserts (Hudson *et al.,* 2008). This modification results in an additional 17 residues in the V domain, however, the impact of this on ligand binding has not been evaluated. Two RAGE mRNA transcripts have been identified in which the majority of the ectodomain is deleted or modified: N-truncated RAGE (RAGE_v2) and RAGE_v13 (Hudson *et al.,* 2008). These forms exhibit no affinity for AGE's and do not initiate signal transduction in response to ligand binding (Yonekura *et al.,* 2003; Ding and Keller, 2005).

One of the first C-terminal splice variants of RAGE identified was an endogenous secretory isoform, hRAGEsec (human secretory RAGE) (Malherbe *et al.,* 1999). This is now classified as RAGE_v16 and contains alterations in introns 2/3 and 7/8 respectively (Malherbe *et al.,* 1999; Hudson *et al.,* 2008). These frame-shift modifications result in a loss of the hydrophobic transmembrane spanning domain, allowing this variant to be secreted (Malherbe *et al.,* 1999). Yonekura *et al.* (2003) identified a secretory isoform (esRAGE), now classified as RAGE_v1. This variant is characterised by the inclusion of intron 9 in place of the exon encoding the transmembrane domain (Yonekura *et al.,* 2003; Hudson *et al.,* 2008). Similar studies identified additional secretory isoforms known as sRAGE 1/2/3 expressed in microvascular and pericyte cell types (Schlueter *et al.,* 2003; Hudson *et al.,* 2008). Of these, sRAGE3 is now considered to be RAGE_v1, with sRAGE1 and sRAGE3 termed RAGE_v14 and RAGE_v15 respectively (Schlueter *et al.,* 2003; Hudson *et al.,* 2008).

This complex array of 23 alternate splice RAGE transcripts does not directly translate into a milieu of RAGE proteins. A large number described by Hudson *et al.,* are predicted to be directed to the nonsense-mediated mRNA decay (NMD) pathway (Hudson *et al.,*

2008). Recent *in vitro* expression studies confirm most of the NMD predictions, supporting the likelihood that RAGE_v1 is the predominant human secretory RAGE isoform (Hudson *et al.,* 2008).

Deregulation of RAGE_v1 expression correlates with progression of a number of disease states including type I and II diabetes, Alzheimer's diseases, atherosclerosis, rheumatoid arthritis, renal disease, numerous cancers and inflammation (Tesarova *et al.,* 2007; Hudson *et al.,* 2008; Nakamura *et al.,* 2008; Romero *et al.,* 2008; Chen *et al.,* 2009). Expression of RAGE_v2 is also thought to reduce RAGE signal transduction by displacing full-length receptor from cell membranes (Yonekura *et al.,* 2003). There is an increasing body of evidence correlating sRAGE plasma and tissue levels with a number of chronic diseases (Basta, 2008; Maillard-Lefebvre *et al.,* 2009; Ramasamy *et al.,* 2009). However, much of the work to date has quantified total sRAGE rather than individual RAGE isoforms. Before sRAGE plasma levels can be used as biomarkers of disease, development of a system that discriminates between the numerous soluble RAGE forms must be developed. Characterisation of the regulatory mechanisms controlling expression of these RAGE isoforms also offers a novel therapeutic opportunity. By controlling expression of RAGE isoforms that antagonise canonical RAGE, a new means of tackling chronic disease may be realised.

The MHC class III region and its highly variable nature correlates with the occurrence of gene polymorphisms within this locus (Traherne, 2008). To date, some 30 polymorphisms in the various gene elements of RAGE have been identified and occur in both coding and non-coding regions (Hudson *et al.,* 1998; Hudson *et al.,* 2001; Kankova *et al.,* 2001; Jang *et al.,* 2007). Of significance is the common Gly82Ser polymorphism located within the V-binding domain, and three mutations within the 5' regulatory region that include -429 T/C, -374 T/A and a 63 bp deletion (Hudson *et al.,* 2001; Hudson *et al.,* 2008; Kalea *et al.,* 2009).

The Gly82Ser polymorphism falls within the V domain, increasing binding affinity with a number of S100 and AGE ligands (Hofmann *et al.*, 2002; Osawa *et al.*, 2007). Not only does this SNP cause local structural changes, but also partially destabilises the entire RAGE structure (Xie *et al.*, 2008). This polymorphism correlates with disease progression in diabetes, and certain cancers (Kim *et al.*, 2009; Kalea *et al.*, 2009b; Jang *et al.*, 2007; Hofmann *et al.*, 2002; Tesarova *et al.*, 2007). This is likely due to increased pro-inflammatory responses and reduced levels of circulating sRAGE observed in

Gly82Ser/Gly82Ser RAGE homozygotes (Hofmann *et al.*, 2002). Hereditary rheumatoid arthritis is known to correlate with the human leukocyte antigen HLA-DR4 (Pall *et al.*, 2008). The RAGE Gly82Ser SNP is reported to occur in disequilibrium with HLA-DR4 in a human case control study of rheumatoid arthritis patients, linking this polymorphism to the progression of this disease (Hofmann *et al.*, 2002).

The precise structural explanation of how the Gly82Ser influences RAGE activation has not yet been determined, however it is postulated to involve disruption of receptor oligomerisation (Xie *et al.*, 2008). This polymorphism is the most prevalent of all RAGE gene mutation. It occurs in approximately 5% of study cohorts compared to 1% for all other RAGE gene alterations (Kalea *et al.*, 2009b).

Alterations within the upstream promoter region of the RAGE locus increase transcription through interference with a negative gene regulatory element (Hudson *et al.*, 2001; Li and Schmidt, 1997). There have been a number of studies looking at the correlation between retinopathies and the -429 T/C and -374 T/A SNPs. Although the study cohorts were small in size, a statistically significant association between the development of retinopathy and the -429 T/C polymorphism was found (Hudson *et al.*, 2001; Ramprasad *et al.*, 2007). This is somewhat surprising, as the -374 T/A SNP results in significantly increased gene transcription and subsequent RAGE expression (Hudson *et al.*, 2001). The -374 T/A SNP is, however, strongly associated with protection against vasculopathies. Studies in both diabetic and non-diabetic populations show -374 T/A homozygotes have decreased occurrence of cardiac and neurovasculopathies, as well as nephropathies (Falcone *et al.*, 2008; Maruyama *et al.*, 2007; Pettersson-Fernholm *et al.*, 2003; Falcone *et al.*, 2005). Identifying correlations between RAGE SNPs and chronic disease is critical in identifying and managing those at risk.

The role and distribution of RAGE in homeostatic and disease states was first investigated by Brett *et al*. (1993) who quantified mRNA and antigenic RAGE levels in bovine organs (Brett *et al.*, 1993). RAGE is present on the surface of numerous cell types including macrophages, monocytes, endothelial cells, and is abundant in whole lung tissue (Schmidt *et al.*, 1992; Brett *et al.*, 1993). Although RAGE is intimately involved in a number of physiological pathways and responses, RAGE -/- mice have been produced with normal macroscopic tissue organisation and histopathology (Chavakis *et al.*, 2003). RAGE expression is now known to be extremely complex. Factors such as homeostatic state, pathophysiology, cell type, developmental stage and genetic predispositions all

affect types and levels of RAGE expression. Briefly, RAGE is present in the central nervous system during pre-natal development where it is involved in neuronal extension and migration (Huttunen *et al.*, 1999; Huttunen *et al.*, 2000; Chou *et al.*, 2004). Under homeostatic conditions, it is detectable in micro and macrovascular endothelium, smooth muscle cells and mesangial cells (Brett *et al.*, 1993; Chou *et al.*, 2004; Fiuza *et al.*, 2003; Warboys *et al.*, 2009; Sterenczak *et al.*, 2009). Numerous organs constitutively express RAGE, with lung and the central nervous system expressing the highest levels of canonical RAGE (Brett *et al.*, 1993; Chou *et al.*, 2004; Fiuza *et al.*, 2003; Warboys *et al.*, 2009; Sterenczak *et al.*, 2009). Needless to say, the predominant form of RAGE expressed within the body is membrane bound. Full length RAGE accounts for some 80% of RAGE mRNA in whole lung homogenate, followed by RAGE_v1 (7%) and RAGE_v5 (4%) (Hudson *et al.*, 2008a). These levels change based on tissue source, the presence of single or multiple polymorphisms, and other multigenetic factors (Brett *et al.*, 1993; Tesarova *et al.*, 2007; Kalea *et al.*, 2009b; Hudson *et al.*, 2008a).

The genetic character and regulation of RAGE expression is extremely complex. Elucidating the relationships between gene polymorphisms, RAGE isoform production and disease states is a challenging task. Efforts to understand these mechanisms will, however, provide exciting therapeutic opportunities to influence the progression of those diseases currently associated with the activation and regulatory dysfunction of RAGE.

1.2.2 Proteomic structure of RAGE

The full length RAGE transcript is translated into a single chain, type I trans membranous receptor of approximately 50 kDa. This 404 amino acid peptide consists of several structural elements including a 22 amino acid N-terminal signal peptide, an Ig V-type domain, two juxtaposed C-type domains, a hydrophobic trans membranous region followed by a negatively charged, highly acidic cytosolic tail (Figure 2).

As with most multi-ligand receptors, RAGE defies simple structural and functional classification, with NMR based information only recently becoming available. It is generally accepted, however, that RAGE is a pattern recognition receptor based on its multi-domain structure and ability to recognise multiple, unrelated ligands (Xie *et al.*, 2008; Chavakis *et al.*, 2003).

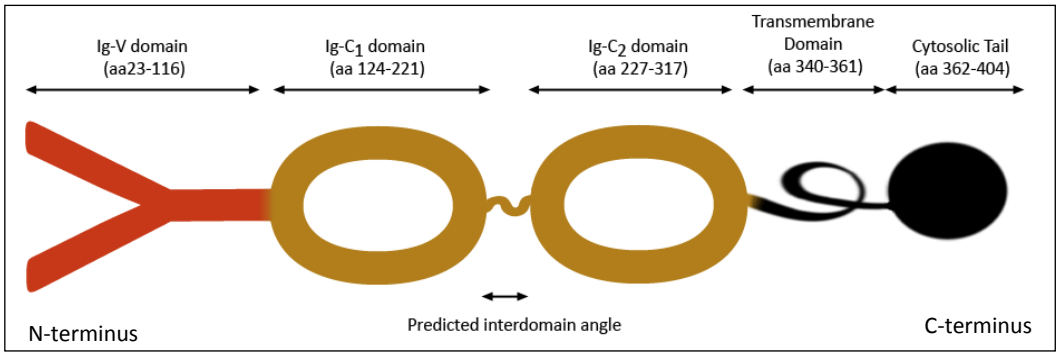

Figure 2. Structural representation of RAGE domains. Full length RAGE consists of an N-terminus Ig-V type domain, two IgG C-type domains separated by a predicted mobile loop, a trans-membranous region and short cytosolic C-terminal tail.

1.2.3 V-type ligand binding domain

Variable Type Ig domains (V domain) are found in a number of cell surface proteins including alternately spliced isoforms of neural cell adhesion molecules (NCAM 140), vascular cell adhesion molecule (VCAM) and CD20 (Neeper *et al.*, 1992; Schmidt *et al.*, 1996). Until recently, the variable domain of RAGE was believed to mediate all ligand binding. A number of RAGE elements are believed to facilitate these interactions, including anionic carbohydrates, a hydrophobic pocket, and an N-terminus cationic patch (Kislinger *et al.*, 1999; Yan *et al.*, 1996; Hofmann *et al.*, 1999; Leclerc *et al.*, 2007).

Two confirmed asparagine glycosylation sequons (Asn81 and Asn25) are located within the RAGE V domain (Figure 2.) (Srikrishna *et al.*, 2002; Neeper *et al.*, 1992). Removal of these glycans reduces RAGE-HMGB1 binding affinity two-fold, while increasing glycoaldehyde-AGE binding three fold (Srikrishna *et al.*, 2002; Osawa *et al.*, 2007). The anionic nature of these glycans almost certainly plays a role in either localising cationic ligands to proximal V domain binding site/s or reducing the rate of association of like-charge ligands. Whether this is their principal role is yet to be determined, as glycans serve a multitude of functions such as protection of proteolytic sensitive sites and stabilization of protein secondary/tertiary structures.

Point mutation and antibody blockade studies of the RAGE V domain identify it as the primary ligand binding region for HMGB1, AGEs, S100B and β-amyloid (Kislinger *et al.*, 1999; Taguchi *et al.*, 2000; Yan *et al.*, 1996). The nature and number of these binding sites, however, remains unclear. Matsumoto *et al.* (2008) produced an NMR solution

structure of the RAGE V domain (Figure 3) (Matsumoto *et al.*, 2008). This structure closely resembles other immunoglobulin variable domains with two β-sheet structures composed of seven β-strands, 6 loops and a single, short α-helix. A disulphide bridge between residues Cys38 and Cys99 links the β-sheets, stabilising the tertiary structure in a β-sandwich like conformation (Matsumoto *et al.*, 2008). Of particular interest is a positively charged area forming a cationic patch around loops 2 and 6 (Figure 3) (Matsumoto *et al.*, 2008). Charge is known to play a significant role in RAGE binding to certain ligands such as HMGB1 and various AGE molecules. However, difficulty dissociating certain RAGE-AGE complexes with 1 M NaCl solutions suggests additional interactions are involved (Xie *et al.*, 2008; Matsumoto *et al.*, 2008).

A hydrophobic cleft with an estimated solvent accessible surface of -300 $Å^2$ is located in close proximity to this cationic centre and located laterally to the disulphide linkage (Matsumoto *et al.*, 2008). Loop 3 of the variable domain is unique to RAGE when compared to canonical Ig variable domain structures. The flexible nature of this loop may enable it to act as a gate to the hydrophobic pocket (Matsumoto *et al.*, 2008). This hydrophobic element of RAGE may explain the high-affinity interactions previously observed for glycaldehyde-AGE structures and various monomeric and fibrillary amyloids. The positively charged region and hydrophobic pocket are, interestingly, closely associated with the Asn81 glycosylation site in loop 4. It is possible that this N-linked glycan interacts with charged ligands to either recruit or retard their interaction with these elements of the V domain. Further studies are required to verify these observations.

Currently, a number of mechanisms by which ligand binds to the RAGE V domain have been proposed: ionic interaction with a cationic patch on the V domain; interaction with a hydrophobic pocket possibly gated by loop 3; and receptor oligomerisation that causes conformational changes influencing ligand accessibility (Xue *et al.*, 2014). Indeed, oligomerisation of RAGE has been shown to increase estimates of affinity by nearly 50-fold (Xue *et al.*, 2011; Xue *et al.*, 2014; Xie *et al.*, 2008; Valencia *et al.*, 2004). There is, however, evidence that some ligands directly bind RAGE at sites associated with the C-type domains of the receptor, and that C_1 is involved in the binding of certain ligands in concert with the V domain (Dattilo *et al.*, 2007; Leclerc *et al.*, 2007).

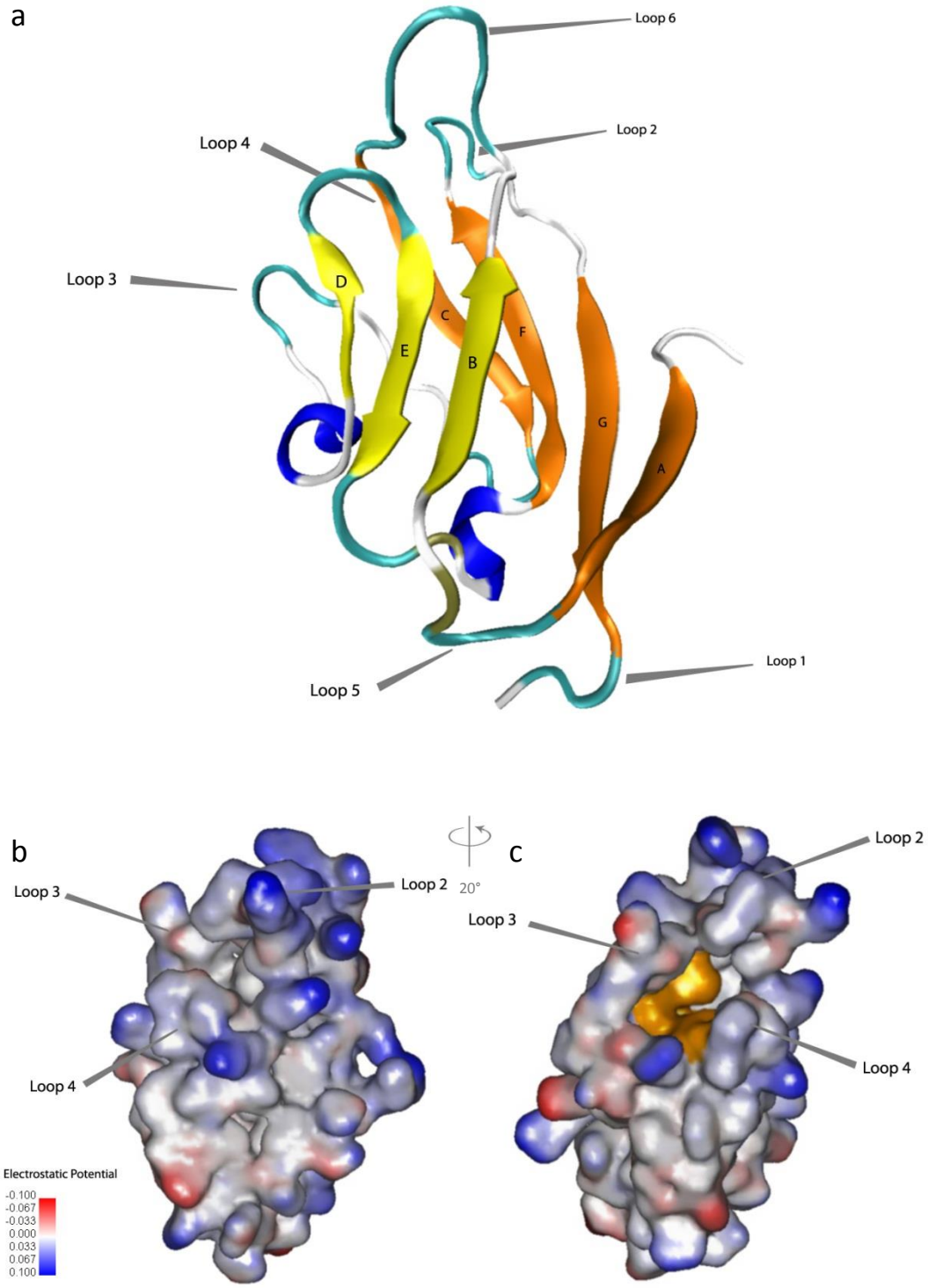

Figure 3. The NMR solution structure of the variable domain of RAGE. (a) The secondary structures in cartoon representation showing two beta sheets coloured in yellow and orange, with the 6 principle loops labelled and alpha helices coloured blue as predicted by VMD. (b) Electrostatic surface profile, as predicted using Accelrys modelling suite, of the domain showing a strong cationic area at the top of the molecule. (c) A hydrophobic cleft coloured gold formed by loops 4, 3 and 2. (PDB Structure: 2E5E.pdb).

1.2.4 C-type lectin domains

C-type lectin domains are found predominantly, but not exclusively, in a wide range of vertebrate immunoglobulin and adhesion molecules such as eosinophil major basic protein and CD22. The function of these animal lectin domains in RAGE biology is poorly understood. They are, however, generally associated with membrane proteins involved in glycoprotein endocytosis and inflammation (Drickamer, 1998).

The role of these domains in RAGE was recently investigated, focusing on the binding of S100 molecules (Dattilo *et al.*, 2007). This study found that the C-domains fulfil separate and important roles. The N-terminus C_1 domain stabilises the V domain structure, while C_2 is a structurally discrete domain with significant rotational freedom provided by a C_1-C_2 interdomain loop (Figure 2.) (Dattilo *et al.*, 2007; Xie *et al.*, 2008). It is possible that the C_1 domain is more important for initial correct folding of the V domain tertiary structures rather than functional requirements such as ligand binding. NMR studies, however, suggest that the C_1 domain is a crucial element that reduces the plasticity of the V domain mobile loops. In the absence of C_1, the V domain demonstrates conformational heterogeneity and significantly weaker affinity for S100B and AGEs (Dattilo *et al.*, 2007; Xie *et al.*, 2008). As the structural studies performed by Matsumoto *et al.* (2008), utilised a V domain-only construct, this structure may not represent an accurate representation of this domain compared to canonical RAGE. Further NMR or modelling studies utilising a VC_1 form of RAGE would provide additional insights into ligand binding and receptor-receptor interactions.

Surface plasmon resonance studies demonstrate that a discrete RAGE C_2 domain construct binds S100A6 (Leclerc *et al.*, 2007). It is proposed that S100B and S100A6 exhibit different cellular outcomes by interacting with separate domains, following the one domain - one ligand paradigm. Xie *et al*. (2007) similarly report that hexameric S100A12 binds to a C_1C_2 RAGE construct independent of the V domain through two symmetric hydrophobic patches available in the presence of Ca^{2+} (Xie *et al.*, 2007). Although there is evidence that C_2 is structurally independent of VC_1, it is not confirmed that C_2 or C_1C_2 constructs used in these studies are comparable to their equivalent domains in eukaryotic VC_1C_2 RAGE. Evaluation of S100A6 and S100A12 binding to eukaryotic V, VC_1 and VC_1C_2 eukaryotic RAGE constructs may help to clarify this observation. Additionally, the concentration of Ca^{2+} and Zn^{2+} in these assays should be carefully considered as calgranulins undergo conformational changes and

oligomerisation in the presence of these divalent cations (Boom *et al.*, 2004; Donato, 2007). Homology modelling of the VC_1 and C_2 domains suggests that the constant domains are connected by a mobile loop comprising 12 residues from Ala223 to Glu236 (Dattilo *et al.*, 2007). Whether the flexible nature of this loop is involved in allosteric signal transduction following ligand binding by the VC_1 structure is unknown.

A number of immunoglobulin superfamily receptors are known to form homodimers (Srikrishna *et al.*, 2002). Recent studies using S100B suggest that RAGE similarly undergoes oligomerisation following ligand binding (Dattilo *et al.*, 2007). Matsumoto *et al*. (2008) observed sRAGE oligomerisation using NMR, while titrating BSA-AGE into a sRAGE solution (Matsumoto *et al.*, 2008). These findings support the hypothesis that in the presence of certain ligands, RAGE forms homophilic receptor superstructures (Matsumoto *et al.*, 2008). RAGE was originally thought to form a heterodimer with a lactoferrin-like molecule based on native PAGE electrophoretic studies showing RAGE in association with a 35 kDa structure (Schmidt *et al.*, 1992). More recently, RAGE purified from mouse lung was found to migrate as part of a 200 kDa complex under non-denaturing conditions (Hanford *et al.*, 2004). Thus, it is generally thought that RAGE forms homodimer/oligomers, however, there is conflicting evidence as to whether RAGE exists in a native oligomerised form, or requires ligand binding to initiate RAGE-RAGE associations (Abel *et al.*, 1995; Leclerc *et al.*, 2007; Ostendorp *et al.*, 2007; Xie *et al.*, 2007; Matsumoto *et al.*, 2008; Xie *et al.*, 2008). The stoichiometry of oligomerisation is uncertain, with reports of dimeric, trimeric and tetrameric RAGE quarternary structures in various contexts (Xie *et al.*, 2007; Xie *et al.*, 2008; Dattilo *et al.*, 2007; Schmidt *et al.*, 1994). Of particular interest is a report that the C_1 domain plays a key role in oligomerisation of sRAGE expressed in a bacterial recombinant protein system (Xie *et al.*, 2007). The role of the interdomain angle between C_1–C_2 mediated by the mobile loop has been proposed as one possible factor influencing RAGE oligomerisation and associated signal transduction (Dattilo *et al.*, 2007; Xie *et al.*, 2007). Indeed, recently Sitkiewicz *et al* (2013) demonstrated the involvement of this loop in the formation of dimer-tetramers of RAGE which is now considered its constitutive form (Xie *et al.*, 2008; Koch *et al.*, 2010).

Clearly, the Ig C-domains of RAGE are not lay bystanders in the activity of this pluripotent receptor. Their roles in directly binding various calgranulins independent of the V domain, stabilisation of the V domain secondary and tertiary structures, as well as RAGE oligomerisation are significant issues requiring further investigation. Do multiple

ligands bind RAGE simultaneously, modifying signal transduction or inhibiting receptor oligomerisation? Do full ectodomain constructs behave differently to the C_1C_2 and C_2 RAGE constructs used in structural studies to date? What is the RAGE-RAGE stoichiometry before and after ligation? These fundamental questions about the structure of RAGE all require significant investigation.

1.2.5 Intracellular C-terminal signalling domain

RAGE is a non-canonical type I transmembrane receptor as it lacks a tyrosine kinase or similar intracellular signalling motif. The RAGE intracellular domain is highly conserved across species including human, bovine, rat and mouse (Ishihara *et al.*, 2003). It is described as consisting of a proximal 17 residue basic region, a central 17 residue glutamic acid region, and a poorly conserved 6 residue C-terminus (Ishihara *et al.*, 2003). The highly acidic, 40 amino acid cytosolic tail (CT) contains more than 30% glutamatic acid residues and assumes a disordered structure (Dattilo *et al.*, 2007). NMR and circular dichroism studies suggest few persistent secondary or tertiary structures within the CT domain (Dattilo *et al.*, 2007). Despite these unusual features, this domain is requisite for RAGE-ligand mediated intracellular signalling (Hudson *et al.*, 2008b; Huttunen *et al.*, 1999; Hassid *et al.*, 2009; Sakaguchi *et al.*, 2003).

Although the CT domain is unusual in structure, two intracellular binding targets have been identified: extracellular signal-regulated protein kinase-1 and -2 (ERK 1/2), and Diaphanous-1 (Dia1) (Ishihara *et al.*, 2003; Hudson *et al.*, 2008b). The RAGE basic amino acid region of the cytoplasmic tail is consistent with a D-domain and directly binds ERK 1/2 (Ishihara *et al.*, 2003). D-domains are essential in mediating the efficient phosphorylation of MAP kinases (Tanoue and Nishida, 2002). The phosphorylation state of the RAGE CT domain does not, however, influence ERK binding, with other members of the MAPK family such as JNK or p38 demonstrating no affinity for this structure (Ishihara *et al.*, 2003). This observation suggests that RAGE is not a substrate for ERK, but a specific intracellular anchor that localizes this kinase to the extracellular membrane (Ishihara *et al.*, 2003). Whether RAGE activation of the ERK signalling pathway is cell, ligand or sub-cellular compartmentally regulated, is yet to be well defined.

More recently, Hudson *et al*. (2008) identified Diaphanous-1 as a key molecule that directly interacts with RAGE to mediate cellular outcomes (Hudson *et al.*, 2008b). Diaphanous-1 is a member of the formin family of Rho GTPase binding proteins

principally involved in actin/cytoskeletal reorganisation (Tominaga *et al.*, 2000; Chardin, 2003). Immunofluorescence and yeast two-hybrid studies confirm that Dia1 co-localises with RAGE at the extracellular membrane and directly interacts with the CT domain (Hudson *et al.*, 2008b). Specifically, RAGE binds to the proline-rich formin homology domain (FH1) as opposed to the Rho binding domain of Dia1 (Hudson *et al.*, 2008b). The interaction of RAGE with Dia1 leads to activation of the Rac/cdc42 pathway involved in cell motility, cytokinesis, membrane protrusion and extension (Yamana *et al.*, 2006). This is in concert with previous observations associating RAGE-ligand binding with neurite outgrowth and macrophage/lymphocyte migration (Huttunen *et al.*, 1999; Chen *et al.*, 2004).

Recently, a number of questions as to the role of receptor oligomerisation and the CT domain have emerged. Does the CT domain undergo re-organisation following oligomerisation? Does this allow other intracellular molecules to interact with the cytosolic domain of RAGE? How does the pleiotropic nature of RAGE manifest through this small 40 amino acid structure?

1.2.6 Lactoferrin-like polypeptide structural association with RAGE

Early research to identify AGE binding proteins led to the discovery of RAGE, along with a 35 kDa Lactoferrin-like polypeptide (LF-L) (Schmidt *et al.*, 1992; Neeper *et al.*, 1992). It was hypothesised that LF-L interacted with RAGE on endothelial and monocyte cell surfaces in a non-covalent, time dependent and reversible manner (Schmidt *et al.*, 1994; Schmidt *et al.*, 1992). Competitive binding studies of bound and free RAGE against LF-L demonstrated specific binding of LF-L to immobilised RAGE, however, the stoichiometry of association was indeterminate (Schmidt *et al.*, 1994). Schmidt *et al.,* observed that when individual components of the LFL-RAGE complex were targeted with IgG antibodies, ligand binding of the entire complex was inhibited (Schmidt *et al.*, 1994). The RAGE–LF-L complex, although non-covalently stabilised, withstood exposure to very high salt (*2 M*) and pH (pH 3), with an affinity estimate (K_D) of 100 pM (Schmidt *et al.*, 1994; Brownlee, 1995). Immunoelectron microscopy studies similarly located LF-L and RAGE in close proximity to each other, with cross-linking producing a single 70 kDa band immune-reactive for both molecules (Schmidt *et al.*, 1992). A Blockade study of the individual LFL-RAGE components and erythrocyte surface AGEs reported that these two AGE receptors bind differing species of AGE structures (Wautier *et al.*, 1994). This observation has not, to date, been confirmed.

At the time of these observations, little was known about RAGE structure. New evidence, however, has revealed that RAGE is capable of forming oligomeric quarternary structures. It is possible that the LF-L-RAGE complex is a heterophilic RAGE dimer; however, significant investigation is required to test this hypothesis.

1.3 RAGE Ligands

A number of RAGE extracellular ligands have been identified including advanced glycation end-products, HMGB1, calgranulins and various amyloids. A few unusual RAGE ligands have also been reported, including the integrin Mac-1, advanced oxidation protein products (AOPP), and hyaluronic acid aggregates (Orlova *et al.*, 2007; Neumann *et al.*, 1999; Guo *et al.*, 2008). This review focuses on the four primary families of molecules known to bind and activate RAGE.

1.3.1 Advanced glycation end-products (AGE)

Advanced glycation end products are a heterogeneous class of irreversibly cross-linked adducts resulting from the non-enzymatic modification of amino acids by aldose sugars (Figure 4) (Brett *et al.*, 1993; Gerrard, 2002). This class of RAGE ligand has been strongly linked to the etiology of diabetic complications and aging, in particular its involvement in the progression of vasculopathies throughout the body (Chong *et al.*, 2006; Leclerc *et al.*, 2009; Salahuddin *et al.*, 2014). These characteristically yellow/brown, pigmented fluorescent adducts are also prevalent in commonly consumed foods such as commercially prepared breakfast cereals, olive oil, butter and various broiled and fried meats (Goldberg *et al.*, 2004; Esposito *et al.*, 1989). Whether ingested exogenous sources of AGEs contribute to the development or progression of AGE related pathologies is yet to be clearly demonstrated.

AGE formation begins with an initial condensation reaction between the free amine group in lysine or arginine, and a carbonyl group associated with reducing sugars such as glucose, ribose, lactose or the glyoxalase system metabolite methylglyoxal (Gerrard, 2002; Westwood *et al.*, 1994). This reaction was first described in 1912 by Louis-Camille Maillard after he observed gentle heating of sugar and amino acids in water produced a yellow brown colour (Gerrard, 2002; Maillard, 1912). Although the chemistry of this reaction was unknown to Maillard, the implication that two common components of

food goods form a biologically active adduct has now been considered extensively in metabolic disorders such as diabetes.

Early stages of protein glycation by this process are reversible from the initial formation of Schiff base products, through to the intermediate Amadori product which has a physiological half-life of 6-8 months (Gerrard, 2002). These intermediate Maillard products undergo further irreversible modification leading to AGE production. In some cases, the Maillard reaction causes protein cross-linking, particularly in proteins with a long half-life such as collagen and lens α-crystallins (Monnier *et al.*, 1999; Nagaraj and Sady, 1996). These structural changes contribute significantly to numerous pathologies such as diabetic complications. Because of this, certain AGEs such as glycated haemoglobin (HbA_{1c}), N^{ε}-Carboxymethyl-lysine (CML), pentosidine and collagen bound furosine are utilised as indicators of diabetes progression (Monnier *et al.*, 1999; Ikeda *et al.*, 1996).

For many years, it has been known that an inverse relationship exists between mammalian longevity and collagen glycation (Kohn, 1982). The distribution of AGEs throughout various tissues appears to correlate strongly with the protein species located in the various organs, protein turn-over and the expression of AGE receptors at these sites (Westwood *et al.*, 1994). The accumulating of AGEs is also often described as a function of protein half-life and sugar availability (Gerrard, 2002; Brownlee *et al.*, 1988; Sell and Monnier, 1989). During homeostasis, intravascular AGEs levels are partially controlled by vascular endothelial endocytosis/transcytosis (Esposito *et al.*, 1989).

The ability of various biological sugars to participate in the Maillard reaction varies greatly. Glucose is the least reactive of the aldohexoses, because of its role as a principle energy carrier in biological systems (Schmidt *et al.*, 2001; Gerrard, 2002). Sugars such as ribose and fructose have reducing power that can lead to highly reactive AGE structures (Gerrard, 2002; Valencia *et al.*, 2004).

AGEs bind a wide array of cell surface receptors other than RAGE, including lactoferrin, scavenger receptor types I and II, oligosaccharyl transferase (OST-48), 80K-H phosphoprotein, galectin-3 and CD36 (Li *et al.*, 1996; Vlassara *et al.*, 1995; el Khoury *et al.*, 1994). The extreme diversity in biological AGE structures makes their *in vivo* characterisation difficult. Numerous radio ligand studies have, however, produced K_D estimates ranging from μM to nM for the binding of common physiological AGEs with RAGE (Xie *et al.*, 2008; Kislinger *et al.*, 1999; Valencia *et al.*, 2004).

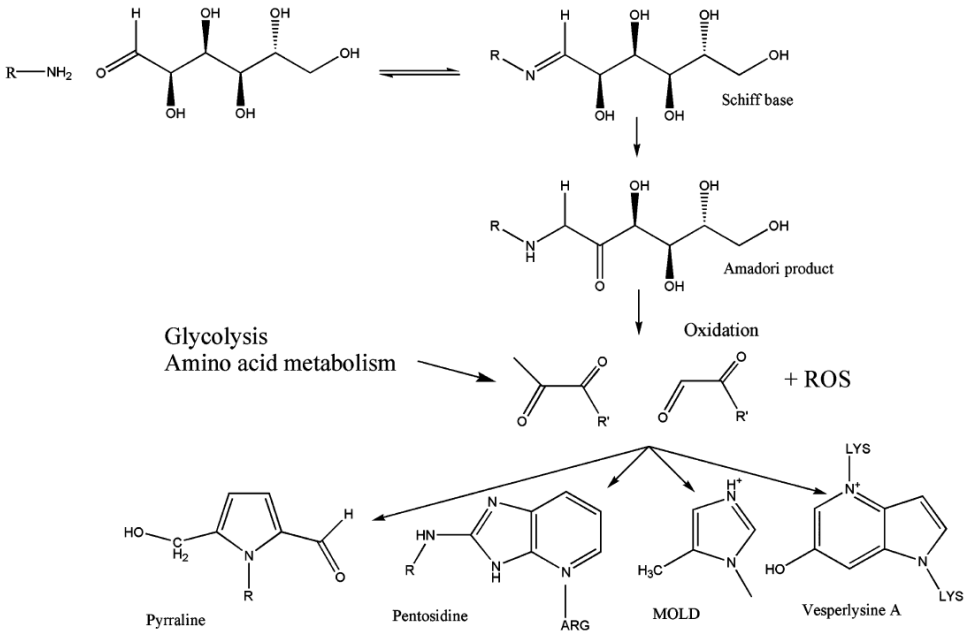

Figure 4. General example of the formation of biologically significant advanced glycation end-products (Schmidt *et al.*, 2001).

Heterogeneity of AGE binding was first demonstrated by competitive binding assays involving radiolabelled methylglyoxal modified BSA (MS-AGE) and BSA-AGE (Westwood *et al.*, 1994). This study reported that radiolabelled AGE ligand is displaced by cold ligand of the same type, but not completely by alternate cold ligand (Westwood *et al.*, 1994). This is possibly explained by the innate ability of MS-AGE to form protein cross-linkages, in this case with BSA-AGE (Gerrard, 2002; Frye *et al.*, 1998). Cross-link formation and polymerisation of AGEs is known to contribute significantly to the robust nature of these macromolecules, reducing their solubility, increasing heat denaturation times and increasing protease resistance *in vivo* (Vlassara *et al.*, 1992; Sell and Monnier, 1989).

The biological activity of AGEs is facilitated through four general mechanisms: intracellular signalling pathway activation following receptor-ligand binding; the structural modification of biological structures via the Maillard reaction; base modification at apurinic/apyrimidinic sites in DNA causing genomic disruption; and the oxidative effect of AGE molecules on nearby contiguous structures (Brownlee, 1995; Sakurai *et al.*, 1990; Xie *et al.*, 2008; Mullokandov *et al.*, 1994; Bao *et al.*, 2014).

The implication of AGE accumulation *in vivo* includes increased endothelial cell permeability, monocyte chemotaxis, expression of cytokine and growth factors, diabetes related renal failure, and nitric oxide dependent vasodilation (Esposito *et al.*, 1989; Kirstein *et al.*, 1990; Vlassara *et al.*, 1992; Bucala *et al.*, 1991; Mallipattu and Uribarri, 2014; Merhi *et al.*, 2014) . Much debate exists as to whether AGEs are a specific RAGE ligand or accidental protagonist. This consideration is, however, moot in the shadow of the severe biological outcomes of AGE accumulation. A greater understanding of the kinetics of interaction between AGEs and RAGE will assist in understanding how this interplay promotes chronic disease.

1.3.2 Amyloids

The term amyloid was first used in 1854 by Virchow to describe an anomalous brain structure, corpora amylacea, which resembled botanical cellulose-like structures referred to at the time as amyloid (Virchow R, 1854). Today, amyloids are characterised as fibrillary structures often composed of amyloid light chain (AL) or amyloid associated (AA) protein with cross-linked β-structures, an affinity for Congo red, and green birefringence (Westermark *et al.*, 2005). A number of *in vivo* amyloid fibril precursors have been identified and associated with local and systemic pathologies generally termed amyloidoses (Figure 5**.**) (Westermark *et al.*, 2005). Endogenous Aβ is a 39-43 amino acid peptide that makes up the majority of extracellular fibrillary aggregates commonly known as amyloid plaques (Balleza-Tapia and Pena, 2009). Aβ exists as a monomer, insoluble (AβF) and soluble (AβO) oligomeric fibrillary structures, and aggregate (AβA) forms (Sturchler *et al.*, 2008).

RAGE directly interacts with amyloid fibrillary structures (Yan *et al.*, 1996; Yu and Ye, 2014; Origlia *et al.*, 2014). The first study showing this found that synthetic amyloid β-peptide (1-40) (Aβ1-40), bound RAGE with nanomolar affinity in both brain endothelium and cortical neurons (Yan *et al.*, 1996). This interaction is inhibited in a dose-dependent manner by anti-RAGE IgG or excess sRAGE in both in-vivo and in-vitro cell binding assays (Yan *et al.*, 1996). The ability of various synthetic Aβ ligands to bind RAGE is now known to involve residues 25-35 of the peptide, with scrambled Aβ25-35 having no binding activity (Yan *et al.*, 1996). These 4-5 kDa peptides are produced by the sequential activity of β- and γ- secretase on transmembrane protein amyloid precursor protein (APP) (Selkoe, 2001; Kimberly *et al.*, 2003). Particular mutations in the gene of APP as well as the presenilins (PS1 and PS2) involved in APP processing, correlate strongly with

familial Alzheimer's disease (Hardy, 1997). These mutations result in the expression of amyloidogenic peptides, namely Aβ1-42, that cause progressive cognitive impairment (Hardy, 1997; Balleza-Tapia and Pena, 2009).

Table I. Amyloid fibril proteins and their precursors in human#.

Amyloid protein	Precursor	Systemic (S) or localized, organ restricted (L)	Syndrome or involved tissues
AL	Immunoglobulin light chain	S, L	Primary Myeloma-associated
AH	Immunoglobulin heavy chain	S, L	Primary Myeloma-associated
$A\beta_2M$	β_2-microglobulin	S	Hemodialysis-associated
		L?	Joints
ATTR	Transthyretin	S	Familial Senile systemic
		L?	Tenosynovium
AA	(Apo)serum AA	S	Secondary, reactive
AApoAI	Apolipoprotein AI	S	Familial
		L	Aorta, meniscus
AApoAII	Apolipoprotein AII	S	Familial
AApoAIV	Apolipoprotein AIV	S	Sporadic, associated with aging
AGel	Gelsolin	S	Familial (Finnish)
ALys	Lysozyme	S	Familial
AFib	Fibrinogen α-chain	S	Familial
ACys	Cystatin C	S	Familial
ABri	ABriPP	S	Familial dementia, British
ADan*	ADanPP	L	Familial dementia, Danish
Aβ	Aβ protein precursor (AβPP)	L	Alzheimer's disease, aging
APrP	Prion protein	L	Spongiform encephalopathies
ACal	(Pro)calcitonin	L	C-cell thyroid tumors
AIAPP	Islet amyloid polypeptide**	L	Islets of Langerhans Insulinomas
AANF	Atrial natriuretic factor	L	Cardiac atria
APro	Prolactin	L	Aging pituitary Prolactinomas
AIns	Insulin	L	Iatrogenic
AMed	Lactadherin	L	Senile aortic, arterial media
AKer	Kerato-epithelin	L	Cornea, familial
ALac	Lactoferrin	L	Cornea
AOaap	Odontogenic ameloblast-associated protein	L	Odontogenic tumors
ASemI	Semenogelin I	L	Vesicula seminalis
ATau	Tau	L	Alzheimer's disease, fronto-temporal dementia, aging, other cerebral conditions

#Proteins are listed, when possible, according to relationship. Thus, apolipoproteins are grouped together, as are polypeptide hormones; *ADan comes from the same gene as ABri; **Also called 'amylin'.

Figure 5. Human precursors for amyloid fibril structures and their associated syndromes (Westermark *et al.*, 2005).

Whether these β-sheet fibrils bind common or discrete V domain binding sites to that of BSA-AGE's and HMGB1 ligands, was investigated in competitive I^{125}-Aβ1-40 binding assays. Each of these ligands reversibly blocked I^{125}-Aβ1-40 interaction with RAGE in a dose-dependent manner, supporting the hypothesis of overlapping or contiguous binding sites (Yan *et al.*, 1996). The conclusion that Aβ exclusively binds the V domain of RAGE was further strengthened by atomic force microscopy and modelling studies (Chaney *et al.*, 2005).

The observation that monomeric and fibrillary forms of amyloid β-peptide bind RAGE with differing affinities prompted the question whether the receptor recognised a sequence motif or a tertiary/quarternary structural motif involving β-sheet structures (Yan *et al.*, 2000; Qosa *et al.*, 2014). To answer this, RAGE binding studies were performed utilizing non-amyloidogenic erabutoxin B - an all β-sheet protein, non-cross-linked β fibril collagen and elastin molecules as ligands. These structures did not interact with the receptor, suggesting that RAGE recognises cross-linked β-structured amyloids only, with the exception of monomeric Aβ-peptide (Yan *et al.*, 2000). The necessity for these quarternary amyloid structures in RAGE binding was further confirmed by the observation that SAA 1 (forming amyloidogenic fibrils) and not SAA 2 (does not form fibrillary structures) binds and initiates cellular stress through RAGE (Malle *et al.*, 2009). Recently, the oligomeric state of Aβ was shown to influence RAGE binding (Sturchler *et al.*, 2008). This study reported that Aβ aggregates specifically interact with the C_1 domain, while monomeric and oligomeric Aβ bind the V domain (Sturchler *et al.*, 2008). Currently, a number of fibrillary RAGE binding molecules have been identified. Serum amyloid A, transthyretin amyloid fibrils (TTR), as well as protein/protein fragments such as amyloid β-peptide, amylin and prion-derived peptides promote cellular dysfunction through RAGE (Yan *et al.*, 2000).

A common factor in RAGE activation by amyloids is oxidative stress through reactive oxygen species (ROS) production and subsequent IκB-α degradation. This event leads to the activation and nuclear translocation of NF-κB by intracellular signalling pathways (Yan *et al.*, 2000). Through this transcription factor, oxidative stress and other signalling pathways, amyloid-RAGE promotes cellular dysfunction and ultimately neuronal apoptosis (Malle *et al.*, 2009; Chong *et al.*, 2006). Inversely, under homeostatic conditions, RAGE facilitates the clearance of amyloid via lysosomal compartment degradation (Chaney *et al.*, 2005).

Although RAGE mediated signal transduction is a significant pathway promoting Aβ outcomes, the promiscuous nature of amyloids suggest it is not the only avenue of action (Balleza-Tapia and Pena, 2009). A multitude of Aβ cell surface binding sites other than RAGE have been identified. These include alpha-5 β-1 integrin, *N*-methyl *D*-aspartate receptor (NMDA-R), nicotinic receptors, formyl-peptide receptor-like-1 (FPRL1) and certain adhesion and tyrosine kinase receptors (Kalea *et al.*, 2009a; Ramprasad *et al.*, 2007; Falcone *et al.*, 2005; Balleza-Tapia and Pena, 2009). Recently, RAGE has been identified as having a role in the transportation of Aβ from the blood

stream into the central nervous system, further confirming it as a key player in the progression of neurodegenerative conditions (Andras *et al.*, 2012).

The mechanistic elements of RAGE-amyloid ligation remain largely unknown. The consequences of this interaction are, however, well documented and include progressing rheumatoid arthritis, neoplasia, systemic amyloidosis, and Alzheimer's disease (Yan *et al.*, 2000; Yan *et al.*, 1996; Malle *et al.*, 2009; Chen *et al.*, 2007).

1.3.3 Calgranulins

Calgranulins are known as S100 proteins due to their solubility in 100% saturated ammonium sulfate (Donato, 2001; Moore, 1965). This heterogeneous family of 21 Ca^{2+} modulated proteins is exclusively expressed by vertebrates in both intracellular and extracellular spaces (Donato, 2007). Calgranulins are characterised by a highly conserved EF-hand tertiary structure composed of two α-helices flanking a Ca^{2+} binding loop that collectively form a helix-loop-helix motif. The first loop in the amino-terminus EF hand structure is long and disordered in comparison to the second carboxyl-terminus EF hand loop which is canonical in arrangement (Donato, 1986; Donato, 2007). These differences result in low and high Ca^{2+} binding affinities respectively (Donato, 1986; Donato, 2007). Although the calcium binding regions are highly conserved within the S100 family, the hinge region joining the two EF hands is highly variable (Santamaria-Kisiel *et al.*, 2006; Yanez *et al.*, 2012).

S100 proteins are an acidic, low molecular weight species often within the range of 9–14 kDa. The human genes encoding 13 members of this family are found in a cluster on chromosome 1 (Donato, 2001; Schafer *et al.*, 1995). The majority of *in vivo* S100 proteins exist as non-covalently bound homophilic oligomers with the exception of S100G which is monomeric (Donato, 2001; Skelton *et al.*, 1994). Extracellular heterodimers of S100A12/S100B, S100A8/S100A9 and S100B/S100A6 are common, with the A8/A9 dimer being the preferred intracellular form for S100A8 and S100A9 (Hunter and Chazin, 1998; Donato, 2001; Leclerc *et al.*, 2009). Monomers stack in an anti-parallel orientation to each other to form non-covalent structures that upon binding of Ca^{2+}, Zn^{2+} or Cu^{2+}, undergo significant conformational change to expose a hydrophobic cleft (Santamaria-Kisiel *et al.*, 2006; Boom *et al.*, 2004). This hydrophobic region is one mechanism by which oligomeric S100 quarternary structures affect intracellular target molecules (Leclerc *et al.*, 2009). It is, however, postulated that other unidentified aspects of calgranulin structure are also involved (Donato, 2007).

S100 molecules are implicated in a broad array of physiological processes that include cell proliferation, differentiation and cytoskeletal organisation, membrane trafficking, protein phosphorylation, gene expression and metabolism (Leclerc *et al.*, 2007; Hofmann *et al.*, 1999; Leclerc *et al.*, 2009). Calgranulins are expressed in a cell specific manner (Leclerc *et al.*, 2009). Whether this explains why certain S100 proteins are associated with diseases affecting particular tissues, or that various calgranulins have unique and specific biological targets from each other, requires considerable clarification.

Based upon the high degree of structural homology within the functional Ca^{2+} binding domain of this family, it is not unreasonable to suggest that S100s may bind a number of common targets. Based on this hypothesis, it was thought likely that a number of calgranulins bind RAGE based on initial observations that S100B and S100A12 are RAGE ligands (Chavakis *et al.*, 2003; Bianchi *et al.*, 2007; Yang *et al.*, 2007). Subsequent studies have shown that S100A1, A4, A6, A7, A8/A9 dimers, A11, A13 and S100P potentially promote physiological outcomes, in part, through RAGE (Donato, 2007; Leclerc *et al.*, 2009; Tothova and Gibadulinova, 2013; Chen *et al.*, 2014b).

S100B is the most studied of the calgranulins, predominantly expressed in brain tissue by astrocytes at levels greater than any other cell type (Santamaria-Kisiel *et al.*, 2006; Donato, 2001). Of all the S100 family, S100B is the only member with an encoding gene located on chromosome 21 (Donato, 2001). The prevalence of S100B in down-syndrome (chromosome 21 trisomy), and a number of neurodegenerative disorders has promoted the hypotheses that S100B-RAGE plays either a neuro-protective role or contributes to neurological pathogenesis. It is known that outcomes of S100B/RAGE interaction are ligand and RAGE concentration dependent. The duality of S100B activity being both neurotrophic and degenerative is apparent at concentrations above 500nM, which promotes neuronal apoptosis (Donato, 2001; Donato, 2007). Low concentrations of both RAGE and S100B inhibit neuronal apoptosis by up-regulating Bcl-2 through the Ras-MEK (MAP-k)-ERK 1/2 pathway (Donato, 2001; Van Eldik and Wainwright, 2003). Exposure of neurons to low-levels of S100B is similarly prophylactic. Subsequent exposure of these cells to high concentrations of S100B or β-amyloid greatly reduces toxicity, likely due to pre-activation of Bcl-2 (Huttunen *et al.*, 2000). The principle effect of persistent high S100B levels on neuronal cells is the over-production of RAGE, and an exaggerated inflammatory response facilitated by ROS, phosphoinositide 3-kinase (PI3K), and NF-κB activation mediated by RAGE (Schafer *et al.*, 1995). The dependency

of S100B on RAGE signal transduction is evident in neurons expressing cytosolic tail deleted RAGE (RAGEΔcyto). These cells show no apparent toxicity to high levels of S100B, while low levels do not trigger normal homeostatic outcomes such as neurite outgrowth (Huttunen *et al.*, 2000). Collectively, these findings support roles for S100B-RAGE mediated cellular outcomes in the development of central nervous tissue and early response to brain injury. Extended and excessive accumulation of S100B, like other RAGE ligands, tends to lead to cellular dysfunction through an exaggerated inflammatory response and ROS production (Hunter and Chazin, 1998; Huttunen *et al.*, 2000; Schafer *et al.*, 1995; Hofmann *et al.*, 1999; Xie *et al.*, 2013; Adami *et al.*, 2004).

The specific cellular outcomes of calgranulins, and the involvement of RAGE in the transduction of intracellular signals is extremely complex. In brief, S100A4 has been clearly shown to progress tumour metastasis and articular pathophysiology as seen in the tumour-like behaviour of rheumatoid arthritis synovium (Shaw *et al.*, 2003; Helfman *et al.*, 2005; Senolt *et al.*, 2006). S100A6 similarly plays a role in tumour development through direct ligation with the tetramerization domain (residues 325-355) of p53, and neuronal apoptosis in a RAGE dependent manner (Leclerc *et al.*, 2007; van Dieck *et al.*, 2009; Gross *et al.*, 2014). S100A8 and A9 are often referred to as neutrophil cytosolic proteins due to their prevalence in neutrophils, monocytes/macrophages, activated glial cells and their roll in leukocyte adhesion and migration (McCormick *et al.*, 2005; Donato, 2007; Ibrahim *et al.*, 2013). Like S100B, S100A8 and A9 are secreted from leukocytes at sites of inflammation in response to proinflammatory stimuli (such as endotoxin), through a positive feedback mechanism involving RAGE and heparan sulphate proteoglycans (Donato, 2007; Ibrahim *et al.*, 2013). These calgranulins are, therefore, often associated with chronic inflammatory disorders such as diabetes and tumour metastasis, making them accurate blood-born markers of ongoing inflammation (Foell *et al.*, 2007). S100A8/A9 heterodimers promote a number of physiological changes in homeostasis that generally increase vascular permeability, platelet aggregation and the recruitment of leukocytes (Roth *et al.*, 2003; Leclerc *et al.*, 2009). NF-κB activation similarly follows S100A8/A9 up regulation, resulting in gene transcription of pro-inflammatory cytokines and cell adhesion receptors such as VCAM (Roth *et al.*, 2003; Donato, 2007; Xu *et al.*, 2012). S100A12 is predominantly expressed in granulocytes and keratinocytes, exerting physiological outcomes such as leukocyte activation and infiltration at sites of inflammation (Roth *et al.*, 2003; Donato, 2007). RAGE mediates S100A12 activity through NF-κB activation, particular in monocytes and endothelium

following exposure to TNF-α and endotoxin (van Zoelen *et al.*, 2011; Wittkowski *et al.*, 2007). These stimuli promote S100A12 expression as seen in synovial fluid of rheumatoid arthritis patients (Chen *et al.*, 2009b). As with S100A8/A9 proteins, RAGE is unlikely the sole receptor mediating S100A12 biological outcomes, with S100A12 activating mast cells not expressing RAGE (Yang *et al.*, 2007).

The S100 family of molecules represents an extremely complex array of molecules with autocrine and paracrine effects on neurons, microglia, astrocytes, monocytes, endothelial cells, vascular smooth muscle cells and numerous tumour cells (Donato, 2007; Bianchi *et al.*, 2007; Ponath *et al.*, 2007; Reeves *et al.*, 1994; Xie *et al.*, 2013; Leclerc *et al.*, 2009). RAGE is clearly a mediator in a number of these cell types for some, but not all calgranulins. This role is central in a number of pathologies involving pro-inflammatory responses, and represents a novel opportunity for intervention in a number of diseases. A greater understanding of the nature of interaction between RAGE and calgranulins is, however, required to realise this ambition.

1.3.4 High-mobility group box chromosomal protein 1

High-Mobility Group - 1 Box Proteins (HMGB1) are a family of essential, multi-functional, non-histone proteins that bind to DNA in a sequence independent manner (Bianchi *et al.*, 2007). Within the HMG set of molecules are sub-groups defined by common functional motifs: HMG-1/2 (HMG box), HMG-14/17 (nucleosome binding domain) and HMG-I/Y (AT-hook) (Hassid *et al.*, 2009). Despite these distinguishing characteristics, all members of the HMG family possess an overarching ability to modify the conformation of DNA, enhancing the efficiency of gene transcription and chromatin plasticity (Hassid *et al.*, 2009). The ability of these molecules to interact with DNA is mediated by two homologous HMG box domains made up of α-helical secondary structures (Read *et al.*, 1993). The original name, amphoterin, reflects the dipolar contiguous arrangement of a basic 185 amino acid domain with a 30 residue anionic region (Hsin *et al.*, 2010).

The role of this family of proteins first identified in the 1970's, was believed to be limited to intra-nuclear functions including gene transcription, replication, repair, and nucleosome stabilization (Kokkola *et al.*, 2005; Fiuza *et al.*, 2003). Recently, however, a number of extracellular roles have been identified for HMGB1. These involve pro-inflammatory responses, central nervous system development, mediation of endotoxicity and modulation of haemostasis and thrombosis (Kokkola *et al.*, 2005; Fiuza *et al.*, 2003; Huttunen *et al.*, 2002; Tanoue and Nishida, 2002; Hassid *et al.*, 2009).

It is known that B16 melanoma, neuroblastoma and immune cells such as monocytes secrete HMGB1 in response to early pro-inflammatory signals including lipopolysaccharide (LPS), TNF-α and interleukin 1 (IL-1) (Kay *et al.*, 2009; Hsin *et al.*, 2010). Normal cytokine secretion occurs through classical endoplasmic reticulum-Golgi exocytosis, in which protein trafficking is determined by a leader sequence (Yamana *et al.*, 2006). Despite functional similarities to cytokines, HMGB1 is exuded into the extracellular milieu by a non-classical, Ca^{2+} -regulated secretory lysosome pathway (Gardella *et al.*, 2002). This process requires a stimulatory element such as LPS, phorbol myristoyl acetate (PMA), TNF-α or IL-1, activation of protein kinase C (PKC), and the bioactive lipid lysophosphatidylcholine (LPC) (Gardella *et al.*, 2002; Wang *et al.*, 1999; Hsin *et al.*, 2010). In the presence of these stimuli, nuclear HMGB1 molecules relocalise to cytoplasmic organelles such as the endolysosomal compartment before undergoing vesicle-facilitated exocytosis (Gardella *et al.*, 2002). Although the majority of circulating HMGB1 relies on this ordered secretory pathway, a small proportion is released from necrotic cells (Kokkola *et al.*, 2005; Stephenson *et al.*, 2010). As with a number of pro-inflammatory molecules, HMGB1 imparts a positive influence at nontoxic levels, recruiting macrophages to sites of injury and promoting monocyte tissue infiltration and senescence (Valencia *et al.*, 2004; Stephenson *et al.*, 2010).

Elevated levels of circulating HMGB1 are a late-stage marker of endotoxicity, immediately followed by increased TNF-α and IL-1 expression (Wang *et al.*, 1999). Inhibitors of both TNF-α and IL-1 have little impact on endotoxicity survival in mice (Wang *et al.*, 1999). Double negative mice for these cytokines, however, demonstrate significant increases in endotoxemic tolerance (Wang *et al.*, 1999). This clinical paradox is explained by the observation that rapid release of TNF-α and IL-1 promotes late-stage secretion of HMGB1 and associated symptoms of endotoxicity (Wang *et al.*, 1999). This is supported by the observation that injection of recombinant HMGB1 into double negative TNF-α and IL-1 mice induces endotoxemia with 60% mortality (Wang *et al.*, 1999).

The pluripotent outcomes of HMGB1 are known to be, in part, mediated by the ligation of HMGB1 with RAGE (Hori *et al.*, 1995; Huttunen *et al.*, 2002; Huttunen *et al.*, 2000; Taguchi *et al.*, 2000; Xie *et al.*, 2013; Ibrahim *et al.*, 2013). The ability of HMGB1 to bind RAGE in a saturable, dose-dependent manner was first reported in 1995, with an estimated K_D of approximately 6-10 nM (Hori *et al.*, 1995). Since this time, a number of groups have reported estimates of binding that range from $K_D \approx$ 90-700 nM (Liu *et al.*,

2009; Ling *et al.*, 2011). The region of HMGB1 interacting with RAGE is refined to amino acids 150-183 that constitute part of a COOH-terminal motif (Huttunen *et al.*, 2002; Hsin *et al.*, 2010). Interestingly, this region of HMGB1 shares sequence similarity with residues 3-39 of S100A12 that constitute the calgranulin EF-hand motif (Huttunen *et al.*, 2002). In endothelial cells, RAGE activation by HMGB1 results in a cell adhesion phenotype characterised by increased expression of intercellular (ICAM) and vascular cell adhesion molecules (VCAM), and activation of β1 and β2 integrins (Patel *et al.*, 2010; Fiuza *et al.*, 2003). Prolonged activation in both endothelia and monocytes results in the secretion of interleukin-8 (IL-8), monocyte chemo attractant protein-1 (MCP-1), TNF-α secretion, RAGE up-regulation and the production of fibrinolysis modulators (Fiuza *et al.*, 2003; Ibrahim *et al.*, 2013; Xie *et al.*, 2013). Activation of these pro-inflammatory elements clearly defines HMGB1 as an agonist of diseases exacerbated by chronic inflammation.

Co-localization of RAGE with HMGB1 in developing rat brain, suggests a homeostatic role for RAGE distinct from chronic disease (Huttunen *et al.*, 2000). Tissue surveys confirmed the expression of RAGE during mammalian development, in particular in the central nervous system (Hori *et al.*, 1995; Brett *et al.*, 1993). HMGB1 coated culture flasks promote neurite outgrowth of cultured rat cortical neurons, with the presence of sRAGE or anti-RAGE antibodies reversibly inhibiting neuronal development (Huttunen *et al.*, 1999; Hori *et al.*, 1995). Cell motility is also in part, influenced by RAGE-HMGB1. A study utilising neuroblastoma cells transfected with a cytosolic domain deleted RAGE (DN-RAGE) construct observed a complete loss of cell migration, otherwise apparent with wild type RAGE (Huttunen and Rauvala, 2004). This observation clearly supports a role for HMGB1-RAGE in cytoskeletal reorganisation affecting cellular outgrowth, cytokinesis and cellular differentiation.

RAGE is clearly involved in mediating HMGB1 physiological outcomes. However, a number of alternative cell surface receptors exist for HMG proteins, including syndecan-1, toll-like receptors (TL2 and TL4), receptor-type tyrosine phosphatise β/ζ, and sulfoglucuronyl carbohydrates on some cell surface adhesion molecules (Salmivirta *et al.*, 1992; Chou *et al.*, 2004; Park *et al.*, 2004b). It is clear that activation of RAGE by HMGB1 in neuronal, tumour, endothelial and leukocyte cells, ultimately leads to the activation of transcription factors NF-κB, Sp1 and cAMP response element binding (CREB) (Huttunen *et al.*, 1999; Taguchi *et al.*, 2000; Fiuza *et al.*, 2003; Rauvala and Rouhiainen, 2007; Urbonaviciute *et al.*, 2008).

The interplay between HMGB1 and RAGE is a significant and complex factor in both disease and health. The myriad of intracellular signalling pathways by which HMGB1-RAGE facilitates these physiological opposites, still requires significant investigation.

1.4 RAGE Intracellular Signalling Pathways

Intracellular signalling is one of the most complex areas of molecular biology investigation. The intrinsic cross-talk, redundancy, subtle mechanisms of regulation/activation and rate of molecular action persistently hamper efforts to understand the inner world of cells.

RAGE is known to mediate multiple, parallel signalling cascades through its cytosolic domain (Hofmann *et al.*, 1999; Taguchi *et al.*, 2000). These cascades have roles in both homeostasis and a number of chronic disease states. RAGE signalling pathways are complex and influenced by cell type, ligand, receptor isoform and oligomeric state, pathophysiology, multigenetic factors and developmental maturity (Kalea *et al.*, 2009b; Ramasamy *et al.*, 2009; Yan *et al.*, 2009; Ishihara *et al.*, 2003). They can, however be described in relation to three general cellular outcomes: actin/myosin cytoskeletal regulation, pro-inflammatory outcomes, and regulation of gene expression.

1.4.1 Cytoskeletal regulation

Regulation of cellular cytoskeletal elements including actin microfilaments, microtubules and myosin motor proteins facilitate cytokinesis, cell adhesion, extension, and motility (Cho and Klemke, 2000; Huttunen *et al.*, 2000; Huttunen and Rauvala, 2004). Cancer cell lines such as N18 neuroblastoma, C6 glioma and glioblastoma are increasingly invasive when RAGE is activated by ligand (Taguchi *et al.*, 2000; Huttunen *et al.*, 2002; Yamana *et al.*, 2006; Bassi *et al.*, 2008). Similarly, homeostatic cells such as neuronal, endothelial and smooth muscle cells exhibit cytoskeletal reorganisation events such as neurite outgrowth, cell spreading and regulated cell adhesion following the interaction of AGE, S100 and HMGB1 with RAGE (Huttunen *et al.*, 1999; Higashi *et al.*, 1997; Christiansen *et al.*, 2009; Leclerc *et al.*, 2007; Rauvala and Rouhiainen, 2010). Inflammatory immune cells such as dendritic cells, monocytes, macrophages, neutrophils and leukocytes all undergo chemotaxis, homing and adhesion to foci of inflammation in response to RAGE-ligand binding (Kokkola *et al.*, 2005; Orlova *et al.*, 2007; Rouleau *et al.*, 2003).

Common to these studies is the observation that inhibiting RAGE-ligand association, cell division cycle 42 (cdc42) or Ras-related C3 botulinum toxin substrate-1 (Rac1) antagonises actomyosin mediated cell behaviours (Huttunen *et al.*, 1999; Hori *et al.*, 1995; Taguchi *et al.*, 2000; Bianchi *et al.*, 2007; Hudson *et al.*, 2008b; Ramasamy *et al.*, 2009). Collectively, these observations support the conclusion that RAGE activates Rac1 and Cdc42 members of the Rho family of small GTPase molecules classically involved in cell adhesion, motility and migration (Figure 6) (Huveneers and Danen, 2009). RhoA directly regulates stress fibres and filamentous actin (f-actin) contraction essential for cell adhesion and spreading (DeMali and Burridge, 2003). Cdc42 and Rac1 generally promote membrane extension and filamentous actin growth. Appropriately, RhoA and Rac1 inhibit each other when active, allowing only one to be functional in the presence of the other. Cdc42 and Rac1 are both required for motility through the recruitment of wiskott-aldrich syndrome protein (WASP) and WASP family verproline-homologous protein (WAVE) respectively (Huveneers and Danen, 2009). In combination, these proteins recruit actin related protein 2/3 (Arp 2/3) that facilitates actin growth (DeMali and Burridge, 2003).

Integrins in collaboration with Src-family kinases, oversee the activity of Rho-GTPases through regulation of guanine-exchange factors (GEFs) and GTPase-activating proteins (GAPs). GEF and GAP are essential in controlling the active conformation of Rho-GTPases by acting as GTP exchange factors (Marignani and Carpenter, 2001). Integrin control of Rac1 and cdc42 was observed in HMGB1-RAGE dependent neutrophil recruitment involving the β2 integrin Mac-1 (Orlova *et al.*, 2007). In this study, HMGB1 induced motility in neutrophils and adhesion in leukocytes in a RAGE dependent manner (Orlova *et al.*, 2007). Crosstalk between growth factor/cell adhesion and integrin/Rho-GTPase signalling pathways facilitates cell-cell adhesion and spreading through Rac1 (Wildenberg *et al.*, 2006). This may explain how RAGE-HMGB1 stimulates migration in one cell type and an adhesion phenotype in another. If the cell, such as endothelia, express high levels of epidermal growth factor receptor (EGFR) or inter-cellular adhesion, cross-talk with the integrin-Rac1 pathway will promote cell spreading and adhesion (Wildenberg *et al.*, 2006; Huveneers and Danen, 2009). Ligation of integrins such as Mac-1, promotes Src phosphorylation and activation of unengaged EGFR (Huveneers and Danen, 2009). EGFR consequently recruits PI3K which mediates activation of Vav2-Rac1-PAK, reducing Arp2/3 levels and promoting cell adhesion/spreading (Figure 6) (Huveneers and Danen, 2009).

PI3K is involved in RAGE-AGE induced cell adhesion (Toure *et al.*, 2008). Inhibition of PI3K following RAGE activation retards cell adhesion and restores cell motility (Toure *et al.*, 2008). In the absence of growth and adhesion cell surface molecules, migration occurs in response to the classic Cdc42-Rac1-Arp2/3 pathway. Src-family of kinases (SFK) and caveolin-1 play a role in S100B-RAGE smooth muscle cell initiated cell motility (Reddy *et al.*, 2006). It has been reported that inhibition of SFK, RAGE or caveolin-1 in smooth muscle cells (SMCs), suppresses cell motility (Reddy *et al.*, 2006). Directional cell migration requires cell polarisation. This manifests in sub-cellular compartmentalisation of Rho-GTPases whereby the rear of the cell contracts towards the migrating front of the cell in unison with extension of lamellipodia at the front of the cell in the direction of migration. Contraction is controlled by RhoA, while extension and cell direction is controlled by Cdc42-Rac1. Activation of Rho GTPases is influenced by SFK-mediated phosphorylation of GAF and GEF intermediates (Huveneers and Danen, 2009). The blockade of SFK in SMC could, therefore, retard cell migration by inhibiting either contraction, extension or both. Caveolin-1 is essential for endosomal recycling and sorting of SFKs and integrins (Huveneers and Danen, 2009). Disruption of this process through caveolin-1 inhibition, ultimately derails RhoA/Cdc42-Rac1 directional chemotaxis in SMC through a loss of SFK activity (Huveneers and Danen, 2009).

Diaphanous-1 is an effector of RhoA activity and was recently identified as a RAGE intracellular ligand (Hudson *et al.*, 2008b). In response to RhoA activation, Dia1 activates Cdc42 at the front of migrating cells along with other intermediates, to promote actin extension and Rac1 activation (Hudson *et al.*, 2008b; Huveneers and Danen, 2009). Interestingly, Hudson *et al.,* observed Rac1 activation following Dia-1 recruitment by RAGE in C6 glioma cells (Hudson *et al.*, 2008b). It may be that RAGE-Dia-1 usurps RhoA-Dia1 regulation of Cdc42/Rac1 and encourages cell motility.

ERK 1 and 2 bind to the RAGE cytosolic domain (Ishihara *et al.*, 2003). It is not known how these members of the MAP kinase family influence cell motility or adhesion. However, ERK in concert with paxillin and myosin light chain kinase (MLCK), increase Rac1-GTP and cdc42-GTP levels at the front of migrating cells, inevitably promoting taxis (Huveneers and Danen, 2009). Alternatively, cytosolic ERK may be activated by Rac-PAK-MEK to promote cell adhesion and spreading (Figure 6). Clarification of the role that ERK plays in cytoskeletal regulation, as discrete from cell survival, is therefore needed.

Interestingly, the HMGB1 receptor syndecan 4, interacts with PKC to facilitate the formation of a Ras-GAP-Rho-GAP complex that inhibits RhoA activation (Huveneers and Danen, 2009). Bianchi *et al*. (2007) reported Ras activation following RAGE-S100B ligation, accompanied by membrane extension (Bianchi *et al.*, 2007). Whether syndecan activation by HMGB1 accounts for the observations of Bianchi *et al.* (2007), or are a result of RAGE activity, still requires further investigation to define the reported role of Ras.

Together, these various complex pathways hypothetically demonstrate how ERK1/2, integrins, Ras, Rac1, cdc42, RhoA and Dia-1 may interact to promote cell adhesion, membrane extension and chemotaxis. Significant experimentation is required to delineate direct outcomes of RAGE activation from those mediated by cross-talk with growth factors and adhesion molecule intracellular cascades.

1.4.1 Pro-inflammatory signalling and gene expression

One of the most significant outcomes of RAGE ligation in disease is the activation of pro-inflammatory signalling pathways and regulation of gene expression. RAGE mediated inflammatory outcomes depend on ligand, cell type, RAGE isoforms, existing pathophysiology, and multigenetic factors.

The first intracellular signalling molecules shown to directly interact with RAGE were extracellular regulated kinases 1 and 2 (ERK 1/2) (Ishihara *et al.*, 2003). ERK is activated in a number of scenarios primarily involving cell proliferation and apoptosis. It is suggested that ERK promotes these antipodal roles through sub-cellular localization (Mebratu and Tesfaigzi, 2009). RAGE activation and subsequent ERK binding is associated with cell death and tumour progression in neuronal and C6 glial cell lines (Chong *et al.*, 2006; Taguchi *et al.*, 2000). RAGE localization of ERK to the cytosolic compartment encourages

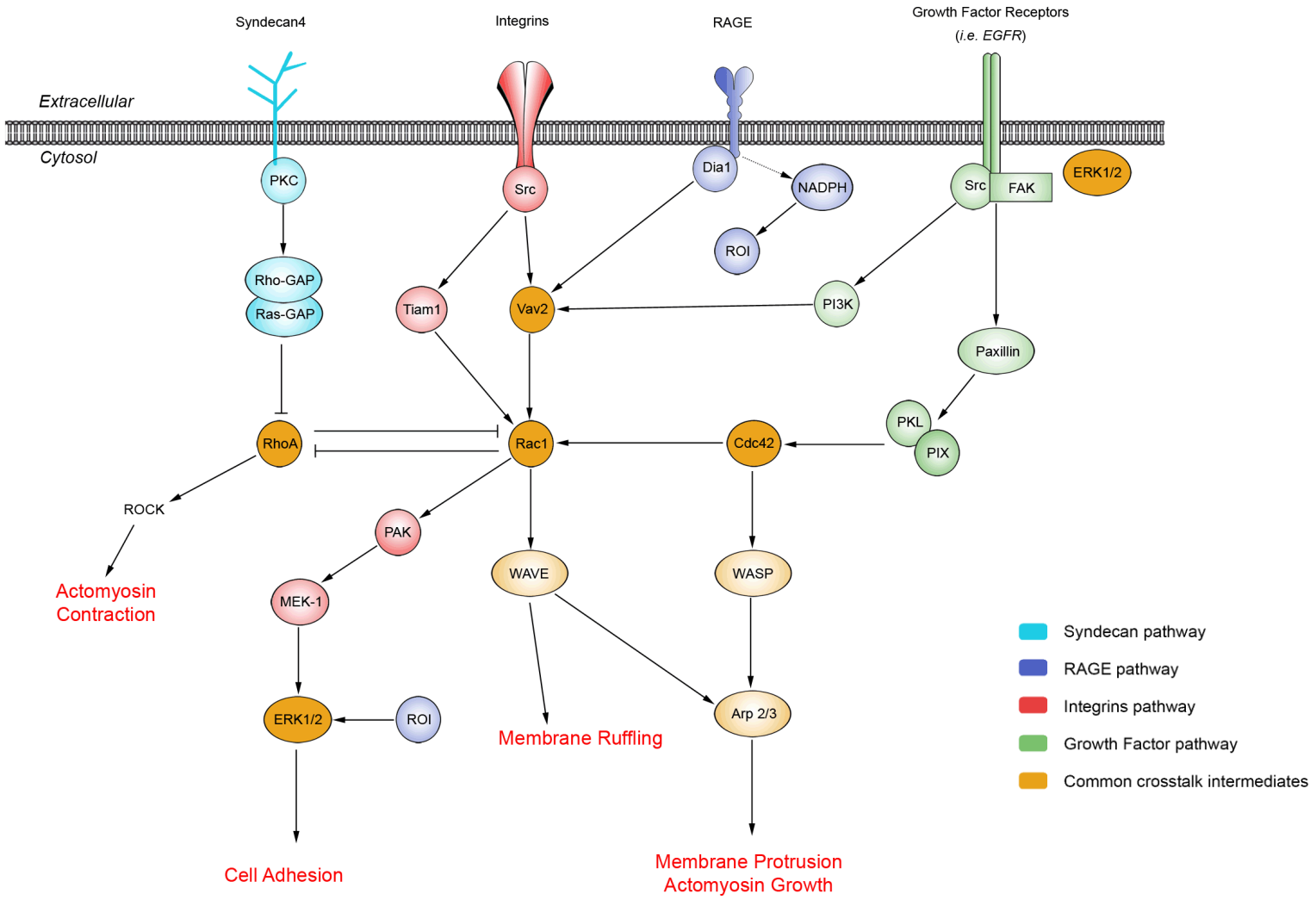

Figure 6. Proposed cytoskeletal cell signalling pathways following RAGE activation. Cytoskeletal regulation pathways involving reported RAGE-dependent signalling intermediates (Cho and Klemke, 2000; Hudson *et al.*, 2008b; Reddy *et al.*, 2006; Toure *et al.*, 2008; Wildenberg *et al.*, 2006; DeMali and Burridge, 2003; Orlova *et al.*, 2007; Taguchi *et al.*, 2000; Rauvala and Rouhiainen, 2010)

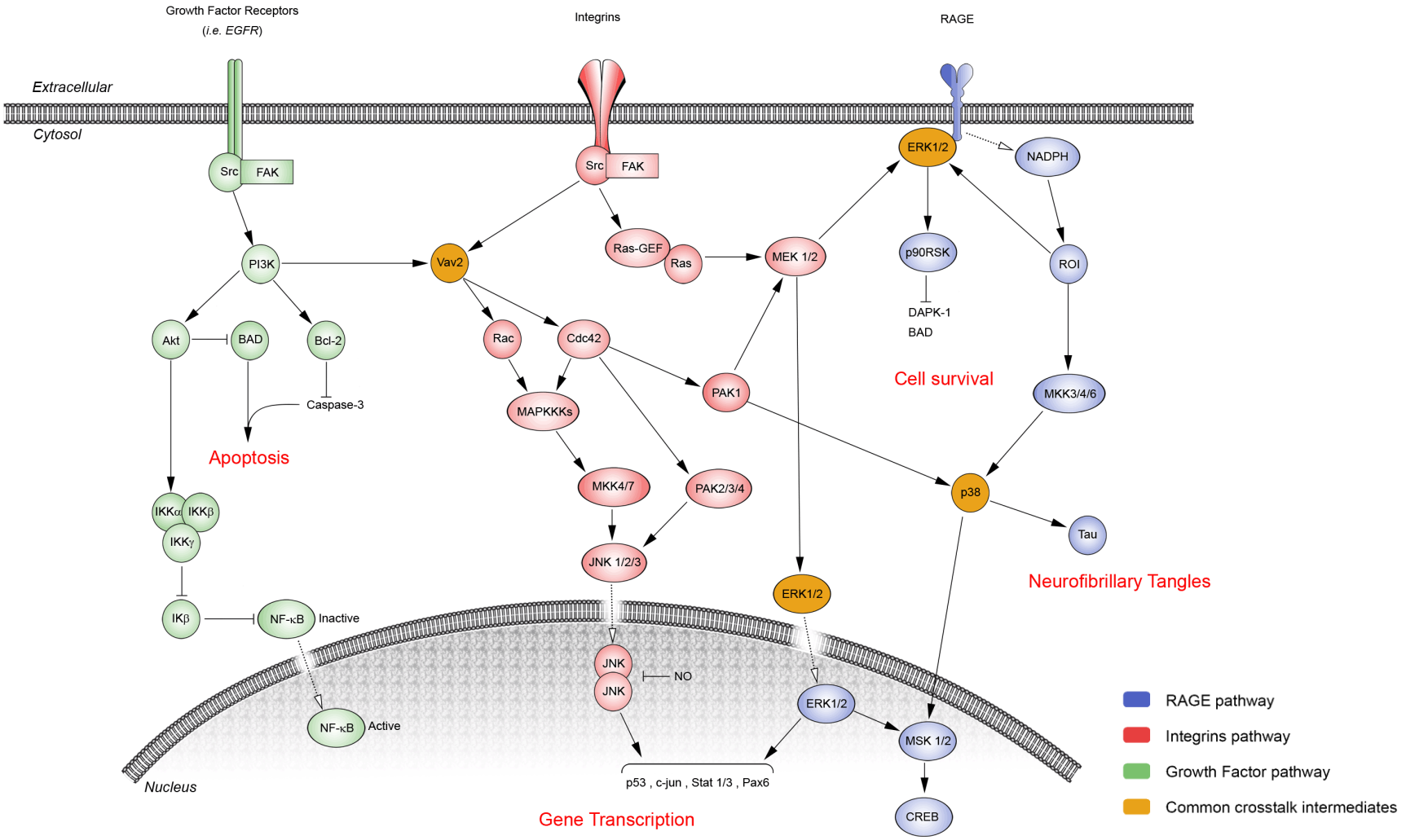

Figure 7. Proposed inflammatory and gene expression signalling pathways associated with RAGE. (Ishihara *et al.*, 2003; Mebratu and Tesfaigzi, 2009; Chong *et al.*, 2006; Xie *et al.*, 2013; Warboys *et al.*, 2009; Nitti *et al.*, 2007; Dukic-Stefanovic *et al.*, 2003; Balleza-Tapia and Pena, 2009; Wautier *et al.*, 1994; Bianchi *et al.*, 2007; Ding and Keller, 2005; Leclerc *et al.*, 2007).

activation of death-associated protein kinase 1 (DAPK-1), a proapoptotic protein, and the formation of tropomyosin-1, which is essential in stress fibre formation (Xie *et al.*, 2013; Houle *et al.*, 2007; Mebratu and Tesfaigzi, 2009). In these scenarios, ERK is commonly activated by oxidative stress. Interestingly, RAGE activation is associated with phospholipase C-mediated activation of Ca^{2+}-dependent PKC, leading to NADPH oxidase production of reactive oxygen species (ROS) (Warboys *et al.*, 2009; Xie *et al.*, 2013; Guo *et al.*, 2008). Increased PKC-NADPH-ERK activity is associated with cell death and altered gene expression following exposure to RAGE ligands such as AGES (Chong *et al.*, 2006; Nitti *et al.*, 2007; Ding *et al.*, 2007; Wautier *et al.*, 2001). Additionally, PI3K/MEK1/2 induces ERK1/2 activation and nitric oxide production in mouse microglia cells following AGE-RAGE binding (Dukic-Stefanovic *et al.*, 2003). These sources of reactive oxygen intermediates (ROI) and localisation of ERK to the cytosolic compartment support the hypothesis that RAGE may mediate apoptosis through RAGE bound, ROI activated ERK1/2.

Interestingly, Aβ1-42 oligomer-RAGE engagement in rat brain leads to ERK 1/2-caspase-3 dependent proteolytic cleavage of Tau (Chong *et al.*, 2006). Inhibition of ERK significantly reduces Aβ toxicity in rats, confirming an association between neurodegenerative pathology and RAGE-ERK signalling (Chong *et al.*, 2006; Balleza-Tapia and Pena, 2009). Currently, the factors determining whether a cell undergoes apoptosis in place of an altered motile/adhesive phenotype are unknown. However, it is known that ligand type and concentration, cell type and intracellular crosstalk, along with RAGE oligomeric state likely influence the outcome (Bianchi *et al.*, 2007; Donato, 2007; Leclerc *et al.*, 2007; Ishihara *et al.*, 2003; Xie *et al.*, 2013; Ibrahim *et al.*, 2013). It is possible that Dia1 competes with ERK for the RAGE cytosolic domain, displacing ERK1/2 which allows it to undergo nuclear translocation. Therefore, those cells with high levels of cytosolic Dia1 such as motile cells, innately promote nucleated ERK1/2 gene transcription that favours cell survival. This proposed interplay correlates with the observed compartmental regulation of ERK mediated biological outcomes (Mebratu and Tesfaigzi, 2009). Although there are studies to support this hypothesis, there are also others in disagreement (Wautier *et al.*, 1994; Hudson *et al.*, 2008b; Wautier *et al.*, 2001; Huttunen *et al.*, 2000). A broad study to control for elements such as activating ligand, RAGE isoform and cell type, and regulation of signalling crosstalk is required to evaluate this hypothesis.

Protein kinase B, commonly known as Akt, is a serine/threonine kinase that plays a critical regulatory role in glucose metabolism, cell survival, angiogenesis and tumour progression (Los *et al.*, 2009). At low levels of S100B exposure (<500 nM), the PI3K-Akt pathways promotes cell survival through phosphorylation of bcl-2 family member BAD (Donato, 2007; Huttunen *et al.*, 2000). Activation of p53 and NF-κB transcription factors by Akt also assists in expression of cell growth and survival factors. Alternately, AGE-RAGE engagement decreases levels of Akt activity in endothelial progenitor cells, leading to increased cell apoptosis mediated by dephosphorylated BAD-Caspase-3 (Chen *et al.*, 2009a). This has similarly been observed in neuronal cells exposed to micromolar concentrations of S100B (Donato, 2007).

S100B, S100A12 and AGEs induce expression of pro-inflammatory cyclooxygenase-2 (COX-2) in human monocytic leukemic cells and peripheral blood monocytes (Shanmugam *et al.*, 2003). COX-2 encourages pro-inflammatory outcomes in a number of diseases through its effector prostaglandin E2. In studies where RAGE mediates COX-2 activation, inflammatory outcomes have been abated through inhibition of RAGE, ROS, PKC, ERK and p38 MAPK (Shanmugam *et al.*, 2003; Nah *et al.*, 2008). This suggests that significant interplay or redundancy exists amongst these intracellular intermediates in what is likely a multi-faceted cellular response, as seen in Rho GTPase signalling.

Signal transduction by RAGE initiates stress activated protein kinase (SAPK), c-jun N-terminal kinase (JNK), janus kinase (JAK) and transcription factor signal transducer and activator of transcription (STAT) (Taguchi *et al.*, 2000; Shanmugam *et al.*, 2003; Reddy *et al.*, 2006; Xie *et al.*, 2013). The common themes of these intracellular signalling intermediates are oxidative stress and activation of gene transcription factors NF-κB, CREB, Sp-1 and STAT. Of those genes up-regulated, a number are pro-inflammatory cytokines. Generally, RAGE activation is associated with increased expression of various RAGE isoforms, early growth response-1, VCAM, matrix metalloproteases (MMP), ICAM-1, tumour necrosis factor – α (TNF-α), interleukins 1β, 2 and 6, and macrophage colony stimulating factor (M-CSF), to name only a few (Yan *et al.*, 2009; Yang *et al.*, 2007; Nakamura *et al.*, 2008; Hofmann *et al.*, 2002; Zhang *et al.*, 1990; Hofmann *et al.*, 1999; Taguchi *et al.*, 2000; Xie *et al.*, 2013). These molecules generally facilitate a positive feed-back mechanism in which RAGE ligands such as calgranulins and HMGB1 are expressed, further activating RAGE and promoting chronic inflammation.

Clearly, RAGE signalling promotes inflammation through the activation of classic MAPK pathways, the production of reactive oxygen intermediates (ROI), and localised expression of pro-inflammatory molecules. Untangling the complex interplay between pathways in differing cell types and contexts requires significant clarification and standardisation of methods to allow accurate comparisons. Furthermore, the presence of different RAGE isoforms, ligand type and concentration, cell phenotypes, existing inflammatory responses and cellular dysfunction, make it difficult to correlate RAGE activation with signalling events and biological outcomes. Controlling for such factors would help elucidate direct RAGE cellular outcomes, as opposed to those influenced by crosstalk with various intracellular cascades.

1.5 Pathophysiologies Associated with RAGE

There is an enormous body of research linking RAGE to a myriad of pathophysiologies including Alzheimer's disease, diabetic complications (such as macrovascular disease), kidney disease, rheumatoid arthritis, tumour outgrowth and migration, and inflammatory diseases (Matrone *et al.*, 2014; Zhao *et al.*, 2014; Gugliucci and Menini, 2014; Alghasham and Rasheed, 2014; Salahuddin *et al.*, 2014). Of particular interest are a number of RAGE blockade studies utilizing sRAGE and RAGE-V domain antibodies as antagonists. These studies utilized a variety of mouse disease models representing diabetic atherosclerosis, inflammatory responses and tumour outgrowth.

1.5.1 Atherosclerosis

Atherosclerosis is a chronic disease, with cardiovascular mortality in diabetic's 2-4 fold higher than recorded in the normal population (Mullarkey *et al.*, 1990; Yan *et al.*, 1994). The interaction between arterial wall low-density lipoproteins (LDL), hyperglycaemia, and hyperinsulinaemia in the formation and progression of atherosclerotic lesions is well established (Mullarkey *et al.*, 1990; Wilson *et al.*, 1985). Oxidatively modified LDL (oxLDL), as opposed to normal LDL, interact with aortic endothelium promoting recruitment of monocytes to sites of oxLDL accumulation (Quinn *et al.*, 1987; Mullarkey *et al.*, 1990). Endocytosis of oxLDL by monocytes transforms them into foam cells commonly associated with atherosclerotic lesions (Quinn *et al.*, 1987; Sparrow *et al.*, 1989).

The formation of vascular abnormalities is in part mediated by smooth muscle and endothelial cells. Expression of various inflammatory and thrombogenic effectors occurs in response to a number of factors including oxidative stress, histamine production, cytokines and blood flow (Hogan *et al.*, 1992; Esposito *et al.*, 1989). An early sign of atherogenesis is the proliferation of smooth muscle cells (Ross, 1986). This mitogenic process is normally regulated by endothelial nitric oxide (NO) mediated quiescence of smooth muscle cells via the guanylate cyclase pathway. Bucala *et al*. (1991) identified a mechanism by which AGE molecules directly interact with and quench nitric oxide *in vitro*. Subsequent studies in rats with AGE accumulation and hyperglycaemia identified an impaired NO response despite normalizing blood glucose and ketone levels (Bucala *et al.*, 1991).

The development of atherosclerotic plaques extends past the common risk factors of dyslipidaemia, hypertension and obesity, to a more specific cellular regulatory element. RAGE was identified as a cell surface receptor in smooth muscle and endothelial cells that promotes the formation of atherosclerotic lesions in heart and aortic tissue following ligation (Daffu *et al.*, 2013; Park *et al.*, 1998; Basta, 2008). A number of RAGE ligands accumulate in vascular lesions, including AGEs, calgranulins and HMGB1 where they induce a pro-inflammatory response (Burke *et al.*, 2004; Inoue *et al.*, 2007; Oimomi *et al.*, 1989). Administration of 40μg/day of sRAGE as a ligand decoy to streptozotocin-induced diabetic mice, reduces the formation and size of lesions to levels seen in non-diabetic mice (Park *et al.*, 1998). This observation clearly implicates RAGE activation in cellular dysfunction associated with lesion development.

Our understanding of RAGE and its role in atherosclerosis and vasculopathies is now better understood. The clarification of RAGE as a significant progressor of atherosclerosis makes it an excellent target for pharmaceutical intervention. By impeding RAGE activation in diabetics and those at risk, significant reductions in cardiovascular mortality may be realised.

1.5.2 Inflammation

Inflammation is a multifaceted physiological response resulting from, and accompanying the “pure” immune response (Stites, 1997). A number of diseases exhibit inflammatory symptoms as a key indicator of progression including colitis, arthritis, sepsis, and delayed type hypersensitivity (DTH) (Hofmann *et al.*, 1999; Foell *et al.*, 2007; Chen *et al.*, 2009b; Chuah *et al.*, 2013; Nogueira-Machado and de Oliveira Volpe, 2012).

Using a CF-1 mouse model, Hofmann *et al*. (1999) observed a DTH response following re-challenge with methylated BSA three weeks after initial exposure (Hofmann *et al.*, 1999). This response was characterised by an influx of inflammatory immune cells, development of localised oedema, erythema, and granuloma (Hofmann *et al.*, 1999). Closer examination of tissue at the nidus of injury revealed a six-fold increase in NF-κB activity associated with pro-inflammatory gene expression (Hofmann *et al.*, 1999). Disruption of S100A12 activation of RAGE in this model reduced NF-κB activation by 70%, clearly implicating RAGE in the pathology of DTH (Hofmann *et al.*, 1999).

The progression of colitis is associated with an accumulation of S100 and AGE RAGE ligands that are indicative of the degree of inflammation (Clynes *et al.*, 2007; Foell *et al.*, 2007). The principle outcome of ligand-RAGE interaction in colitis also involves the activation of NF-κB. Recent studies have similarly implicated HMGB1 in the development of colitis and associated colorectal carcinomas in a RAGE-dependent manner (Maeda *et al.*, 2007; Clynes *et al.*, 2007). Inhibition of p38 or the application of sRAGE as a ligand decoy in a mouse model of colitis reduces active NF-κB levels and inflammation (Andrassy *et al.*, 2006).

As previously mentioned, the occurrence of the Gly82Ser RAGE SNP is observed in disequilibrium with the HLA-DR4 locus implicated in hereditary rheumatoid arthritis (RA). Canonical RAGE activation by HMGB1, S100s and various AGEs is a key factor in the progression of rheumatoid arthritis (Rouleau *et al.*, 2003; Chen *et al.*, 2009b; Chen *et al.*, 2013). Serum amyloid A promotes NF-κB activation in fibroblast-like synovial cells that invade rheumatoid arthritic joints, where they promote inflammation (Okamoto *et al.*, 2008). Inhibition of RAGE-SAA interaction reduces NF-κB mediated expression of pro-inflammatory molecules, reducing invasiveness of immune cells to the site or injury that is linked to RA (Okamoto *et al.*, 2008)

Clearly, RAGE activation following ligation promotes inflammation in a number of pathologies. Although various intermediate signalling molecules involved in propagating the inflammatory cascade are known (Section 1.4.1), clear delineation of RAGE signalling from crosstalk with other pathways is required to fully understand the role of RAGE in inflammation (Figure 7).

1.5.3 Cancer and tumour development

RAGE is known to play a role in a number of cancers and tumour outgrowth and metastasis. Early reports of RAGE signal transduction promoting neurite outgrowth, angiogenesis and inflammation, highlighted a possible role of RAGE in cancer and tumour metastasis (Huttunen *et al.*, 1999; Sasahira *et al.*, 2007; Taguchi *et al.*, 2000; Chen *et al.*, 2014a). Elevated levels of RAGE and its ligands are observed in pancreatic, breast, prostate, and oral square cell carcinoma cancers (Tesarova *et al.*, 2007; Arumugam *et al.*, 2005; Fuentes *et al.*, 2007; Bhawal *et al.*, 2005).

RAGE co-localisation with HMGB1 at the leading edge of advancing tumour cells was one of the first reported observations implicating RAGE with cancer (Taguchi *et al.,* 2000). In vivo studies by Taguchi *et al*. (2000) found that intravenously administered sRAGE decreases growth and metastasis of both implanted tumours, and induced tumours in susceptible mice (Taguchi *et al.,* 2000). Soluble RAGE reduced tumour size and invasion of surrounding tissue, as well as down-regulated p38 and JNK mediated signalling cascades associated with tumour proliferation (Taguchi *et al.*, 2000).

There is a growing body of research into RAGE and cancer progression particularly investigating HMGB1 and calgranulin involvement, however, little is known as to the role of AGEs or amyloids in these pathologies. Further studies in this area will likely identify roles for RAGE in metastasis, angiogenesis of tumours, and the progression from chronic inflammatory states to cancer in a number of tissues.

1.5.4 Diabetes

Despite our increasing understanding of diabetes and the plethora of research over the last 40 years, diabetics continue to develop serious complications (Brownlee *et al.*, 1988). It is known that AGE molecules accumulate within the extracellular matrix of vessel walls in correlation with increased glycaemia associated with diabetes and age (Brownlee *et al.*, 1988; Schmidt *et al.*, 1993; Singh *et al.*, 2014; Manigrasso *et al.*, 2014). Diabetic levels of AGEs in plasma are often 10-45 fold greater than those of non-diabetics (Brownlee, 1995). Injection of AGEs into otherwise normal animals induces vascular abnormalities in the absence of hyperglycaemia, strongly linking AGEs to vascular disease and the progression of diabetic complications (Vlassara *et al.*, 1992).

The production of mitogenic cytokines including interleukin-1β and platelet derived growth factor (PDGF) is associated with AGE-RAGE interaction in mononuclear phagocytes (MP) (Schmidt *et al.*, 1993; Kirstein *et al.*, 1992). The expression of these cytokines is a normal part of the removal of senescent material and ongoing tissue remodelling (Kirstein *et al.*, 1992). Disproportionate expression of these endothelial and fibroblast progression factors results in foam cell formation and atherogenesis commonly observed in chronic diabetes (Miki *et al.*, 1993). Early research identified the importance of macrophages and monocytes in wound healing through the secretion of mitogenic factors and cytokines (Leibovich and Ross, 1975). Decreased migration of monocytes to sites of tissue damage through AGE-RAGE induced cell adherence to endothelia, may account for impaired wound healing common to diabetics (Greenhalgh *et al.*, 1990). Transcytosis of AGE moieties from plasma to the endothelial extracellular matrix causes intercellular gap formation (Esposito *et al.*, 1989). These gaps result in endothelium permeability and increased AGE accumulation in the vascular basement membrane (Esposito *et al.*, 1989).

In addition to increased vascular permeability and impairment of wound healing, diabetes is associated with dysfunctional vasodilation and vascular narrowing. Bucala *et al*. (1991) observed that increased levels of AGEs reversibly impaired endothelial production of nitric oxide (NO) and resultant smooth muscle cell relaxation mediated by the guanylate cyclase pathway (Hogan *et al.*, 1992; Bucala *et al.*, 1991). Additionally, glycated collagen fibres facilitate cross-linking of low density lipoprotein (LDL) and immunoglobulins in vessel walls (Brownlee, 1995). This leads to narrowing of vascular lumen and dysfunction of normal extracellular matrix interactions.

Intervention of AGE formation using aminoguanidine treatment markedly reduces the progression of diabetic retinopathy, hypertension, renal disease, vascular leakage and peripheral nerve function in animal models (Huijberts *et al.*, 1993; Hammes *et al.*, 1994; Ellis and Good, 1991). Injection of exogenous AGEs in these animals promotes the rapid developed of diabetic vasculopathies, and the deposition of AGEs in vessel walls (Vlassara *et al.*, 1992).

The link between AGEs and thrombogenicity has been well documented following the observation that erythrocytes possess non-enzymatically glycated haemoglobin surface structures (Esposito *et al.*, 1989; Wautier *et al.*, 1981). It was hypothesised that the formation of thromboses may be in part, mediated by AGE-RAGE binding between

endothelial cell surface RAGE and glycated erythrocyte haemoglobin groups (Wautier *et al.*, 1994). This interaction initiates ROS production through autoxidative glycosylation and activation of RAGE intracellular signalling pathways (section 1.4.1) (Wolff and Dean, 1987; Wautier *et al.*, 1994).

The association between glycated proteins and production of reactive oxygen species (ROS) is now well established (Galkina and Ley, 2009; Xie *et al.*, 2013). RAGE-AGE ligation promotes oxidative stress in intravascular spaces following the infusion of AGE into rats (Ramasamy *et al.*, 2012; Naka *et al.*, 2004). These oxidative species elevate the levels of malondialdehyde and thiobarbituric acid reactive substances (TBARS), which promote vascular permeability and endothelial cell dysfunction (Yan *et al.*, 1994; Schmidt *et al.*, 1996). The quenching of O^{2-} species through self-reduction of Fe^{3+}-CML-AGE *in vitro*, reportedly reduces TBARS formation by 30% (Sakurai *et al.*, 1990). Therefore, the reducing power of AGEs modulates cell intracellular stress pathways independent of RAGE (Sakurai *et al.*, 1990; Wolff and Dean, 1987).

The biological consequences of advanced protein glycation accumulation manifest in impaired vessel tone and wound healing, progression of atherosclerosis, and suppression of normal aortic smooth muscle cytostasis (Brownlee, 1995; Hogan *et al.*, 1992). Therapies to reduce AGE formation or AGE-RAGE interaction offer significant hope in treating the symptoms of diabetes that often manifest as debilitating retinopathies, nephropathies and vasculopathies.

1.5.5 Amyloidoses

The binding of various amyloid products to RAGE progresses a number of diseases that includes Alzheimer's disease and vascular dementias, amyloid peripheral neuropathies and nephropathies (Lue *et al.*, 2005; Matsunaga *et al.*, 2005; Emanuele *et al.*, 2005; Deane, 2012; Kook *et al.*, 2012).

Serum amyloid A (SAA) is a generic term referring to a family of acute-phase proteins composed of 12-14 kDa apolipoproteins found predominantly in the high-density lipoprotein (HDL) fraction of plasma (Patel *et al.*, 1998; Yan *et al.*, 2008; Yan *et al.*, 2000). These peptides are expressed by hepatic and extrahepatic tissues, including cancer cell lines in response to inflammatory cytokines such as IL-1, IL-6 and TNF-α (Yan *et al.*, 2008). In acute inflammation, these molecules provide a protective benefit in promoting homeostasis. The positive outcomes of SAA expression are similarly

mediated by leukocyte secretory interleukins, including IL-8 and IL-10 (Patel *et al.*, 1998). Yan *et al*. (2000) reported that RAGE was the mechanism by which SAA and amyloid-A fibrils induce pro-inflammatory outcomes in systemic amyloidoses. This finding was based on the co-localisation of RAGE with amyloid fibrils in splenic tissue in a systemic amyloidosis mouse model, and the ability of sRAGE and anti-RAGE IgG to immunise these animals against chronic inflammation (Yan *et al.*, 2000).

Familial amyloid polyneuropathy (FAP) is a neurodegenerative disorder associated with the accumulation of transthyretin (TTR) amyloid fibrillary structures in peripheral nervous tissue (Sousa *et al.*, 2001). Sousa *et al*. (2001) observed that the interaction of TTR with RAGE promotes an exaggerated inflammatory response (Sousa *et al.*, 2001). Activation of RAGE in FAP patients correlates with significant localised increases in TNF-α, IL-1β and iNOS, and is followed by a delayed activation of caspase-3 and DNA fragmentation (Sousa *et al.*, 2001). These effects of TTR appear to act largely on endothelial and neuron-like Schwann cells, mimicking the effects seen *in vitro* CNS neuronal cell types following challenge with Aβ (Lue *et al.*, 2001b; Sousa *et al.*, 2001).

The accumulation of amyloid fibrils in FAP kidney tissue is accompanied by RAGE activation and AGE accumulation (Matsunaga *et al.*, 2005). The aggregation of these ligands causes significant RAGE activation, promoting chronic inflammation and associated kidney dysfunction and disease (Lee and Park, 2013; Matsunaga *et al.*, 2005).

RAGE is up-regulated in the brain of Alzheimer's Disease (AD) sufferers (Yan *et al.*, 1996; Lue *et al.*, 2001a; Matrone *et al.*, 2014). As previously mentioned, RAGE binds a number of Aβ forms (section 1.3.2), leading to apoptotic signal transduction in microglia, endothelia and neurons (Lue *et al.*, 2001a; Yan *et al.*, 1996; Wilson *et al.*, 2009; Sturchler *et al.*, 2008; Origlia *et al.*, 2008). The precise means by which Aβ ligands promote apoptosis through RAGE is yet to be clearly delineated. Complexities in intracellular signal crosstalk, alternate activation of Aβ receptors, the presence of differing RAGE isoforms, and the ability of various Aβ forms to bind distinct RAGE domains are all complicating factors (section 1.3.2). The role of RAGE as a transporter of Aβ across the blood brain barrier has further drawn attention to it as a therapeutic target in the treatment of Alzheimer's disease (Matrone *et al.*, 2014; Sharma *et al.*, 2012).

1.6 RAGE as a Target for Pharmaceutical Intervention

As our understanding of RAGE biology has increased, so too has the search for small molecule antagonists. The use of sRAGE and anti-RAGE/anti-ligand antibodies has clearly demonstrated that inhibition of RAGE ligation abates the progression of tumour outgrowth, inflammation, neuronal death and the formation of atherosclerotic lesions (Taguchi *et al.,* 2000; Hofmann *et al.,* 1999; Park *et al.,* 1998). Soluble forms of RAGE are naturally secreted in both mice and humans, allowing it to be intravenously administered without prompting an immune response (Schlueter *et al.,* 2003). The limitations of sRAGE as a therapeutic agent are however its inability to cross the blood brain barrier for treatment of Alzheimer's disease and tumour growth. Additionally, the intrinsic costs associated with producing suitable quantities of RAGE, difficulties in storing and shipping tend against its use as a viable treatment option.

The development of potent, small-molecule antagonists of RAGE capable of crossing the blood-brain barrier would provide a novel strategy for the inhibition of RAGE. The design of such molecules greatly depends on the elucidation of the receptor structure for application to rational drug design methodologies. It wasn't until 2010 that the first crystal structures of RAGE were published (Park *et al.*, 2010; Koch *et al.*, 2010). In combination with a small number of NMR studies, this structural information will contribute significantly to the development of antagonists. Currently a number of pharmaceutical companies, including Transtech and Pfizer are developing small molecule antagonists such as TTP488 for the treatment of Alzheimer's disease (Burstein *et al.*, 2014).

Alternative strategies targeting RAGE intracellular signalling intermediates, ROI production through antioxidant therapies and RAGE ligand production may also offer novel opportunities for pharmaceutical intervention.

1.7 Recombinant Protein Production Hosts

Since the first recombinant protein was produced in 1977, significant leaps forward in the range and complexity of hosts used for heterologous protein production have been made (Itakura *et al.*, 1977). The post-genomic era has placed increasing demands on protein expression methodologies and hosts for active, authentically processed

enzymes, large eukaryotic multi-subunit complexes and intramembranous, multi-domain proteins (Fernandez and Vega, 2013; Rosano and Ceccarelli, 2014; Ferrer-Miralles and Villaverde, 2013). This has driven the development of specialty vectors tailored for the production of proteins with particular transcription, translation and post-translational requirements (discussed further in section 4.2). The use of a host organism capable of implementing these functional requirements is pivotal in producing recombinant protein of sufficient form, function, yield and space time yield for application to modern day structural, functional and pharmacological investigations (Porro *et al.*, 2011).

Bacterial systems are still considered the work horse organism of recombinant protein expression due to its unparalleled growth kinetics, versatility, simplicity of manipulation and low cost of production (Rosano and Ceccarelli, 2014; Sezonov *et al.*, 2007). The current day catalogue of commercially available forms of *Escherichia coli* (*E. coli*) is immense and is largely based upon the B and K12 background strains used over the last 30 years (Ferrer-Miralles and Villaverde, 2013). The last decade has seen the emergence of alternative bacterial hosts due to the need for greater metabolic diversity and biosynthetic potential as discussed by Ferrer-Miralles and Villaverde (2013). The lack of post-translational modification performed by prokaryotic hosts as discussed in section 4.3, has ensured eukaryotic organisms such as insect, mammalian, yeast and fungal systems have continued to be used and developed for the production of complex heterologous proteins (Ferrer-Miralles and Villaverde, 2013). Today, a wide selection of organisms, molecular tools and technologies are commercially available for the production of recombinant proteins in both prokaryote and eukaryote hosts, with the choice of system often defined by the protein of interest and its intended use (Sahdev *et al.*, 2008). RAGE was almost exclusively expressed in insect cells for the first 10 years following its discovery. Over the last 10 years, RAGE is increasingly expressed in prokaryotic hosts (Hofmann *et al.*, 1999; de Arriba *et al.*, 2003; Srikrishna *et al.*, 2002; Xue *et al.*, 2011; Park *et al.*, 2010). With more than 93% of all known three-dimensional protein structures being produced by either bacterial or insect hosts, this study focuses on the integrity of RAGE and RAGE ligands produced in these systems as representative molecules of their endogenous forms (Fernandez and Vega, 2013). These hosts, their characteristics and the implication of these traits for heterologous protein production are discussed in detail in sections 4.2 and 4.3.

1.8 The Present Study

The principle aim of this study is to investigate a common method for expressing not only RAGE and its many forms, but a number of its ligands as well. This common 'toolbox' approach has the enormous potential of simplifying the production of the both RAGE and it's common ligands, as well as a means of simply, safely and reliably evaluating functionality.

To date, much of the research investigating the kinetics of interaction between RAGE and its ligands has involved combinations of endogenous, bacterial and baculoviral expressed RAGE and ligand molecules. This study aims to:

1. Evaluate the suitability of a rapid recombinant gene technology for use in insect expression as an alternative to baculoviral expression.

2. Evaluate a range of bacterial hosts and factors impacting the heterologous production of RAGE.

3. Determine which host organism is optimal for the expression of both RAGE and a number of its ligand molecules, in particular S100s and HMGB1.

4. Develop a simplified method for measuring RAGE-ligand binding that is safe, flexible and robust. Use this method to demonstrate the functionality of the RAGE and ligand molecules produced through the course of this study.

2.0 MATERIALS AND METHODS

2.1 Materials

Reagent	Manufacturer/Supplier
3M Filter Paper	Whatman, Brentford, Middlesex - U.K
4-16% Precast PAGE gel	Gradipore, Sydney, NSW - Australia
Acetic Acid	
Agarose LE, Analytic Grade	Promega, Madison, WI - U.S.A
Ampicillin	Royal Perth Hospital, Perth, W.A. - Australia
Antibody Goat Anti-Human RAGE - Biotinylated	R&D Systems, Minneapolis, MN - U.S.A
Antibody Goat Anti-Mouse IgG Alkaline Phosphatase Conjugate	Santa Cruz Biotechnology, Santa Cruz, CA - U.S.A
Antibody Mouse Anti-Human RAGE	R&D Systems, Minneapolis, MN - U.S.A
Antibody Mouse Anti-V5 IgG	Invitrogen, Carlsbad, CA - U.S.A
Apoprotein	Sigma-Aldrich, St Louis, MO - U.S.A
Aurum Plasmid Purification Kit	Bio-Rad, Hercules, CA - U.S.A
Biacore CM5 Sensor Chip	GEHealthcare, Little Chalfont, Buckinghamshire, U.K
Blasticidin S-HCl	Invitrogen, Carlsbad, CA - U.S.A
Borate	Sigma-Aldrich, St Louis, MO - U.S.A
Bovine Serum Albumin	Sigma-Aldrich, St Louis, MO - U.S.A
Cellfectin®	Invitrogen, Carlsbad, CA - U.S.A
Coomassie blue R350	Sigma-Aldrich, St Louis, MO - U.S.A
Deoxyribonucleotide Triphosphates (dNTP's)	Invitrogen, Carlsbad, CA - U.S.A
Dimethyl Sulfoxide	Sigma-Aldrich, St Louis, MO - U.S.A
Dithiothreitol	Sigma-Aldrich, St Louis, MO - U.S.A
D-Ribose	Sigma-Aldrich, St Louis, MO - U.S.A
Ethanolamine Hydrochloride	GEHealthcare, Little Chalfont, Buckinghamshire, U.K

Reagent	Manufacturer/Supplier
Ethidium Bromide	Invitrogen, Carlsbad, CA - U.S.A
Ethylenediaminetetraacetic Acid	Sigma-Aldrich, St Louis, MO - U.S.A
Ex-Cell® 405 Serum Free Media	Sigma-Aldrich, St Louis, MO - U.S.A
Express Five® Serum Free Media	Invitrogen, Carlsbad, CA - U.S.A
Foetal Calf Serum (FCS)	Thermo Scientific, Waltham, MA - U.S.A
Glycerol	Ajax Chemicals, Auburn, N.S.W – Australia
Glycine	Sigma-Aldrich, St Louis, MO - U.S.A
10x glycoprotein denaturation buffer	New England Biolabs - USA
HBS-EP Buffer	GEHealthcare, Little Chalfont, Buckinghamshire, U.K
High-Five® Insect Cells (High Five™)	Invitrogen, Carlsbad, CA - U.S.A
Human RAGE gene, full length	University of Helsinki, Rauvala Laboratory - Finland
Hybond™-P PVDF	GEHealthcare, Little Chalfont, Buckinghamshire, U.K
Imidazole	Sigma-Aldrich, St Louis, MO - U.S.A
Isopropyl β-D-1-thiogalactopyranoside	Sigma-Aldrich, St Louis, MO - U.S.A
LB Agarose	Royal Perth Hospital, Perth, W.A. - Australia
LB Broth	Royal Perth Hospital, Perth, W.A. - Australia
LB Broth Powder	USBiological, Swampscott, MA - U.S.A
Leupeptin	Sigma-Aldrich, St Louis, MO - U.S.A
Lowry Protein Assay kit	Sigma-Aldrich, St Louis, MO - U.S.A
Magnesium Chloride	Sigma-Aldrich, St Louis, MO - U.S.A
Methanol	Merck, Kilsyth, VIC - Australia
Na_2HPO_4	Sigma-aldrich – Sydney, NSW - Australia
NAH_2PO_4	Sigma-aldrich – Sydney, NSW - Australia
N-ethyl-N'-(3-dimethylaminopropyl) carbodiimide hydrochloride	GEHealthcare, Little Chalfont, Buckinghamshire, U.K

Reagent	Manufacturer/Supplier
N-hydroxysuccinimide	GEHealthcare, Little Chalfont, Buckinghamshire, U.K
Nonidet P-40	Roche, Sydney, NSW - Australia
Origami™ B *Escherichia coli*	EMD Millipore, Sydney, NSW - Australia
pcDNA3 Expression Vector	Invitrogen, Carlsbad, CA - U.S.A
PCR Grade Magnesium Chloride	Invitrogen, Carlsbad, CA - U.S.A
PCR Primers	Geneworks, Hindmarsh, S.A. - Australia
PCR Reaction Buffer	Invitrogen, Carlsbad, CA - U.S.A
Phenylmethanesulphonylfluoride	Sigma-Aldrich, St Louis, MO - U.S.A
Phosphate Buffered Saline Concentrate	Invitrogen, Carlsbad, CA - U.S.A
pIB/V5 His TOPO® TA Vector	Invitrogen, Carlsbad, CA - U.S.A
pIB/V5 His-CAT plasmid	Invitrogen, Carlsbad, CA - U.S.A
Platinum® Taq Polymerase	Invitrogen, Carlsbad, CA - U.S.A
RAGE Duoset ELISA	R&D Systems, Minneapolis, MN - U.S.A
Recombinant Human RAGE-Fc Standard	R&D Systems, Minneapolis, MN - U.S.A
Rosetta-gami™ B	EMD Millipore – Sydney, NSW - Australia
S100A6-GST	MBL International, Woburn, MA - U.S.A
S100B (Bovine)	Sigma-Aldrich, St Louis, MO - U.S.A
S100P-GST	MBL International, Woburn, MA - U.S.A
Sf21 Insect Cells	Invitrogen, Carlsbad, CA - U.S.A
Sf9 Insect Cells	Invitrogen, Carlsbad, CA - U.S.A
Sf9 00™-II Serum Free Media	Invitrogen, Carlsbad, CA - U.S.A
Skim Milk Powder	Coles, Tooronga, VIC - Australia
SOC Media	Invitrogen, Carlsbad, CA - U.S.A
Sodium Acetate (anhydrous)	Sigma-Aldrich, St Louis, MO - U.S.A
Sodium Chloride	Merck, Kilsyth, VIC - Australia
Sodium Dodecyl Sulphate	Bio-Rad, Hercules, CA - U.S.A

Reagent	Manufacturer/Supplier
Streptavidin Conjugated Horseradish-Peroxidase	R&D Systems, Minneapolis, MN - U.S.A
Sulphuric Acid	Merck, Kilsyth, VIC - Australia
T7 Shuffle® B	New England Biolabs - USA
T7 Shuffle® K12	New England Biolabs - USA
TMB+ AP Substrate	Dako, Carpinteria, CA - U.S.A
TOP10 Chemically Competent *E. coli*	Invitrogen, Carlsbad, CA - U.S.A
Trichloroacetic Acid	Sigma-Aldrich, St Louis, MO - U.S.A
Tris	Sigma-Aldrich, St Louis, MO - U.S.A
Trypan Blue	Sigma-Aldrich, St Louis, MO - U.S.A
Tween-20	MP Biomedicals, Solon, OH - U.S.A

2.2 Ethics approval

Animal or Human ethics approval were not required at any stage of this project.

2.3 Genetically Modified Organism Approval and Safety

This project utilized commercially available expression systems developed by Invitrogen™. These systems are classified as exempt dealings under parts 1 & 2 of Schedule 2 of the Gene Technology Regulations 2001 (Commonwealth Government of Australia) due to the well-defined nature of the vectors. Notice of the use of these vectors and the associated genes to be expressed is registered with the Curtin University Institutional Biosafety Committee.

2.4 Molecular Biology Methods

2.4.1 Primer design

Forward and reverse primers for use in polymerase chain reaction (PCR) were designed using an open source, web based application known as Primer3 (Peters *et al.*, 2008). The primers for canonical RAGE gene sequence amplification were designed against the RAGE complete coding sequence (2000) (Genbank accession number: AB036432), and the optimal forward and reverse products are described in Table 1. Melting temperatures included were determined by the primer manufacturer. Primers for amplification of human HMGB1 were designed against human mRNA for high mobility group-1 protein (GenBank accession number X12597), and are described in Table 2. Primers for amplification of the endogenous human RAGE V, VC_1 and VC_1C_2 domains for expression in a prokaryote system that exclude the leader sequence are described in Table 3 and designed against both a synthetic optimised form of the human RAGE gene and canonical RAGE (2000) (Genbank accession number: AB036432). Primers to amplify human calgranulins S100B, S100P and S100A6 were designed against GenBank accession numbers: BC001766, BC006819 and BC001431 respectively, and are described in Table 4. Sequencing primers for the entry vector pENTR SD/D-TOPO were designed against the manufacturers provided plasmid sequence.

Table 1. Forward and reverse primers used to amplify the V, VC_1 and VC_1C_2 domains of human RAGE for expression in insect cells.

Melting behavior (delta H degree) of the oligomers was calculated as per the method of Breslauer *et al.* (1986).

Primer	Sequence	T_m (°C)
Ins-Forward-RAGE (F1)	AGGATGGCAGCCGGAACAGCAGTTG	62
Ins-Reverse V (R1)	GACACGGACTCGGTAGTTGGACTTGGT	62
Ins-Reverse VC_1 (R2)	GACACGGGGCTGGATGGGGGC	64
Ins-Reverse VC_1C_2 (R3)	TTCCTGGGGCCCGTGGCTGGA	64

Table 2. Forward and reverse primers used to amplify full length and truncated human HMGB1.

Primer	Sequence	Tm (°C)
Forward-truncHMGB1	TGGGTAAAGGCGATCCGA	55
Reverse-truncHMGB1	CTTTTTCTTTTTAGATTTTTCTGCTTTCAC	54
Forward-HMGB1	GCATGCATGGGCAAAGGCGATCCG	62
Reverse-HMGB1	TTCGTCGTCGTCGTCTTCTTCTTCG	59

Table 3. Forward and reverse primers used to amplify human RAGE V, VC_1 and VC_1C_2 domains for expression in a prokaryote system.

Primer	Sequence	T_m (°C)
Prok-Forward-RAGE native (N-pF1)	ATGGCTCAAAACATCACAGCC	59
Prok-Forward-RAGE (pF1)	ATGGCCCAAAACATTACCGCT	61
Prok-Reverse V (pR1)	TTCCGGTTTGCCCGGAATTT	61
Prok-Reverse VC1 (pR2)	CAACCACCAGTTGCACTTCT	58
Prok-Reverse VC1C2 (pR3)	CAGACCGCTGCCACCAA	59

Table 4. Forward and reverse primers used to amplify human calgranulins S100B, S100P and S100A6 for expression in a prokaryote system.

Primer	Sequence	T_m (°C)
S100B-Forward	ATGTCTGAGCTGGAGAAGGC	59
S100B-Reverse	TCACTCATGTTCAAAGAACTCGT	58
S100P-Forward	ATGACGGAACTAGAGACAGCC	59
S100P-Reverse	TCATTTGAGTCCTGCCTTCTCA	59
S100A6-Forward	ATGGCATGCCCCCTGGATC	55
S100A6-Reverse	TCAGCCCTTGAGGGCTTCATT	54

Table 5. Forward and reverse primers used for sequencing pENTR-SD/D-TOPO.

Primer	Sequence	T_m (°C)
pENTR-Forward	GCATGCATGGGCAAAGGAGATCCT	59°
pENTR-Reverse	AAGCTTTATTCATCATCATCATCA	49°

2.4.2 Transformation of chemically competent Escherichia coli

Chemically Competent TOP10 or Library Efficiency® DH5 *Escherichia coli* (*E. coli*) (Invitrogen™) were transformed with plasmid containing various PCR inserts. A microfuge tube containing 50 µL of chemically competent *E. coli* stored at -80°C, was thawed on ice. Two µL of plasmid (50-150 ng) was added and mixed by gentle vortex. This mixture was placed on ice for 25 minutes before being heat shocked for 30 seconds without shaking at 42°C in a water bath. The mixture was immediately placed back on ice for 2 minutes and 450 µL of room temperature super optimal broth with catabolite repression (SOC) medium added. The mixture was then shaken for 1 hour (37°C) at 200 rpm on a horizontal platform shaker. Aliquots of this mixture were diluted with Lysogeny broth (LB) 100-fold, 10-fold and 5-fold to a final volume of 200 µL. Each diluted sample and an undiluted aliquot were plated onto LB agarose containing 100 µg/mL of an appropriate selective antibiotic (section 2.4.4).

2.4.3 Preparation of ampicillin selective LB agarose plates

Solid 1.2% LB agarose (100 mL) was heated in an 800 W microwave for 5 minutes or until melted. The agarose was allowed to cool to 55°C in a water bath. Ampicillin, kanamycin or chloramphenicol (water soluble) was reconstituted in 1 mL of LB broth to a working concentration of 5 mg/mL before being combined with the molten agarose. The LB agarose + antibiotic (50 µg/mL), was immediately poured into 60 mm petri dishes and allowed to set at room temperature. Plates were sealed with parafilm and stored at 4°C until needed.

2.4.4 Selection of positive TOP10 E. coli using selective media

LB agarose plates containing a selective antibiotic were prepared as outlined in section 2.4.3. Onto these plates, 25 µL, 75 µL and 200 µL aliquots of transformed *E. coli* (section 2.4.2) were pipetted and gently spread over the agarose surface using a flame sterilised glass hockey stick. Plates were sealed and incubated overnight at 37°C before being inspected for colony forming units (cfu). A flame-sterilised loop was used to pick a cfu and inoculate 10 mL of LB broth containing 100 µg/mL of ampicillin. The LB broth containing the appropriate antibiotic was then shaken at 160 rpm (37°C) overnight or until a spectrometric $O.D^{600nm}$ of 0.8-1 was achieved, representing mid log-phase.

2.4.5 Whole cell PCR

A PCR master mix was prepared at 4°C using Invitrogen™ Platinum° Taq DNA Polymerase kit components at 1x PCR Buffer, 0.2 mM dNTPs, 2.5 mM $MgCl_2$, 0.25 µM forward and reverse primer and 1U of Platinum Taq. Then, 15 µL of master mix was added to a sterile, nuclease free 0.5 mL microfuge tube on ice. From the LB-Amp+ plates containing positive colony forming units (section 2.4.4), single colonies were picked using a sterile pipette tip and transferred into each microfuge tube containing master mix. The tubes were immediately capped and labelled, and placed in a PTC-100 thermocycler where they were amplified according to the following program:

1) 10 minutes at 94°C to activate the hot start polymerase and lyse cells
2) 30x cycles of:
    a. 0.5 minute at 94°C
    b. 0.5 minute at 60°C
    c. 1 minute at 72°C

3) 7 minutes at 72°C

At the end of the program, reaction mixtures were stored at -20°C until needed.

2.4.6 Plasmid purification

Plasmid was prepared by inoculating 10 mL LB Amp+ broth (100 µg/mL Ampicillin) with a single cfu picked from an LB-Amp+ plate (section 2.4.4), or with a 100 µL aliquot of bacterial-plasmid glycerol stock (section 2.4.6). The broth was sealed and shaken at 160 rpm (37°C) overnight or until an $O.D^{600nm}$ of 0.6-0.8 was reached. The culture was then centrifuged at *1000 g* for 15 minutes at 4°C. All subsequent steps were performed on ice or using buffers stored at 4°C unless otherwise specified.

The supernatant was carefully poured off and the bacterial pellet gently resuspended in 250 µL Bio-Rad Aurum™ Plasmid mini-prep spin kit (BAP) resuspension buffer. The mixture was transferred to a 1.5 mL eppendorf tube to which 400 µL of BAP lysis buffer was added. The lysed cell suspension was carefully mixed by inverting the tube 6-8 times. BAP neutralization buffer (450 µL) was then added and the tube mixed by gently inverting the solution a further 4-6 times. The suspension was centrifuged at *12,000 g* for 5 minutes before the clear cell lysate was transferred to a BAP mini-spin column, which was centrifuged at *12,000 g* for 1 minute. The flow-through was discarded and 750 µL of BAP wash buffer was added to the column. The column was again centrifuged at *12,000 g* for 30 seconds, and this wash step was repeated a further two times. The BAP mini-spin column was loaded into a sterile 1.5 mL eppendorf tubes and 50 µL of ultra-pure water was added to the column. The column was placed upright for 2 minutes at room temperature to allow even distribution of the water across the frit surface. The plasmid was then eluted by centrifuging the mini-column at *12,000 g* for 2 minutes. DNA eluate quality and quantity was evaluated as described in section 2.4.8 before being stored at -20°C until required.

2.4.7 PCR amplification and restriction enzyme digest of pGEX-6P1-deltaHMGB1

PCR amplification of truncated HMGB1 was performed as described in section 2.4.11, however, the plasmid used was pGEX-6P1-deltaHMGB1 and the primers are those described in Table 2. Following amplification, a 10 µL aliquot of the PCR reaction mixture was added and incubated with 10U of restriction enzymes *BamHI* and *EcoRI*

over night at 37°C. The entire mixture was then visualised on a 2% agarose gel as described in section 2.4.9.

2.4.8 Evaluation of plasmid DNA quantity and quality

Purified plasmid (section 2.4.6) was assessed spectrophotometcially by comparing the ratio of absorbance at 260 nm/280 nm. This ratio was determined by aliquoting 2 µL of purified plasmid into 998 µL of high pure DNase free water and gently mixing twice by inversion. The DNA sample was measured against a blank of high pure water.

2.4.9 DNA agarose gel electrophoresis

DNA was visualised on a 1.2% agarose gel which was prepared by mixing 3.6 g LE grade agarose with 300 mL of Tris Borate EDTA buffer (pH 8.3) (TBE) containing 0.09 M Tris, 0.09 M borate, 0.0025 M EDTA. The mixture was heated in an 800 W microwave oven for approximately 4 minutes or until it boiled. The agarose mixture was gently swirled to ensure the agarose was completely dissolved and allowed to cool in a 60°C oven until needed.

A gel cassette was sealed on both sides with tape and a 12-well comb placed in position. The 1.2% molten agarose was poured into the cassette and the gel allowed to set for 20 minutes at room temperature. Once set, the gel was placed into an electrophoresis tank which was filled with sufficient TBE buffer (pH 8.3) to completely cover the gel. A 10 µL aliquot of PCR reaction mixture was combined with 5 µL of DNA loading buffer, which was then loaded onto the gel. The gel was subsequently run for approximately 1 hr at 90 V or until the dye front approached the edge of the gel.

2.4.10 Visualisation of agarose gel electrophoresis PCR product or plasmid DNA

The agarose gel and cassette (2.4.9) were removed from the electrophoresis tank and the gel carefully submerged in a solution containing 0.5 µg/mL ethidium bromide at room temperature. The gel was allowed to sit for 10-15 minutes before being removed from the bath and placed on a UV transilluminator to visualize the DNA bands. The images were captured using a Polaroid camera system.

2.4.11 PCR amplification of plasmid inserts

Amplification of plasmid vector gene inserts was done using the same protocol outlined in 2.4.5. The bacterial cell template was substituted with 50-150 ng of purified plasmid and the initial Taq activation cycle was 5 minutes instead of 10 minutes.

2.4.12 Cloning of PCR product into pIB/V5 His TOPO expression vector

The pIB/V5 HIS vector (Figure 78) mixture contains linearized plasmid in the presence of activated topoisomerase-I. The cloning reaction was setup according to the manufacturer's instructions. Briefly, in a 0.5 mL sterile microfuge tube, 2 µL of PCR product was mixed with 1 µL of salt solution (1.2 M $NaCl_2$, 60 mM $MgCl_2$), 1 µL of pIB/V5 His TOPO® vector mixture and made up to a final volume of 5 µL with sterile high pure water. The reaction mixture was incubated at room temperature for 10 minutes before being placed on ice. TOP10 *E. coli* was then transformed with the reaction mixture as outlined in protocol 2.4.2.

2.4.13 Sub-cloning of PCR products in to pGS-21a expression plasmid

PCR product was produced as outlined in method 2.4.11 and single bands excised and purified using a Qiagen QIAquick PCR Purification Kit according to the manufacturer instructions. GenScript pGS-21a plasmid (Figure 77) was produced in TOP10 *E. coli* and purified as outlined in section 2.4.6. Purified plasmid was linearized by incubating 1 µg of pGS-21a with 5U of XbaI and 5U of HindIII Restriction enzymes in NEBuffer (1x final working concentration) for a total working volume of 50 µL. The reaction was incubated at 37°C for 60 minutes before being placed on ice. Vector containing RAGE/HMGB1/S100 recombinant protein constructs were similarly digested and combined at a molar insert to vector ration of 3:1 and the solution made up to 10 µL in ice cold hpH_20 and mixed with 10 µL New England Biolabs (NEB) 2x quick ligation buffer. To this mixture, 1 µL of NEB Quick T4 DNA Ligase was added and the mixture incubated at room temperature for five minutes before being placed back on ice. The mixture was immediately used to transform TOP 10 *E. coli* as outlined in 2.4.2 and the culture plated out on selective media.

2.4.14 Preparation of ultra-low temperature bacterial glycerol stocks

Colonies identified by PCR as containing correctly oriented gene inserts were used to inoculate 10 mL of LB Amp+ broth (100 µg/mL ampicillin). The LB Amp+ broth was

shaken at 160 rpm (37°C) until an $O.D_{600nm}$ of 0.6-0.8 was achieved. The cultures were then diluted two-fold with sterile 80% glycerol in 1.5 mL sterile eppendorf tubes in 1 mL aliquots. The glycerol stocks were stored at -72°C until needed.

2.5 Cell Culture Methods

2.5.1 Thawing of Sf9 and Sf21 insect cells

Stocks of *Sf9* , *Sf21* and *Tn5* insect cells were sealed in 1.5 mL cryovials containing $1x10^7$ cells and stored in liquid nitrogen (vapour phase) until required. A frozen cryovial was rapidly thawed by placement in a 27°C water bath until the cell pellet was almost completely thawed. The cell suspension was immediately transferred to a 10 mL centrifuge tube containing 9 mL of pre-warmed *Sf9* 00-II serum free medium (SFM) containing 16 mM L-glutamine. A 3 mL aliquot of this mixture was transferred to a 75 cm^2 Nunclon™ tissue culture flask and left to sit for 20 minutes at 28°C. The cell media was subsequently aspirated and replaced with 10 mL of *Sf9* 00-II SFM, 2.5% FCS, 16 mM L-glutamine (28°C) and then kept at 27°C in a non-humidified incubator until cells reached confluency.

2.5.2 Thawing of Tn5 Insect Cells

Tn5 insect cells were thawed and seeded using the same steps outlined in section 2.5.1, however the *Sf9* 00-II SFM was substituted with Express Five® SFM supplemented with 16 mM L-glutamine.

2.5.3 Freezing of insect cells

The medium used for freezing insect cells was prepared by mixing equal volumes of conditioned culture medium with fresh culture medium, dimethyl sulphoxide (DMSO) to a final concentration of 7.5% v/v and Foetal Calf Serum (FCS) to a working concentration of 5% v/v. Cells were grown to 80% confluence (sections 2.5.4, 2.5.6) with cell viability and total count determined as described in section 2.5.7. The cell suspension was centrifuged at *50 g* for 5 minutes and the supernatant decanted. The cell pellet was resuspended to a cell density of $1x\ 10^7$ cells/mL in the medium described above chilled to 4°C. The cell suspension was quickly aliquoted (1 mL) into 1.5 mL Nunc cryovials and then refrigerated at -20°C for 30 minutes, followed by -80°C for 24 hr, before being placed into liquid nitrogen for long-term storage.

2.5.4 Passaging Sf9, Sf21 and Tn5 insect cells in adherent culture

Sf9 00-II media was used to culture *Sf9* and *Sf21* insect cells, and Ex-Cell 405 or Express Five® SFM media was used to culture *Tn5* insect cells. Conditioned media containing cell debris was aspirated from an 80% confluent insect cell monoculture grown in a 75 cm^2 culture flask. Five millilitres of pre-warmed (27°C) medium was added to the culture and gently washed across the surface of the flask by tipping it back and forth, before being aspirated. After being washed, 10 mL of culture media was streamed directly over the adhered cells 3-4 times at maximum output using an electronic transfer pipette until >90% of the cells were sloughed from the surface. The cell culture was split five-fold, with 2 mL of the cell suspension being added to a new 75 cm^2 culture flask containing 8 mL of fresh media. The cells were left to adhere to the flask surface for 20 minutes before the media and cellular debris were aspirated and 10 mL of fresh media added. The culture was left to grow at 27°C in a non-humidified incubator until confluent.

2.5.5 Adaptation of Lepidoptera insect cells from adherent to suspension culture

Cells were cultured to confluence and >95% cell viability in 75cm^2 monoculture flasks as described in section 2.5.4, with one flask on average producing 1x10^7 viable cells. Sufficient flasks were cultured to yield 5x10^7 viable cells. Sloughed cells suspensions were combined in a 50 mL Falcon centrifuge tube, with cell density and viability determined as outlined in section 2.5.7. The suspension was centrifuged at *50 g* for 5 minutes to pellet the insect cells. The supernatant was removed and the cells resuspended in 10 mL of suitable serum-free culture media (*Sf9* 00-II medium for *Sf9* and *Sf21* or Express Five® SFM media for *Tn5* insect cells). The cell suspension was then transferred to a 250 mL Erlenmeyer shaker flask containing 90 mL of pre-warmed (27°C) culture medium to yield a final cell density of 5x10^5 viable cells/mL. The shaker flask was incubated at 27°C with constant orbital agitation of 100 rpm. Cells were considered confluent at 2x10^6 cells/mL and passaged according to section 2.5.6.

2.5.6 Passaging Sf9, Sf21 and Tn5 insect cells in suspension culture

Cells were grown in suspension to a density of 2x10^6 viable cells/mL. The culture was transferred to two 50 mL centrifuge tubes and centrifuged at *50 g* for 5 minutes. The supernatant was collected and stored at 4°C for further analysis if required. The cell pellet was resuspended in 10 mL of fresh culture media (*Sf9* 00-II medium for *Sf9* and *Sf21* or Express Five® SFM media for *Tn5* insect cells). From the cell suspension, 2.5 mL

was transferred to a 250 mL spinner flask containing 97.5 mL fresh media yielding a final cell density of $5x10^5$ viable cells/mL. Samples were taken from each freshly seeded flask to ensure correct seeding density and cell viability greater than 95% was observed. Cultures were grown at 27°C with constant orbital agitation at 90 rpm until confluent.

2.5.7 Determining cell density and viability

A 0.4% trypan blue solution was prepared using an isotonic phosphate buffered saline (pH 7.4) (PBS). To 100 µL of cell suspension, 10 µL of trypan blue solution was added. Ten microliters of the cell suspension-trypan mixture was then loaded onto a haemocytometer. The number of blue stained cells and the number of total cells in a single large chamber were counted and the cell viability and density determined according to the following formula:

Cell viability (%) = [1.00 – (Number of blue cells / Number of total cells) x 100]

Cell density (cells/mL) = number of viable cells x 10^4 x 1.1

2.5.8 Transient expression of RAGE domain constructs in Lepidoptera insect cell cultures

A transfection mixture was prepared (1 mL serum free cell culture media, 1 µg of pIB/V5-His-TOPO-hRAGE construct and 20 µL Cellfectin®reagent) in a 1.5 mL microfuge tube and gently mixed for 10-15 seconds before being incubated at room temperature for 30 minutes (Bierhaus *et al.*, 1997). A positive control transfection mixture using pIB/V5-His-TOPO-CAT in place of the human RAGE (hRAGE) expression vector was similarly prepared and used alongside the hRAGE constructs.

Insect cells were seeded the day before into a 60 mm culture dish so that 60% confluence would be achieved within 24 hr. The media from these cultures was carefully aspirated and the transfection mix added drop wise evenly over the monolayer. The culture dish was incubated at room temperature for 4 hr on a side-to-side rocking platform at two side motions per minute. Following the incubation period, 2 mL of serum-free culture media (27°C) was carefully added and the dish incubated for 48 hr at 27°C in a humidified incubator. Conditioned media was then collected and evaluated for the presence of recombinant protein. Cells were carefully sloughed from the surface of the 60 mm culture dish with 2 mL of suitable pre-warmed (27°C) media and transferred

to T-75 flasks containing 8 mL of the appropriate media. Cells were grown to confluency and media was collected for evaluation of secretory recombinant protein expression.

2.5.9 Stable expression of RAGE domain constructs in Lepidoptera insect cell cultures

Transfected insect cells were grown to confluence before being sloughed from the monoculture flask surface using 10 mL of the conditioned media. The cell suspension was split into four T-75 culture flasks containing 7.5 mL of fresh culture media for a total volume of 10 mL. The cells were allowed to attach for 1 hour at room temperature and adherence determined using an inverted microscope. Selective media was prepared by dissolving Blasticidin-S HCl in culture media to a working concentration of 80 µg/mL. Media was aspirated from the cultures and replaced with 10 mL of selective media pre-warmed to 27°C. Cells were incubated at 27°C for 3-6 days depending on the cell line, or until large foci formed. Cells were then passaged as outlined in section 2.5.4, using selective culture media every third passage to maintain selection.

2.5.10 Lysis of insect cells

Cells from monocultures were sloughed from the flask surface and transferred to a centrifuge tube before being centrifuged at *50 g* for 5 minutes. The cell pellet was gently resuspended in 5 mL of PBS chilled to 4°C, and again centrifuged at *50 g* for 5 minutes. The supernatant was again decanted and the cell pellet resuspended in 250 µL of ice cold lysis buffer (50 mM Tris (pH 7.8) containing 150 mM NaCl, 1% Nonidet P-40, 1 mM PMSF, 1 µM Leupeptin and 0.1 µM aprotinin) before being vortexed for 1 minute. The cell suspension was allowed to sit for 30 minutes on ice. Cellular debris was removed by centrifugation at *11,000 g* (4°C) for 30 minutes. The supernatant was collected and analysed for the presence of recombinant protein.

2.6 Protein Expression and Purification

2.6.1 Prokaryote transformation and expression of human RAGE V, VC_1 and VC_1C_2 extracellular domains

Lysogeny Broth (LB) was prepared by mixing 7.75 g of LB powder (USBiological) with 500 mL of high-pure H_2O before being autoclaved at 121°C for 15 minutes. The broth was allowed to cool to room temperature before ampicillin was added to a final concentration of 100 µg/mL. The LB + Amp mixture was stored at 4°C until needed.

TOP10 *E. coli* were transformed with both optimised and canonical V, VC_1 and VC_1C_2 domain constructs in pGS-21a as described in section 2.4.2 and plasmid purified and quantified as outlined in section 2.4.6. Expression host strains to be transformed were BL21 (DE3), Rosetta-gami™ B, Origami™ B, T7 Shuffle® K12 and T7 Shuffle® B. Their respective genotypes are described in Table 10.

A vial of each prokaryote expression strain was thawed on ice for 10 minutes. Fifty nanograms of purified pGS-21a RAGE construct was added to each vial, which was gently mixed by flicking. The mixture was placed back on ice for 30 seconds before being heat shocked for 30 seconds at 42°C and then returned to ice for five minutes. Super optimal broth with catabolite repression (SOC) was warmed to room temperature and 950 µL added to each vial before each mixture was incubated at 30°C for 60 minutes with vigorous shaking (250 rpm). Serial dilutions of each vial were made and then plated on selective media and incubated overnight at 37°C. After 24 hours, individual colonies were screened for the presence of the expected gene insert by PCR before being used to inoculate starter cultures comprising 5 mL Lysogeny Broth and 100 µg/mL ampicillin. Starter cultures were incubated overnight at 30°C with 250 rpm agitation. A 1 L preparation of LB containing 100 µg/mL ampicillin was inoculated with the starter culture and agitated at 250 rpm at 30°C until the culture reached an $O.D^{600}$ of 0.6-0.8. A liquid stock of 250 mM isopropyl β-D-1-thiogalactopyranoside (IPTG) was added to the culture to achieve a final concentration of 1 mM to induce recombinant protein expression. The culture was then shaken at 200 rpm at 30°C for six hours. The entire culture was subsequently split into four 250 mL centrifuge pots and centrifuged at *12,000 g* for 30 minutes. The supernatant was discarded and the cell pellets resuspended in 10 mL of ice cold PBS before being combined in a single 50 mL centrifuge tube which was centrifuged again at *12,000 g* for 30 minutes. The supernatant was discarded and the cell pellet which contained the expressed protein was stored at -20°C until needed.

2.6.2 Microplate culturing of Escherichia coli transformed with RAGE V, VC_1 and VC_1C_2 extracellular domains.

Lysogeny Broth was prepared by mixing 7.75 g of LB powder (USBiological) with 500 mL of high-pure H_2O before being autoclaved at 121°C for 15 minutes. The broth was allowed to cool to room temperature before ampicillin was added to a working concentration of 100 µg/mL. 200 µL of Luria broth was added to each well on a round

bottom 96-well sterile microtitre culture plate (Greiner) and the plate warmed to 30°C in a humidified cabinet. Wells were inoculated in triplicate with 20 µL aliquots of log-bacterial expression hosts transformed with a range of pGS-21a expression vectors for RAGE, HMGB1 and S100s. A gas permeable adhesive seal (Thermo Scientific) was placed over the plate and the plate agitated at 400rpm, with growth monitored photometrically at 600 nm. The culture was induced using IPTG at a working concentration of 1 mM once an $O.D^{600}$ of 0.6-0.8 was achieved. Cultures were induced for 6 hours (RAGE) or 2.5 hr (HMGB1). Individual well cultures were transferred to 0.5 mL microfuge tubes containing 250 µL of 50 mM Tris-HCl (pH 7.5) containing 50 mM NaCl, 5 mM DTT (Lysis Buffer) with Roche COmplete™ Protease Inhibitor Cocktail (EDTA-free) and lysed on a thermocycler at 95°C for 20 minutes. Samples were centrifuged at, *9,000 g* for 15 minutes at 4°C. The concentration of RAGE expressed within the soluble fraction of each well was determined by ELISA (Section 2.6.19) and visualised on a denaturing SDS-PAGE gel (section 2.6.16) by Coomassie staining (section 2.6.17) and Western blotting (section 2.6.18).

2.6.3 Lysis of prokaryote cells by sonication

Prokaryote cell pellets stored at -20°C were thawed on ice for 10 minutes before being resuspended in ice cold 50 mM Tris-HCl (pH 7.5) containing 50 mM NaCl and 1 mM DTT (Lysis Buffer) with Roche COmplete™ Protease Inhibitor Cocktail (EDTA-free) following the manufacturer instructions. Lysis buffer was added at a ratio of 1:3 cell wet weight to buffer volume. The mixture was gently vortexed to ensure thorough re-suspension of the cell pellet and left on ice for 10 minutes. The mixture was loaded into the sonication chamber and immersed in an ice bath before being sonicated 10 times for 10 second bursts with 20 second intervals to prevent over-heating. Care was taken to prevent frothing or heating of the mixture. Upon completion, the mixture was centrifuged at *20,000 g* for 15 minutes at 4°C to pellet the insoluble cell debris, leaving the soluble fraction containing the expressed recombinant protein. The soluble fraction was filter sterilised using a 0.22 µm syringe filter before being snap frozen in liquid nitrogen and then stored at -80°C until needed. If the fraction was to be used within 24 hr, the filtered sample was stored at 4°C.

2.6.4 Prokaryote expression of S100B, S100P and S100A6

The expression of S100B, S100P and S100A6 was done using the same methodology employed in the expression of RAGE constructs in section 2.6.1. The calgranulin gene

sequences were optimised for prokaryote expression and synthesised by GenScript before being supplied in pUC57 cloning vector and subsequently sub-cloned into pGS-21a as described in section 2.4.13. The vector was transformed in to T7 Shuffle® K12 as described in section 2.6.1 and expressed as outlined in section 2.6.1. Cells were pelleted and lysed as described in 2.6.3.

2.6.5 Prokaryote expression of HMGB1

The expression of full length and truncated HMGB1 was done using the same methodology employed in the expression of RAGE constructs in section 2.6.1. Truncated HMGB1 was expressed using the canonical human sequence for HMGB1, kindly provided by the Rauvala laboratory, Helsinki in pGEX-6P1-deltaHMGB1. Full length HMGB1 was optimised and synthesised by GenScript and supplied in pUC57 cloning vector. The gene insert was sub-cloned into pGS-21a as described in section 2.4.13. Both plasmids were transformed in to T7 Shuffle® K12 and expression carried out as described in section 2.6.1 with a number of variations. Induction took place at $O.D^{600nm}$ of 1.0 and expression was only allowed to continue for 2.5 hr before cells were pelleted and lysed as described in 2.6.3.

2.6.6 Perchloric acid extraction of HMGB1

All steps in this section were performed at 4°C except where otherwise specified. The cell pellet produced in section 2.6.3 was thawed out in a 25°C water bath for 10 minutes. For each gram of cell pellet, 3 mL of 6% perchloric acid solution was added and the cell pellet completely resuspended by vortexing. The mixture was centrifuged at *12,000 g* for 10 minutes and the supernatant transferred to a 15 mL centrifuge tube on ice. One part 10x 20 mM Tris (pH 7.4) containing 50 mM NaCl, 0.5 mM DTT and protease inhibitor cocktail (Roche) was added to 9 parts of the perchloric acid fraction, and the pH adjusted to 7.4 by adding 2 M NaOH drop-wise.

2.6.7 De-glycosylation of recombinant RAGE

Samples of conditioned culture media containing each RAGE construct were filtered using a 0.22 µm syringe filter before being concentrated to a final volume of 100 µL using an Amicon Ultra-4 centrifugal filter unit (nominal molecular weight limit of 3 kDa). Nine microliters of each RAGE construct was mixed with 1 µL of 10x glycoprotein denaturation buffer (New England Biolabs) and heated at 100°C for 10 minutes. The

mixture was allowed to cool at room temperature for 10 minutes before adding 2 µL of 10x G7 Reaction Buffer supplied with the glycosidase, 2 µL of 10% NP40, 10U of PNGaseF and 4 µL of high pure water. The mixture was incubated for 2 hours at 37°C. The reaction mixture was then prepared and run on an SDS PAGE gel as outlined in section 2.6.16.

2.6.8 Generation of ribose-AGE (Advanced Glycation End products)

A 5.4 mg/mL BSA in 400 mM sodium phosphate buffer (pH 7.4) containing 500 mM D(-) Ribose was filter-sterilised using a 0.22 µm syringe filter. The ribose-BSA solution was stored in a dark container at 37°C for 10 weeks as described in the method of Valencia *et al* (2004), before being separated into 0.5 mL aliquots and stored at -20°C until needed. AGE content was determined by taking optical measurements (OD^{405}) as previously described by Muench *et al* (2004).

2.6.9 Phenyl Sepharose® chromatography

All chromatography is performed at 4°C unless otherwise indicated. A 1 mL column pre-packed with phenyl Sepharose CL-4B (GE) was connected to a Bio-Rad Biologic FPLC and pre-equilibrated with 20 column volumes (CV) of 20 mM sodium phosphate buffer (pH 7.4) containing 150 mM NaCl, 1 mM DTT and 5 mM $CaCl_2$ (column buffer). The soluble fraction of T7 Shuffle® K12 induced to express S100B, S100P or S100A6 was supplemented with a working concentration of 5 mM $CaCl_2$ and applied to the column at 0.25 mL/min. The column was washed at 0.25 mL/min with 5-7 CV of column buffer or until a stable $O.D^{280nm}$ base line was reached. Bound protein was eluted by washing the column with column buffer plus 2 mM EGTA and collected in 1 mL fractions.

2.6.10 Heparin-Sepharose® affinity chromatography

Sample containing recombinant RAGE was filtered using a 0.45 µm syringe filter immediately before being applied to the chromatography column. A 5 mL pre-packed heparin Sepharose® HiTrap™ column (GE Healthcare) was connected to a Bio-Rad Biologic FPLC system and pre-equilibrated with 25 mL of 50 mM Tris-HCl buffer (pH 7.5) containing 50 mM NaCl and 1 mM DTT (binding buffer) at a flow rate of 1 mL/min. The recombinant RAGE samples were applied to the column at 0.5 mL/min with a single pass and the flow-through retained for analysis of unbound RAGE. The column was washed with 25 mL of binding buffer at a flow rate of 1 mL/min. The column was eluted at a

flow rate of 1 mL/min using binding buffer with different concentrations of NaCl in a step gradient as outlined in Table 6.

Table 6. Step gradient used for the elution of protein bound to a heparin-Sepharose® 1 mL column

Step	Concentration NaCl (mM)	Elution time (min)
1	50	15
2	150	15
3	250	15
4	500	15
5	1000	15

The column was regenerated by applying 10 mL of binding buffer containing 0.01% SDS, followed by 20 mL of binding buffer and 5 mL of 20% ethanol prepared in high pure water at 1 mL/min. The column was stored in 20% ethanol at 4°C until needed.

2.6.11 Size exclusion chromatography

A HiPrep 16/60 Sephacryl S-200 (GE) column was connected to an AKTA Purifier FPLC (GE) and equilibrated with 15 mL distilled water followed by 60 mL of 50 mM sodium phosphate buffer (pH 7.2-7.4) containing 150 mM NaCl and 1 mM DTT (wash buffer) at 0.5 mL/min. The sample to be fractionated was concentrated using an Amicon® Ultra centrifugal filter to 0.5-1 mL and injected onto the column using a 50 mL superloop (GE). The sample was washed through the column using wash buffer at 0.5 mL/min and eluates collected in 2 mL fractions.

2.6.12 Nickel Sepharose® affinity chromatography

A 1 mL pre-packed HisTrap HP column (GE Healthcare) was equilibrated with 10 column volumes (CV) of 20 mM Sodium Phosphate (pH 7.4) containing 500 mM NaCl, 25 mM imidazole and 1 mM DTT (buffer A) at a flow rate of 0.5 mL/min. Pooled heparin Sepharose® eluates containing RAGE were applied to the column at a flow rate of 0.25 mL/min and the flow through collected for analysis of unbound RAGE. The column was

washed with 10 CV of buffer A or until a stable $O.D^{280nm}$ base line was reached. The column was then eluted by washing the column with 10 CV of buffer A containing 250 mM imidazole at 0.5 mL/min. Eluates were collected in 1 mL fractions and RAGE content determined by ELISA (section 2.6.19). The column was regenerated after 4-5 purifications at a flow rate of 0.5 mL/min using 10 mL of buffer C containing 50 mM EDTA, followed by 10 mL of distilled water. The resin was recharged with nickel by injecting 1 mL of 100 mM $NiSO_4$ onto the column and incubating for 10 minutes. The column was washed with 10 mL of distilled water and stored in 20% ethanol at 4°C.

2.6.13 Glutathione S-transferase affinity chromatography

A 1 mL prepacked GSTrap column (GE) was connected in-line with a Bio-Rad Biologic FPLC system and equilibrated with 5 column volumes of 25 mM sodium phosphate (pH 7.4) containing 140 mM sodium chloride, 2.7 mM potassium chloride and 1 mM DTT (wash buffer). Clarified cell lysates from bacteria expressing recombinant protein in pGEX-6P vectors were prepared as described in section 2.6.3, ensuring the protease cleavage site is in-frame. The sample was applied to the column at a flow rate of 0.3 mL/min with the system housed in a refrigerated cabinet at 4°C. The column was then washed with 5 column volumes of wash buffer and the flow through collected in 1 mL fractions at a flow rate of 1 mL/min. The system was paused and the GSTrap column carefully removed. Using a syringe, 20U of PreScission Protease in wash buffer was added to the column, with a 1 mL HisTrap column connected in series to the bottom of the GSTrap to bind the protease upon elution. Both columns were re-connected to the FPLC system and left for 4 hours at 4°C. The system was resumed at a flow rate of 0.5 mL/min and the eluates collected in 1 mL fractions.

2.6.14 Bradford microtitre protein assay

Bio-Rad Bradford 1x dye solution was gently inverted to ensure it was evenly mixed before 150 µL of the dye was added to 150 µL of sample or standard in triplicate in wells of a 96-well microtitre plate. The plate was gently mixed on a plate shaker for 5 minutes at room temperature, and read in a microplate reader at a 595 nm wavelength. The concentration of samples was determined relative to the standards loaded on the plate.

2.6.15 Modified Lowry protein assay

Assay samples were diluted to a total volume of 1 mL with ddH2O and mixed with 100 µL of sodium deoxycholate (1.5 mg/mL). The diluted samples were vortexed before being left to stand for 10 minutes at 22°C. To each sample, 100 µL of 72 % w/v trichloroacetic acid was added before the solution was left to stand at 22°C for 10 minutes. The samples were subsequently centrifuged at *11,000 g* for 15 minutes and the supernatant aspirated off to leave the pellet. The pellet was suspended in 1 mL of Lowry reagent for 30 minutes at 22°C. Folin & Ciocalteaus phenol reagent (0.5 mL) was then added to each tube with vigorous mixing, and the samples again left at 22°C for 30 minutes. The absorbance of each sample was measured at 660 nm using a Shimadzu UVmini-1240 UV-Vis spectrophotometer. The sample absorbance readings were compared against a bovine serum albumin standard curve.

2.6.16 Denaturing polyacrylamide gel electrophoresis (SDS-PAGE)

A 4-16 % pre-cast polyacrylamide gel was placed into a Bio-Rad™ electrophoresis tank filled with 25 mM Tris-HCl (pH 8.3) containing 250 mM glycine and 0.1 % SDS. The first well was loaded with 10 µL of a broad range pre-stained molecular weight marker. Samples to be run on the gel were prepared by mixing 10-15 µL of starting material that was made up to 20 µL using 25 mM Tris-HCl, (pH 8.3) containing 6 % SDS, 20 % glycerol, 0.05 % bromophenol blue and 200 mM dithiothreitol. This mixture was heated for 5 minutes at 99°C before being loaded onto the gel. The gel was run at 90 V (constant current) for approximately two hours, or until the dye front reached the base of the gel.

2.6.17 Coomassie staining of SDS-PAGE gel

A Coomassie staining solution was prepared by dissolving 0.4 g of Coomassie blue R350 in 200 mL of 40% (v/v) methanol in distilled water. The staining solution was filtered through Whatman filter paper before adding 200mL of 20% (v/v) acetic acid. The staining solution had a final concentration of 0.1% (w/v) Coomassie blue R350, 20% (v/v) methanol, and 10% (v/v) acetic acid. Destaining solution stock consisted of 50% (v/v) methanol and 10% (v/v) acetic acid. Following completion of PAGE (section 2.6.16), the precast gel was removed from the plastic cassette and immediately placed into a solution comprising 50% stain and 50% destain solutions so that the gel was completely covered. The gel was allowed to stain overnight with gently agitation at room temperature. The staining mixture was poured off and replaced with 100% of the

destain solution. This was replaced every 30 minutes or when needed until the desired level of clarity was achieved. The gel was wrapped in plastic film and stored at 4°C until needed.

2.6.18 Western blot

An SDS-PAGE gel prepared as described in section 2.6.16 was immediately placed into ice-cold 1.25 M glycine (pH 8.3), containing 0.125 M Tris, 0.1 % SDS and 20 % methanol (transfer buffer) for 15 minutes at 22°C. A sheet of PVDF membrane and two pieces of 3M filter paper were cut so that they were just larger than the polyacrylamide gel. The PVDF membrane was then rinsed for 5 seconds in methanol, followed by two 30-second washes in 100 mL high pure water. The membrane was then left in transfer buffer until needed. All components were pre-washed with transfer buffer before being placed into the PAGE transfer sandwich. The transfer sandwich assembly was then loaded into an electrophoresis transfer tank filled with ice-cold transfer buffer. The entire unit was placed on ice to maintain the temperature below 4°C. A small magnetic stirrer was placed into the electrophoresis tank and gently rotated for the duration of the run. The transfer was run at a constant current of 90 V for 75 minutes. The primary antibody was prepared by diluting the antibody stock 100-fold in 0.125 M Tris (pH 8.0) containing 5 % w/v skim milk powder, 0.15 M NaCl and 0.05 % Tween-20. The primary antibody solution was kept at 4°C until needed. Once the transfer was completed, the PVDF membrane was removed from the transfer sandwich and placed in 15 mL of 0.125 M Tris (pH 8.0) containing 5 % w/v skim milk powder, 0.15 M NaCl and 0.05 % Tween-20 (blocking buffer) for 60 minutes at 4°C with gentle shaking. The membrane was then placed into a shallow tray containing the primary antibody solution and incubated over night at 4°C with gentle shaking. Following this, the membrane was washed 3 times for 10 minutes in 15 mL of blocking buffer at 4°C. The secondary detection antibody conjugated to alkaline phosphatase was diluted in blocking buffer according to the manufacturer directions. The PVDF membrane was incubated in 20 mL of this solution with gentle agitation for 45 minutes at 22°C. The membrane was again washed three times for ten minutes in blocking buffer. The colorimetric reaction solution was prepared by mixing 800 µl of 25 x alkaline phosphatase colour development buffer (Bio-Rad™), with 200 µl of Solution A (Bio-Rad™), 200 µl of Solution B (Bio-Rad™) and 10 mL of colour reaction buffer (Bio-Rad™). The membrane was washed for 10 minutes with 10 mL of the colorimetric reaction solution until the desired band intensity was

achieved. The membrane was washed with high pure water to stop the colour development, and the membrane was air dried for two hours at room temperature.

2.6.19 RAGE enzyme-linked immunosorbent assay (ELISA)

A mouse anti-human extracellular RAGE domain capture antibody (R&D Systems) was reconstituted in phosphate buffered saline (pH 7.4) to 180 µg/mL and a biotinylated goat anti-human RAGE detection antibody (R&D Systems) was reconstituted in phosphate buffered saline (pH7.4) (PBS) to 36 µg/mL. The capture antibody was further diluted to a working concentration of 1 µg/mL and 100 µL added to each well on a 96-well NUNC Maxisorp plate. The antibody was left to stand overnight at room temperature to adsorb to the well surface. The wells were washed three times with PBS containing 0.05% Tween-20 (wash buffer) and blocked with 300 µL of phosphate buffered saline (pH 7.4) containing 2% BSA (reagent diluent) for 2 hours at room temperature. The wells were aspirated and 100 µL of sample containing RAGE was added to each well. The plate was incubated at room temperature for 2 hours before being carefully washed three times with 300 µL of wash buffer per well. A 100 µL aliquot of biotinylated goat anti-human RAGE detection antibody was incubated with each well for 2 hours at room temperature. The wells were subsequently washed three times with 300 µL of wash buffer before 100 µL of Streptavidin-Horse Radish Peroxidase (HRP) conjugate was added and allowed to bind to the detection antibody for 20 minutes at room temperature. Each well was then washed three times with 300 µL of wash buffer before 100 µL of TMB containing HRP substrate chromogen was added to each well. The plate was allowed to sit for a maximum of 20 minutes at room temperature or until sufficient colour development was observed. Colour development was stopped by adding 50 µL of 2N sulphuric acid to each sample. Wells were read at 450 nm on a microplate reader and compared to a human RAGE standard (R&D systems).

2.7 Receptor-Ligand Binding and Kinetic Evaluation

2.7.1 AGE-RAGE colorimetric microwell binding assay

RAGE ligand was diluted in 20 mM phosphate buffer (pH 7.4) containing 150 mM NaCl and 1 mM DTT (PBS) to a working concentration of 20 µg/mL. A 100 µL aliquot was added to each well of a 96-well NUNC Maxisorp plate and allowed to adsorp at 4°C overnight. The wells were aspirated and blocked with 300 µL of PBS containing 1% BSA

w/v (reagent diluent) for two hours at room temperature. The wells were again aspirated and washed three times with 150 µL of reagent diluent. RAGE recombinant protein was serially diluted in reagent diluent to 300 nM, 200 nM, 100 nM, 50 nM, 30 nM and 15 nM. A 100 µL of each RAGE concentration was added in triplicate to the ligand coated wells and the plate left overnight a 4°C to allow binding to reach equilibrium. Each well was carefully washed three times with 100 µL of ice-cold reagent diluent and 100 µL of goat anti-human RAGE polyclonal antibody conjugated to horse radish peroxidase added to each well and left to incubate for four hours at 4°C. The wells were then aspirated and washed three times with 300 µL of ice cold reagent diluent. A 100 µL of TMB+ substrate was added to each well and the plate left to develop for a maximum of 20 minutes at room temperature or until sufficient colour was present. Colour development was stopped by adding 50 µL of 2 N sulphuric acid to each well. The plate was read at 450 nm on a Bio-Rad 3550 micro plate reader and compared to a human RAGE standard (R&D systems) developed on the same plate.

2.7.2 Circular dichroism (CD)

Prior to all CD experiments, all protein constructs were dialyzed into 10 mM phosphate buffer (pH 7.4) to remove interfering additives. The CD instrument used for this experiment was a JASCO J-815 spectropolarimeter. All runs were performed with standard sensitivity (100 mdeg), data pitch of 1 nm, continuous scanning mode with speed of 100 nm/min, response of 1 s and band width of 1 nm. Absorbance was monitored over the range of 260-185 nm. A 10 mm path length rectangular Spectrosil(R) Quartz cuvette (Starna®) was blanked over 5 accumulated scans using 400 µL of 10 mM phosphate buffer (pH 7.4). CD measurement of proteins was conducted in the same solution as the blank and the CD absorption spectrum was accumulated over five scans. The secondary structure components of the protein constructs were evaluated using online analysis website DichroWeb [DichroWeb references] with an optimized wavelength range of 185-240 nm used as reference. CONTIN, a ridge regression method was used for analysis, generating a linear combination of known spectra of reference proteins with known conformations. Only reference proteins with similar spectral characteristics were used to give a best fit for the sample. A Normalized Root Mean Square Deviation (NRMSD) value is given as a parameter to determine whether the Circular Dichroism profile is reliable.

2.7.3 Beta amyloid 1-42 preparation for surface plasmon resonance immobilisation

Human synthetic beta amyloid 1-42 (Aβ42) peptide was purchased from W.M. Keck Biotechnology Resource Laboratory. Stock Aβ42 was prepared by dissolving lyophilised peptide in 10% dimethyl sulfoxide (DMSO) to a concentration of 1 mg/ml. The stock was diluted in 0.01 M HEPES buffered saline (pH 7.4) containing 3 mM EDTA, 0.15 M NaCl, and 0.005% vol/vol surfactant polysorbate 20 (P20)) (HBS) to a working concentration of 10 ng/mL immediately before use to ensure monomeric and not aggregated Aβ42 was the principal form immobilised.

2.7.4 Surface plasma resonance

A Biacore 3000 and Biacore T200 were used for all surface plasma resonance methods referred to within this thesis. A CM5 amine coupling chip (GE Healthcare) was prepared using flow cell 1 and or 3 as blank surfaces. The blank cell was prepared using the built-in method in which the dextran matrix was activated by passing a mixture of 0.4 M N-ethyl-N'-(3-dimethylaminopropyl) carbodimide hydrochloride (EDC) and 0.1 M N-hydroxysuccinimide (NHS) across the flow cell. Following esterification of the dextran matrix, the chip surface was blocked by passing 1 M ethanolamine hydrochloride-NaOH (pH 8.0), across the flow cell for three minutes at a flow rate of 5 µL/min. Where beta-amyloid was to be immobilised as the target ligand, a scrambled beta-amyloid 42 amino acid peptide was first immobilised to flow cells 1 and 3. Any remaining unreacted sites where then blocked with 1 M ethanolamine hydrochloride-NaOH (pH 8.0), across the flow cell for three minutes at a flow rate of 5 µL/min. The chip was washed with 10 mM sodium acetate buffer (pH 5.0) containing 1 M NaCl for 30 seconds at 30 µL/min to remove any non-specific binding of blocking agent.

RAGE constructs or RAGE ligands were immobilised to cells 2 or 4 following their activation using a mixture of 0.4 M EDC and 0.1 M NHS as per the blank cell surfaces. For insect expressed RAGE SPR binding assays, mouse Anti-V5 monoclonal antibody (Invitrogen™) was diluted to a working concentration of 1 µg/mL in degassed 10 mM sodium acetate buffer (pH 5.0). The antibody mixture was passed across the activated flow cell using an adaptive immobilisation strategy at 5 µL/min until 300 response units (RU) was achieved. For all other SPR assays with other RAGE ligands, a working concentration of 100 ng/mL was prepared in the running buffer immediately before immobilisation. Where less than 10 RU cell loading was required, as was the case with beta-amyloid, samples were prepared at 10 ng/mL. Following immobilisation of ligand,

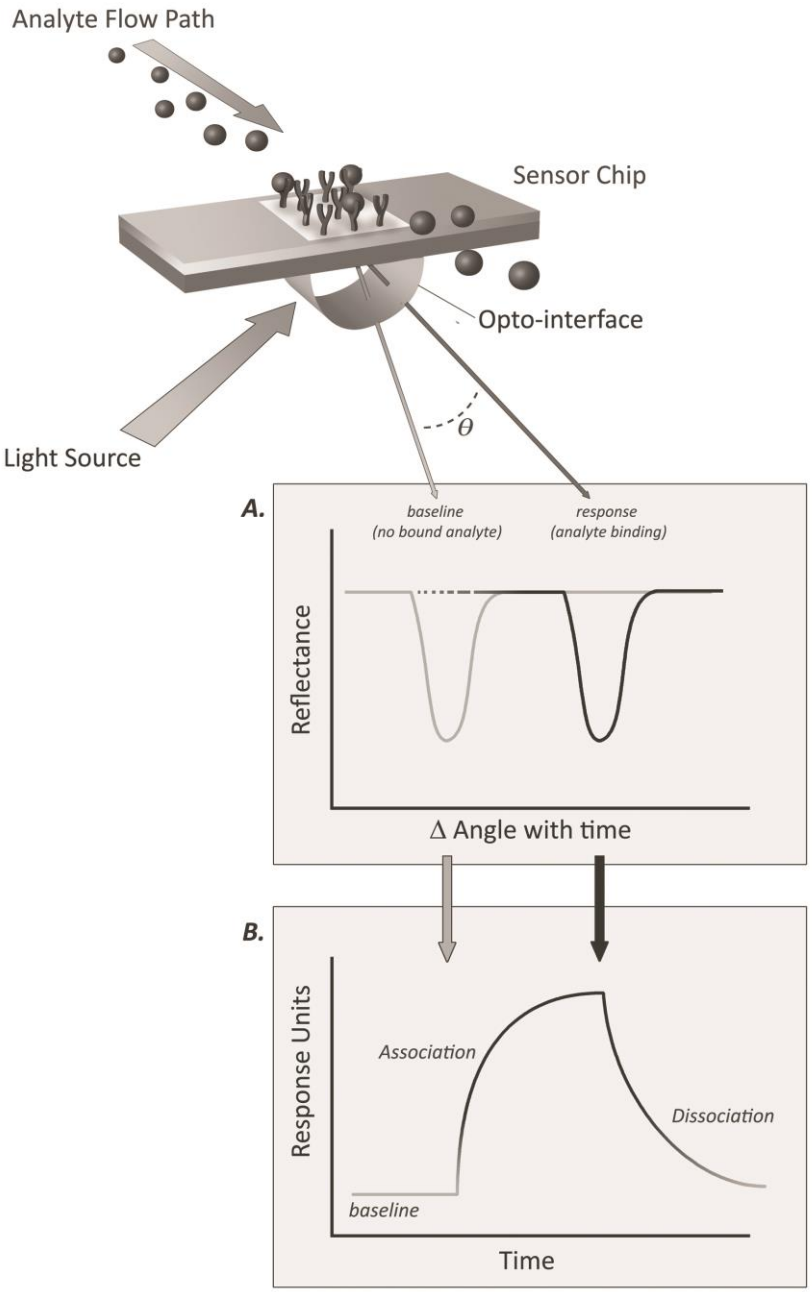

Figure 8. Principles of surface plasmon resonance (SPR).

A molecule (ligand) is immobilised to a dextran matrix while a second molecule in solution (analyte) is passed across the surface. As analyte binds, the change in reflectance at the opto-interface **a**) is directly proportional to the change in mass at the chip surface and recorded as response units **b**). Where an already captured analyte dissociates and immediately rebinds (avidity) or is simultaneously bound by a second ligand molecule, no change in mass or response units is registered.

as per the blank cells, remaining unreacted sites on the surface was blocked by passing 1 M ethanolamine hydrochloride-NaOH (pH 8.0) across the flow cell at 5 µL/min for three minutes. Unreacted ethanolamine was eluted by passing 10 mM sodium acetate buffer (pH 5.0) containing 1 M NaCl across the flow cell at 30 µL/min for 30 seconds. The flow cell was then pre-equilibrated with 0.01 M HEPES buffered saline (pH 7.4) containing 3 mM EDTA, 0.15 M NaCl, and 0.005% vol/vol surfactant P20) (HBS) in preparation for binding and kinetic assays. Where binding required the presence of divalent cation co-factors such as Ca^{2+}, HBS without EDTA was used (HBS-N).

2.7.5 Surface plasma resonance multi-cycle and single-cycle kinetics analysis

Both single and multi-cycle analysis of surface plasmon resonance response data utilise measurements across a range of analyte concentrations. The predominant difference is that single-cycle kinetics involves the sequential injection of increasing concentrations of analyte without the need to regenerate the chip surface between cycles. Single-cycle kinetic method increase the likelihood for slow interactions to approach equilibrium and are significantly shorter in total run time due to removal of intermediate regeneration steps. However, it is more sensitive to drift due to the long cycle duration and is limited in the complexity of interactions that it is appropriate for. The multicycle method regenerates the chip surface between cycles, removing all bound analyte before injecting another sample. This method is therefore significantly longer and may degrade the immobilised molecule through exposure to harsh regeneration conditions, however, it is the traditional format for investigating kinetics of interaction by surface plasmon resonance analysis.

For single-cycle, five concentrations of analyte are prepared in series in 10 mM HEPES (pH 7.4) containing 150 mM NaCl, 3 mM EDTA and 0.005% v/v Surfactant P20 (HBS-EP). A start-up cycle injects HBS-EP three times in place of sample to equilibrate the system followed by regeneration of the chip surface with 10 mM NaOH for 10 seconds. Sample is injected in sequence from the lowest to highest concentration without intermediate regeneration. Samples are injected across immobilised flow cells at 30 µL/min and allowed to associate for 120 seconds with no stabilisation period. Following the injection of all five sample concentrations, bound analyte is allowed to dissociate for 600 seconds before the surface is regenerated by the injection of 10 mM NaOH through the flow path.

Multi-cycle analysis involved the preparation of 5-12 concentrations of a sample molecule such as RAGE VC_1C_2 for use as an analyte. The system is first equilibrated by injecting HBS-EP across the flow path for association/dissociation times of 120 seconds and 600 seconds respectively before being regenerated using 10 mM NaOH. This is repeated for all samples with two being performed in duplicate. Following the association and dissociation of each sample, the flow path is regenerated by injecting 10 mM NaOH across the flow path for 10 seconds. All models of interaction are designed and fitted using Biaevaluate 4.0 (GE).

3.0 RESULTS

3.1 Development of human RAGE insect cell expression constructs

3.1.1 Verification of full length human RAGE in pcDNA3 plasmid

The gene encoding full length human RAGE was provided in a mammalian expression vector, pcDNA3 (Invitrogen™). Sequencing primers for pcDNA3 were used to amplify the insert to confirm the presence of the full length gene (section 2.4.11). A product of approximately 1400 bp was observed following agarose gel electrophoresis, correlating with an expected size of 1364 bp (Figure 9).

3.1.2 Transformation of TOP10 E. coli with pcDNA3-hRAGE

The pcDNA3-hRAGE plasmid was transformed into chemically competent TOP10 *E. coli* for the purpose of plasmid replication. Whole-cell PCR amplification (section 2.4.5) of individual colonies was performed using RAGE forward primer F1 in combination with reverse primer R2 (Table 1) to ensure that the plasmid containing hRAGE was retained by transformed cells. All six colonies selected displayed a PCR product of approximately 650 bp, corresponding with the expected product of 687 bp (Figure 10). These PCR amplicons confirmed the presence of pcDNA3-RAGE and the presence of the RAGE leader sequence, to which the F1 forward primer is complementary.

3.1.3 Amplification of RAGE extracellular domains V, VC_1 and VC_1C_2

Purified pcDNA3-hRAGE plasmid was used as template in the PCR amplification of gene segments encoding the V, VC_1 and VC_1C_2 RAGE extracellular domains (section 2.4.11) (Figure 11). Primer combination F1-pR1 (lane 2) produced a band representing the RAGE V domain, while F1-R2 amplified the VC_1 domains (lane 3) and F1-R3 amplified extracellular domains VC_1C_2 (lane 4) (Table 1). The three products resolved using a 1.2% agarose gel were approximately 350 bp (lane 2), 700 bp (lane 3), and 950 bp (lane 4) (Figure 11). These products correspond with the expected sequence lengths of 351 bp for the V domain, 687 bp for VC_1, and 936 bp for VC_1C_2. No other PCR products were present, confirming the suitability of the primers and product for sub-cloning.

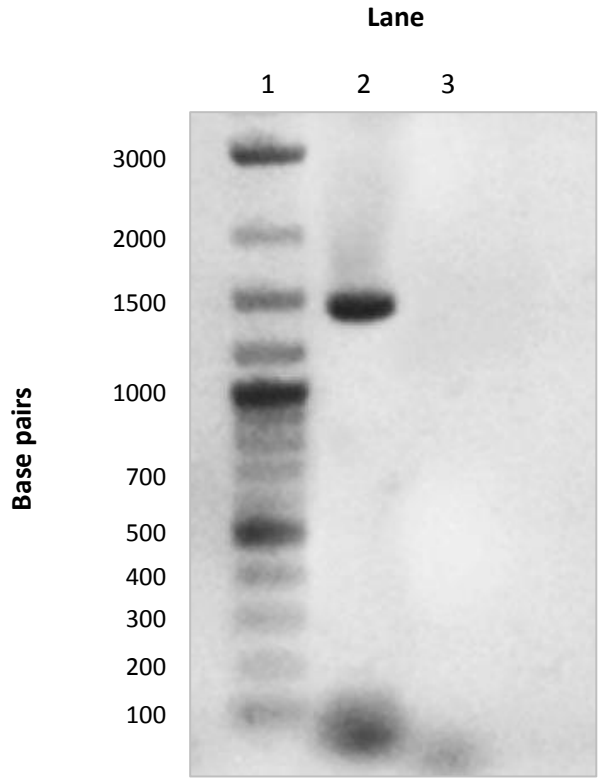

Figure 9. Amplification of the full length gene encoding human RAGE.

Mammalian expression plasmid pcDNA3 (Invitrogen™) containing the gene for human RAGE (hRAGE) was amplified using forward and reverse pcDNA3 sequencing primers (lane 2). A negative control without template was also amplified (lane 3). The reaction products were run on a 1.2% agarose gel against a log-2 (New England Biolabs®) base ladder (lane 1).

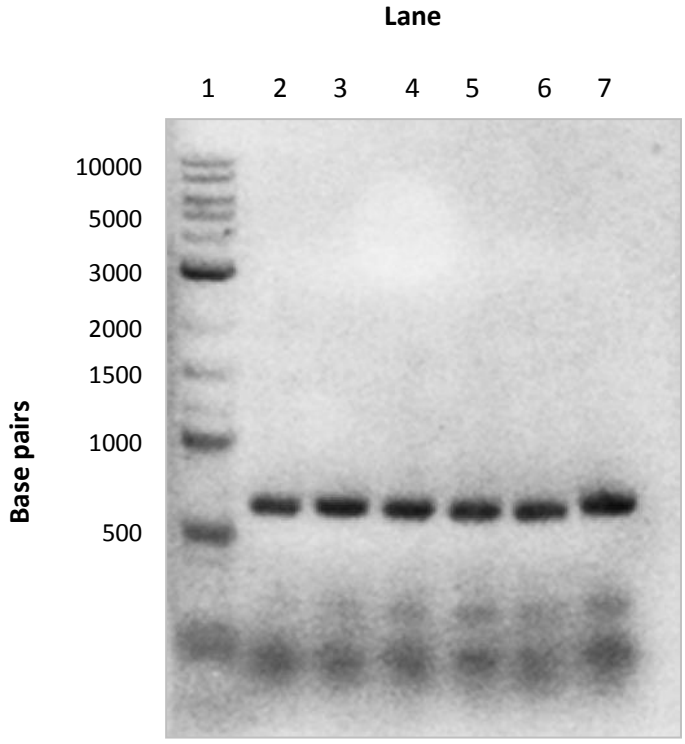

Figure 10. Selection of TOP10 *E. coli* transformed with pcDNA3-hRAGE by PCR.

TOP 10™ *E. coli* transformed with pcDNA3-hRAGE were cultured on LB + Amp agarose (section 2.4.4). Whole cell PCR screening of six colonies chosen at random was carried out with amplification products representing colonies 1-6 respectively (lanes 2-7), run on a 1.2% agarose gel against a log-2 base ladder (lane 1) (New England Biolabs®) as described in section 2.4.9.

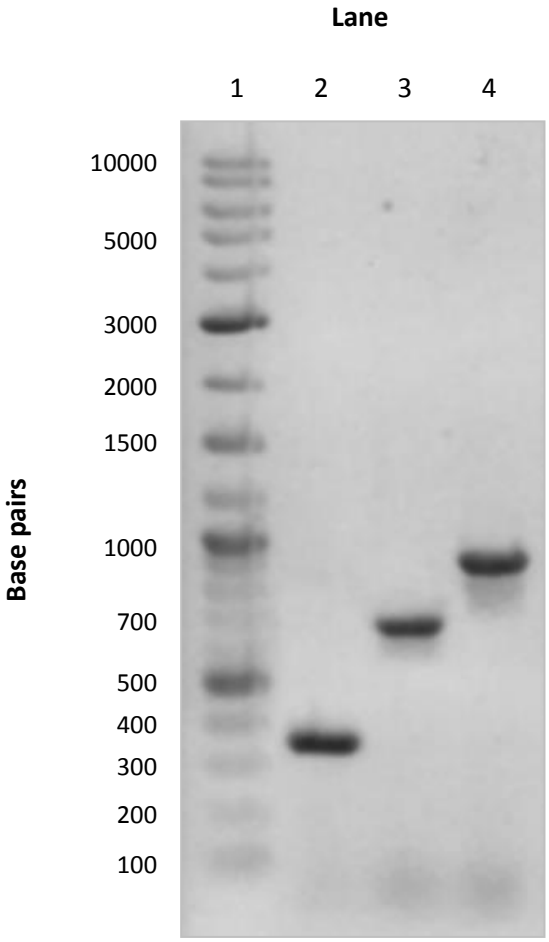

Figure 11. Amplification of human RAGE extracellular domains V, VC_1 and VC_1C_2.

Purified pcDNA3-hRAGE was used as a template in PCR reactions amplifying the V (lane 2), VC_1 (lane 3) and VC_1C_2 (lane 4) extracellular domains of RAGE as described in section 2.4.11. PCR products were visualised on a 1.2% agarose gel as outlined in section 2.4.9. A log-2 base pair ladder (New England Biolabs®) was loaded in lane 1 to help approximate product size.

3.1.4 Identification of transformed TOP10 colonies containing correctly oriented RAGE domain inserts in pIB/V5-HIS TOPO®

Following successful amplification of the RAGE V, VC_1 and VC_1C_2 extracellular domain segments, the PCR products were cloned into an insect pIB/V5-HIS expression vector as described in section 2.4.12. Identification of colonies containing vector with product inserted in the correct orientation was performed by whole cell PCR using pIB/V5 forward sequencing primer (Invitrogen™) and reverse primers R1, R2 and R3 for V_1, VC_1 and VC_1C_2 respectively. Of the colonies containing the RAGE V domain, colony 10 in lane 11 (Figure 12) resulted in a PCR product of approximately 450 bp, with this domain construct having a transformation efficiency of $1.25x10^5$ cfu/µg DNA. Colonies 1, 2 and 7 in lanes 2, 3 and 8 respectively (Figure 13) were transformed with pIB/V5-HIS-VC_1, producing a PCR product of approximately 800 bp, with a transformation efficiency of $3.12x10^3$ cfu/µg DNA. RAGE pIB/V5-HIS-VC_1C_2 had the lowest transformation efficiency of $9.24x10^2$ cfu/µg DNA, with only colony 25 having a gene insert in the correct orientation (Figure 14). All positive colonies were sent for sequencing. Both the V and VC_1C_2 single colonies were confirmed as containing the correct RAGE construct sequences. Colonies 1 and 7 containing VC_1 both returned correct sequences. Colony 2 (lane 3, Figure 13) of the positive pIB/V5-HIS-VC_1 transformants was discarded due to the presence of a single point mutation in the V domain that resulted in an amino acid shift. This finding is surprising because the V domain had the highest rate of transformation with only 6% of colonies ligating in the correct orientation. The VC_1 and VC_1C_2 constructs had 43% and 4% respectively of colonies with inserts in the correct orientation.

3.2 Development of RAGE and ligand constructs for prokaryote expression

3.2.1 PCR amplification of synthetic RAGE V, VC_1 and VC_1C_2 domain constructs optimised for prokaryote expression.

Human RAGE V, VC_1 and VC_1C_2 domain constructs were optimised for prokaryote expression by modifying codon bias, GC content and possible secondary structures using the GenScript OptimumGene™ algorithm. The gene sequences were synthesised by GenScript and provided in pUC57 vectors, which were used as PCR template. Single bands of approximately 300, 600 and 1000 bp were visible following PCR amplification

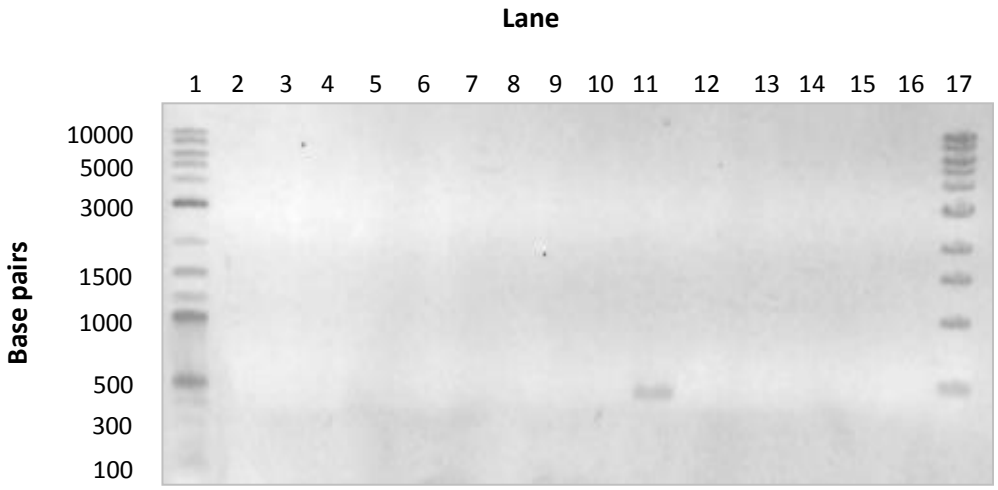

Figure 12. PCR screening of TOP10 *E. coli* transformed with pIB/V5-hRAGE-V.

TOP10 *E. coli* were transformed with pIB/V5-HIS TOPO® insect expression vector (Invitrogen™) containing a human RAGE V domain insert. Transformants were plated on selective LB agarose plates (section 2.4.4) and 15 randomly selected colonies screened by whole-cell PCR (section 2.4.5). PCR reaction mixtures were loaded into lanes 2-16 of a 1.2% agarose gel along with a log-2 base pair ladder (New England Biolabs®) (lane 1) and then visualised (section 2.4.9).

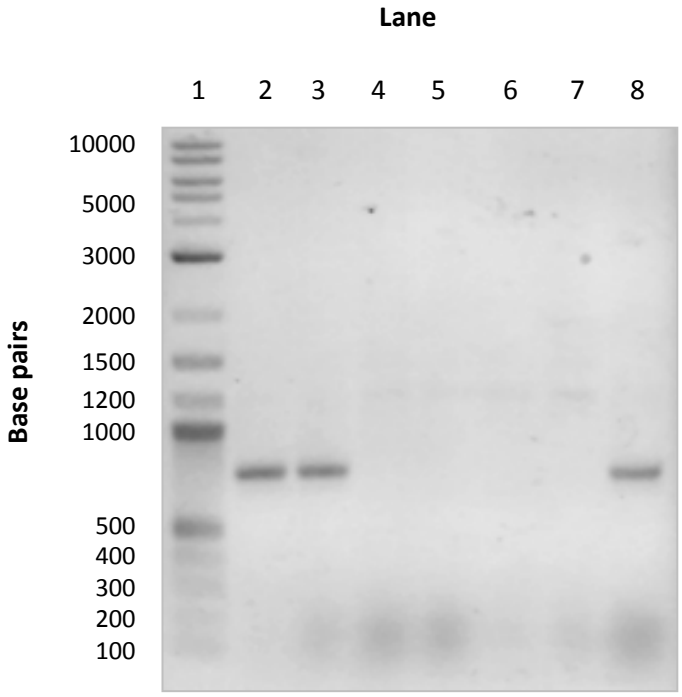

Figure 13. PCR screening of TOP10 *E. coli* transformed with pIB/V5-hRAGE-VC_1.

TOP10 *E. coli* were transformed with pIB/V5 insect expression vector (Invitrogen™) containing extracellular RAGE domains VC_1 (sections 2.4.2 and 2.4.12). The transformation mixture was spread over a selective agarose media (section 2.4.4). Seven colonies were picked at random and screened by PCR using pIB forward sequencing vector and the RAGE-VC_1 reverse primer (R2) for correct insert orientation (section 2.4.5, Table 1). The PCR reactions representing the seven colonies were loaded in wells 2-8 respectively on a 1.2% agarose gel alongside a log-2 base ladder (lane 1) (New England Biolabs®). The gel was run and visualised as described in section 2.4.9.

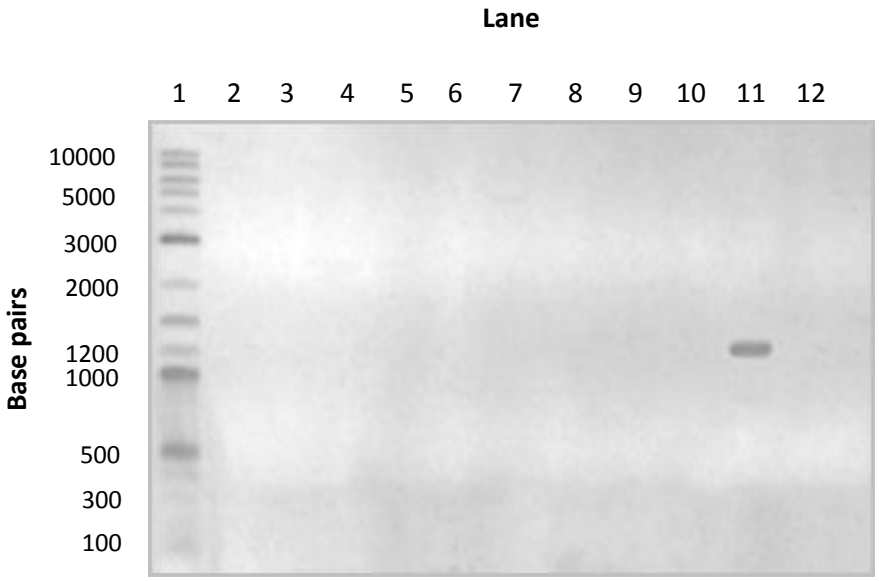

Figure 14. PCR screening of TOP10 *E. coli* transformed with pIB/V5-hRAGE-VC_1C_2.

TOP10 *E. coli* were transformed with pIB/V5 insect expression vector (Invitrogen™) containing hRAGE-VC_1C_2 and grown on selective media (section 2.4.4). A 20 µL pipette tip was used to transfer randomly selected colonies into separate PCR reaction mixtures containing pIB/V5 forward sequencing vector (Invitrogen™) and RAGE-VC_1C_2 reverse primer (R3) (section 2.4.5, Table 1). This was repeated for 24 colonies. PCR product for colonies 16-26 were loaded into lanes 2-12 respectively of an 1.2% agarose gel, alongside a log-2 base ladder (lane 1) (New England Biolabs®), and visualised according to section 2.4.9.

for pUC57-RAGE_V, pUC57-RAGE_VC_1 and pUC57-RAGE_VC_1C_2 respectively, closely approximating the theoretical sizes of 312 (V), 666 (VC_1) and 957 (VC_1C_2) base pairs (Figure 15). The pUC57 plasmids containing the RAGE inserts were subsequently digested with XbaI and HindIII with the gene fragments sub-cloned into pGS-21a as described in section 2.4.13.

3.2.2 PCR amplification of TOP10 E. coli transformed with RAGE V, VC_1 and VC_1C_2 domain constructs containing the native gene sequences.

Synthetic human RAGE V, VC_1 and VC_1C_2 domain constructs were sub-cloned into pGS-21a and used to transform TOP10 *E. coli* as outlined in method 2.4.13. To identify colonies with the RAGE gene insert, RAGE/vector primers were used in whole-cell PCR screening of transformants according to section 2.4.5. All five colonies transformed with the V-domain had a single band of approximately 500 bp, with colonies 8, 9, 11 and 12 (RAGE-VC_1) and 14, 15, 18 (RAGE- VC_1C_2) all producing a single band of 850 and 1150 bp, respectively (Figure 16). Factoring in the additional 160 bp added by the sequencing primer, these bands approximated the expected size of RAGE V, VC_1 and VC_1C_2. The percentage of positive clones followed the standard dogma of decreasing sub-cloning efficiency as the insert size increases with 100%, 80% and 60% of clones positively identified to contain their respective V, VC_1 and VC_1C_2 inserts (Figure 16). Similarly the canonical sequence for the identical gene segments encoding V, VC_1 and VC_1C_2 were synthesised with the same XbaI and HindIII digest sites. Following sub-cloning and preliminary screening, one positive clone for each domain construct was used as PCR template in whole-cell amplifications of the complete V, VC_1 and VC_1C_2 insert. Figure 17 shows the presence of three single bands that each correspond with the expected size of the three domain constructs, confirming that a single insert approximating the expected gene size is present in each clone. Sequencing of the pGS-21a-nativeV, pGS-21a-nativeVC_1 and pGS-21a-nativeVC_1C_2 confirmed that the inserts had ligated and replicated without error when compared to Genbank accession number AB036432 and the sequence submitted to GenScript.

3.2.3 Verification of the truncated HMGB1 gene insert in expression vector pGEX-6P1.

Plasmid pGEX-6P1-deltaHMGB1 (ΔHMGB1) was kindly supplied by Dr Rouhiainen (University of Helsinki, Finland). A restriction digest was performed as described in section 2.4.7 to quickly confirm the presence of HMGB1 in the pGEX-6P1 vector.

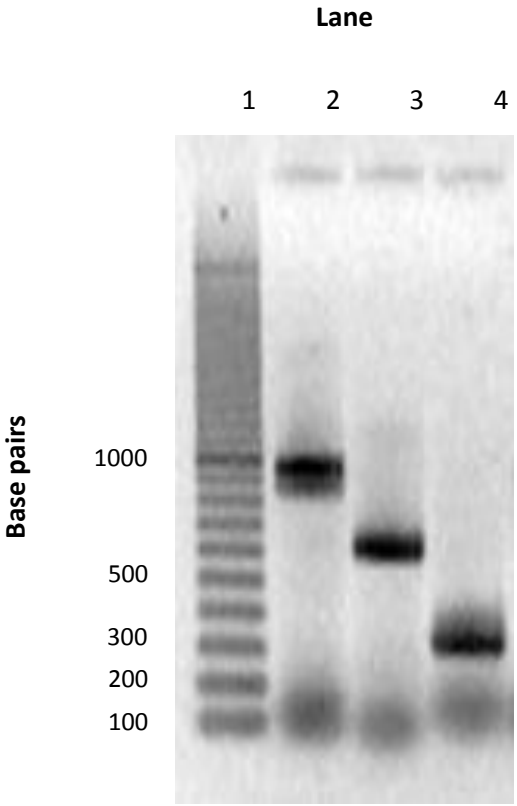

Figure 15. PCR amplification of prokaryote optimised human RAGE V, VC_1 and VC_1C_2 domain constructs.

The sequence for human RAGE V, VC_1 and VC_1C_2 domain constructs was optimised for prokaryote expression, synthesised and provided in a pUC57 plasmid by GenScript. To confirm the identity of the gene inserts, primers specific to the three domains were used to amplify each construct. Lane 1 was loaded with a 100 bp ladder (Fisher Biotec), with VC_1C_2, VC_1 and V PCR product loaded into lanes 2, 3 and 4 respectively on a 1.2% agarose gel and visualised by translumination.

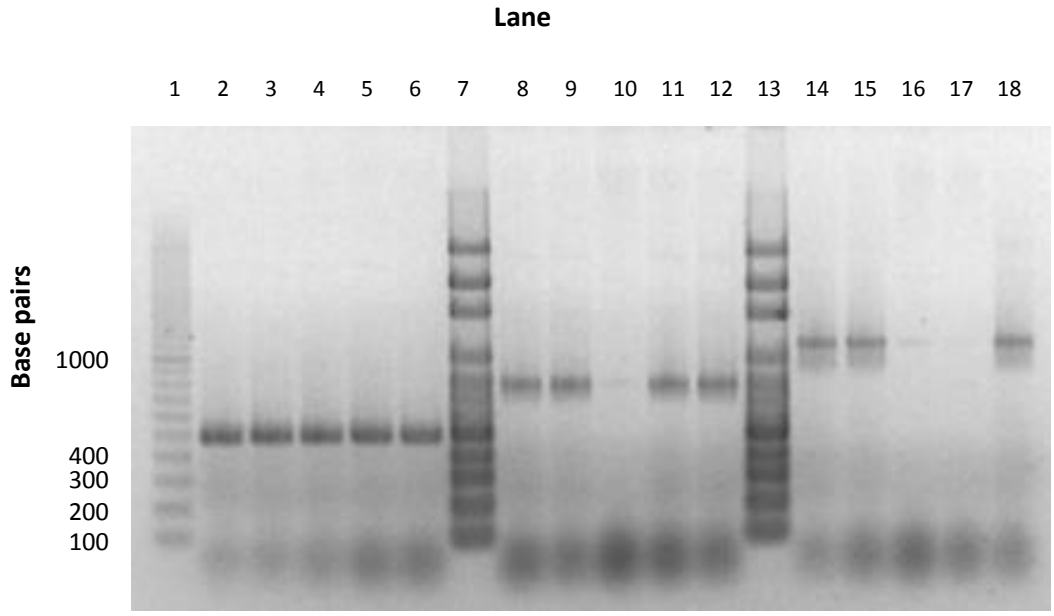

Figure 16. Whole cell PCR screening of TOP10 *E. coli* transformed with RAGE domain constructs sub-cloned into pGS-21a expression vector.

Cloning vector pUC57 containing optimised synthetic human RAGE V, VC_1 and VC_1C_2 gene sequences were sub-cloned into pGS-21a expression vector and subsequently transformed into TOP10 *E. coli* as described in sections 2.4.13 and 2.4.2. Transformants were screened by whole cell PCR for the presence of V, VC_1 and VC_1C_2 gene inserts (section 2.4.5). PCR product from five V, VC_1 and VC_1C_2 transformants was loaded into wells 2-6, 8-12 and 14-18 respectively on a 1.2% agarose gel. Lane 1 was loaded with a 100 bp ladder (Fisher Biotec). The gel was visualised as described in section 2.4.10.

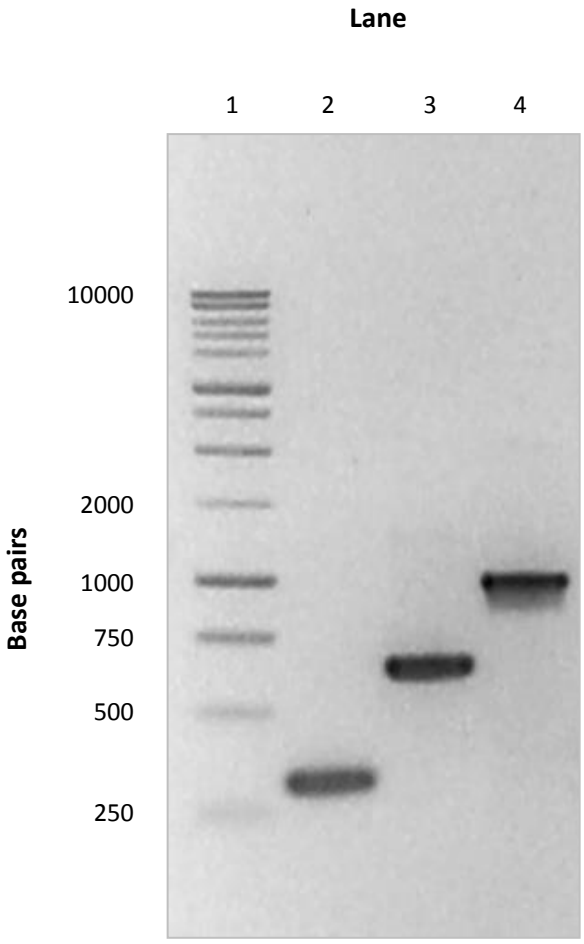

Figure 17. Amplification of native gene sequences for human RAGE extracellular domains V, VC_1 and VC_1C_2 in pGS-21a expression vector.

TOP10 *E. coli* transformed with pGS-21a containing the canonical sequences for human RAGE domains V, VC_1 and VC_1C_2 was used as template in whole cell PCR reactions (section 2.4.5). Primers designed to amplify each of the RAGE gene inserts end-to-end were used, with the reaction products for V, VC_1 and VC_1C_2 loaded into lanes 2, 3 and 4 respectively on a 1.2% agarose gel. A 1kb DNA ladder (Promega) was loaded into lane 1 to allow estimation of PCR amplicon sizes.

Two products of approximately 290 bp and 3900 bp (Figure 18) were visualised following electrophoresis of the digest mixture on a 1.2% agarose gel (section 2.4.9), correlating with expected digest products based on sequence analysis. PCR amplification of truncated human HMGB1 was performed using the forward and reverse primers described in section 2.4.7 with pGEX-6P1-deltaHMGB1 used as template. PCR product was visualised on a 1.2% agarose gel, with a single PCR product of approximately 380 bp visible in lane 3, alongside a negative control in lane 2 and a 100 bp DNA ladder in lane 1 (Figure 19). A product of 374 bp was expected for HMGB1 based upon its known sequence (Accession number NM_002128) and the primers designed. The synthetic human HMGB1 gene insert was provided by GenScript in a pUC57 cloning vector and sub-cloned into pGS-21a utilising the identical methodology used to produce the three RAGE domain constructs (section 2.4.13). A positive clone was used as template, with a single PCR product of approximately 470 bp visible in lane 3, alongside a negative control in lane 2 and a 100 bp DNA ladder in lane 1 (Figure 20). A product of 464 bp was expected based upon the primers used, correlating well with the band observed in lane 3 (Table 2) (Figure 20). The insert was subsequently verified by sequencing as a 100% match to the synthetic sequence provided to GenScript, with a synonymous primary amino acid sequence to human HMGB1 (Accession number NM_002128).

3.2.4 PCR amplification of S100B, S100P and S100A6 cloned into vector pGS-21a.

The gene sequences encoding human calgranulins S100B, S100P and S100A6 were optimised for prokaryotic host expression and synthesised by GenScript. The restriction digest sites for XbaI and HindIII designed into synthetic RAGE and HMGB1 were similarly incorporated into each of the calgranulin gene inserts, which were then provided in pUC57 cloning vectors by GenScript. The inserts were sub-cloned into pGS-21a and subsequently transformed and screened in TOP10 *E. coli* using the identical methods used for RAGE and HMGB1 (sections 2.4.2 to 2.4.5). Primers designed for end-to-end amplification of the three calgranulin sequences were used in whole-cell PCR to confirm the presence of a single gene insert in the pGS-21a vector. All three reactions produced well defined, single bands approximately 300 base pairs in size which approximates the expected sequence sizes of 276 bp (S100B), 285 bp (S100P) and 270 bp (S100A6) respectively (Figure 21). Sequencing of plasmid collected from these three clones confirmed the inserts were a match to the sequences submitted to GenScript for synthesis.

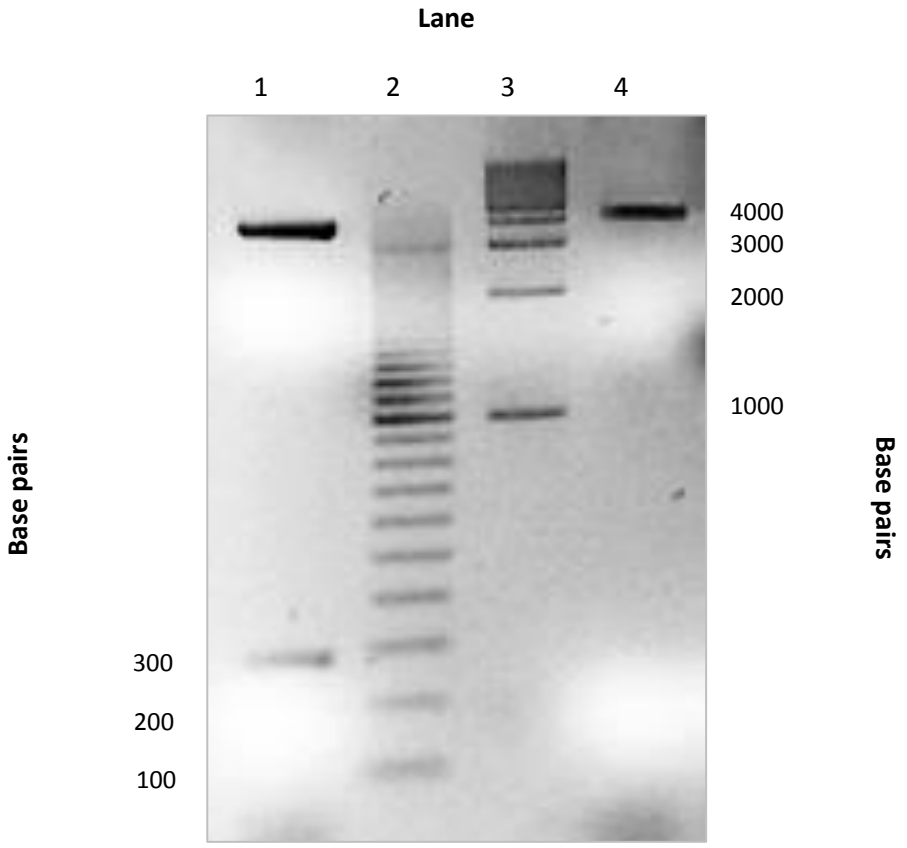

Figure 18. Restriction enzyme digests of pGEX-6P1-deltaHMGB1.

pGEX-6P1-deltaHMGB1 was harvested from transformed TOP10 *E. coli* as described in section 2.4.6. A restriction enzyme digest of pGEX-6P1-deltaHMGB1was performed according to section 2.4.7 and the reaction mixture visualised on a 1.2% agarose gel (section 2.4.9). Digest mixtures for BamHI + EcoRI + pGEX-6P1-deltaHMGB1 was loaded into lane 1, EcoRI + pGEX-6P1-deltaHMGB1 in lane 4, with a 100 bp (Promega) and 1000 bp ladder (EZ Bioresearch) loaded in lanes 2 and 3 respectively.

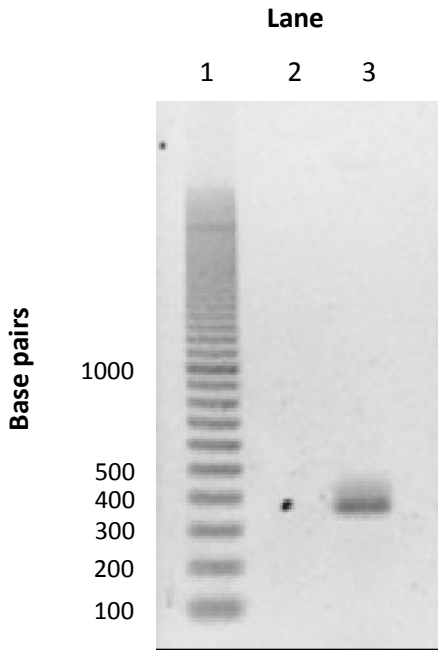

Figure 19. PCR Amplification of truncated human HMGB1.

Amplification of truncated human HMGB1 was performed as outlined in section 2.4.7 using primers designed against HMGB1 amino acids 1-185 (Table 2). PCR reaction mixture containing pGEX-6P1-deltaHMGB1 as template was loaded into lane 3 on a 1.2% agarose gel, along with a 100 bp ladder (Promega) in lane 1, and negative control in lane 2.

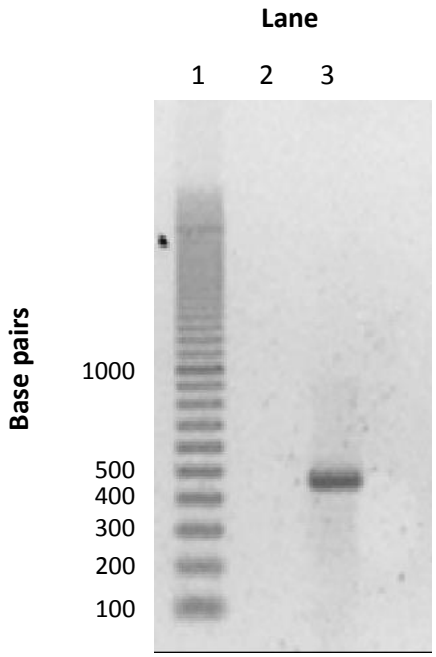

Figure 20. PCR amplification of full length human HMGB1.

PCR amplification of synthetic human HMGB1 cloned into pGS-21a expression vector was performed as outlined in section 2.4.7 (Table 2). PCR product from reaction mixtures with and without pGS-21a-hHMGB1 as template, were loaded into lanes 3 and 2, respectively on a 1.2% agarose gel. A 100 bp ladder (Promega) was loaded into lane 1 and the samples visualised as described in section 2.4.9.

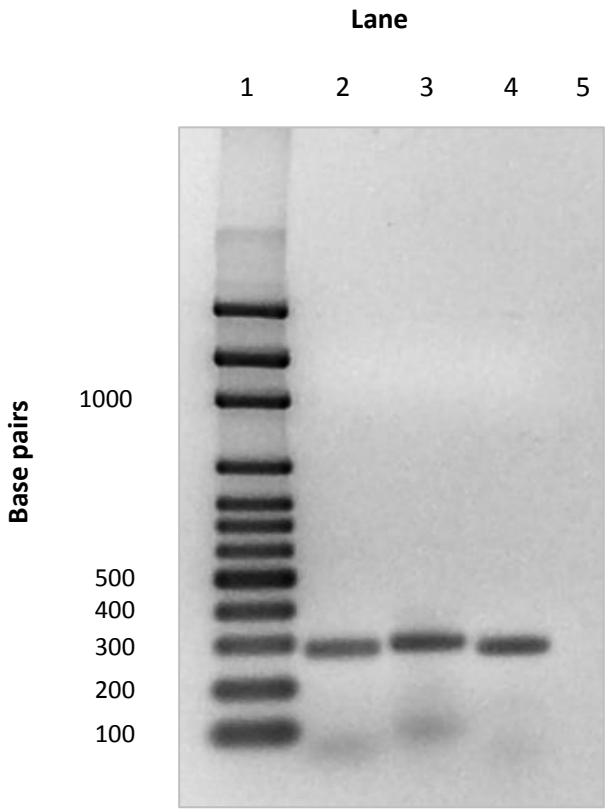

Figure 21. PCR amplification of human S100B, S100P and S100A6 in pGS-21a expression vector.

Synthetic genes encoding human S100B, S100P and S100A6 ligated into pGS-21a and subsequently transformed into TOP10 *E. coli* was used as template in whole cell PCR. Primers amplifying up the entire length of the gene inserts were used, with reaction products for S100B, S100P and S100A6 loaded into lanes 2, 3 and 4, respectively on a 1.2% agarose gel. A 100 bp base ladder (Promega) was loaded into lane 1 along with a negative control containing no template in lane 5.

3.3 Cell culture and recombinant protein expression

3.3.1 Transient expression of pIB/V5 RAGE constructs in insect cells.

Lepidoptera cell lines *Sf9*, *Sf21* and High Five™ (*Tn5*) were transfected with pIB/V5 vector containing canonical human RAGE V, VC_1 and VC_1C_2 extracellular domains as outlined in section 2.5.8. Cells were incubated at 27°C and the conditioned media collected 48 hours post-transfection. Western blots of *Sf9* (Figure 22) and *Sf21* (Figure 23) conditioned media confirmed the presence of pairs of RAGE immunoreactive bands for V, VC_1 and VC_1C_2 that were 20-22 kDa, 30-32 kDa and 46-48 kDa in size, respectively. *Tn5* expressed recombinant RAGE appeared as single bands for the V, VC_1 and VC_1C_2 constructs of 21 kDa, 31 kDa and 45 kDa, respectively (Figure 24). Accounting for the additional amino acids encoding the V5 and 6xHis tag which add approximately 7 kDa, the size of the immunoreactive proteins correlates closely to the theoretical molecular weights of 14, 24 and 38 kDa for V, VC_1 and VC_1C_2, respectively. Optimisation of the DNA transfection quantity was done using the *Tn5* host for all three domain constructs (Figure 25). It was observed that as the quantity of DNA increased past 4 µg, the culture viability decreased significantly, with cultures transfected with 8 µg of vector becoming unviable. The optimal amount of vector for use in transfection without impeding survival rates post-transfection was 4 µg for all constructs (Figure 25). Although the cultures frequently survived when 6 µg was used, the passage times and molecular burden placed on the hosts resulted in unhealthy cultures with ongoing issues of poor viability and long passage times (data not shown).

3.3.2 Stable expression of pIB/V5 RAGE constructs in insect cells

Sf9, *Sf21* and High Five™ insect cells confirmed to be transiently expressing RAGE constructs V, VC_1 and VC_1C_2 were grown to confluency before being passaged as described in section 2.5.8. The monocultures were grown to approximately 40% confluency before the nucleoside antibiotic Blasticidin was added at a 80 µg/mL working concentration to select for chromosomally incorporated transfectants (section 2.5.9) (Figure 24). Approximately 40% of the transfected cell cultures were dead 48 hr post-administration of Blasticidin, with foci of resistant cells clearly visible in e), h) and k) of Figure 26, after only 24 hr. The untransfected control culture (Figure 26a-c) was extinct 48 hr post-selection, with membrane blebbing and cytosolic vacuols visible within 24 hr (Figure 26b). The high concentration of selective antibiotic ensured cells containing multiple inserts were successfully selected and maintained as stable transfectants.

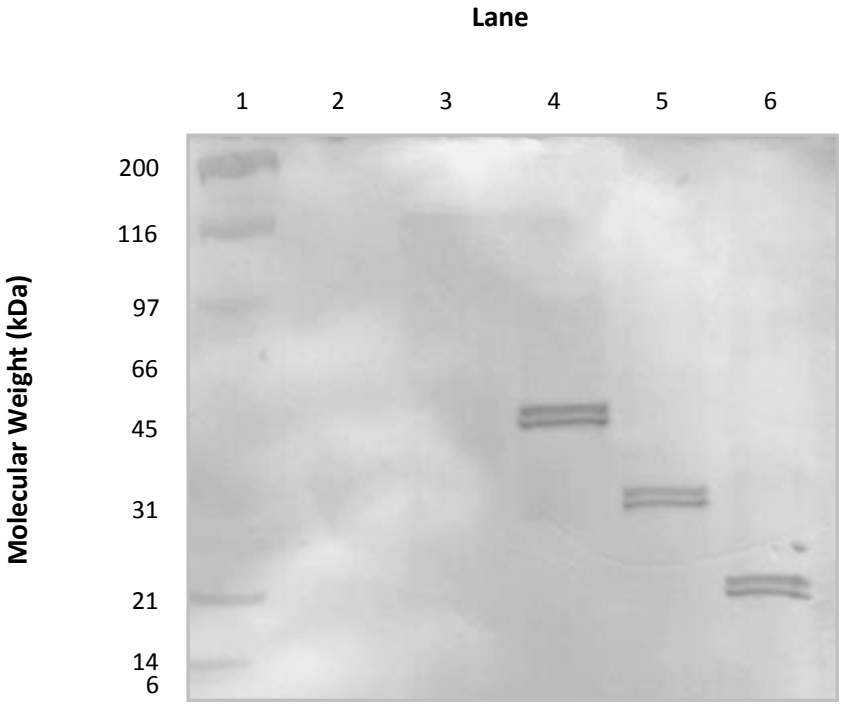

Figure 22. Western blot for the presence of pIB/V5 RAGE constructs in conditioned media 48 hr post-transfection of *Sf9* cells.

Sf9 insect cells grown in monocultures were transfected with pIB/V5 human RAGE constructs described in section 3.1.4. Cultures were grown for 48 hr before being passaged. Samples of conditioned media from all transfected cultures was prepared for visualisation on an SDS-PAGE 4-12% precast gradient gel as described in section 2.6.16. Lane 1 was loaded with broad range prestained molecular weight standards, while mock transfectant media was loaded into lane 3 (lane 2 left blank). Denatured RAGE VC_1C_2, VC_1, and V domain samples were loaded into lanes 4, 5 and 6 respectively and electrophoresed. A Western blot was performed on the gel as outlined in section 2.6.18 using an anti-V5 specific monoclonal detection antibody (Invitrogen™).

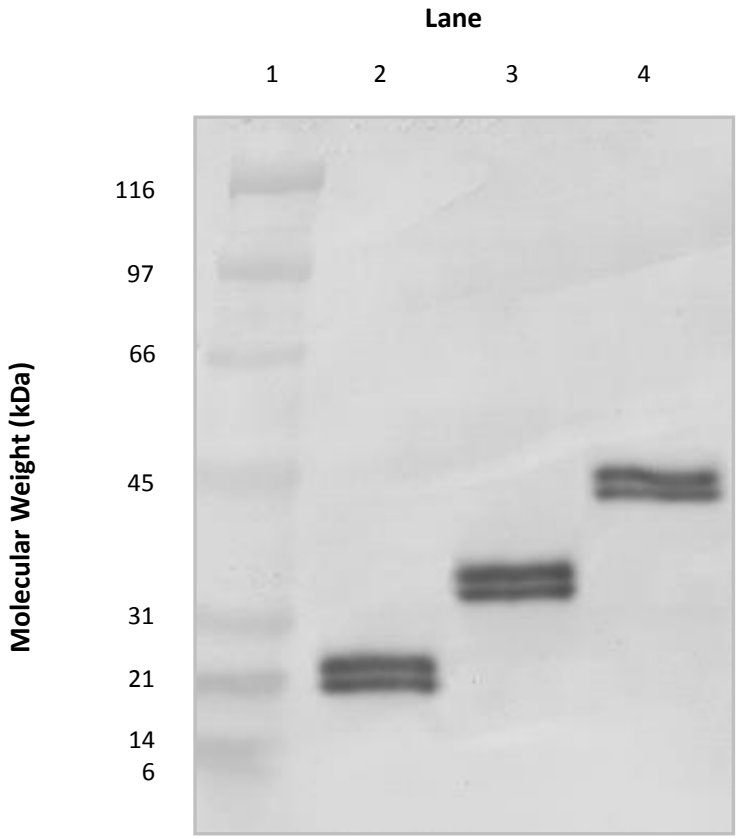

Figure 23. Western blot for the presence of pIB/V5 RAGE constructs in conditioned media 48 hr post-transfection of *Sf21* cells.

Sf21 insect cells grown in monocultures were transfected with pIB/V5 human RAGE constructs described in section 3.1.4. Cultures were grown for 48 hr before being passaged. Samples of conditioned media from all transfected cultures was prepared for visualisation on an SDS-PAGE 4-12% precast gradient gel as described in section 2.6.16. Lane 1 was loaded with broad range prestained molecular weight standard (Bio-Rad). Denatured RAGE V, VC_1 and VC_1C_2 conditioned media samples were loaded into lanes 2, 3 and 4, respectively and electrophoresed. A subsequent Western blot was performed on the gel as outlined in section 2.6.18 using an anti-V5-specific monoclonal antibody for detection (Invitrogen™).

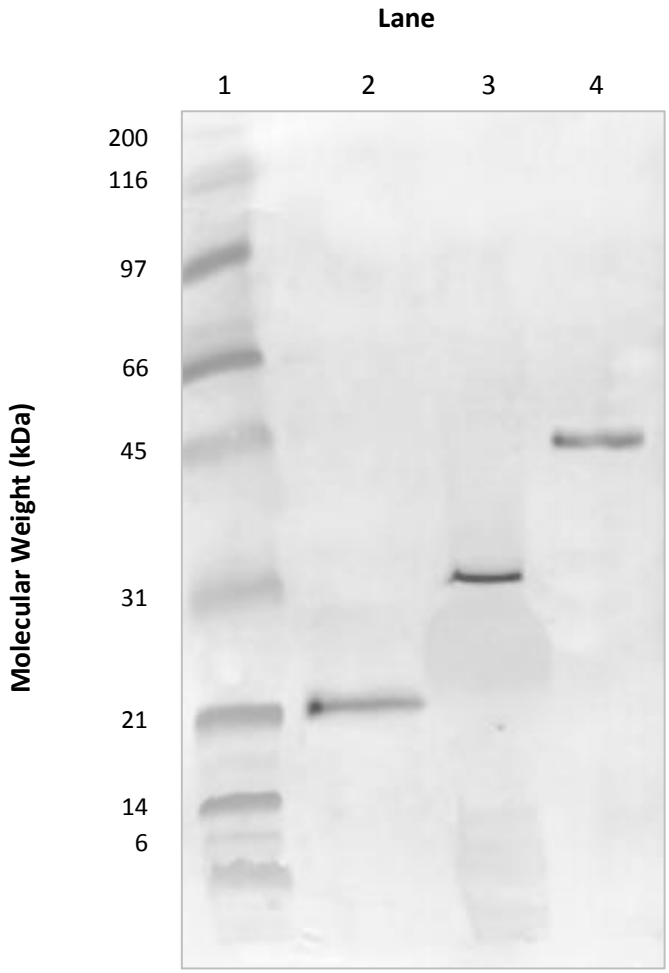

Figure 24. Western blot for the presence of pIB/V5 RAGE constructs in conditioned media 48 hr post-transfection of *Tn5* insect cells.

Tn5 insect cells grown in monocultures were transfected with pIB/V5 human RAGE constructs described in section 3.1.4. Cultures were grown for 48 hr before being passaged. Samples of conditioned media from all transfected cultures was prepared for visualisation on an SDS-PAGE 4-12% precast gradient gel as described in section 2.6.16. Lane 1 was loaded with broad range prestained molecular weight standard (Bio-Rad). Denatured RAGE V, VC_1, and VC_1C_2 conditioned media samples were loaded into lanes 2, 3 and 4, respectively and electrophoresed. A Western blot was performed on the gel as outlined in section 2.6.18 using an anti-V5 monoclonal detection antibody (Invitrogen™).

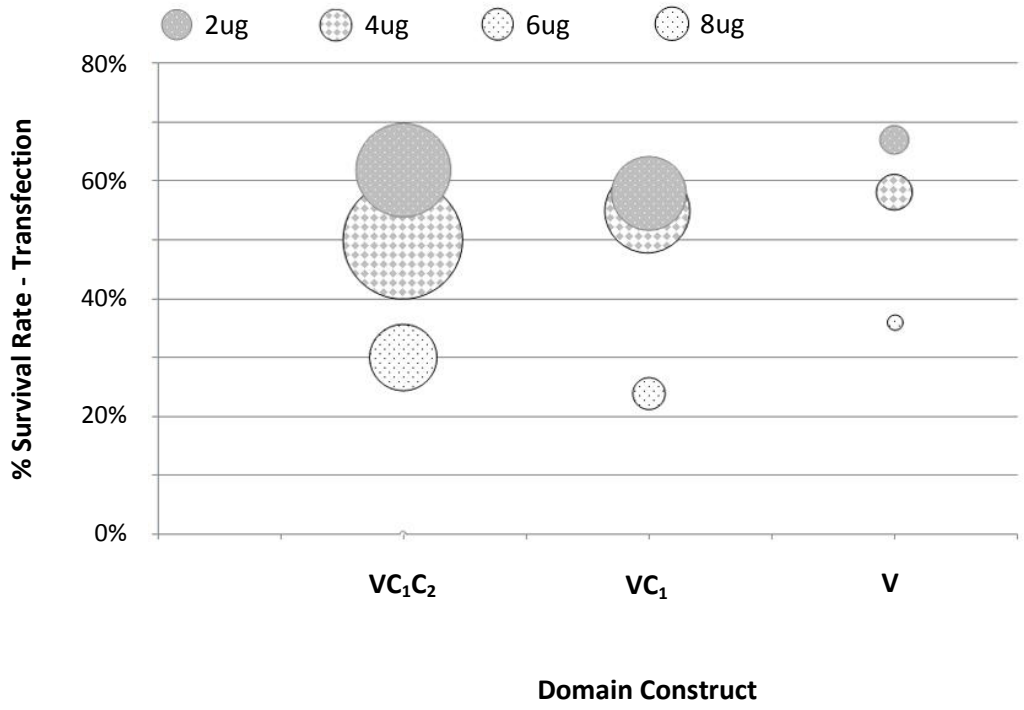

	VC_1C_2		VC_1		V	
cDNA	µg/L	%survival	µg/L	%survival	µg/L	%survival
2ug	450	62%	280	58%	42	67%
4ug	715	50%	362	55%	65	58%
6ug	226	30%	52	24%	12	36%
8ug	4	unviable	2	unviable	<1	unviable

Figure 25. Bubble plot of transient protein expression levels and cell survival rates following transfection of *Tn5* cells with different quantities of DNA.

Tn5 insect cells were transfected with 2 µg, 4 µg, 6 µg and 8 µg of high pure pIB/V5-nativeV, pIB/V5-nativeVC_1 and pIB/V5-nativeVC_1C_2 cDNA using a lipid transfection system. Cell survival was evaluated by trypan blue exclusion and viable cells manually counted using a haemocytometer (2.5.8). The size of the bubble is indicative of the level of expression (µg/L) as determined by RAGE ELISA. The corresponding data is tabulated below the chart.

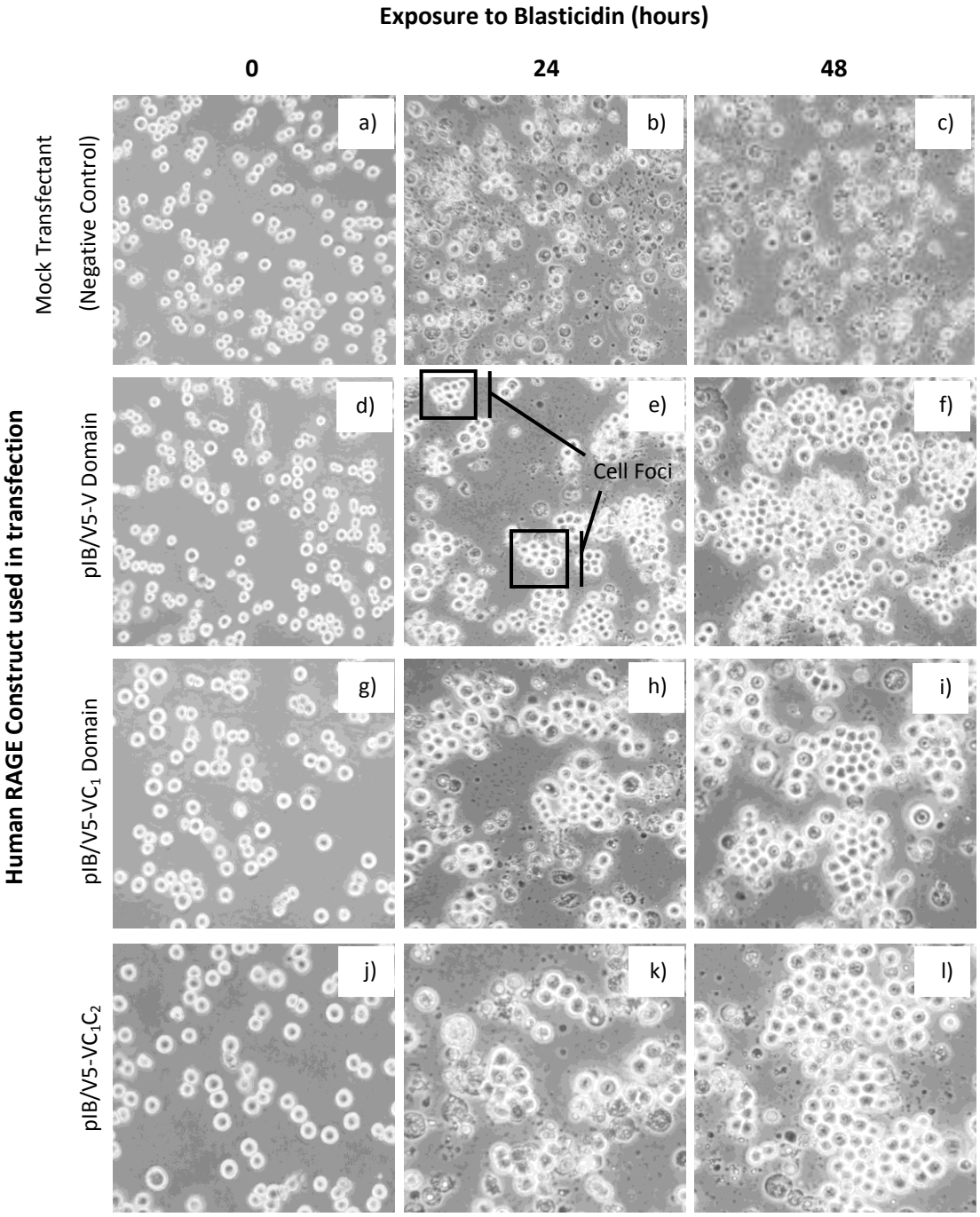

Figure 26. Selection of *Tn5* insect cells stably expressing human RAGE extracellular domain constructs V, VC_1 and VC_1C_2.

Tn5 insect cell cultures were transfected with human RAGE V, VC_1, VC_1C_2 and mock pIB/V5 vector (Figure 24) as described in section 2.5.4. The cultures were allowed to adhere to the flask surface before treatment with the nucleoside antibiotic Blasticidin (80 µg/mL working concentration) to select stable transfectants and cultured as described in section 2.5.9. Cells were imaged at 0, 24 and 48 hrs post-treatment with Blasticidin with image e) highlighting the formation of normal cell foci.

3.3.3 De-glycosylation of recombinant RAGE constructs expressed in insect cells.

Sf9 and *Sf21* expressed recombinant RAGE (Figures 21-22) was treated with N-glycosidase to evaluate the heterogeneity of glycosylation as described in section 2.6.7. Western blotting before and after digest demonstrated the reduction of the two bands to a single band approximately 26 kDa, 38 kDa and 46 kDa in size respectively (Figure 27). Deglycosylation of *Tn5* expressed recombinant RAGE similarly produced V, VC_1 and VC_1C_2 RAGE proteins approximately 2 kDa smaller in size (data not shown). This confirms that the recombinant RAGE constructs expressed by all Lepidoptera cell lines were glycosylated, with *Tn5* cells producing homogeneously glycosylated recombinant protein.

3.3.4 Quantitative analysis of recombinant RAGE constructs expressed by Sf9, Sf21 and Tn5 insect cells in suspension culture.

The *Sf9*, *Sf21* and *Tn5* cultures stably expressing recombinant V, VC_1 and VC_1C_2 were adapted to suspension culture as outlined in section 2.5.5. Shaker flasks with 50 mL of serum free media were seeded and allowed to grow to confluence before total recombinant RAGE in each culture was determined by ELISA (section 2.6.19). *Sf9* cells expressed 1.10 ± 0.05 µg, 1.43 ± 0.28 µg, and 2.16 ± 0.12 µg of V, VC_1 and VC_1C_2 respectively over a 4 day period (Figure 28). *Sf21* cells expressed 1.10 ± 0.22 µg, 3.56 ± 0.41 µg, and 5.03 ± 0.19 µg of V, VC_1 and VC_1C_2 respectively over a single passage (Figure 28). *Tn5* cells produced 3.16 ± 0.17 µg, 14.49 ± 0.57 µg, and 20.8 ± 2.28 µg of V, VC_1 and VC_1C_2 respectively over a three day single passage (Figure 28). A positive correlation between increasing levels of expression and protein size was observed for all cell lines.

Sf21 levels of VC_1 and VC_1C_2 expression were approximately 2-fold higher than those of *Sf9*, with no significant difference between V domain levels. The *Tn5* cells expressed V, VC_1 and VC_1C_2 recombinant RAGE proteins at levels 2.5-fold, 5-fold and 4-fold higher than *Sf21* over a single passage, clearly demonstrating that *Tn5* is the most efficient Lepidoptera cell line for expressing homogeneous glycosylated recombinant human RAGE constructs with the greatest yield.

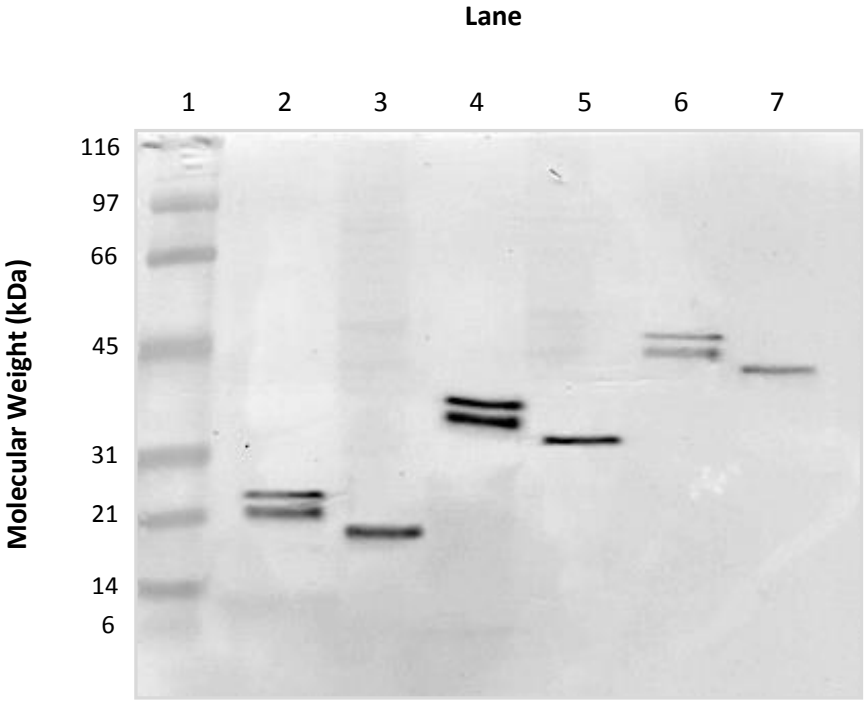

Figure 27. Western blot of de-glycosylated recombinant human RAGE constructs expressed in *Sf21* insect cells.

Recombinant RAGE expressed by *Sf21* insect cells transfected with the V, VC_1 and VC_1C_2 constructs was denatured and incubated with the N-glycosidase, PNGaseF (New England Biolabs®) as described in section 2.6.7. Glycosylated V, VC_1 and VC_1C_2 recombinant protein was prepared for denaturing SDS-PAGE (section 2.6.16), and loaded into lanes 2, 4 and 6, respectively. Corresponding de-glycosylated forms of V, VC_1 and VC_1C_2 RAGE were loaded into lanes 3, 5 and 7, with a broad-range molecular weight standard (Bio-Rad) run in lane 1. Western blot analysis of the gel was performed as described in section 2.6.18, using an anti-V5 monoclonal antibody (Invitrogen™).

a)

	V	VC_1	VC_1C_2	V	VC_1	VC_1C_2
Sf9	5%	7%	15%	<1%	<1%	<1%
Sf21	5%	17%	71%	<1%	<1%	2%
Tn5	15%	23%	100%	<1%	<1%	3%
	Culture Media			Cytosolic Fraction		

b)

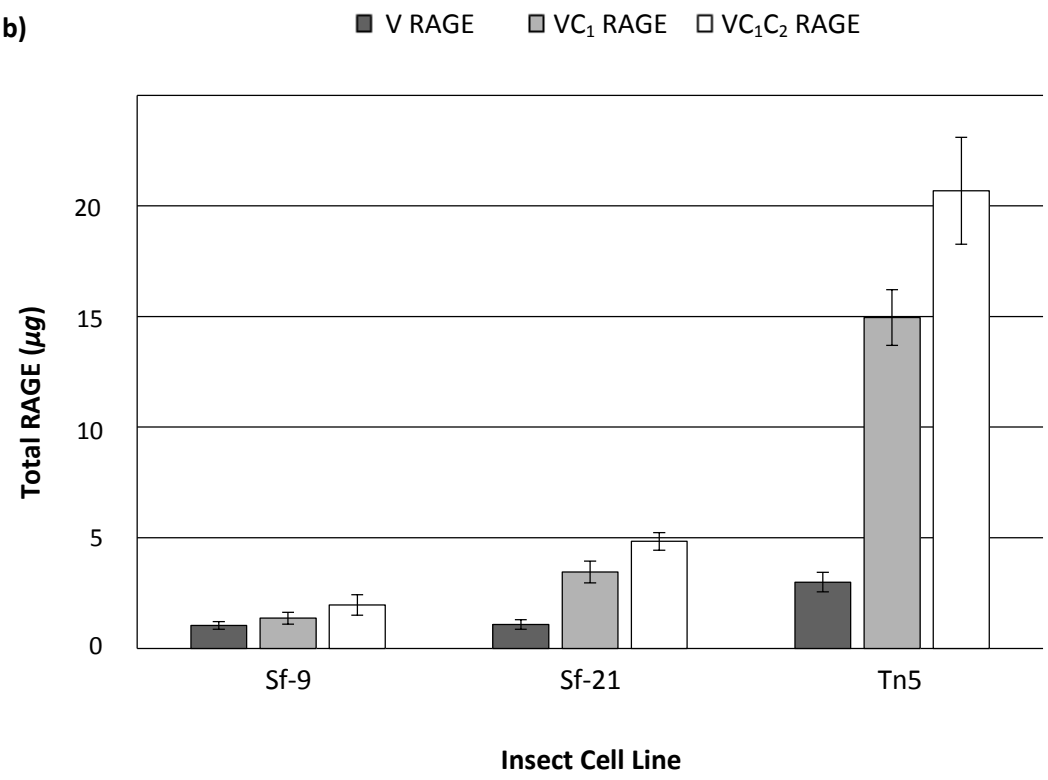

Figure 28. Total recombinant VC_1C_2 RAGE expressed by *Sf9*, *Sf21* and *Tn5* insect cells over a single passage in suspension culture (mean ± se).

a) Heat map showing levels of expression as a percentage of the highest expressing RAGE construct (VC_1C_2) for both secreted and cytosolic located protein (n=3), with the colour intensity correlating with the relative level of expression **b)** *Sf9*, *Sf21* and *Tn5* insect cells stably expressing recombinant RAGE constructs V, VC_1 and VC_1C_2, were grown in 50 mL suspension cultures as described in section 2.5.6. Once cells reached confluence, conditioned media was collected and total recombinant RAGE determined by ELISA (section 2.6.19). Samples were measured in triplicate.

3.3.5 Comparison of insect cell growth rates in suspension culture.

Sf9, *Sf21* and *Tn5* cells stably transfected with V, VC_1 and VC_1C_2 recombinant RAGE constructs were grown in 50 mL cell suspension cultures according to section 2.5.6. Viable cell counts were performed every 24 hours to assess culture health and growth rates between constructs (section 2.5.7). No discernible difference was observed in growth rates of either *Sf9* or *Sf21* cells expressing different constructs, with a maximum cell density of approximately $2.7x10^6$ viable cells/mL achieved after 96 hr (Figure 29 and Figure 30). Similarly, no differences were observed in growth rates of the *Tn5* cells expressing the different RAGE constructs, with a maximum cell density of $2.87x10^6$ viable cells/mL 72 hr post-seeding (Figure 31). This demonstrated that *Tn5* insect cells go through a single passage 33% faster (24 hr) than both *Sf9* and *Sf21* cells transfected with identical RAGE constructs. As such, all further work was carried out using only *Tn5* stable transfectants due to their homogeneous glycosylation of recombinant protein, faster passage times and higher levels of RAGE expression. Further optimisation of media exchange regimes and brand of culture media were carried out using *Tn5*. Approximately 40% higher cell densities for *Tn5* cells were achieved after 72 hours in culture using Ex-Cell 405™ media in comparison to Express Five™ (Figure 32). Passaging of cells into conditioned media was done to evaluate nutrient exhaustion and cell viability under poor media conditions, again demonstrated that *Tn5* cells grown in Ex-Cell 405™ had both higher viability and cell density under adverse conditions. This was clearly demonstrated by the non-viability of the p3 culture grown in Express Five™ media, with the Ex-Cell 405™ culture returning to normal growth kinetics in p4 (Figure 32). The levels of protein expression of VC_1C_2 as an archetypal RAGE domain construct in the two different media were 19% greater in yield for cultures grown in Ex-Cell 405™ media compared to those grown in Express Five™ (Figure 33). This clearly demonstrated that Ex-Cell 405™ is the preferred Lepidoptera culture media in suspension culture, producing not only more viable cultures with higher cell densities, but 19% higher levels of protein expression relative to the Express Five™ media.

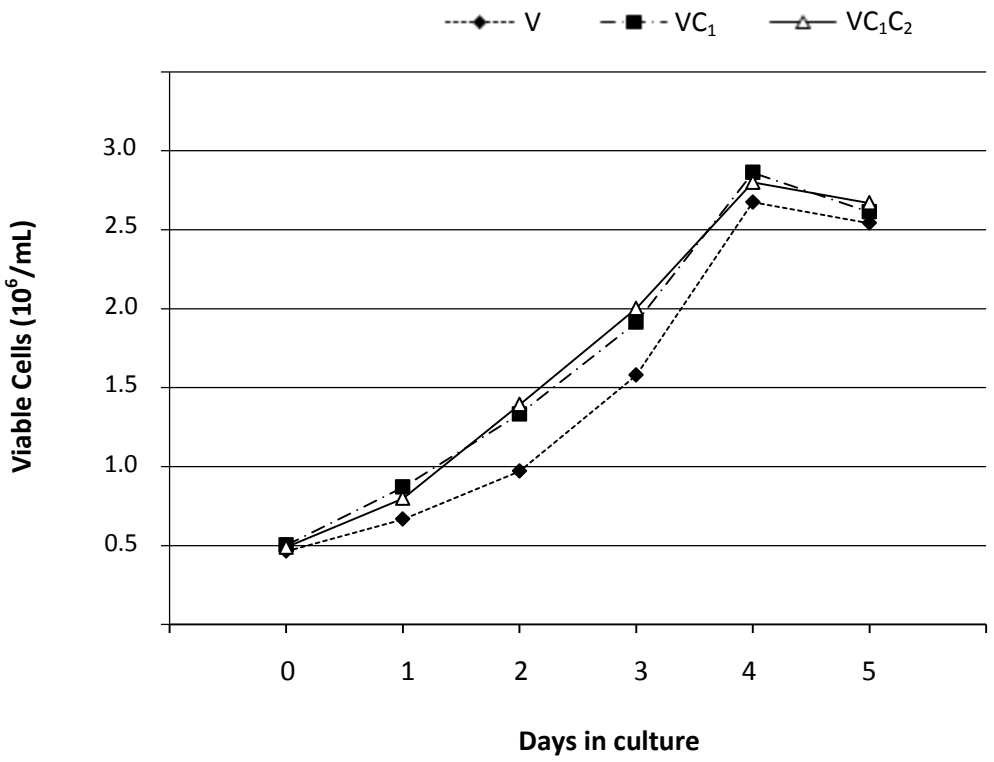

Figure 29. Growth rate of *Sf9* insect cells in suspension culture expressing different soluble RAGE domain constructs.

Sf9 insect cells stably transfected with V, VC_1 and VC_1C_2 recombinant RAGE domain constructs were grown in parallel in suspension culture (section 2.5.6) using Express Five™ (Invitrogen™). Total viable cell counts were performed as described in section 2.5.7.

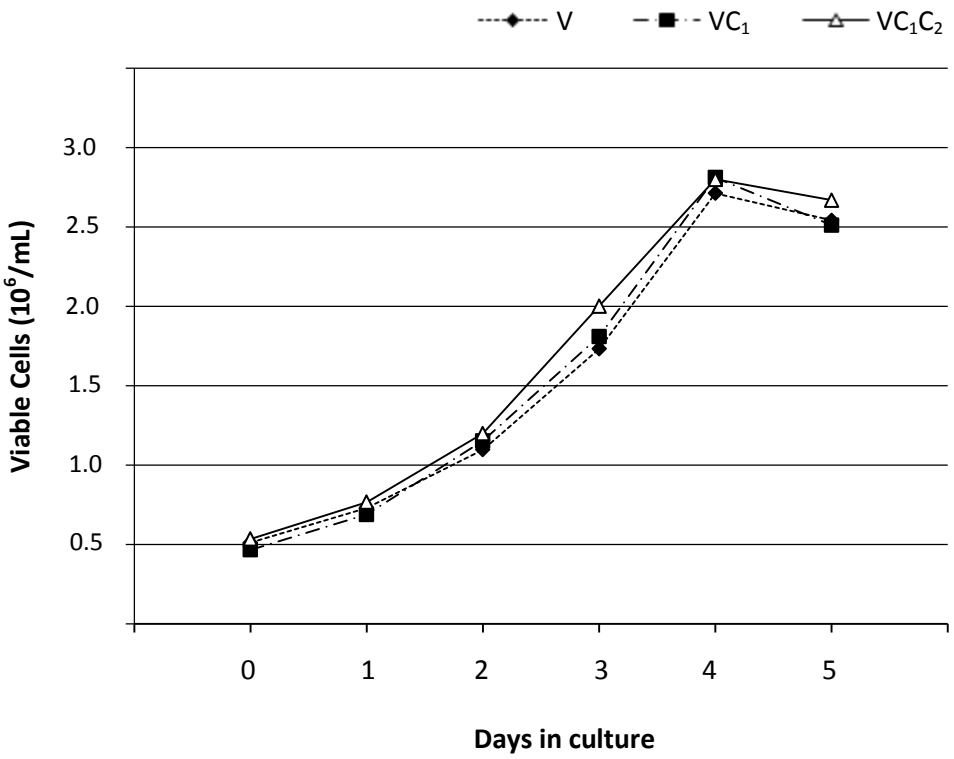

Figure 30. Growth rate of *Sf21* insect cells in suspension culture expressing different soluble RAGE domain constructs.

Sf21 insect cells stably transfected with V, VC_1 and VC_1C_2 recombinant RAGE domain constructs were grown in parallel in suspension culture (section 2.5.6) using Express Five™ (Invitrogen™). Total viable cell counts were performed as described in section 2.5.7.

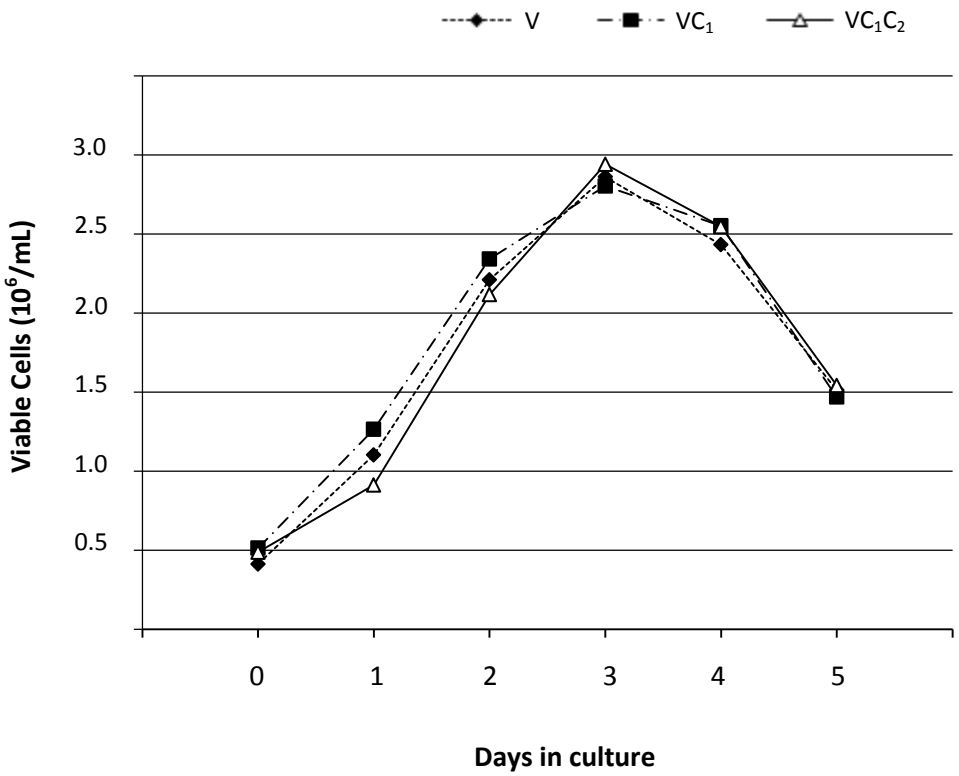

Figure 31. Growth rate of *Tn5* insect cells in suspension culture expressing different soluble RAGE domain constructs.

Tn5 insect cells stably transfected with V, VC_1 and VC_1C_2 recombinant RAGE domain constructs were grown in parallel in suspension culture (section 2.5.6) using Express Five™ serum free media (Invitrogen™). Total viable cell counts were performed as described in section 2.5.7.

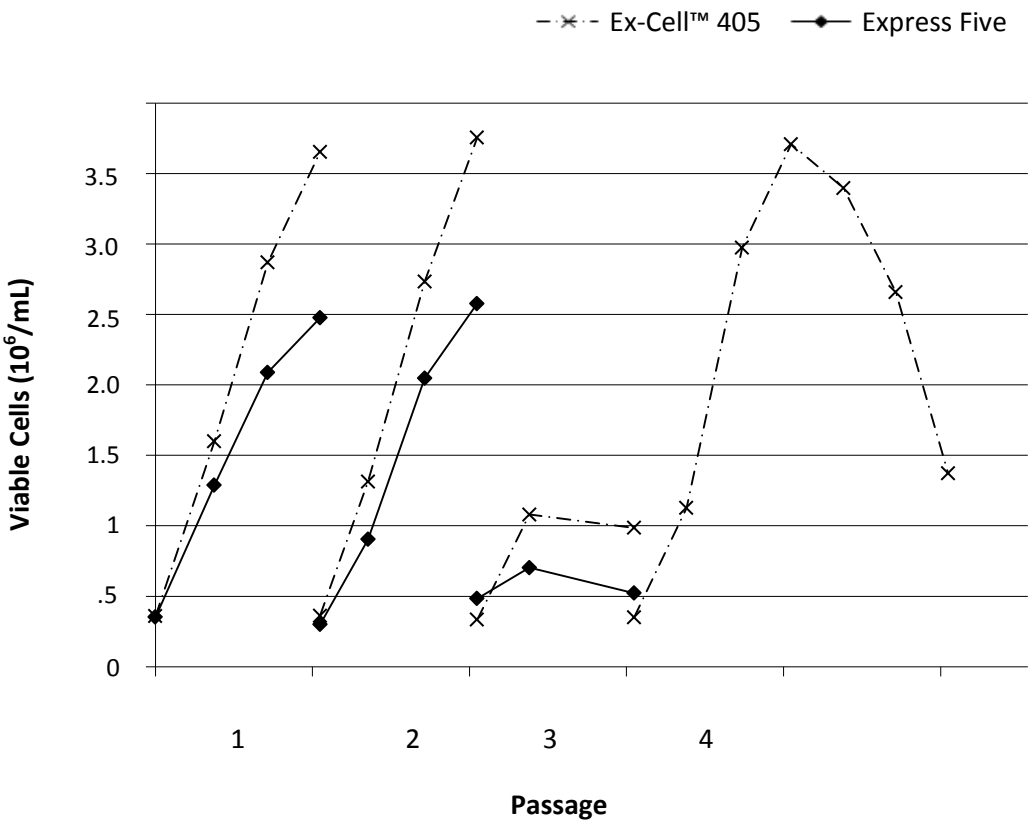

Figure 32. Growth rate of *Tn5* insect cells in different media over multiple passages.

Tn5 insect cells were grown in suspension as described in section 2.5.6. Two cultures were grown in parallel using Express Five™ SFM (Invitrogen) and Ex-Cell™ 405 (Sigma) media. Passages 1 and 2 had a single media change when cultures were split. Passage 3 was split and seeded at the same cell densities as p1 and p2. However, conditioned media from passage 2 was used for the culture media of p3. Cells were finally allowed to grow to extinction in passage 4 in fresh media.

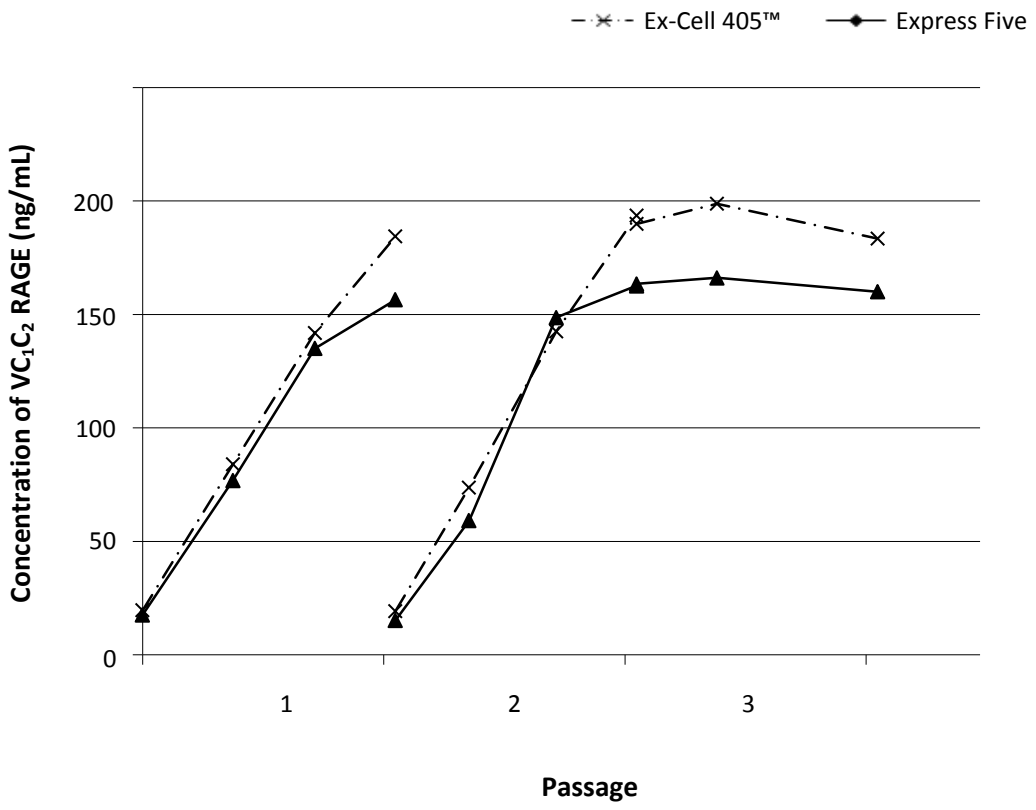

Figure 33. Insect cell expression of recombinant VC_1C_2 RAGE under different culture media conditions.

Tn5 insect cells stably expressing recombinant VC_1C_2 were grown in suspension as described in section 2.5.6. Levels of recombinant protein expressed every 24hr of culture were measured by ELISA (2.6.19). Two cultures were grown in parallel using Express Five™ SFM (Invitrogen) and Ex-Cell™ 405 (Sigma) media. Passages 1 and 2 had a single media change when cultures were split. Passage 3 was split and seeded as per p1 and p2, however, conditioned media from p2 was used for the culture media of p3.

.

3.3.6 Prokaryote expression of human RAGE V, VC_1 and VC_1C_2 extracellular domains.

Prokaryote protein expression strains BL21 (DE3), Rosetta-gami™ B, Origami™ B, T7 Shuffle® K12 and T7 Shuffle® B were transformed with optimised human RAGE domain constructs pGS-21a-optV, pGS-21a-optVC_1 and pGS-21a-optVC_1C_2 as outlined in section 2.4.2. The Rosetta-gami™ B, Origami™ B and T7 Shuffle® K12 were similarly transformed with pGS-21a-nativeV, pGS-21a-nativeVC_1 and pGS-21a-nativeVC_1C_2 and cultured as outlined in method 2.6.2. Each culture was induced to express, with samples from T7 Shuffle® K12 collected for reducing PAGE, Coomassie staining (method 2.6.17) and Western blotting with anti-RAGE antibody (method 2.6.18). The pGS-21a-optV construct did produce a visible band by Coomassie post-induction of approximately 18 kDa in size. The native V-domain construct similarly showed the presence of a band approximately the same size as the synthetic construct, with Western blot confirming immunoreactivity of the post-induction bands with anti-RAGE antibody (Figure 34). T7 Shuffle® K12 transformed with pGS-21a-optVC_1 and pGS-21a-nativeVC_1 produced single bands post-induction visible by Coomassie of approximately 32 kDa and 28 kDa (Figure 35). This 4 kDa difference in size is likely due to differences in PAGE conditions, apparatus used, gels and running buffers, as the electrophoresis of the native and optimised samples were done separately with a significant period of time elapsing between runs. Similarly, T7 Shuffle® K12 transformed with pGS-21a-optVC_1C_2 and pGS-21a-native VC_1C_2 produced prominent single bands post-induction of approximately 47 kDa and 49 kDa in size respectively (Figure 36). Western blot analysis demonstrated the presence of a strong immunoreactive band of approximately 50 kDa when probed with an anti-RAGE antibody, confirming the expressed protein was recombinant RAGE (Figure 36). Rosetta-gami, Origami™ B and T7 Shuffle® K12 were the only hosts transformed with native gene sequence constructs for RAGE. The Shuffle® strain expressed canonical RAGE constructs at levels 4-fold, 3-fold and 0.5-fold lower than those of optimised RAGE constructs for VC_1C_2, VC_1 and V, respectively (Figure 37). Rosetta-gami™ B produced V, VC_1 and VC_1C_2 at levels 4-fold, 3-fold and 2-fold higher than those of its parent strain, Origami™ B (Table 7). The soluble fraction of each culture following collection, sonication and clarification (section 2.6.3) was assayed for recombinant RAGE by ELISA (method 2.6.19). The BL21 strain contained most of the expressed RAGE in the insoluble fraction, with very low levels of recombinant protein in the soluble fraction (Table 7). A significant reduction in levels of RAGE expression was observed in all strains with the deletion of C-domains in both the native and optimised constructs (Table 7).

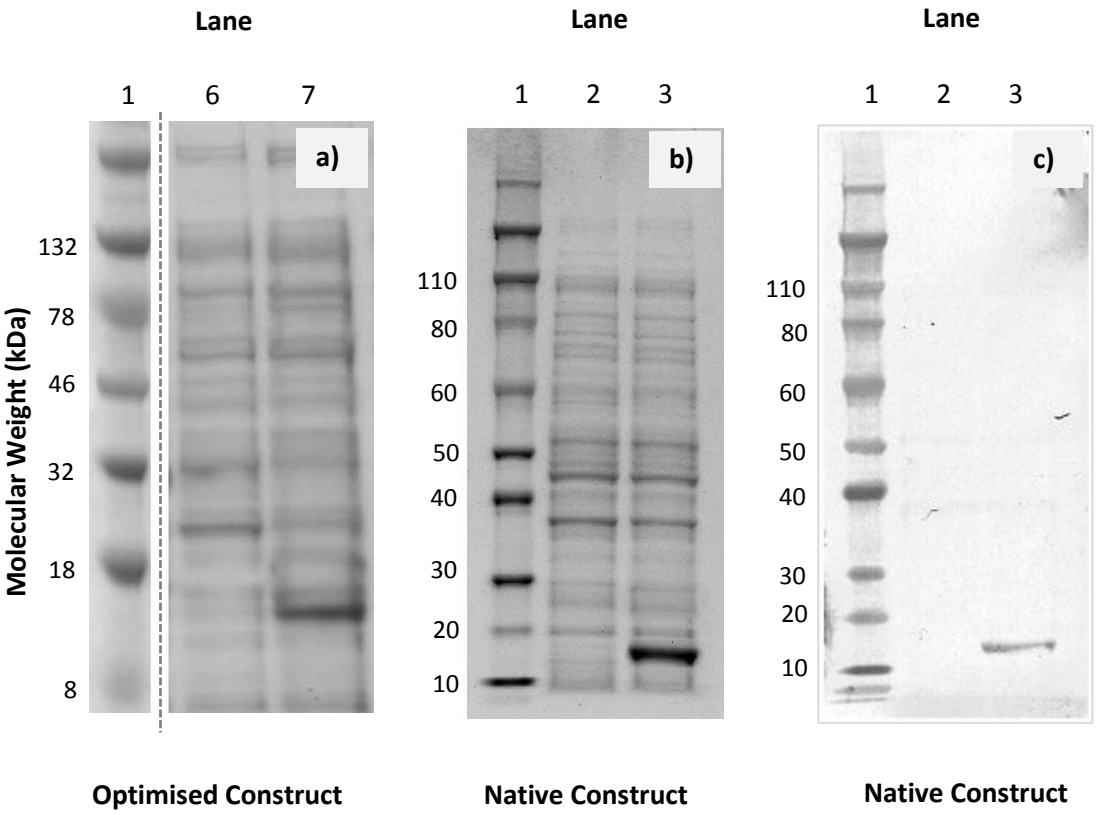

Figure 34. Coomassie and Western blot analysis of both native and optimised recombinant RAGE V domain expressed in *E. coli* T7 Shuffle® K12.

T7 Shuffle® K12 *E. coli* transformed with **a)** pGS-21a-optV and **b)** pGS-21a-nativeV were induced and the soluble fractions pre and post-induction induction loaded into lanes **b)** 2 and 3; or **a)** lanes 6 and 7 of reducing SDS-PAGE gels respectively (section 2.6.1). Gels **a)** and **b)** were Coomassie stained as outlines in section 2.6.17, while gel **c)** was transferred to nitrocellulose for Western blotting with an anti-RAGE antibody (NEB) as described in 2.6.18. Lane 1 of each gel was loaded with a prestained broad range marker (Life Technologies).

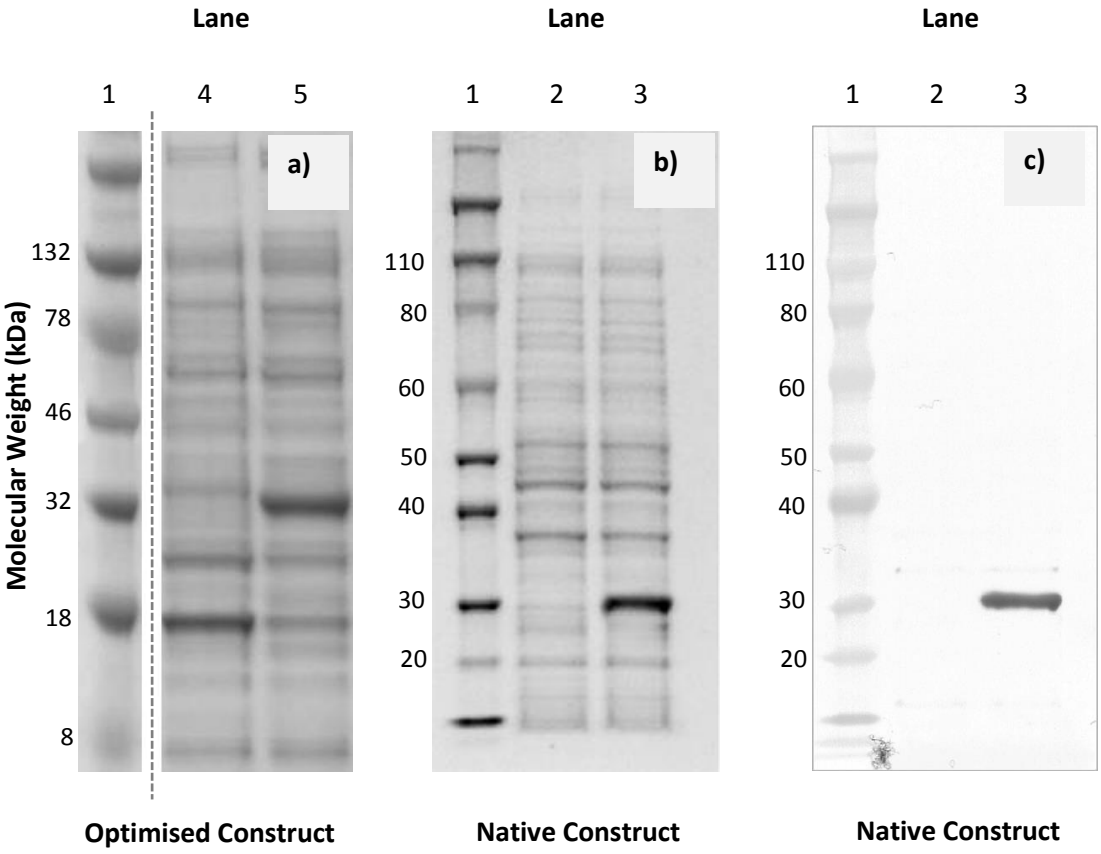

Figure 35. Coomassie and Western blot analysis of both native and optimised RAGE VC_1 recombinant expression in *E. coli* T7 Shuffle® K12.

T7 Shuffle® K12 *E. coli* transformed with **a)** pGS-21a-optVC_1 and **b)** pGS-21a-nativeVC_1 were induced and the soluble fractions pre and post-induction induction loaded into lanes **b)** 2 and 3; or **a)** lanes 4 and 5 of reducing SDS-PAGE gels respectively (section 2.6.1). Gels **a)** and **b)** were Coomassie stained as outlines in section 2.6.17, while gel **c)** was transferred to nitrocellulose for Western blotting with an anti-RAGE antibody (New England Biolabs®) as described in 2.6.18. Lane 1 of each gel was loaded with a prestained broad range marker (Life Technologies).

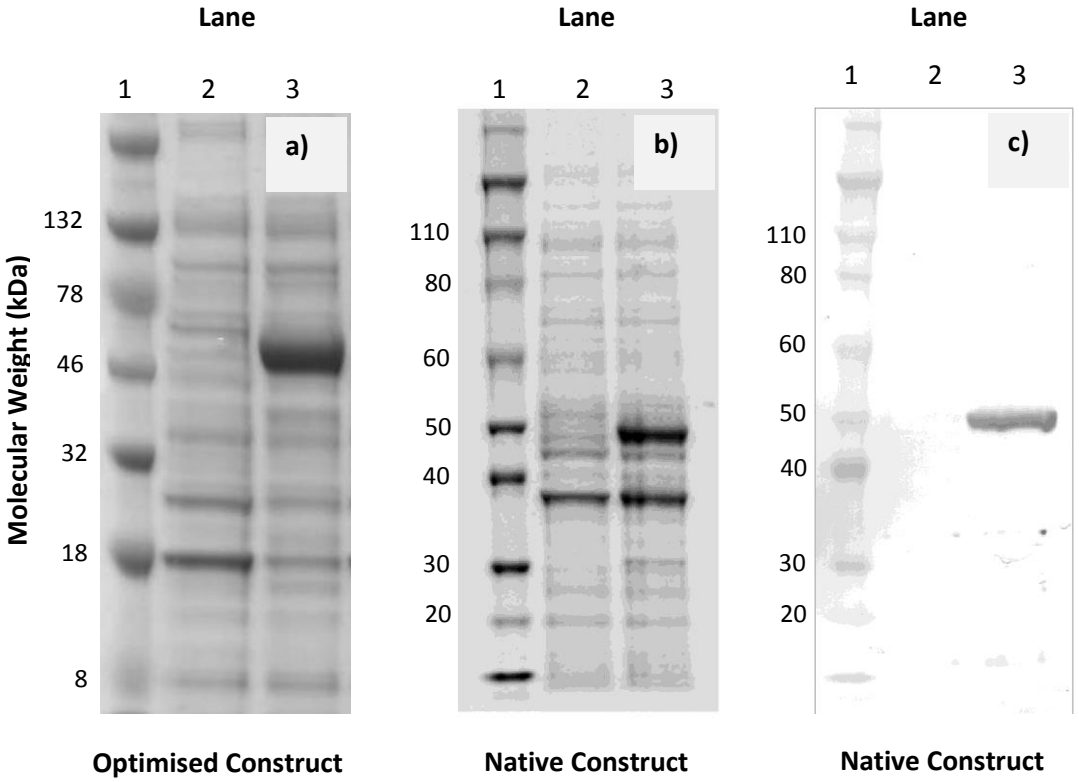

Figure 36. Coomassie and Western blot analysis of both native and optimised RAGE VC_1C_2 domain constructs expressed in *E. coli* T7 Shuffle® K12.

T7 Shuffle® K12 *E. coli* transformed with **a)** pGS-21a-optVC_1C_2 and **b)** pGS-21a-nativeVC_1C_2 were induced and the soluble fractions pre and post-induction induction loaded into lanes 2 and 3 of reducing SDS-PAGE gels respectively (section 2.6.1). Gels **a)** and **b)** were Coomassie stained as outlines in section 2.6.17, while gel **c)** was transferred to nitrocellulose for Western blotting with an anti-RAGE antibody (New England Biolabs®) as described in 2.6.18. Lane 1 of each gel was loaded with a prestained broad range marker (Life Technologies).

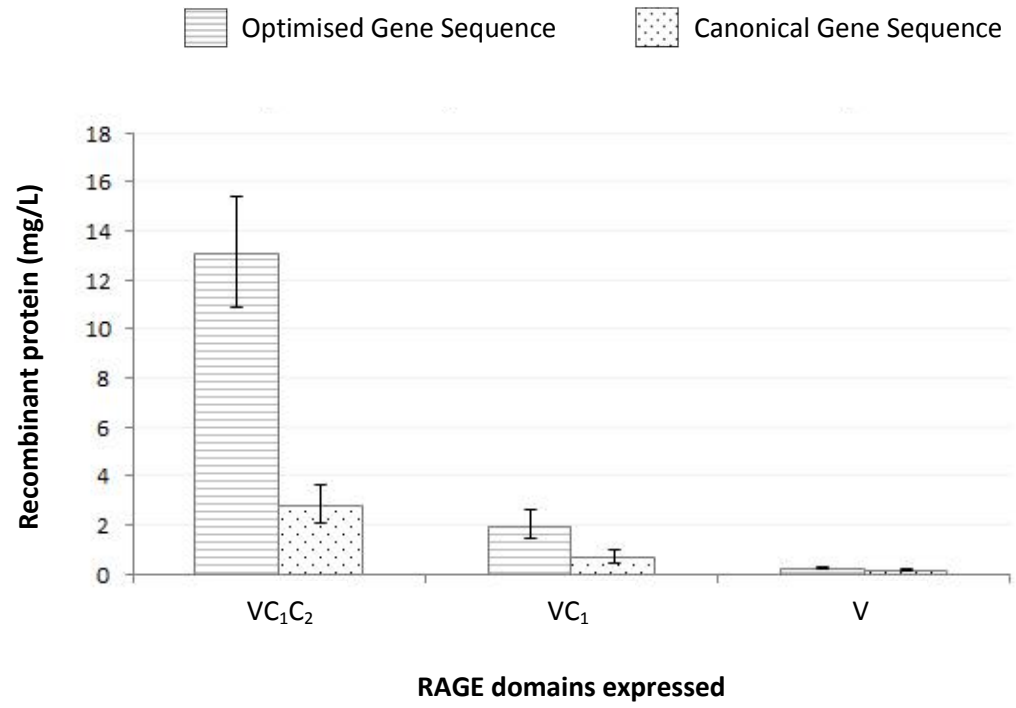

Figure 37. Expression of canonical and optimised RAGE gene sequences encoding different forms of the RAGE extracellular domains in *Escherichia coli* strain T7 Shuffle® K12 (mean ± se).

Escherichia coli strain T7 Shuffle® K12 was transformed with pGS-21a plasmid containing either the canonical or optimised gene encoding human RAGE VC_1C_2, VC_1 or V domains as described in (2.6.1). Micro cultures were prepared and induced (section 2.6.2), with the quantity of soluble recombinant forms of each RAGE domain construct measured by ELISA (section 2.6.19) (n=3).

Table 7. The expression of endogenous and optimised human RAGE V, VC_1 and VC_1C_2 domain constructs in various bacterial hosts.

Bacterial strains were transformed with either optimised or native RAGE gene sequence constructs, and grown to equivalent densities before being induced as described in section 2.6.2. Cultures were lysed by sonication and the total recombinant RAGE in the soluble fraction quantified by ELISA and recorded in mg/L. See Table 8 for comparison with expression in insect cells.

	Optimized Sequence			Native Sequence		
Host	**V**	**VC_1**	**VC_1C_2**	**V**	**VC_1**	**VC_1C_2**
T7 Shuffle® B	0.1	1.15	14.9			
T7 Shuffle® K	0.27	2.04	13.1	0.18	0.72	2.8
Rosetta-gami™ B	0.04	0.71	4.4	0.04	0.7	4.1
Origami™ B	0.09	0.96	3.725	0.02	0.21	0.9
BL21(DE3)	0.08	0.06	0.18			

As the V domain had the lowest level of expression, the T7 Shuffle® K12 strain which expressed this construct at levels three-times greater than all other strains, was selected as the preferred host for use in further RAGE expression of the V, VC_1 and VC_1C_2 recombinant proteins.

3.3.7 Prokaryote expression of full length human HMGB1

T7 Shuffle® K12 was transformed with pGS-21a-hHMGB1 and induced with IPTG as described in section 2.6.3. During the course of this study, it was found that HMGB1 was bactericidal, causing the rapid drop-off in culture growth post-induction (Figure 38). Comparison of induced and uninduced hHMGB1 transformants confirmed that tight regulation of the T7 RNA Polymerase was suppressing basal expression of hHMGB1, with no reduction in growth between cultures containing mock-pGS-21a transformants and pGS-21a-hHMGB1 (Figure 38). The soluble fraction of samples pre and post-induction were collected and clarified as described in section 2.6.3. The induced soluble fraction was loaded in lane 2 of a 4-12% PAGE gel, with lane 3 loaded with the un-induced soluble fraction of the same culture. Coomassie staining shows the presence of a significant band in lane 2 of approximately 30 kDa which strongly correlates with the expected size of full length human HMGB1 being 28 kDa (Figure 39). Western blotting of a parallel SDS-PAGE gel with an anti-HMGB1 antibody detected a single band of approximately 30 kDa in the post-induction soluble fraction, confirming the presence of full length recombinant human HMGB1 in the soluble fraction of T7 Shuffle® K12 transformed with pGS-21a-hHMGB1.

3.3.8 Prokaryote expression of truncated human HMGB1

T7 Shuffle® K12 *E. coli* transformed with pGEX-6P1-deltaHMGB1 was induced by the addition of IPTG as outlined in section 2.6.5 and allowed to express for 2.5 hr. The soluble fractions from this culture pre and post-induction were collected as described in section 2.6.3. The presence of a protein post-induction of approximately 50 kDa in size was observed in a Coomassie stained SDS-PAGE gel loaded with both soluble fractions (Figure 40). This correlates very closely with the expected size of truncated HMGB1 (24 kDa) tagged with GST (25 kDa), estimated to be 49 kDa (Figure 40). Western blotting with an anti-HMGB1 antibody detected a single 50 kDa band post-induction, confirming the expression of hHMGB1-GST.

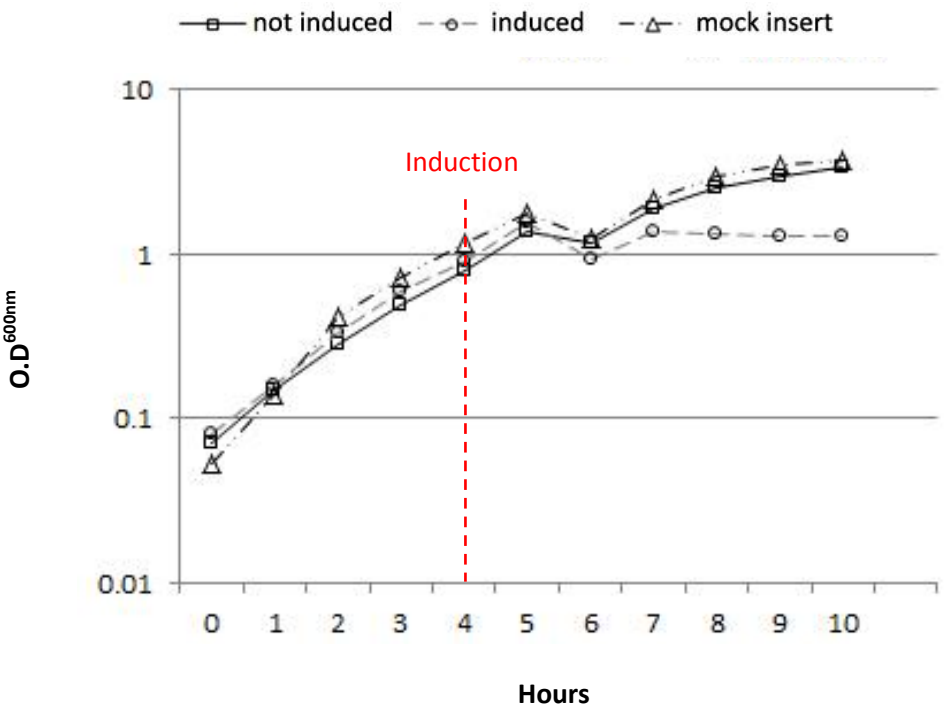

Figure 38. Growth rates of T7 Shuffle® K12 transformed with full length human HMGB1 pre and post induction.

T7 Shuffle® K12 was transformed with pGS-21a-hHMGB1 containing the human HMGB1 gene or pGS-21a without a gene insert as described in section 2.6.5. Two cultures containing no insert (*mock insert*) and one with hHMGB1 (*induced*) were induced to express by the addition of IPTG. A second culture transformed with HMGB1 (*not induced*) was not induced. Growth was measured at $O.D^{600}$ every hour.

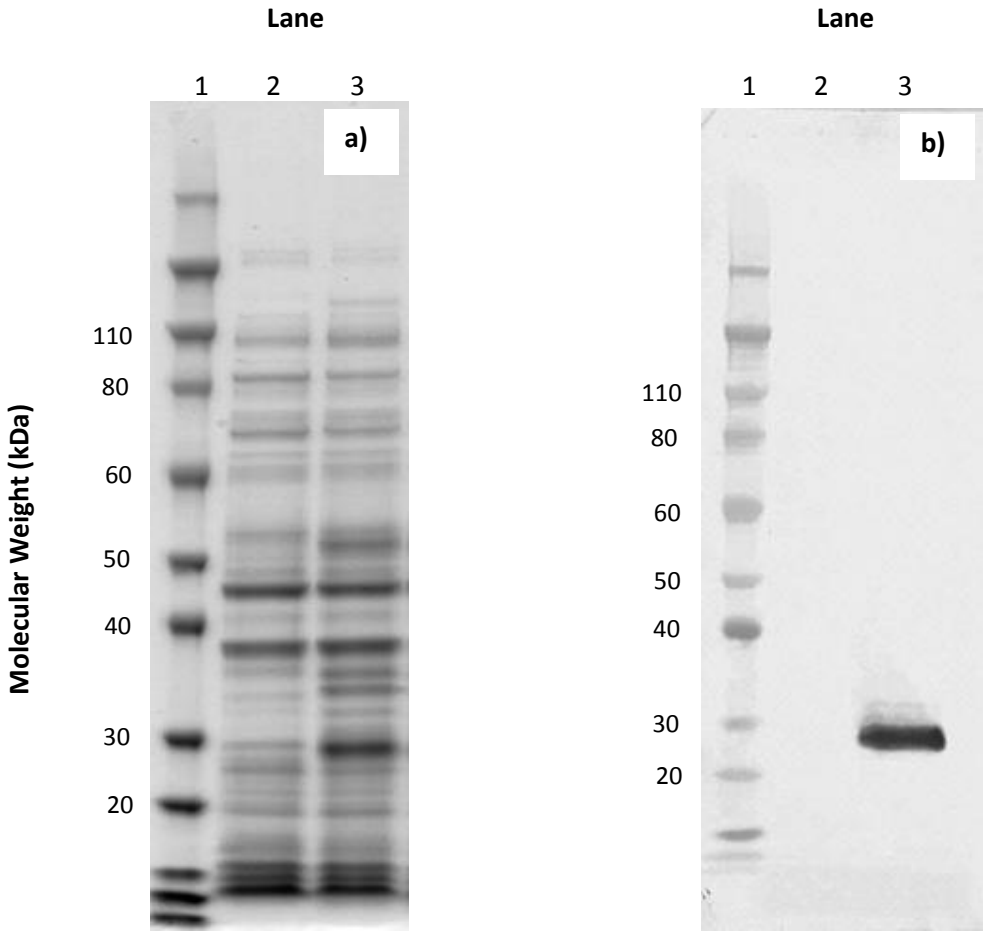

Figure 39. Western blot and Coomassie stain of full length human HMGB1.

T7 Shuffle® K12 *E. coli* pGS-21a-hHMGB1 was induced with the addition of IPTG to express full length human HMGB1 (section 2.6.5). Lane 1 contains a broad range molecular weight marker (Life technologies). Soluble fractions from pre and post-induction were loaded into lanes 2 and 3 respectively of 4-12% SDS-PAGE gels. Gel **a)** was Coomassie stained as described in 2.6.17, with the second gel transferred to nitrocellulose for **b)** Western blotting with anti-human HMGB1 (Merck Millipore) (section 2.6.18).

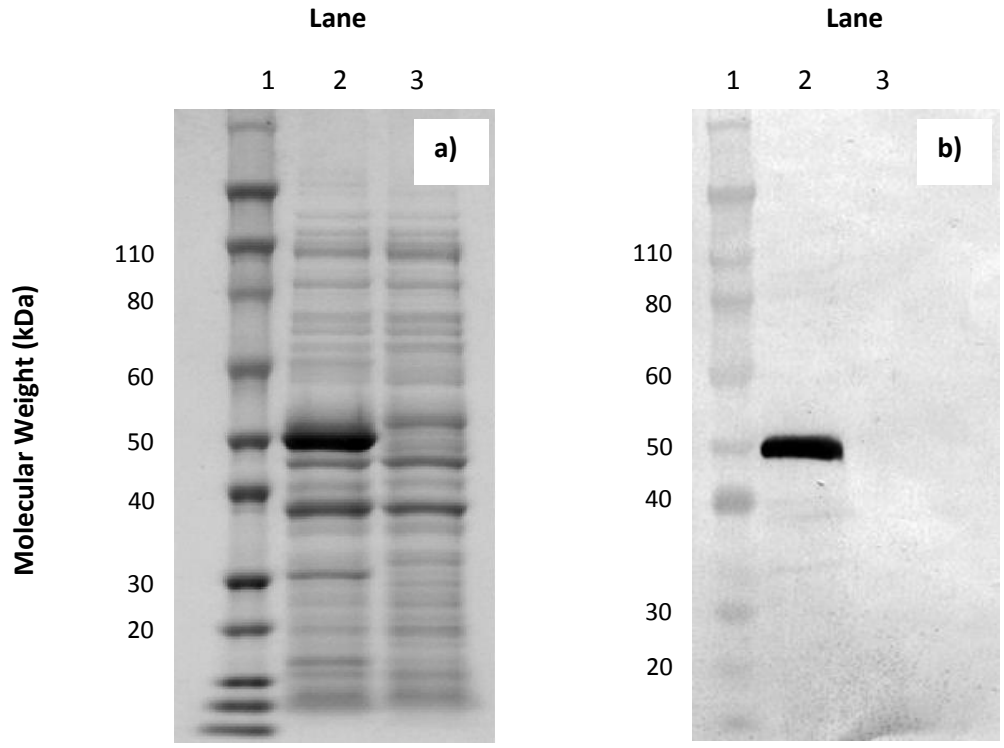

Figure 40. Western blot and Coomassie staining of truncated human HMGB1-GST.

T7 Shuffle® K12 *E. coli* transformed with pGEX-6P1-deltaHMGB1 was induced for 2.5 hr as described in section 2.6.5 before being sonicated and clarified (method 2.6.3). Soluble cell fractions pre (lane 3) and post (lane 2) induction were loaded onto two 4-12% SDS-PAGE gels and subsequently **a)** Coomassie stained and transferred to nitrocellulose for **b)** Western blotting with anti-human HMGB1 (Merck Millipore) (section 2.6.18). Lane 1 contains a broad range molecular weight marker (Life technologies).

3.3.9 Prokaryote expression of human S100B, S100P and S100A6

T7 Shuffle® K12 was transformed with pGS-21a-S100B, pGS-21a-S100P and pGS-21a-S100A6 and induced to express recombinant protein as described in method 2.6.4. Soluble fraction aliquots from pGS-21a-S100B pre and post-induction were collected and clarified (section 2.6.3), before being loaded onto a 4-12% SDS-PAGE gel (Figure 41a). A band approximately 10 kDa in size was visible post-induction with subsequent Western blotting confirming this band was immunoreactive to an anti-S100B antibody (Figure 41b). A second lighter band approximately 20 kDa in size also demonstrated immunoreactivity to the anti-S100B antibody with no other prominent band visible. The pGS-21a-S100P soluble fractions pre and post-induction were similarly collected and loaded onto a 4-12% SDS-PAGE gel. A very faint band was visible by Coomassie post-induction of approximately 10 kDa, with the corresponding Western blot confirming the identity of this band as S100P (Figure 42b). Again, an additional faint band was visible by Western blot of approximately 20 kDa in size that was not visible by Coomassie staining. T7 Shuffle® K12 culture transformed with pGS-21a-S100A6 was induced, lysed and clarified, with the subsequent pre and post-induction soluble fractions again loaded onto a 4-12% SDS-PAGE gel. Following Coomassie staining, a band approximately 10 kDa in size was visible in the post-induction fraction (Figure 43a). Western blotting with anti-S100A6 antibody confirmed the identity of the induced 10 kDa band as S100A6, with a minor band approximately 20 kDa in size once again visible (Figure 43b). Collectively, T7 Shuffle® K12 transformed with these three calgranulin expression vectors and cultured as outlined in section 2.6.4, produced 10.6 mg/L, 14.4 mg/L and 6.9 mg/L of S100B, S100A6 and S100P respectively post-purification (Figure 44).

3.4 Protein Purification

3.4.1 Heparin chromatography of prokaryote RAGE domain constructs V, VC_1 and VC_1C_2

RAGE domain constructs V, VC_1 and VC_1C_2 were expressed as outlined in section 2.6.1 and the bacterial soluble fraction clarified through sonication and centrifugation as described in 2.6.3. A protease inhibitor cocktail was used to minimise proteolytic degradation of the recombinant protein along with 0.5 mM dithiothreitol (DTT) to prevent oxidation of recombinant RAGE. The soluble fraction for each domain was applied to a 5 mL Heparin column at 1 mL/min and the flow through collected. Analysis

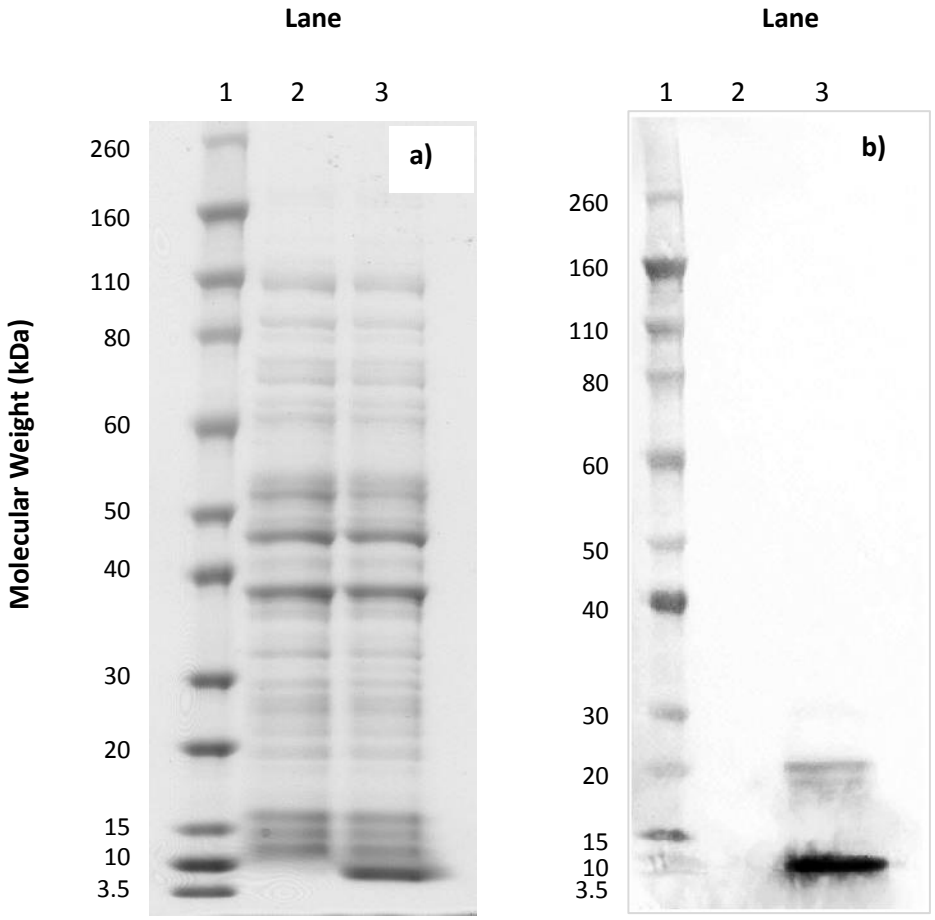

Figure 41. Coomassie and Western blot of prokaryote expressed recombinant human S100B.

T7 Shuffle® K12 *E. coli* was transformed with pGS-21a-S100B and expression induced by the addition of IPTG (section 2.6.4). Soluble fractions collected pre (lane 2) and post (lane 3) induction were loaded on two denaturing 4-12% SDS-PAGE gels. Gel **a)** was Coomassie stained while gel was transferred to PVDF membrane for **b)** Western blotting with an anti-S100B antibody (Abcam). The first lane of each gel was loaded with a broad range, pre-stained molecular weight marker (Life technologies).

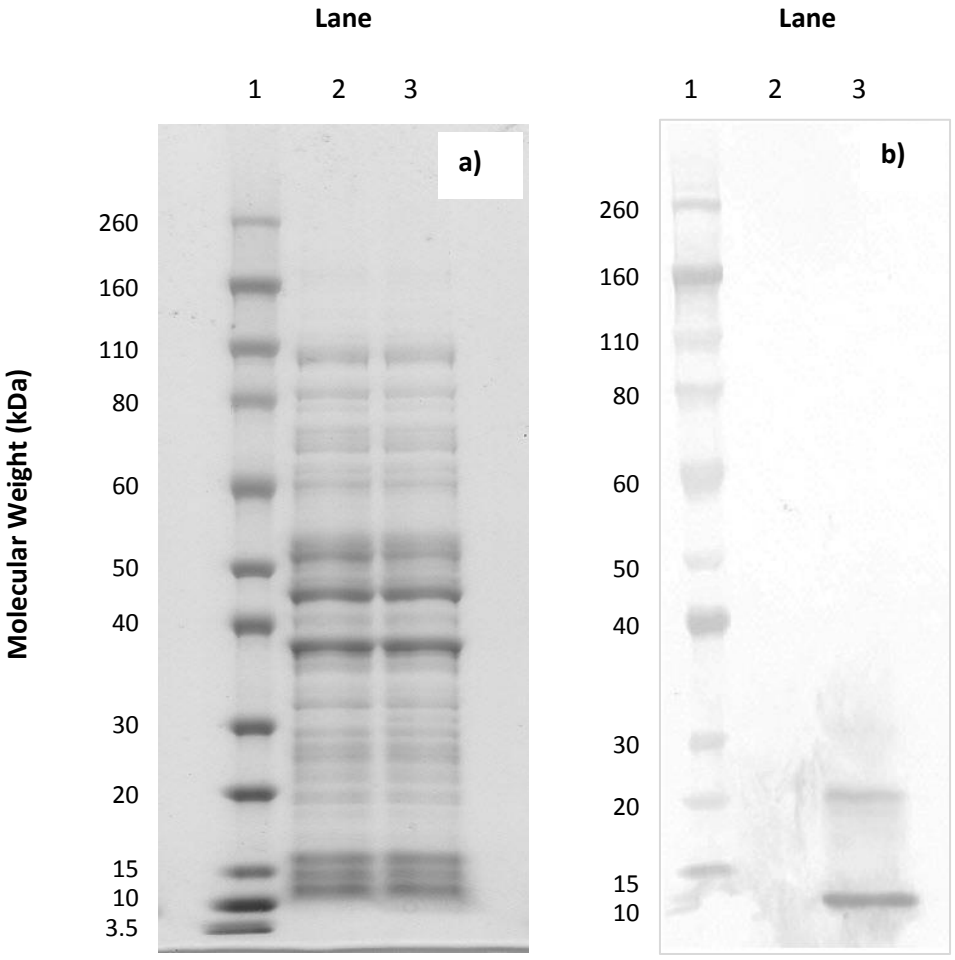

Figure 42. Coomassie and Western blot of prokaryote expressed recombinant human S100P.

S100P was recombinantly expressed in T7 Shuffle® K12 *E. coli* using the vector pGS-21a-S100P (section 2.6.4). Soluble fraction samples pre (lane 2) and post (lane 3) induction were collected and loaded on two identical 4-12%SDS-PAGE gels. Gel **a)** was Coomassie stained, with gel **b)** Western blotted and probed with an anti-S100P antibody (Abcam). The first lane of each gel was loaded with a broad range, pre-stained molecular weight marker (Life technologies).

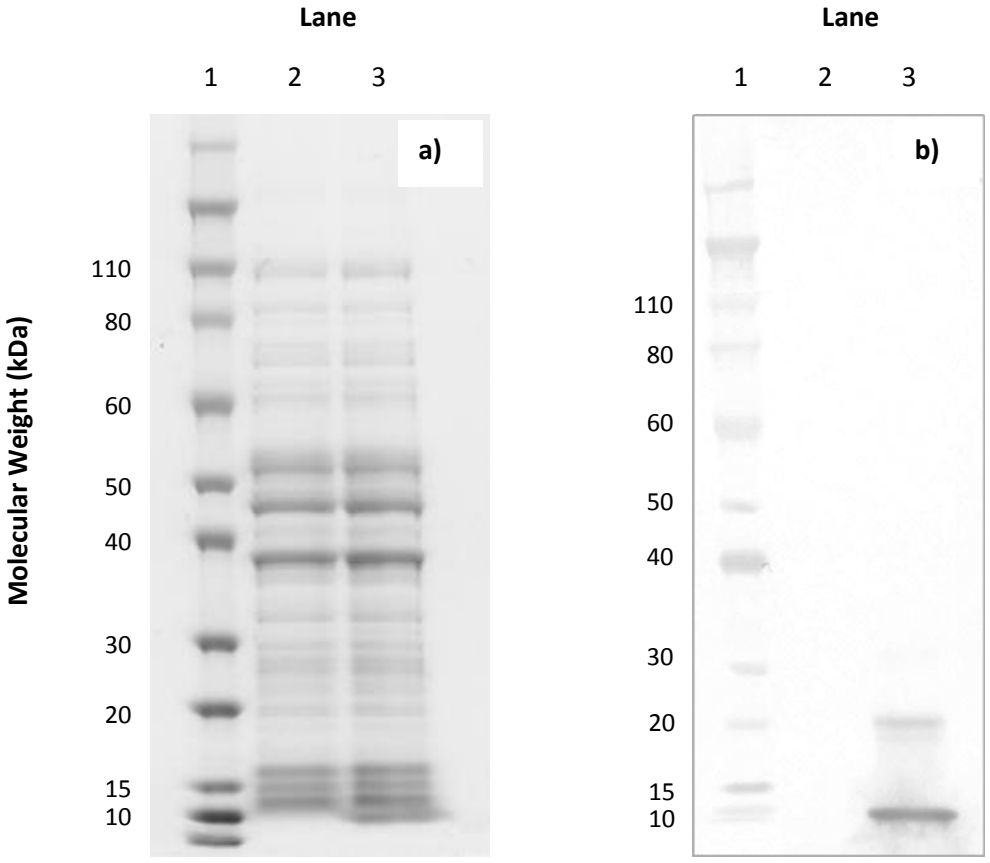

Figure 43. Coomassie and Western blot of prokaryote expressed recombinant human S100A6.

T7 Shuffle® K12 transformed with pGS-21a-S100A6 was induced and soluble fractions pre and post-induction collected as outlined in section 2.6.4 and loaded into lanes 2 and 3 respectively on two 4-12% SDS-PAGE gels. Gel **a)** was Coomassie stained as described in section 2.6.17, while gel was transferred to a PVDF membrane and **b)** Western blotted with an anti-S100A6 antibody (Abcam) (section 2.6.18). Both gels had a broad range pre-stained marker loaded in lane 1 (Life technologies).

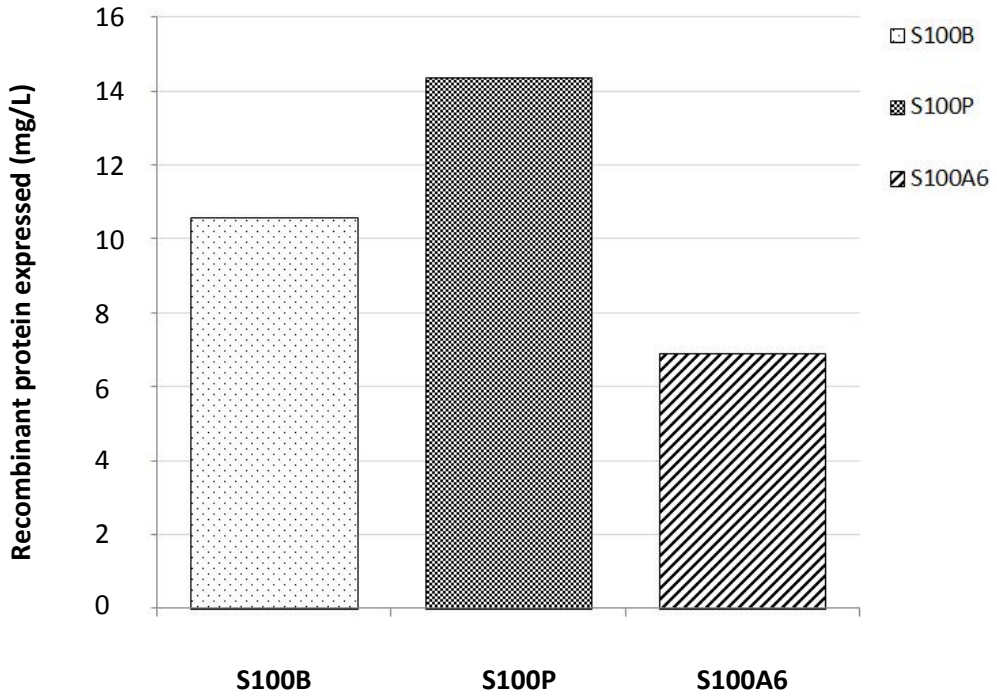

Figure 44. Yields of human S100B, S100P and S100A6 expressed in T7 Shuffle® K12 following phenyl Sepharose® purification.

T7 Shuffle® K12 was used as an expression host for pGS-21a-S100B, pGS-21a-S100P and pGS-21a-S100A6 as described in section 2.6.4. Following induction, host cells were lysed by sonication and the clarified soluble fraction applied to a phenyl Sepharose® column (2.6.9). Eluates were estimated to contain recombinant calgranulins at >95% purity by Coomassie (data not shown), with the concentration of eluates measured by modified Lowry (2.6.15) (n=1).

of the starting soluble fractions and flow-throughs by ELISA revealed approximately 80% of RAGE present in the bacterial lysate bound and was eluted from the heparin resin. Multiple elution peaks were seen in the purification of V, VC_1 and VC_1C_2 (Figure 45, Figure 46 and Figure 47 respectively), correlating with the five isocratic steps of increasing ionic strength used for elution as outlined in section 2.6.10. The V domain of RAGE eluted using 1 M NaCl (Figure 45), while VC_1 and VC_1C_2 were eluted by 500 mM NaCl (Figure 46 and Figure 47 respectively). The fractions were subsequently assayed by polyacrylamide gel electrophoresis, dot blot or ELISA for the presence of RAGE, with only those fractions containing the recombinant protein retained for further analysis. Those fractions containing RAGE were subsequently applied directly to nickel Sepharose® without buffer exchange.

3.4.2 Nickel chromatography of prokaryote RAGE domain constructs V, VC_1 and VC_1C_2

Recombinant V, VC_1 and VC_1C_2 RAGE domain constructs eluted from heparin Sepharose were applied to a nickel HisTrap column (GE) as described in section 2.6.12 and the column washed to remove unbound protein. Approximately 70% of RAGE VC_1C_2 eluted from the nickel column in fractions 17 to 19 (Figure 48) with an overall recovery of 56% of VC_1C_2 recovered in a two-step purification strategy that yielded approximately 7 mg/L of purified RAGE VC_1C_2. Approximately 65% of RAGE VC_1 present in the starting heparin eluate was recovered using nickel chromatography (Figure 49), with a final yield of approximately 1.1 mg/L of pure protein. Approximately 70% of the heparin eluted V domain of RAGE was recovered in elution fractions 17-19 of the HisTrap nickel column, with a yield of approximately 0.2 mg/L as determined by ELISA (Figure 50). The final purified V, VC_1 and VC_1C_2 recombinant RAGE domains were estimated to be greater than 95% pure as determined by Coomassie (Figure 51). Following elution of bound protein, fractions containing RAGE were dialysed into HEPES buffered saline (HBS) in the presence of 2 mM EDTA. Interestingly in the absence of EDTA, a white flocculate appeared in the dialysis cassettes that correlated with a loss of much of the soluble eluted protein. It is reasonable to speculate that nickel ions leeching from the column are co-ordinating the histidine tags at the C-terminus of the eluting RAGE to promote aggregation. The inclusion of EDTA to chelate any co-eluting nickel ions, followed by dialysis, circumvented the precipitation of the VC_1C_2 and VC_1 domains. The V domain eluate still formed a small amount of white flocculate even in the presence of EDTA, however, this resulted in almost no loss of protein.

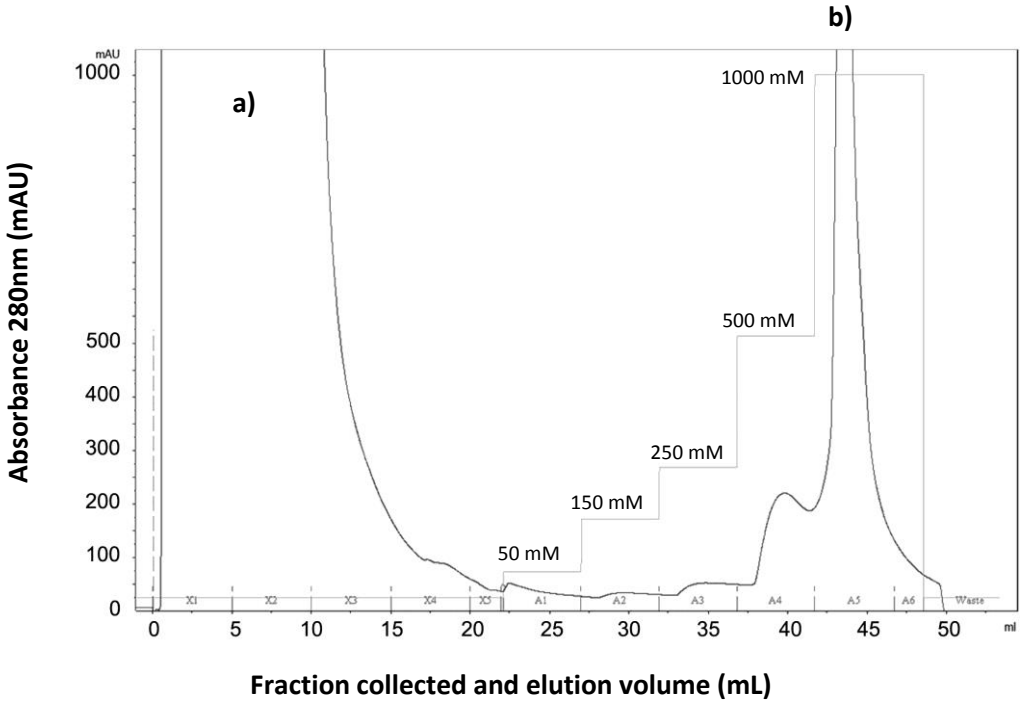

Figure 45. Heparin Sepharose® purification of prokaryote expressed V RAGE domain construct.

T7 Shuffle® K12 *E. coli* expressing recombinant RAGE V domain was clarified as outlined in section 2.6.3. This soluble fraction was **a)** applied to a Heparin HiTrap™ column (GE) on an AKTA Purifier FPLC (GE). The column was washed and eluted using five isocratic steps with increasing salt concentrations to a maximum of 1 M NaCl as detailed in method 2.6.10. The V domain was eluted in peak **b)** and yield determined by ELISA (section 2.6.19).

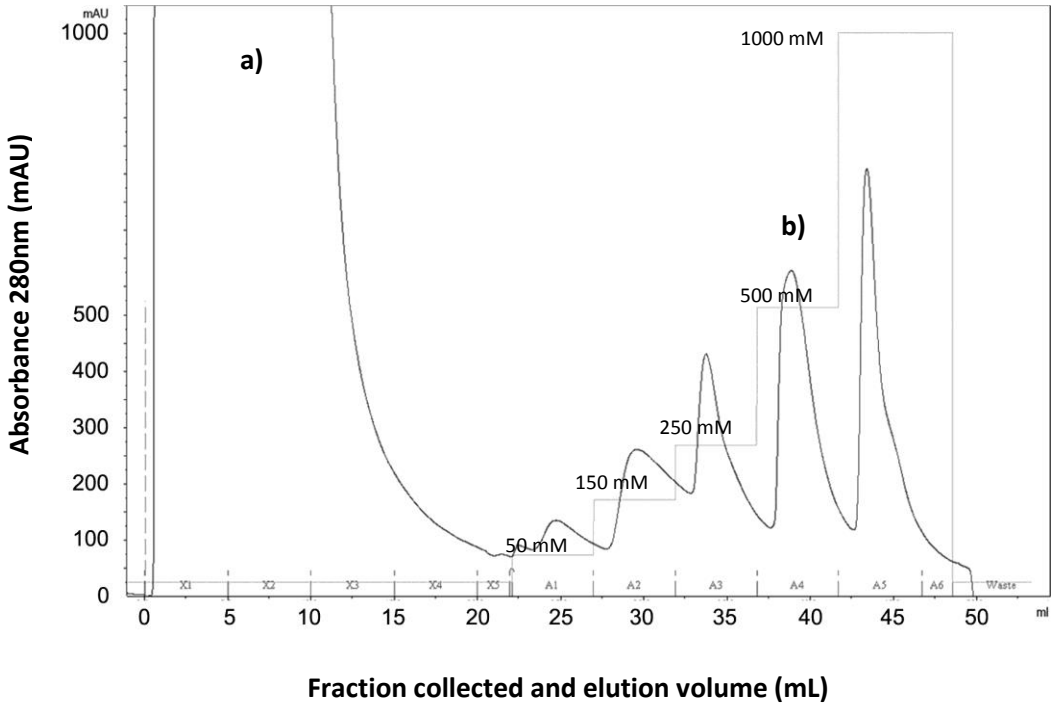

Figure 46. Heparin Sepharose® purification of prokaryote expressed VC_1 RAGE domain.

The clarified soluble fraction of T7 Shuffle® K12 *E. coli* containing recombinant RAGE VC_1 was **a)** applied to a Heparin HiTrap™ column (GE) on an AKTA Purifier FPLC (GE). The column was washed before bound VC_1 domain RAGE was eluted in fraction **b)** using isocratic steps with a final eluting salt concentration of 1 M as detailed in method 2.6.10 with the yield of RAGE VC_1 determined by ELISA (section 2.6.19).

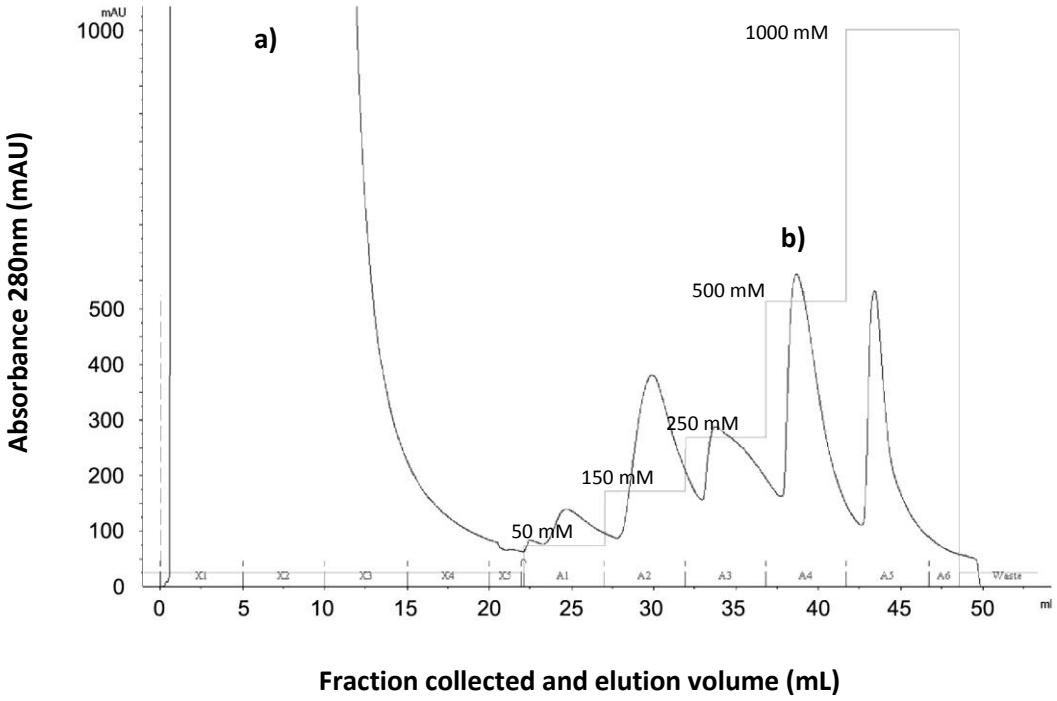

Figure 47. Heparin Sepharose® purification of prokaryote expressed RAGE VC_1C_2 domain.

The soluble fraction of T7 Shuffle® K12 *E. coli* expressing recombinant RAGE VC_1C_2 was clarified as outlined in section 2.6.3 before being applied to a heparin Sepharose® HP column (GE) on an AKTA Purifier FPLC (GE). The column was **a)** washed before bound RAGE was eluted in fraction **b)** using five isocratic salt concentrations ranging from 50 mM to a final concentration of 1 M as detailed in method 2.6.10 with the yield of RAGE VC_1C_2 determined by ELISA (section 2.6.19).

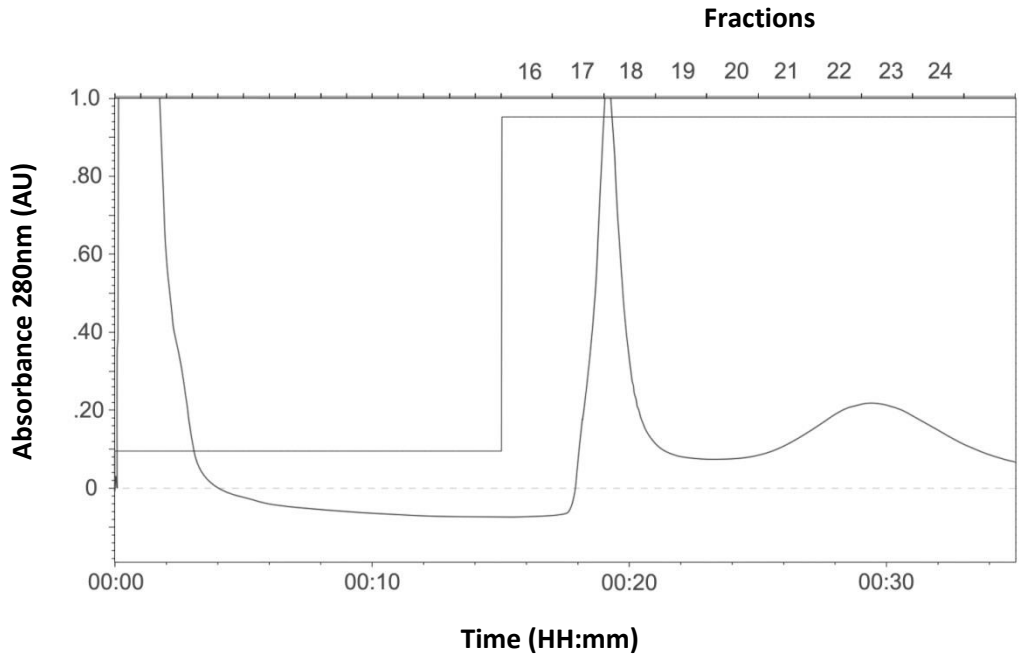

Figure 48. Nickel Sepharose® purification of 6xhis tagged prokaryote expressed VC_1C_2 RAGE domains.

Heparin Sepharose® fractions containing RAGE VC_1C_2 were pooled and applied to a Nickel Sepharose® HisTrap HP column (GE) on a Bio-Rad Biologic FPLC. The column was washed and then eluted with a 250 mM imidazole buffer as described in section 2.6.12.

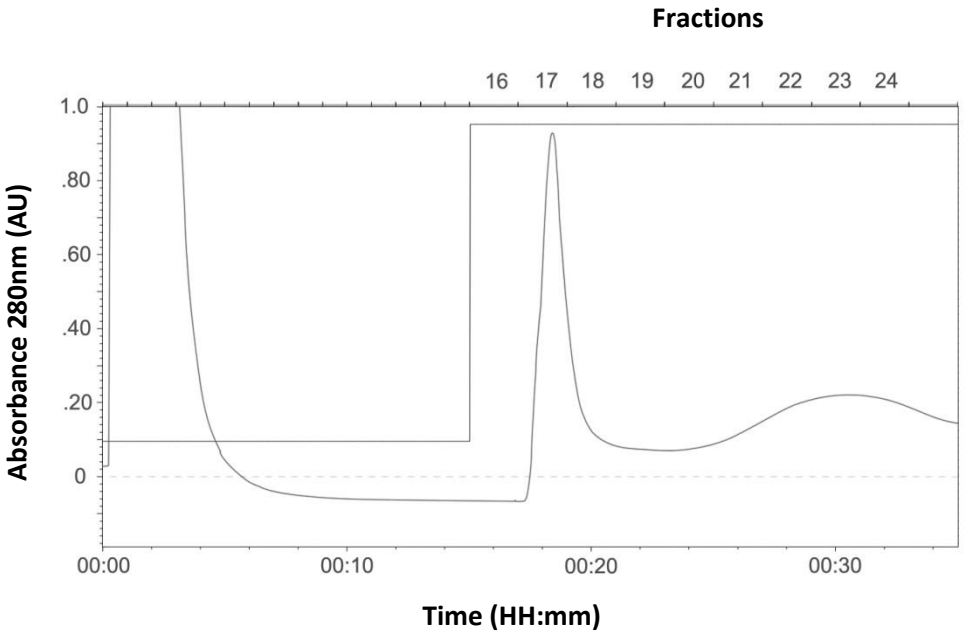

Figure 49. Nickel Sepharose® purification of 6xhis tagged prokaryote expressed VC_1 RAGE domains.

Heparin Sepharose® eluate containing RAGE VC_1 was loaded onto a HisTrap HP column (GE) connected to a Bio-Rad Biologic FPLC. The column was washed and protein eluted using 250 mM imidazole buffer, as detailed in section 2.6.12.

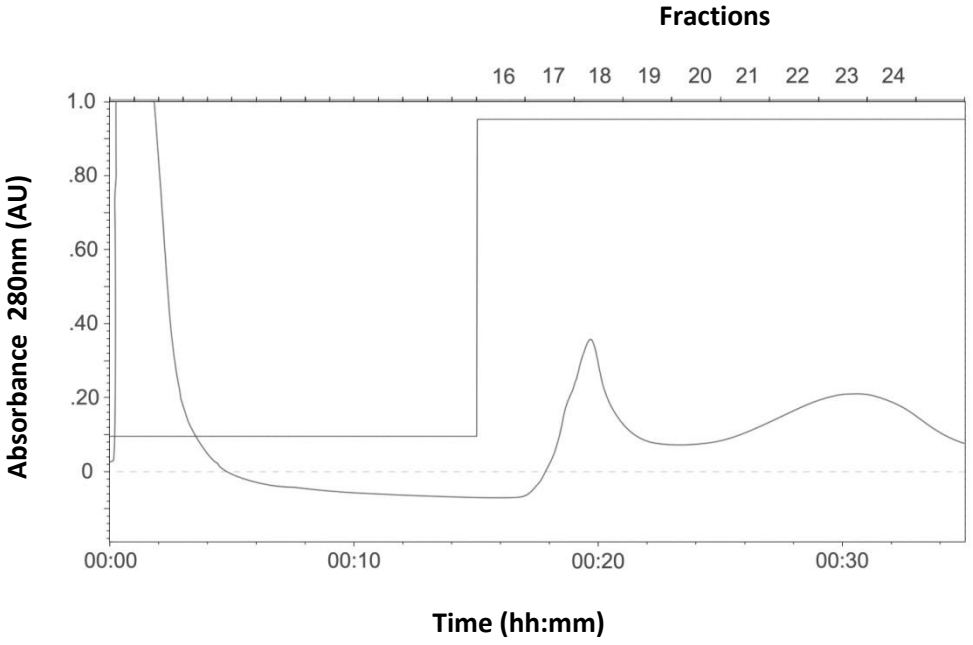

Figure 50. Nickel Sepharose® purification of 6xhis tagged prokaryote expressed V RAGE domain.

Heparin Sepharose eluate containing V domain recombinant protein was loaded onto a HisTrap HP column (GE) connected to a Bio-Rad Biologic FPLC. The column was washed and protein eluted using a 250 mM imidazole buffer (pH 7.4) as described in 2.6.12.

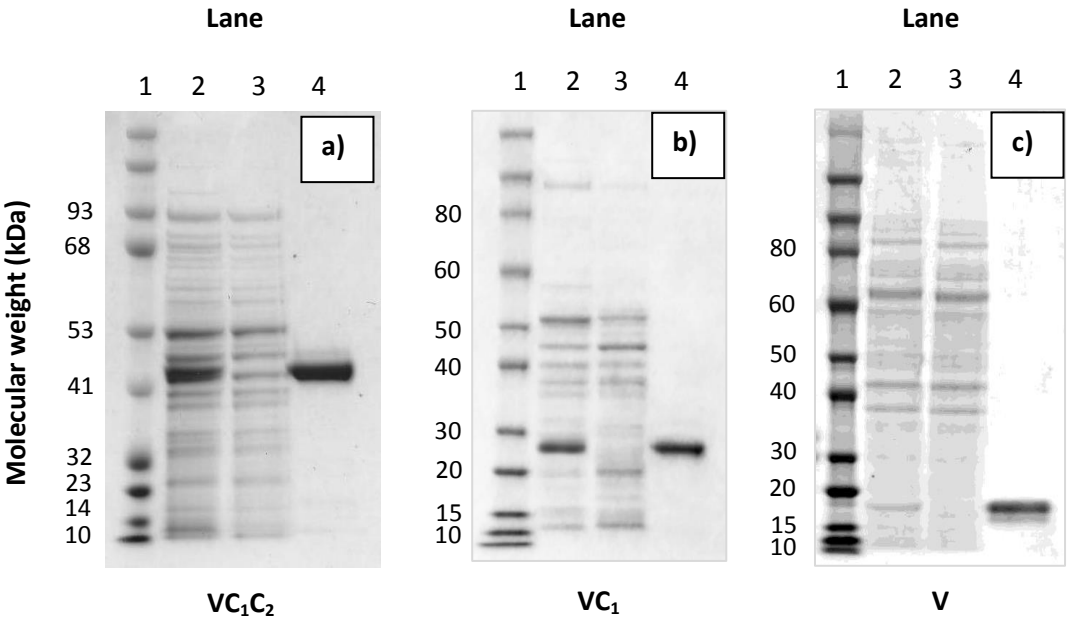

Figure 51. Coomassie stain of purified recombinant V, VC_1 and VC_1C_2 RAGE domains.

RAGE recombinant proteins present in the soluble fractions of T7 Shuffle® K12 pre and post-induction was loaded into lanes 3 and 2, respectively of gels **a)** VC_1C_2, **b)** VC_1 and **c)** V, respectively. The recombinant proteins of each RAGE construct, purified by successive heparin and nickel affinity chromatography (Figure 45 to Figure 47, and Figure 48 to Figure 50 respectively) are shown in lane 4 of each gel. Lane 1 of each gel was loaded with a prestained broad range marker (Life technologies). All gels were run as described in method 2.6.16 before being Coomassie stained (section 2.6.17).

3.4.3 Purification of full length and truncated human HMGB1

Full length HMGB1 in subcloned into pGS-21a was expressed in T7 Shuffle® K12, with the pelleted culture subsequently solubilised using perchloric acid as outlined in method 2.6.6. The protein retained in the acid soluble fraction was visualised on a reducing SDS-PAGE gel and Coomassie stained to evaluate the heterogeneity of remaining protein (Figure 52, lane 3). A main band of approximately 28 kDa was apparent, along with some minor, low molecular weight species also visible. Subsequent size exclusion chromatography (SEC) of this soluble fraction demonstrated the presence of a single main peak collected in fractions B2 and B3 (Figure 53), with further Coomassie gel analysis showing a single band representing HMGB1 of greater than 95% purity (Figure 54). Approximately 1.8 mg/L of full length HMGB1 was purified from a 1 litre starting culture.

Truncated human HMGB1 (ΔHMGB1) was kindly provided by the Rauvala laboratory, Helsinki and is the only recombinant protein not expressed using vector pGS-21a. Following induction for 2.5 hours, T7 Shuffle K12 transformed with pGEX-6P1-deltaHMGB1 was sonicated and the soluble fraction clarified as described in 2.6.3. A 1mL GSTrap column was connected to a Bio-Rad Biologic FPLC before loading the soluble fraction and continuing to wash the column until all unbound protein was eluted. The system was paused (Figure 55a) and the GSTrap column carefully removed for the addition of protease. This disconnection is reflected by an upward shift in the absorbance base line. Following cleavage of the GST tag as described in section 2.6.13, a number of fractions were collected, with fraction 18 containing a large peak (Figure 55) shown to mostly consist of a single protein approximately 24 kDa in size (Figure 56), as visualised by Coomassie stain on a reducing gel. This fraction was further purified by perchloric acid extraction (section 2.6.6) and loaded alongside T7 Shuffle® K12-ΔHMGB1 samples pre and post-induction (Figure 57). Figure 57, lane 4 showed the presence of ΔHMGB1, with the minor bands previously seen no longer visible. Approximately 2.4 mg/L of ΔHMGB1 was purified from a 1 litre starting culture (Figure 58).

3.4.4 Purification of S100B, S100P and S100A6

Baudier *et al* (1982) reported the use of phenyl Sepharose® for the selective purification of S100B through the use of zinc dications to induce conformational change that enable some calgranulins to bind hydrophobic moieties. T7 Shuffle® K12 was used to express

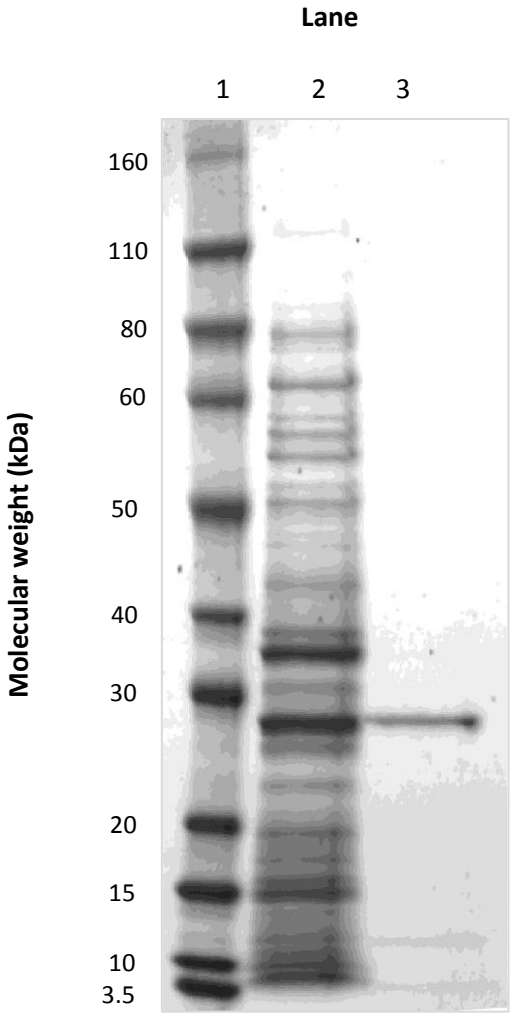

Figure 52. Perchloric acid purification of full length HMGB1.

T7 Shuffle® K12 transformed with pGS-21a-hHMGB1 was induced to express full length HMGB1. An aliquot of total protein in the induced culture immediately prior to acid solubilisation is shown in lane 2, with a broad range molecular weight marker present in lane 1 (Life technologies). The culture was pelleted and solubilised in perchloric acid as described in section 2.6.6. The soluble fraction was loaded in lane 3 and the SDS-PAGE gel Coomassie stained (section 2.6.17).

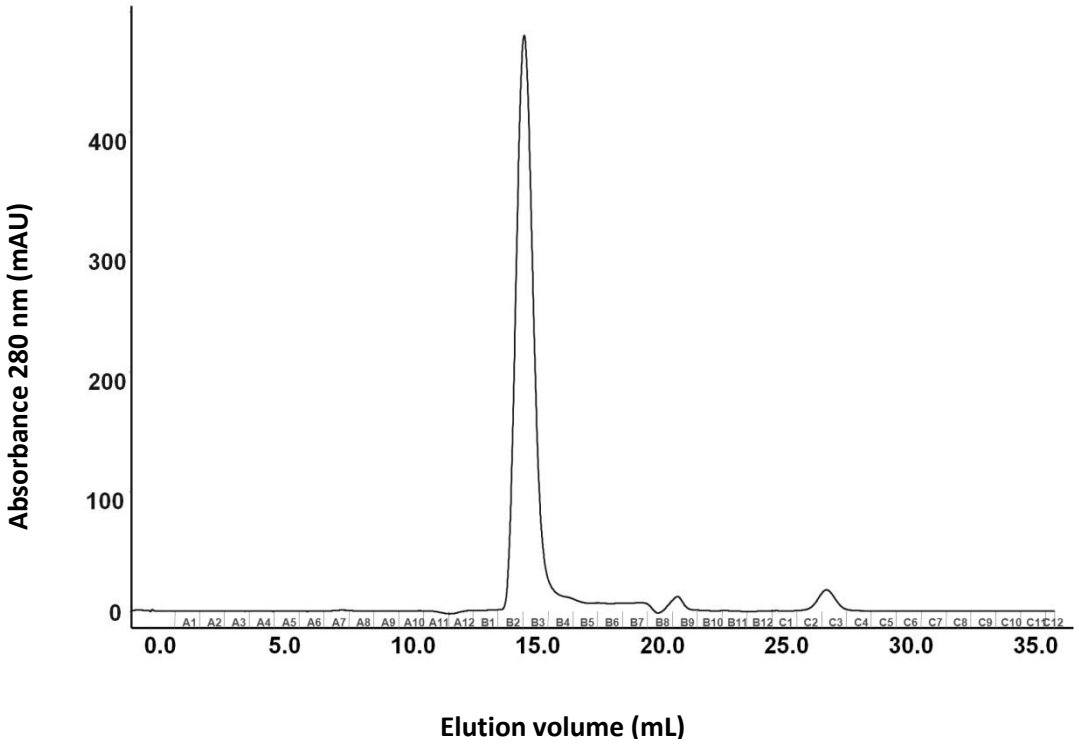

Figure 53. Purification of full length HMGB1 by size exclusion chromatography.

Perchloric acid purified HMGB1 was titrated back to pH 7-7.4 and concentrated to 0.5 mL. The HMGB1 fraction was applied to a HiPrep 16/60 Sephacryl S-200 (GE) on an AKTA Purifier (GE) and fractionated as described in section 2.6.11.

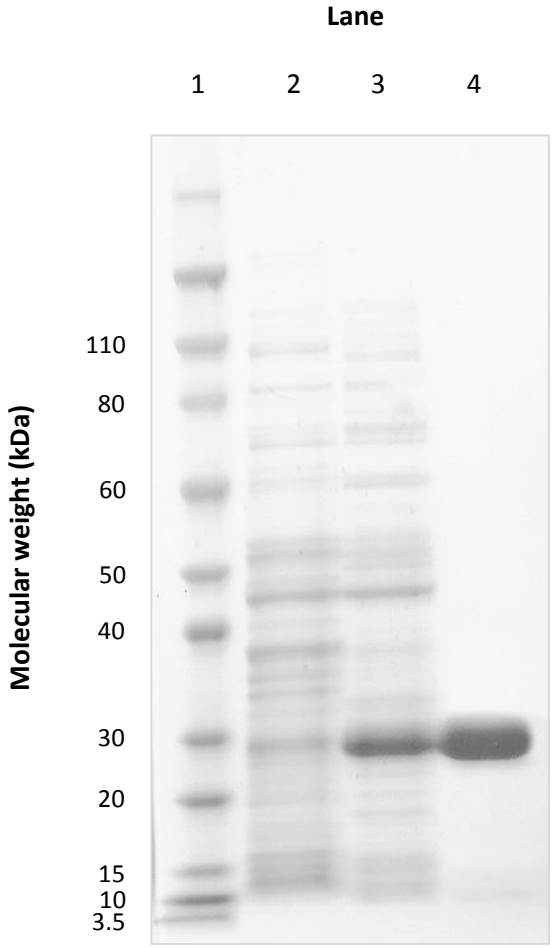

Figure 54. Coomassie stain of purified full length human HMGB1.

Recombinant HMGB1 was expressed by T7 Shuffle® K12. Soluble fractions pre and post induction were loaded in lanes 2 and 3, respectively. HMGB1 purified by successive perchloric acid and size exclusion steps (Figure 52 and Figure 53 respectively) is shown in lane 4. A molecular weight marker was loaded in lane 1 (Life technologies). The samples were run on a reducing SDS-PAGE gel and Coomassie stained as described in section 2.6.17.

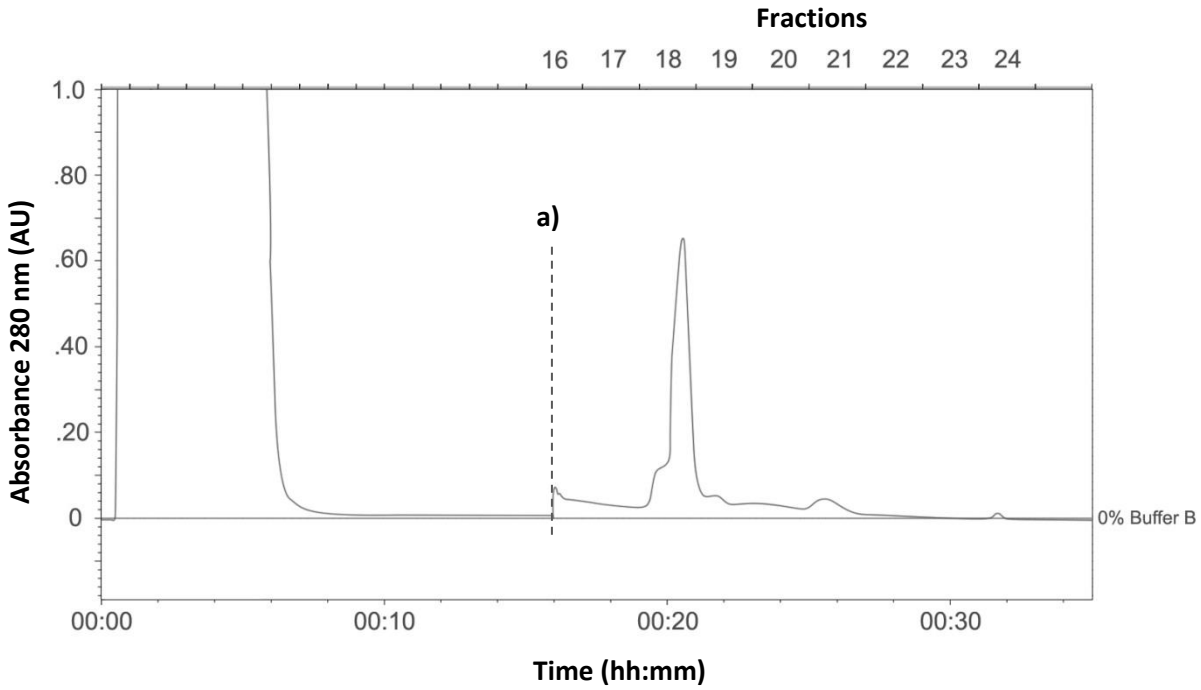

Figure 55. Glutathione affinity chromatography and on-column cleavage of recombinant truncated human HMGB1-GST.

T7 Shuffle® K12 transformed with pGEX-6P1-deltaHMGB1 was induced as outlined in section 2.6.5. The soluble fraction was applied to a GSTrap™ HP column on a Bio-Rad Biologic FPLC and washed until the 280 nm absorbance was steady. The system was paused **a)** and PreScission Protease manually injected onto the column. A HisTrap column was connected in series to the end of the GSTrap column and the two columns re-connected to the FPLC to incubate for 4 hours at 4°C (section 2.6.13). The wash was then resumed and the eluates collected.

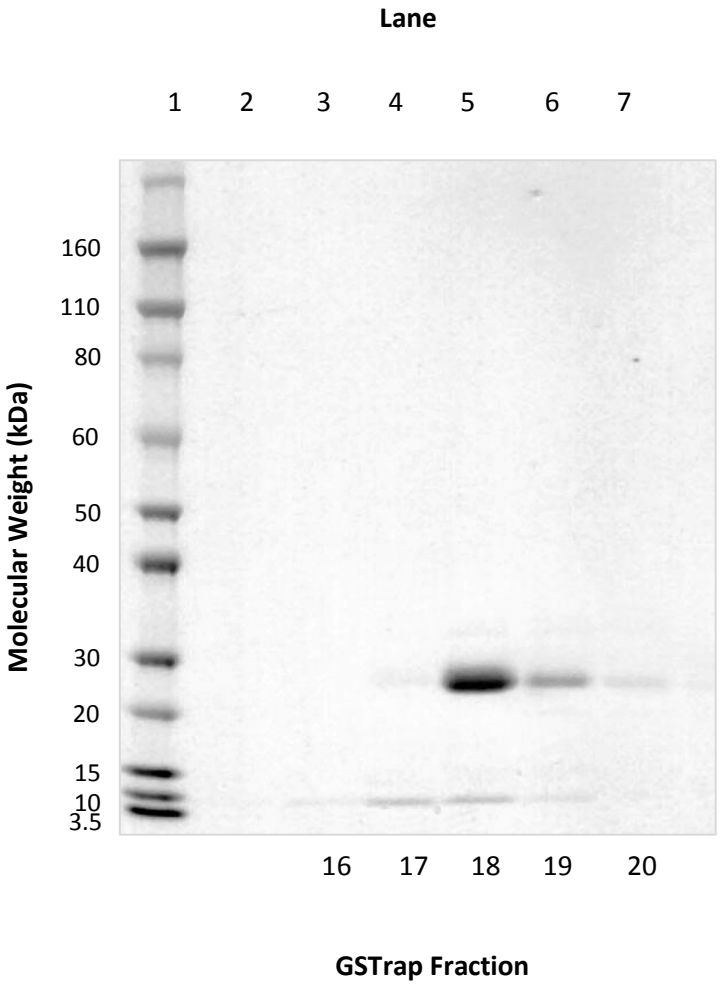

Figure 56. Glutathione chromatography eluates containing truncated HMGB1.

GSTrap HP fractions 16-20 (Figure 55) were run on a 4-12% SDS-PAGE reducing gel in lanes 3-7 respectively, before being Coomassie stained (section 2.6.16). A broad range molecular weight marker was loaded in to lane 1 (Life technologies).

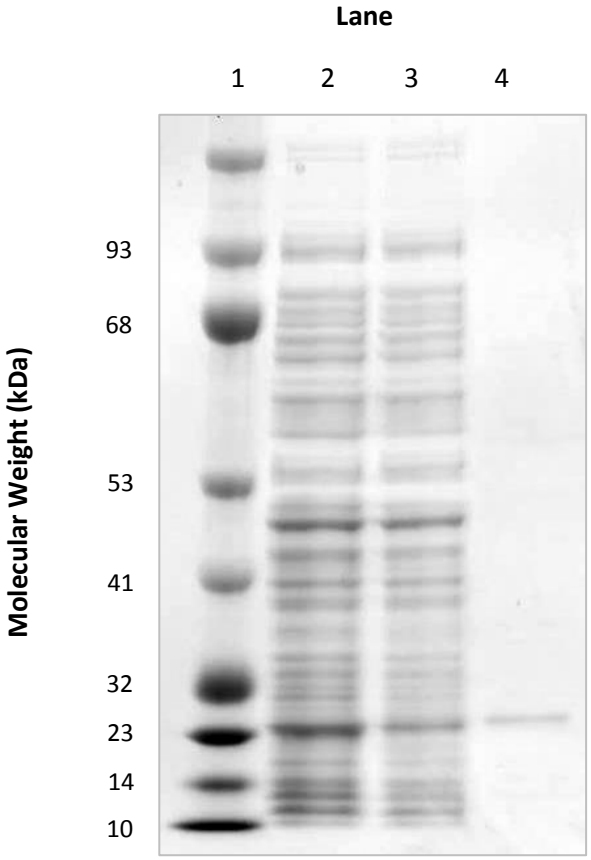

Figure 57. Coomassie stain of purified truncated human HMGB1.

Truncated HMGB1 was expressed by T7 Shuffle® K12 using pGEX-6P1-deltaHMGB1, with samples pre and post induction loaded in lanes 2 and 3 of an SDS-PAGE gel respectively. Fractions 19 and 20 from GST affinity chromatography (Figure 56) were pooled, perchloric acid purified as outlined in section 2.6.6, and loaded into lane 4. The samples were run on a reducing SDS-PAGE gel with a broad range molecular weight marker in lane 1 (Fermentas) and Coomassie stained as described in section 2.6.17.

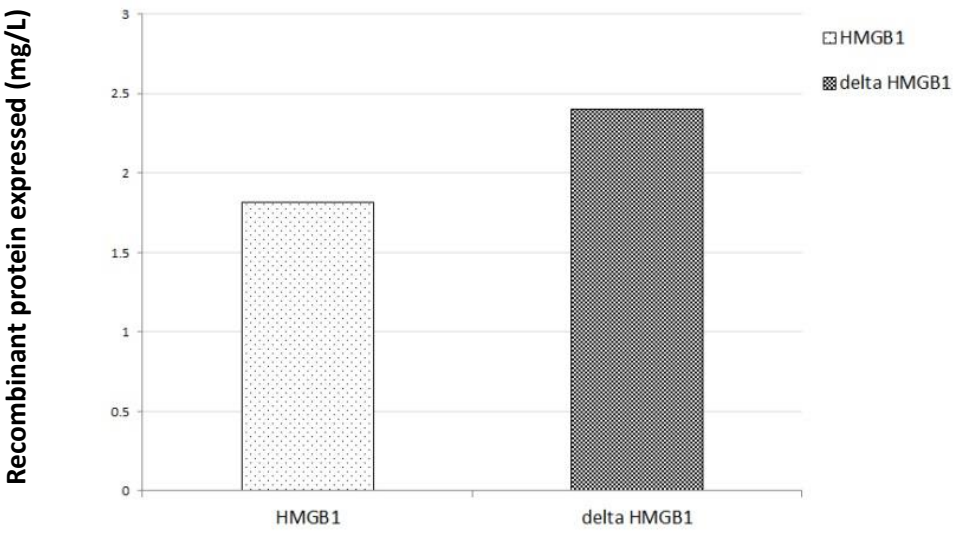

Figure 58. Yields of full length HMGB1 and truncated HMGB1 from T7 Shuffle® K12 following acid precipitation of the host.

T7 Shuffle® K12 was used as an expression host for pGS-21a-hHMGB1 (full length) and pGEX-6P1-deltaHMGB1 (truncated). Following induction, cells were harvested and solubilised using 6% perchloric acid as described in section 2.6.6. The clarified, soluble fraction was titrated back to pH 7-7.4 and protein content estimated by the Bradford method (2.6.14) (n=1).

S100B, S100P and S100A6 as described in section 2.6.4. The clarified soluble fractions were purified by phenyl Sepharose® chromatography (Figure 59 to Figure 61) on a Bio-Rad Biologic FPLC as described in section 2.6.9. All three calgranulins eluted in the presence of wash buffer containing 2.5 mM EGTA (buffer B) and appeared as single peaks in fraction 17 for both S100B (Figure 59) and S100P (Figure 60), with S100A6 eluting as part of a large single peak across fractions 17 and 18 (Figure 61). The flow-through and fraction 17 of the S100B and S100P phenyl Sepharose® eluates was run on an SDS-PAGE and Coomassie stained as described in section (2.6.17). A single band of approximately 10 kDa in size was visible in the fraction 17 eluates for both S100B (Figure 62a) and S100P (Figure 62b), with no equivalent band present in either flow-through. Similar Coomassie staining of S100A6 phenyl Sepharose® samples (Figure 62c), did show the presence of a notable 10 kDa band in the flow-through, along with a prominent single protein of the same size in fraction 17. This likely indicates saturation of the phenyl Sepharose® resin. The binding capacity for phenyl Sepharose® CL-4B varies between 5-20 mg/mL of resin depending on the protein species bound. It is likely that for calgranulins, the binding capacity is approximately 14 mg/mL. The concentration of each purified calgranulin was 10.6 mg/L, 14.4 mg/L and 6.9 mg/L respectively as determined by the Bradford assay (section 2.6.14).

3.5 Protein Purification and Function

3.5.1 Binding of insect and bacterial expressed RAGE recombinant domain constructs to ribose-AGE

A novel assay was developed to evaluate whether RAGE constructs expressed in insect cells were able to bind one of their key ligands, ribose-AGE (section 2.7.1). Briefly, ribose-AGE was adsorbed onto NUNC Maxisorp plate well walls with unabsorbed surface subsequently blocked with a PBS + casein solution. Conditioned media from insect cells stably secreting RAGE V, VC_1 and VC_1C_2 was added to the wells in triplicate and allowed to bind to the ribose-AGE. The media was removed and free RAGE removed by gentle washing of the wells with PBS+casein. Anti-RAGE antibody conjugated to horse radish peroxidase (HRP) was used to detect bound RAGE, with free antibody removed by gentle washing. The amount of antibody present was determined in a similar manner to an ELISA, using a TMB HRP substrate mixture to generate a chromogen. The amount of

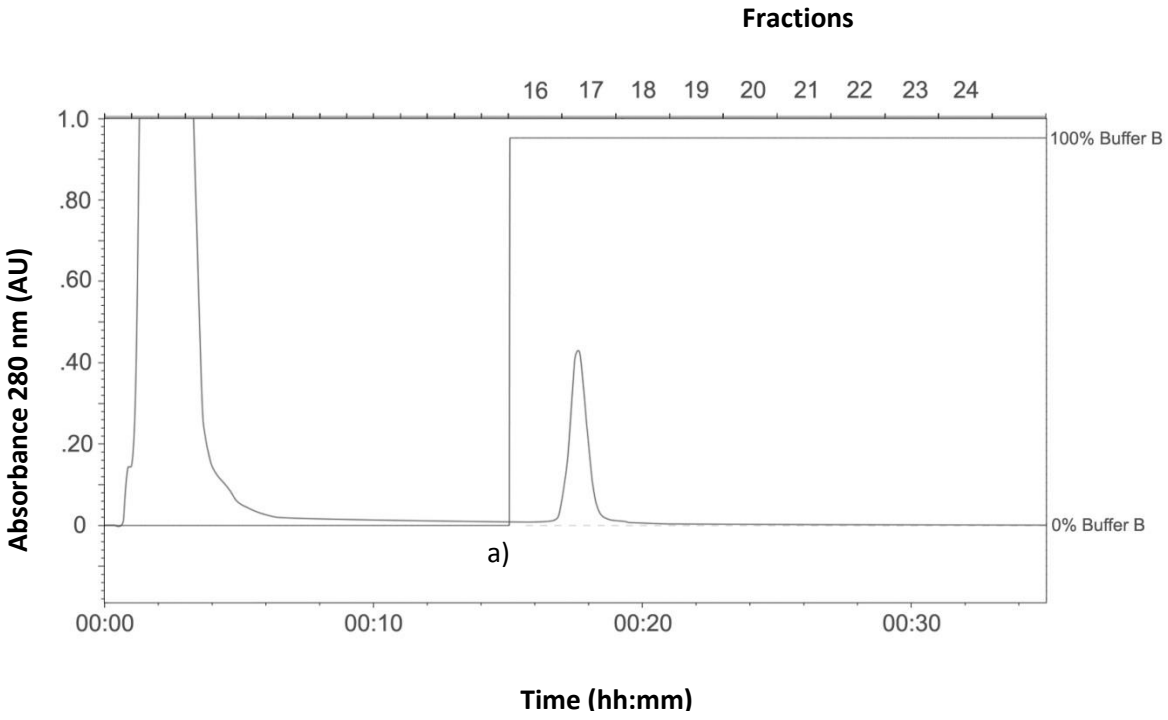

Figure 59. Phenyl Sepharose® purification of S100B.

Human S100B was expressed in T7 Shuffle® K12 and the soluble fraction clarified as described in section 2.6.3. Calcium chloride was added to the soluble fraction for a final working concentration of 5 mM and the solution applied to a 1 mL phenyl Sepharose® column at 0.25 mL/min as described in section 2.6.9. The column was washed and eluted with **a)** 100% buffer B (wash buffer containing 2.5 mM EGTA) as described in section 2.6.9.

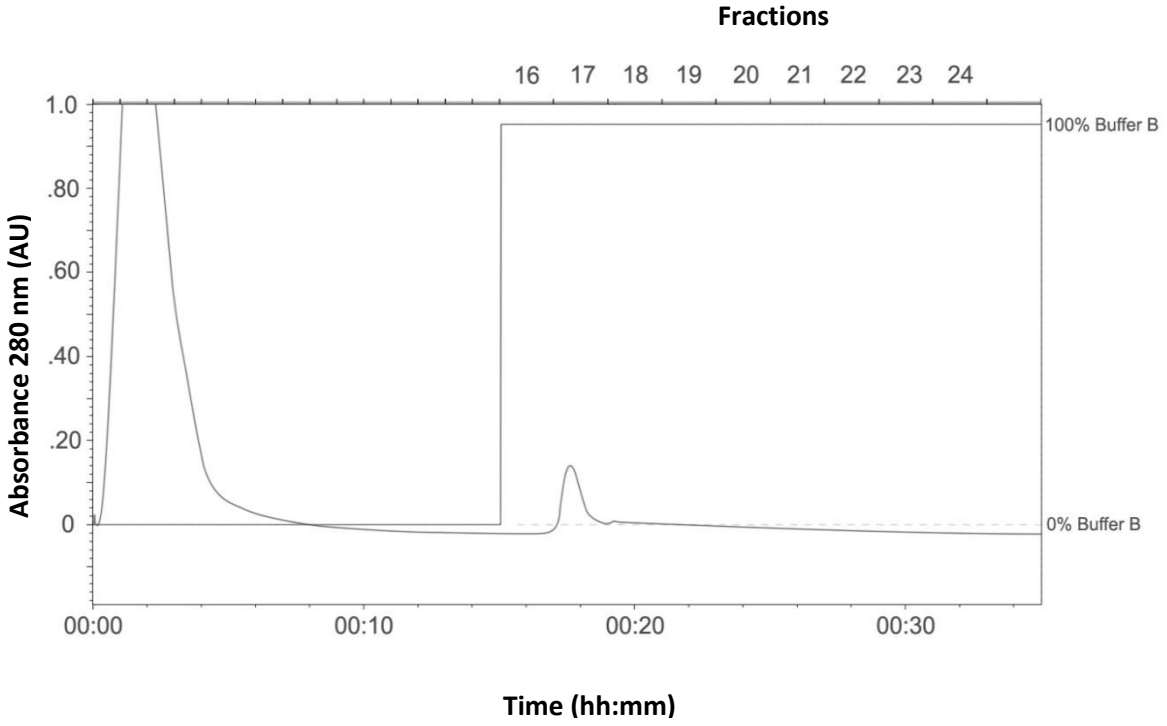

Figure 60. Phenyl Sepharose® purification of S100P.

Human S100B was expressed in T7 Shuffle® K12 and the soluble fraction clarified as described in section 2.6.3. Calcium chloride was added to the soluble fraction for a final working concentration of 5 mM and the solution applied to a phenyl Sepharose® column as described in section 2.6.9. The column was washed and eluted with **a)** 100% buffer B (wash buffer containing 2.5 mM EGTA) and fractions collected as described in section 2.6.9.

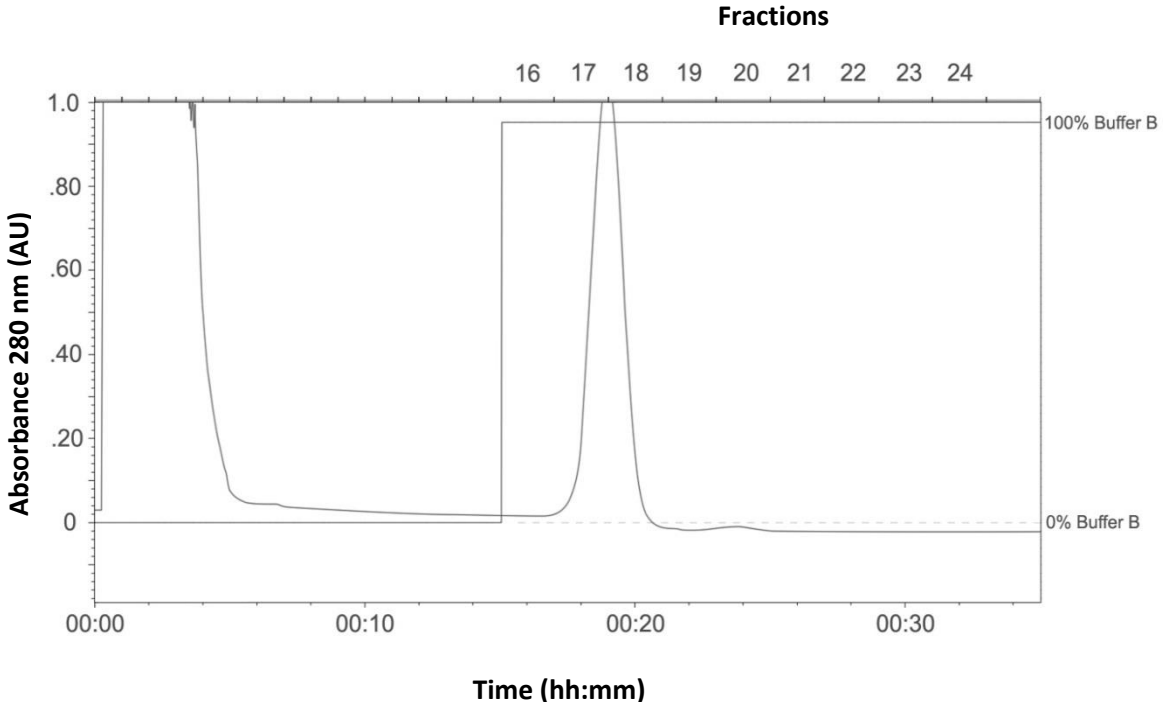

Figure 61. Phenyl Sepharose® purification of S100A6.

T7 Shuffle® K12 transformed with pGS-21-S100A6 was induced and the clarified soluble fraction supplemented with a working concentration of 5 mM $CaCl_2$. This sample was immediately applied to a phenyl Sepharose® column as described in section 2.6.9. The column was washed and eluted with **a)** 100% buffer B (wash buffer containing 2.5 mM EGTA), with fractions collected as described in section 2.6.9.

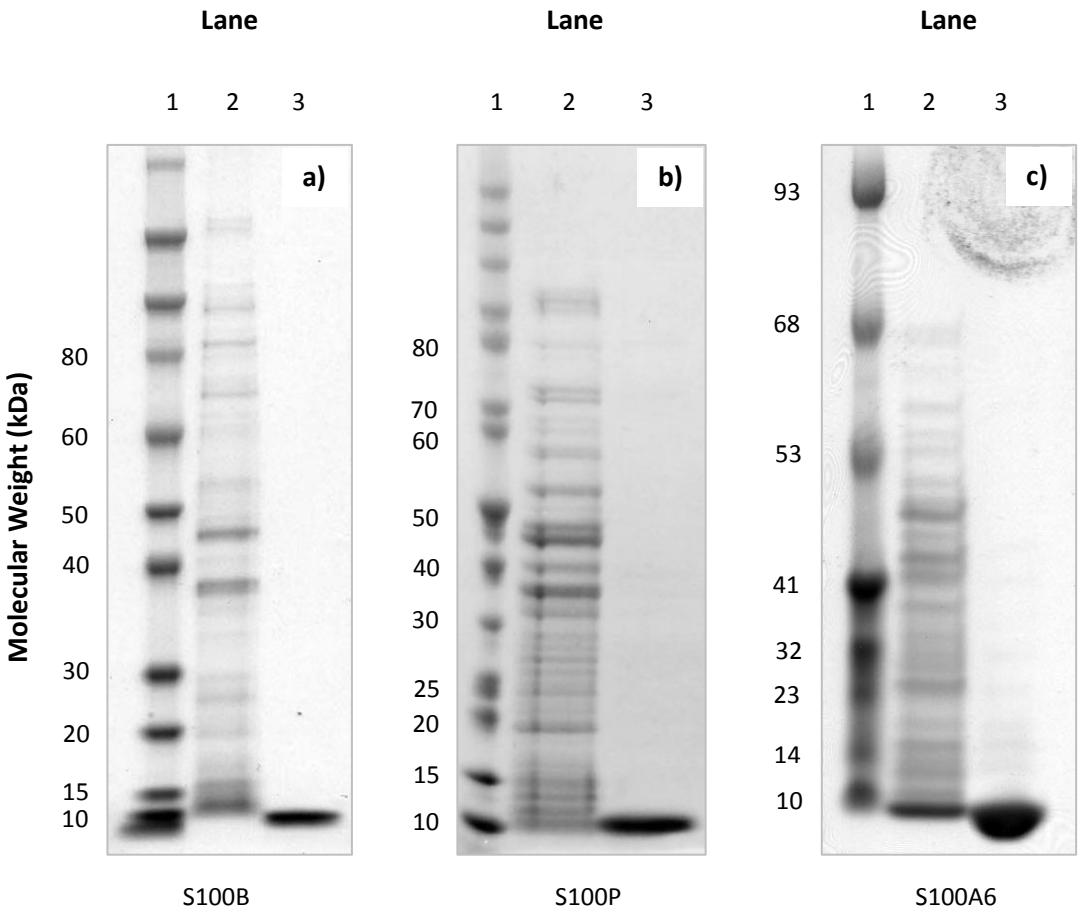

Figure 62. Phenyl Sepharose® purified S100B, S100P and S100A6.

a) S100B, **b)** S100P and **c)** S100A6 fractions from phenyl Sepharose® (Figure 59 to Figure 61 respectively), were loaded onto a reducing 4-12% SDS-PAGE gel. Lanes 2 on each gel was loaded with a sample of flow through, alongside fraction 17 in lane 3. A broad range marker was loaded in lane 1 of each gel (a) and b) Life technologies, c) Fermentas) and run as outlined in section 2.6.16, before being Coomassie stained (method 2.6.17).

chromogen generated was proportional to the amount of bound RAGE and was measured at 450 nm spectrophotometrically. Both RAGE VC_1 and VC_1C_2 expressed in insect and prokaryotic hosts bound in a concentration dependent manner with a saturation effect at the higher concentrations of RAGE suggesting specificity of binding to ribose-AGE (Figure 63, Figure 64). Insect expressed RAGE VC_1C_2 (K_D ≈ 58nM ± 11nM) (Figure 63a) and VC_1 (K_D ≈ 71nM ± 13nM) (Figure 63b), bound ribose-AGE with slightly higher affinities than the corresponding prokaryote expressed VC_1C_2 (K_D ≈ 80nM ± 13nM) (Figure 64a) and VC_1 (K_D ≈ 89nM ± 28nM) (Figure 64b); however the differences are not statistically significant. The V domain expressed by both insect (Figure 63c) and bacterial hosts (Figure 64c), did demonstrate a concentration effect, however, affinities were in the micromolar molar range (K_D ≈ 1.6-4.3 µM) with ambiguous fits. The interaction was specific for RAGE binding to ribose AGE as there was no demonstrable binding in any of the control wells (data not shown).

3.5.2 Binding of insect expressed RAGE recombinant domain constructs to ribose-AGE

Calgranulins S100B, S100P and S100A6 were expressed in T7 Shuffle® K12 and purified as described in section 2.6.9. Calcium chloride was added to stock solutions of each S100 and left to form multimeric homodimers, before being used to coat the wells of a 96-well NUNC MaxiSorp® T7 Shuffle® K12 RAGE VC_1C_2 bound all immobilised S100 proteins in a dose dependent, saturable manner (Figure 65) using the novel plate based binding assay described in section 2.7.1. Nonlinear regression analysis using the least squares fitting method, along with Scatchard analysis of S100B-VC_1C_2 (Figure 65a), S100P-VC_1C_2 (Figure 65b) and S100A6-VC_1C_2 (Figure 65c), generated estimates of affinity in the order of K_D ≈ 36.3 ± 22 nM, K_D ≈ 19.8 ± 6 nM and K_D ≈ 154 ± 41 nM respectively. All Scatchard insets had an approximate y value of 6 when x=0, indicating that all wells were evenly coated with their respective S100 molecules.

3.5.3 Binding of bacterial expressed recombinant RAGE domain constructs V, and VC_1C_2 to HMGB1

Purified HMGB1 expressed in T7 Shuffle® K12 was absorped to the surface of NUNC MaxiSorp wells overnight as described in section 2.7.1. Purified V and VC_1C_2 RAGE expressed in the T7 Shuffle® K12 host, along with VC_1C_2 produced in *Tn5* insect cells was serially diluted as described in section 2.7.1 and added to the plate in triplicate, along

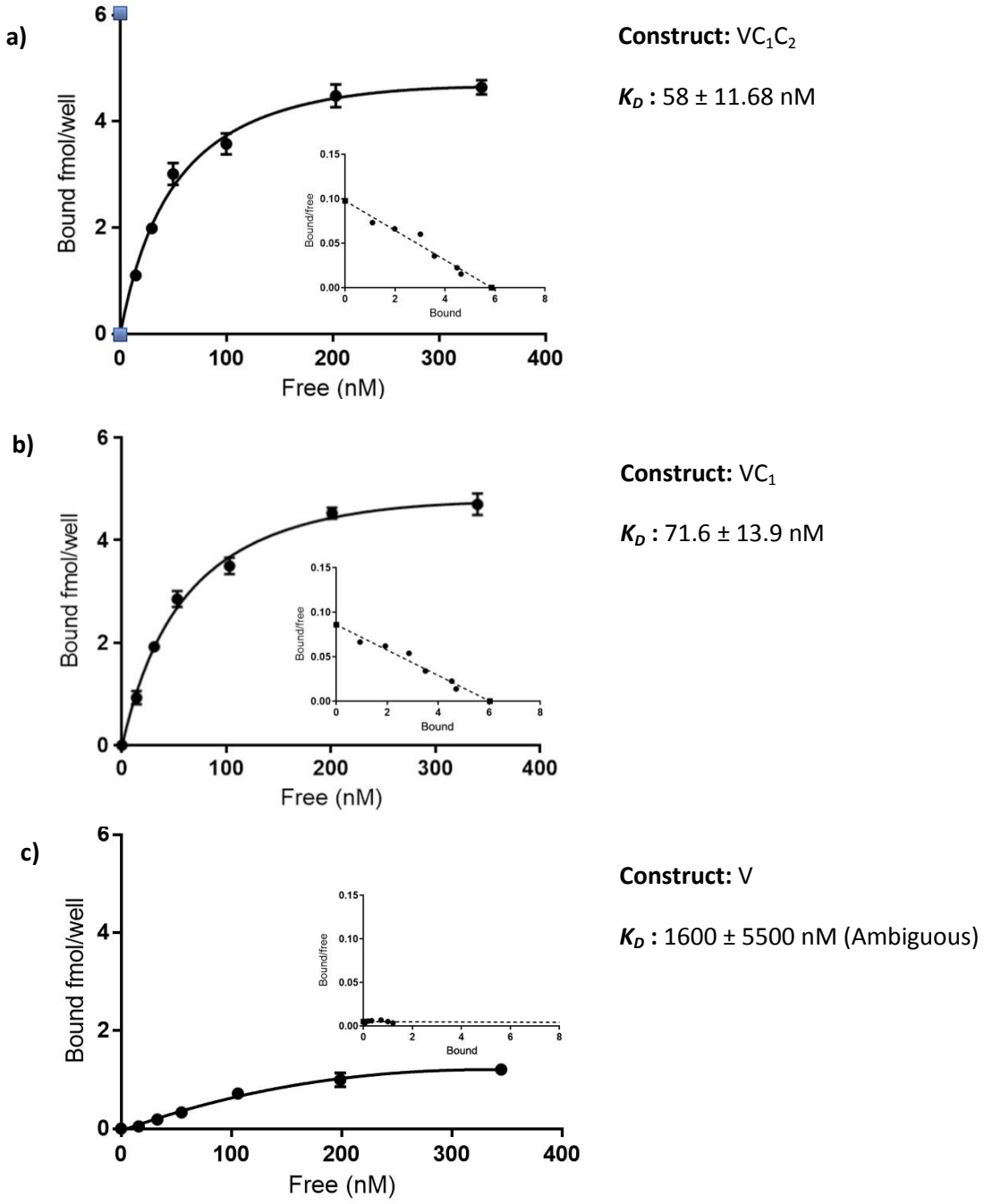

Figure 63. Microtitre plate binding assay of insect expressed RAGE V, VC_1 and VC_1C_2 to ribose-AGE (mean ± se).

Culture media conditioned by *Tn5* insect cells and containing secreted human RAGE **a)** VC_1C_2, **b)** VC_1 or **c)** V recombinant forms, was added to wells on a 96-well NUNC Maxisorp microplate coated with ribose-AGE at various concentrations (section 2.7.1). The ribose-AGE - RAGE interaction was allowed to reach equilibrium, before the media was aspirated (section 2.7.1). Bound RAGE was measured as described in section 2.7.1 and GraphPad Prism used to generate a non-linear regression and Scatchard plot (insets). Three replicates per concentration were used.

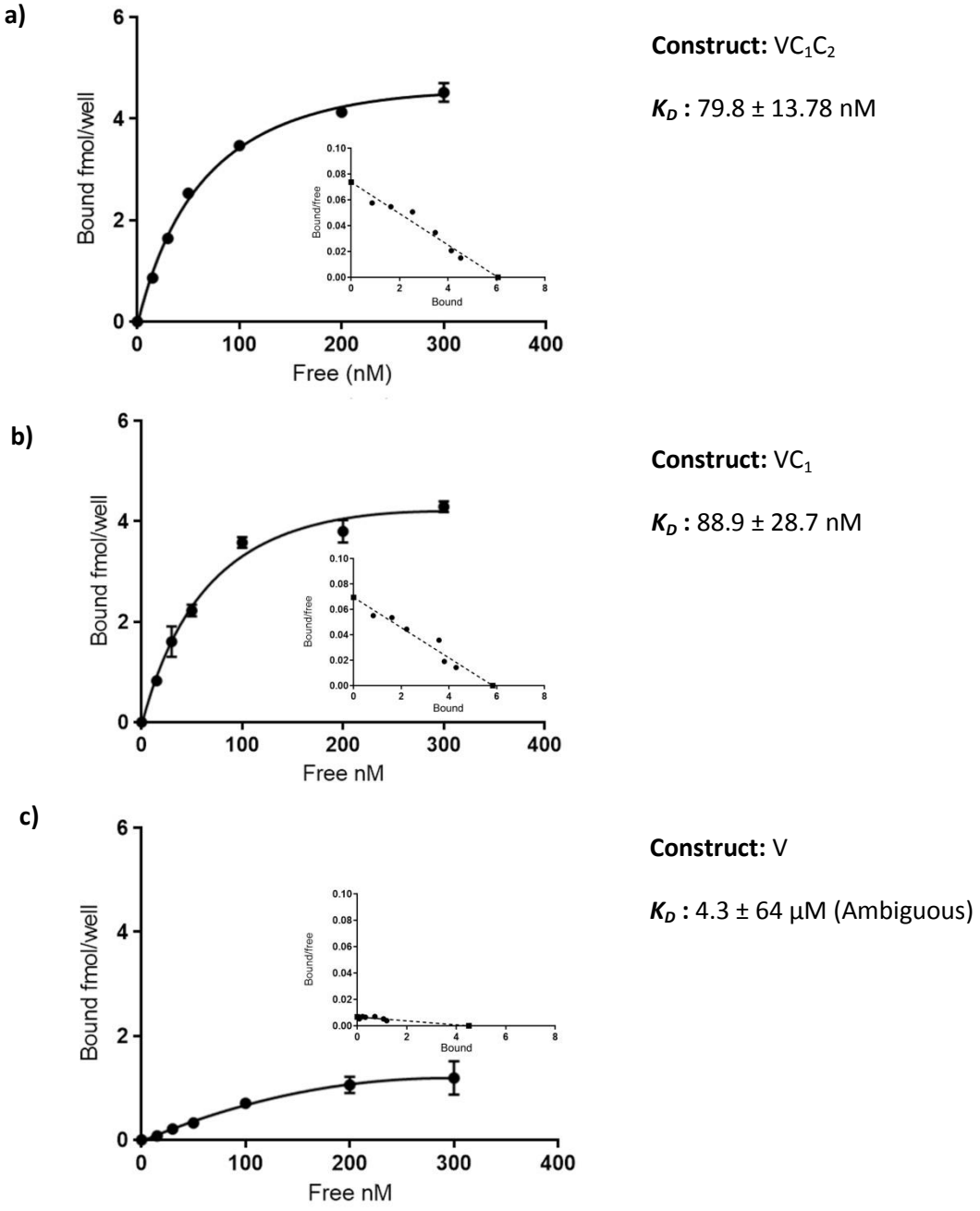

Figure 64. Microtitre plate binding assay of prokaryote expressed RAGE V, VC_1 and VC_1C_2 to ribose-AGE (mean ± se).

Human RAGE domains **a)** VC_1C_2, **b)** VC_1 and **c)** V, and were expressed in T7 Shuffle® K12 as described in section 2.6.1. Serial dilutions of each form of recombinant RAGE was added in series to wells on a 96-well NUNC Maxisorp microplate coated with ribose-AGE (section 2.7.1). The ribose-AGE - RAGE interactions came to equilibrium and free RAGE removed by washing before bound RAGE was measured as described in 2.7.1. The data was fitted by non-linear regression and Scatchard analysis (inset) in GraphPad Prism using three replicates per concentration.

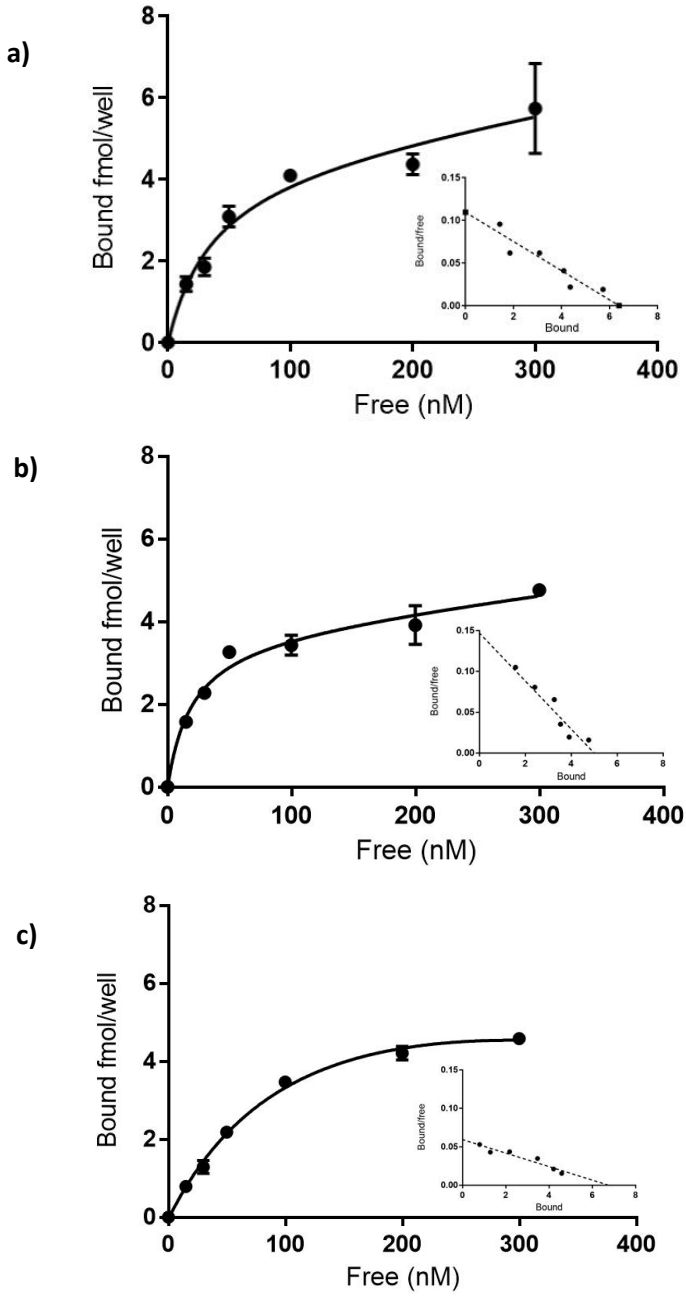

Ligand: S100B

K_D **:** 36.3 ± 22 nM

Ligand: S100P

K_D **:** 19.8 ± 6 nM

Ligand: S100A6

K_D **:** 154 ± 41 nM

Figure 65. Microtitre plate binding assay of prokaryote expressed RAGE VC_1C_2 to S100B, S100P and S100A6 (mean ± se).

Prokaryote expressed RAGE VC_1C_2, was serially diluted and added to a 96-well microplate coated with **a)** S100B, **b)** S100P or **c)** S100A6 (section 2.7.1). The S100-RAGE interaction was allowed to reach equilibrium as described in section 2.7.1 before the media was aspirated. Bound RAGE was measured as described in 2.7.1 and the data fitted by non-linear regression and Scatchard analysis (inset) in GraphPad Prism using three replicates per concentration.

with RAGE ELISA standards. The binding of RAGE to HMGB1 was evaluated by nonlinear regression and Scatchard analysis, returning estimates of affinity for V, and VC_1C_2 of $K_D \approx$ 486 ± 845 nM and $K_D \approx$ 58.6 ± 19 nM; with insect VC_1C_2 binding HMGB1 with a $K_D \approx$ 64.3 ± 14 nM. There was no statistically significant difference in the affinity of interaction between VC_1C_2 expressed in bacterial or *Tn5* for HMGB1 (p=0.9425, two-tailed t-test). The V domain bound with approximately 8-fold lower affinity ($K_D \approx$ 486 ± 845 nM) than bacterial VC_1C_2, which is statistically significant (p=0.045, two-tailed t-test) (Figure 66c). The x-axis intercept at y=0 for all three Scatchard plots was consistent (Figure 66), indicating the wells were evenly coated and the interaction was specific for HMGB1.

3.5.4 Circular dichroism (CD) of prokaryote expressed RAGE VC_1V_2 and full length HMGB1

Purified VC_1C_2 is the most complex of the three RAGE domain constructs, having three intra-domain disulphide bonds and three immunoglobulin type domains requiring correct folding. HMGB1 is also a complex protein comprising two boxes and highly charged acidic tail and basic region. Therefore, circular dichroism was completed as described in section 2.7.2 with the subsequent spectra (Figure 67a) analysed using the circular dichroism online analysis program DichroWeb. Both RAGE and HMGB1 appeared to be largely α-helical dominated proteins with significant unordered components (Figure 67 and Figure 68, respectively).

3.5.5 Surface plasmon resonance analysis (SPR) of RAGE VC_1 binding to beta-amyloid 1-42

RAGE binds amyloids and, in particular, is reported to interact with β-amyloid (Aβ1-42) to progress a range of inflammatory diseases (Lue *et al.*, 2001a; Yan *et al.*, 1996; Wilson *et al.*, 2009; Sturchler *et al.*, 2008; Origlia *et al.*, 2008). Lyophilised synthetic Aβ1-42 peptide was reconstituted using a method that resuspends the peptide in its monomeric form in solution (section 2.7.3). Monomeric Aβ1-42 was immediately immobilised on the surface of a CM5 chip (GE) at very low levels to prevent on-chip aggregation. To confirm Aβ1-42 was accessible, an anti- Aβ1-42 antibody was passed across the chip surface, binding with an estimated $K_D \approx$ 0.5nM using a 1:1 Langmuir fit (Figure 69a). Purified bacterial VC_1C_2 was subsequently passed across the chip surface using a single-cycle methodology (section 2.7.5) and the affinity of interaction estimated using a two-state model (Figure 69b). The RU range over which binding was observed is very small due to the diffuse loading of peptide to minimise on-chip aggregation of Aβ.

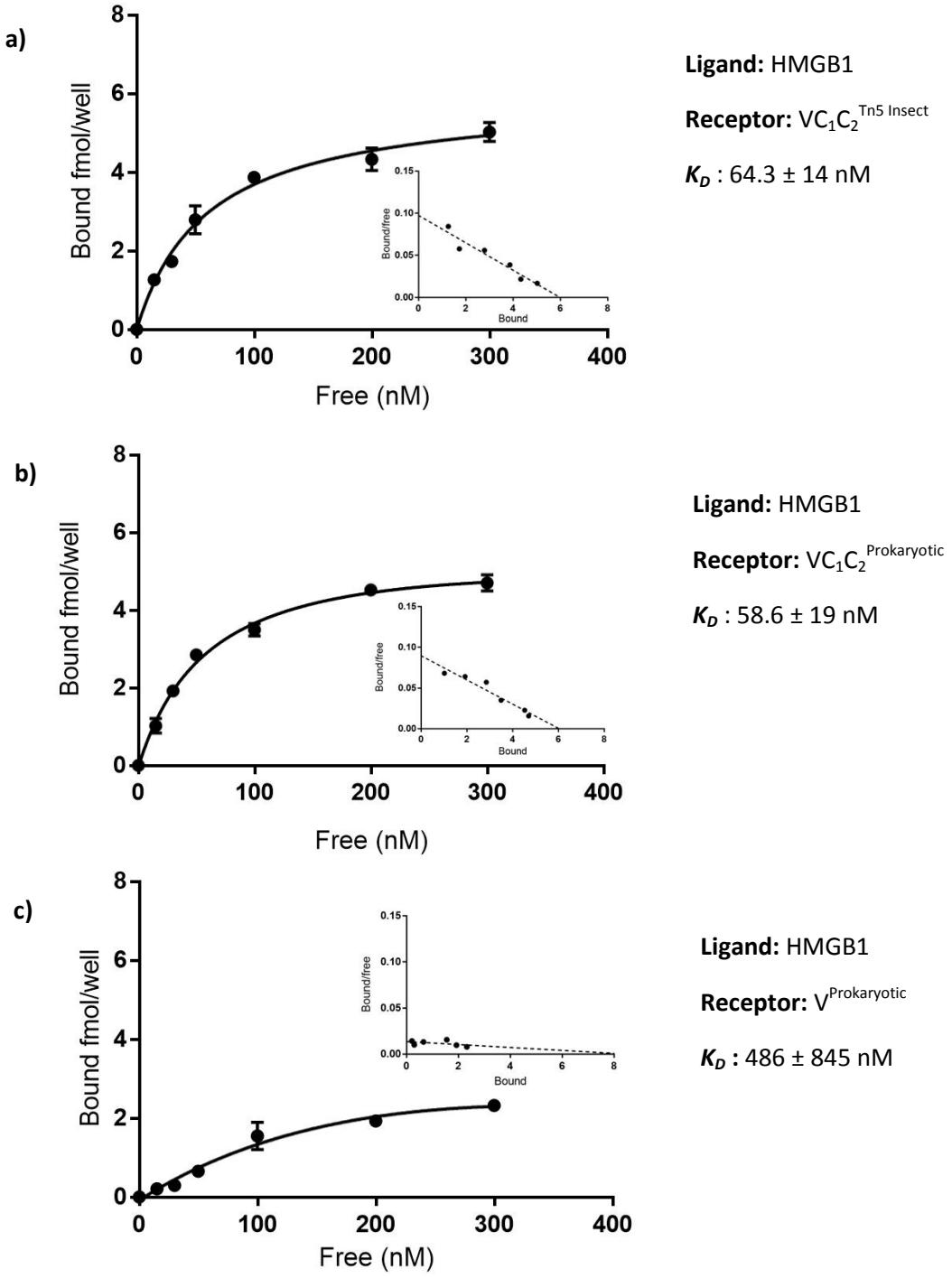

Figure 66. Microtitre plate binding assay of V, VC_1 and VC_1C_2 RAGE domains with HMGB1 (mean ± se).

A 96-well NUNC Maxisorp microplate was coated with HMGB1 before serial dilutions of **a)** insect and **b)** prokaryote expressed VC_1C_2 and **c)** prokaryote expressed V-domain were added and allowed to reach binding equilibrium (section 2.7.1). Unbound RAGE was removed by washing and bound RAGE measured as described in 2.7.1. Data fitted by non-linear regression and Scatchard analysis (inset) in GraphPad Prism using three replicates per concentration.

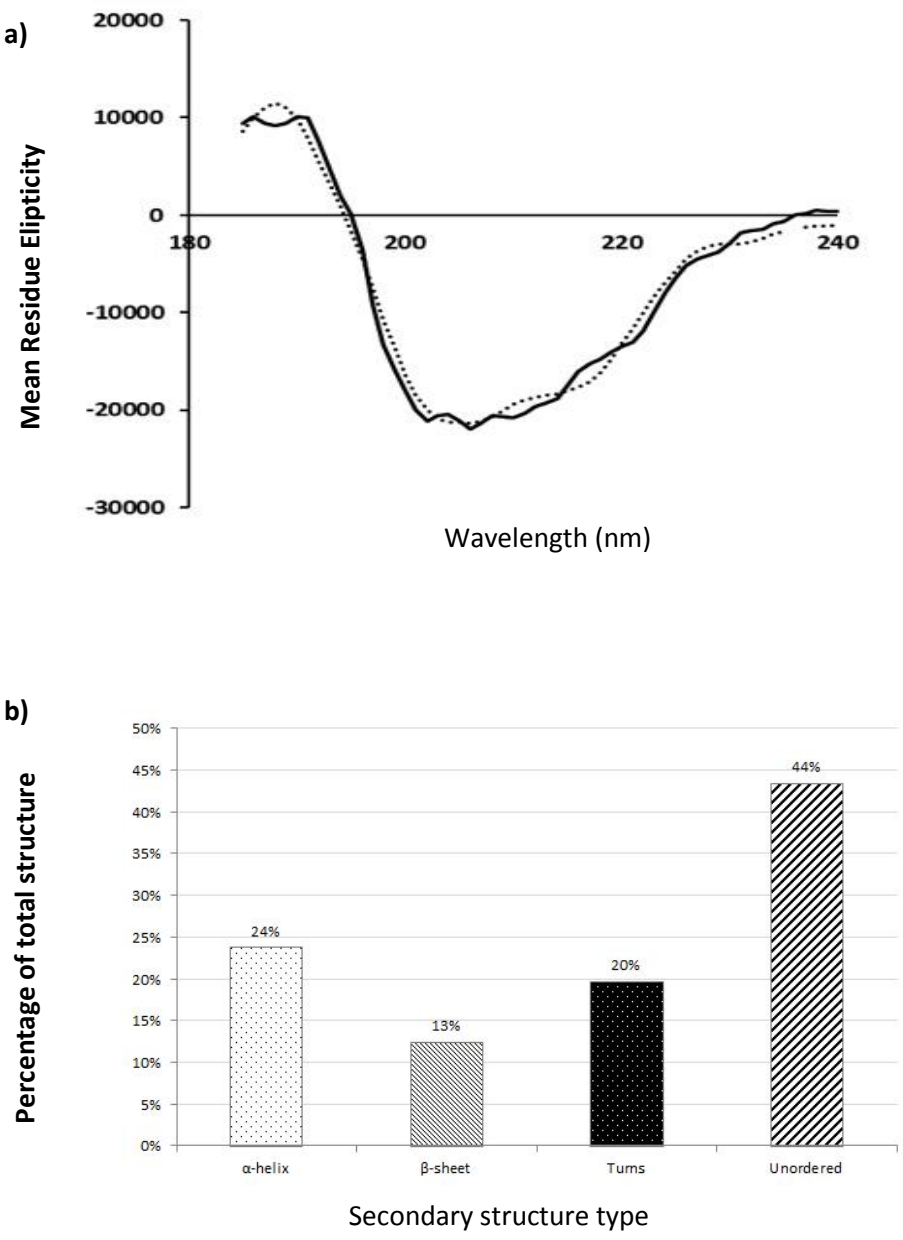

Figure 67. Circular dichroism profile of prokaryote expressed RAGE VC_1C_2.

The secondary structure composition of purified RAGE VC_1C_2 was determined by circular dichroism as described in section 2.7.2. The spectral profile **a)** was analysed using DichroWeb to estimate the α-helix, β-sheet, turn and unordered composition **a)** (in collaboration with Wresti Anggayasti).

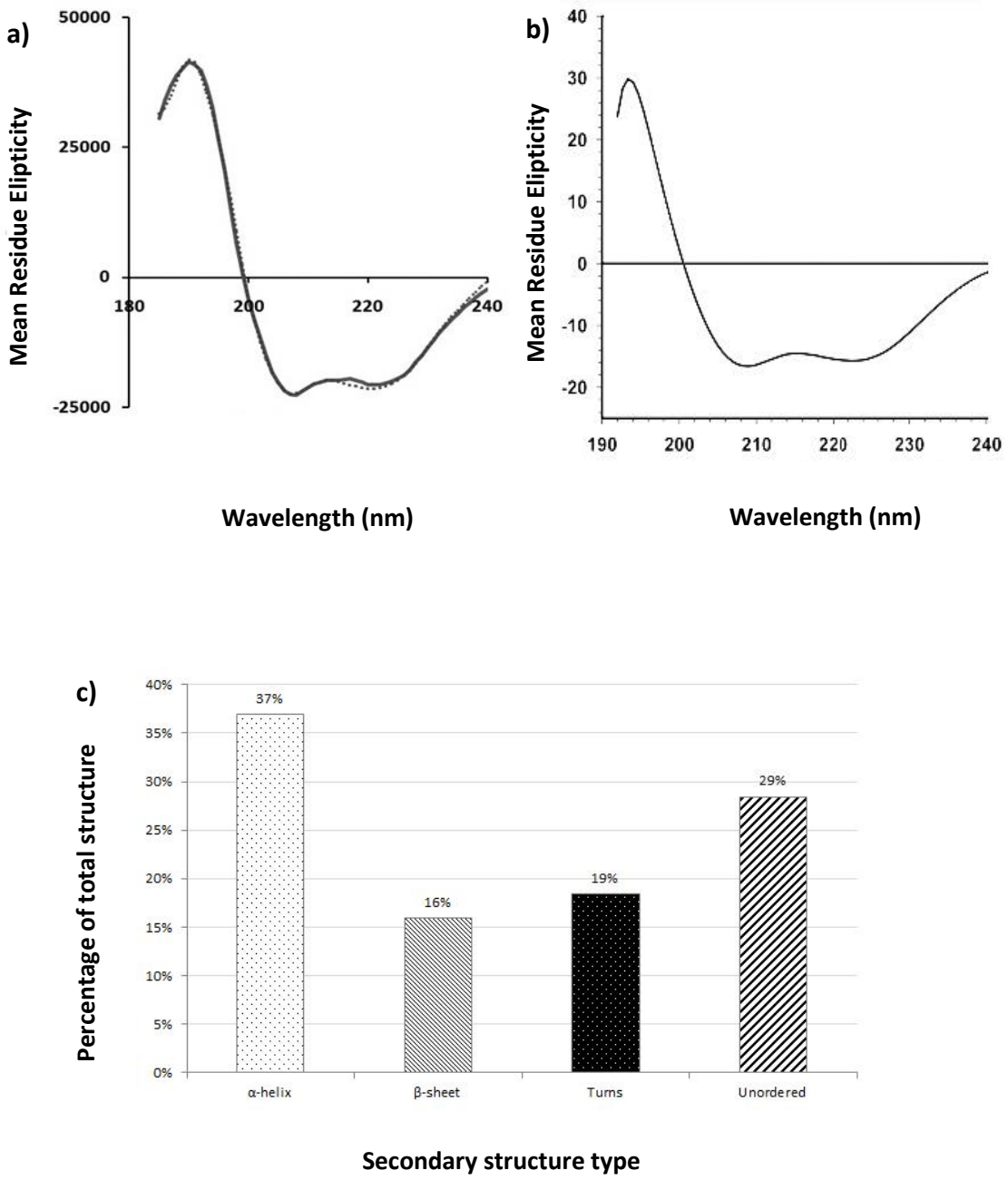

Figure 68. Circular dichroism profile of prokaryote expressed human HMGB1.

The **a)** CD spectra of purified HMGB1 was determined by circular dichroism at 25°C as described in method 2.7.2 and compared to the **b)** CD spectra of HMGB1 published by Belgrano *et al* (2013). **c)** The secondary structure composition was determined using DichroWeb (section 2.7.2) (in collaboration with Wresti Anggayasti).

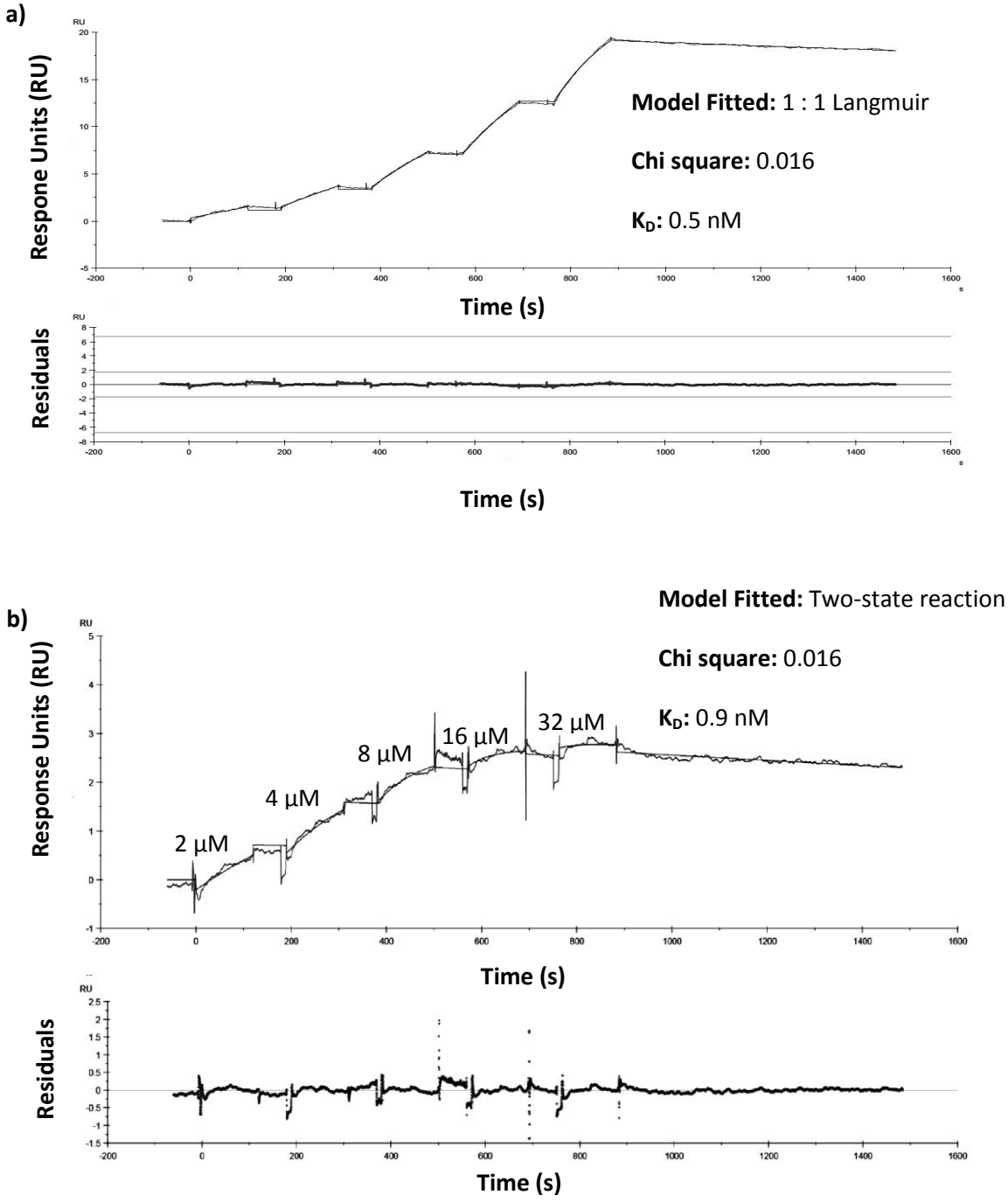

Figure 69. Single-cycle kinetic evaluation of prokaryote expressed RAGE VC_1 binding to immobilised beta amyloid 1-42.

Beta amyloid was prepared as described in 2.7.3 and immediately immobilised as ligand on Fc 4 of a CM5 chip (GE Healthcare). **a)** Anti Aβ1-42 antibody was used to confirm availability of the immobilised β-amyloid1-42 for binding with **b)** serial dilutions of RAGE VC_1 passed across flow cells 3 and 4 at 30 µL/min using a single-cycle method to determine kinetics of interaction.

Despite this, an estimate of affinity of K_D ≈ 0.9 nM was calculated with an acceptable Chi^2 value of 0.02 (Figure 69b). The binding was specific as demonstrated by an absence of binding to a control flow cell immobilised with a randomly scrambled Aβ1-42 peptide. These controls were subtracted from the response flow cells in the analysis of binding.

3.5.6 Surface plasmon resonance analysis (SPR) of RAGE VC_1 binding to ribose-AGE

The binding of *Tn5* insect or T7 Shuffle® K12 expressed VC_1 to ribose-AGE was investigated through the use of surface plasmon resonance. Briefly, VC_1 was passed across the chip surface and captured by an immobilised V5 antibody as described in section 2.7.4. Ribose-AGE was passed across the surface at a range of concentration using a multicycle methodology (section 2.7.5). Evaluation of the kinetics of interaction of the *Tn5* derived VC_1 with a 1:1 Langmuir model did not best describe the observed binding data, with a Chi^2 of 0.38 (Figure 70a). Further analysis using BIAevaluation 4.0 (GE) to fit a custom tetrameric analyte model yielded an affinity estimate of K_D ≈ 1.9 μM and a much smaller Chi^2 of 0.1 (Figure 70b). The same tetrameric model was fitted to the observed binding between bacterial VC_1 and ribose-AGE to produce an estimate of K_D ≈ 1.16 μM which is not significantly different from that observed for insect VC_1 (p=0.31 two-tailed t-test) (Figure 71). This estimate of affinity only describes the first encounter binding event, with subsequent interactions not contributing additional response units. The drifting baseline was approximately 0.6 RU/min and was a result of RAGE dissociating from the immobilised anti-V5 antibody.

3.5.7 Surface plasmon resonance analysis (SPR) of HMGB1-RAGE and HMGB1-DNA binding.

Full length human HMGB1 was immobilised on the surface of a CM5 chip as described in section 2.7.4. A single-cycle method of kinetic evaluation was used to measure the binding of pBluescript II KS(–) (analyte) as archetypal DNA to immobilised HMGB1. Applying five increasing concentrations of analyte to HMGB1 produced a response that was best described by a 1:1 Langmuir model of binding with a K_D ≈ 3.1 pM and Chi^2 of 0.02 using Biaevaluate 4.0 (GE) (Figure 72). Following regeneration of the chip (section 2.7.5), a multicycle analysis of bacterial produced VC_1C_2 binding to the immobilised HMGB1 was carried out, with a two-state model estimate of K_D ≈ 54 nM providing the best fit to the observed data (Figure 73).

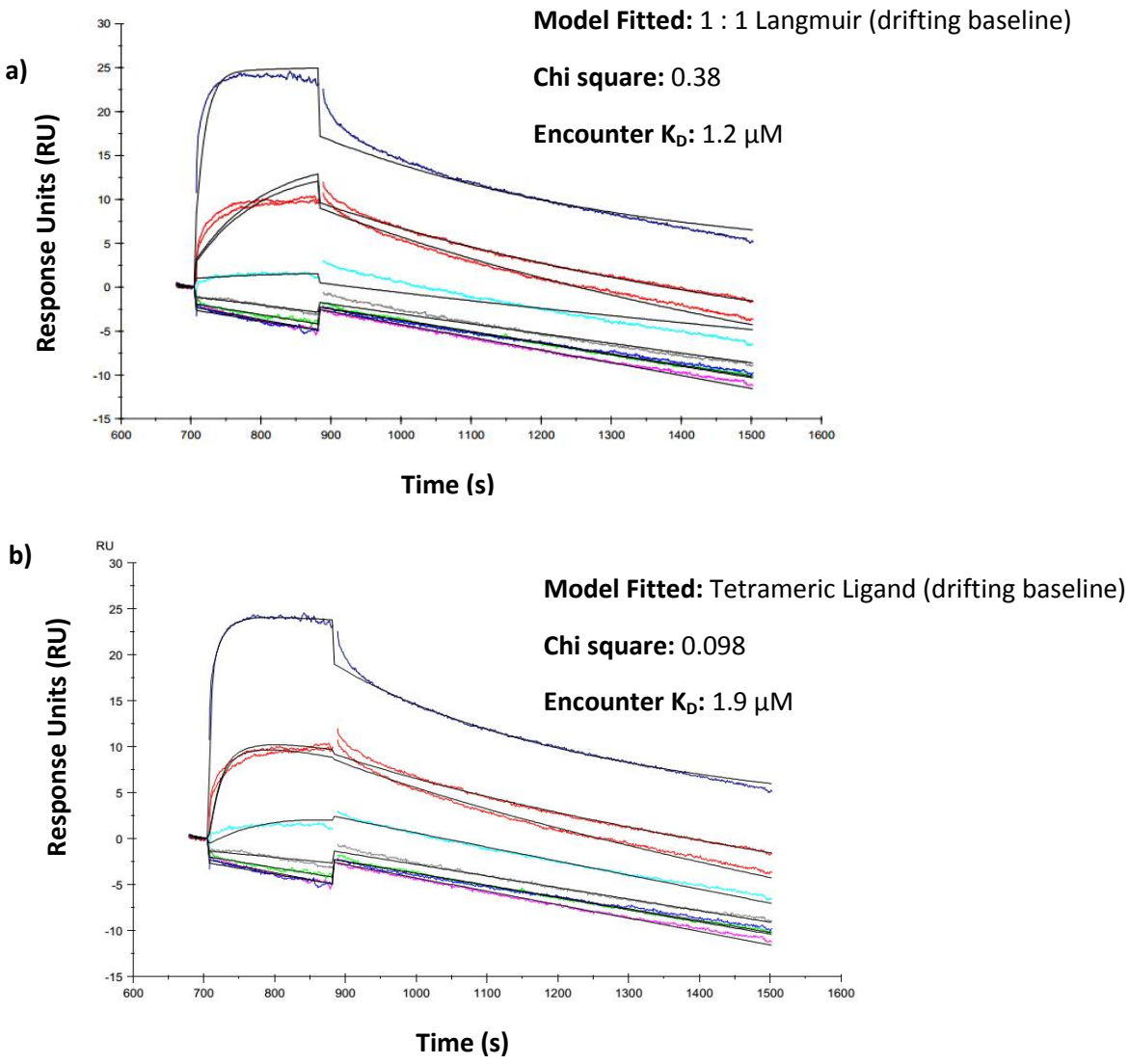

Figure 70. Multi-cycle surface plasmon resonance analysis of insect expressed RAGE VC_1 binding to ribose-AGE with different models of interaction.

RAGE VC_1 conditioned insect cell media was captured at the surface of a CM5 chip by immobilised anti-V5 antibody on a Biacore 3000 instrument (GE Healthcare) (section 2.7.4). Ribose generated AGE molecules were subsequently passed across the cells and following the association and dissociation phases of each cycle, the chip surface was regenerated. Analysis of the multi-cycle kinetic response was done using Biaevaluate software to fit **a)** 1:1 Langmuir model and **b)** a tetrameric ligand model used to best fit the interaction of ribose-AGE with immobilised RAGE VC_1.

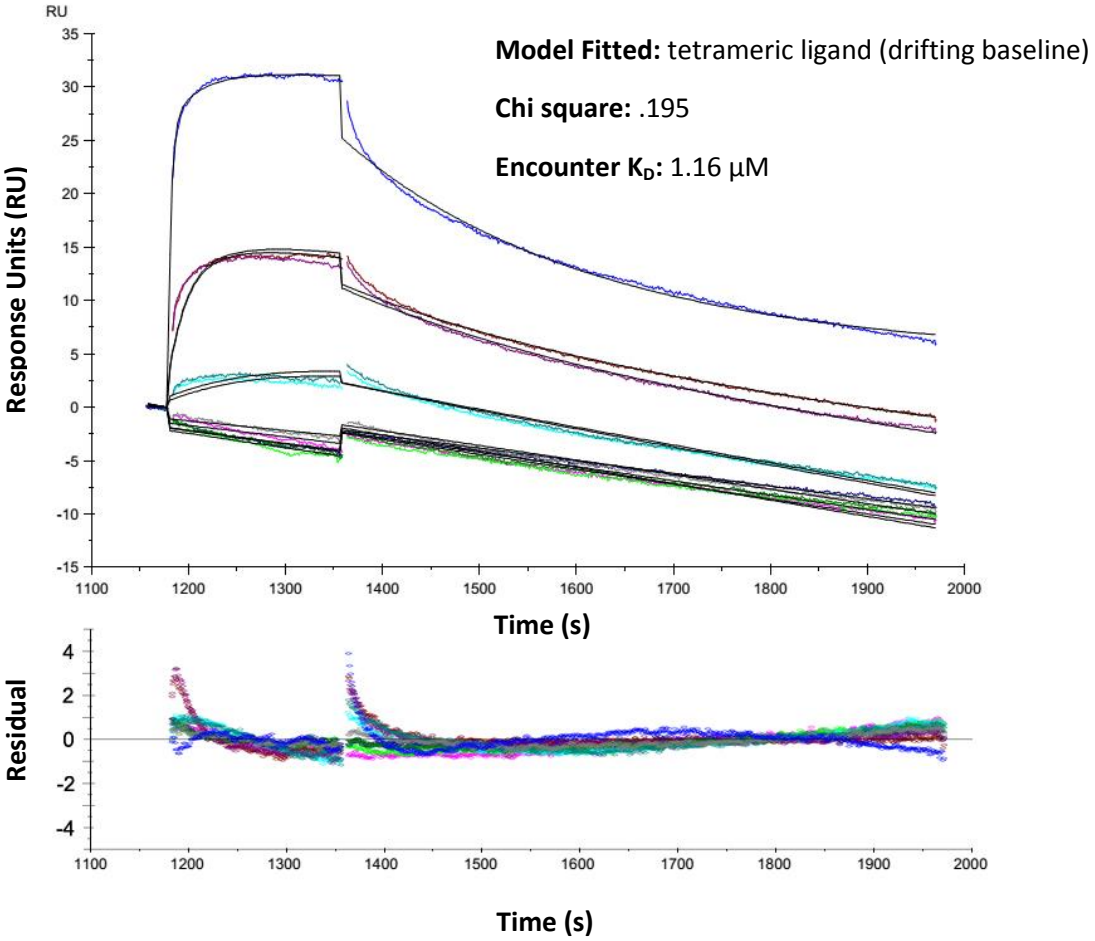

Figure 71. Multi-cycle surface plasmon resonance analysis of prokaryotic expressed RAGE VC_1 binding to ribose-AGE with a tetrameric model of interaction.

Monoclonal anti-V5 antibody was immobilised onto the surface of a CM5 chip, using a Biacore 3000 instrument (GE Healthcare) (section 2.7.4). Conditioned insect cell media was passed across the chip surface and RAGE VC_1 captured by immobilised antibody. Ribose generated AGE molecules were subsequently passed across the cells and following the association and dissociation phases for each concentration, the chip surface was regenerated as described in section 2.7.5. Analysis of the multi-cycle kinetic responses was done using Biaevaluate 4.0 (GE) software and a tetrameric model used to best fit the interaction of ribose-AGE with immobilised RAGE VC_1.

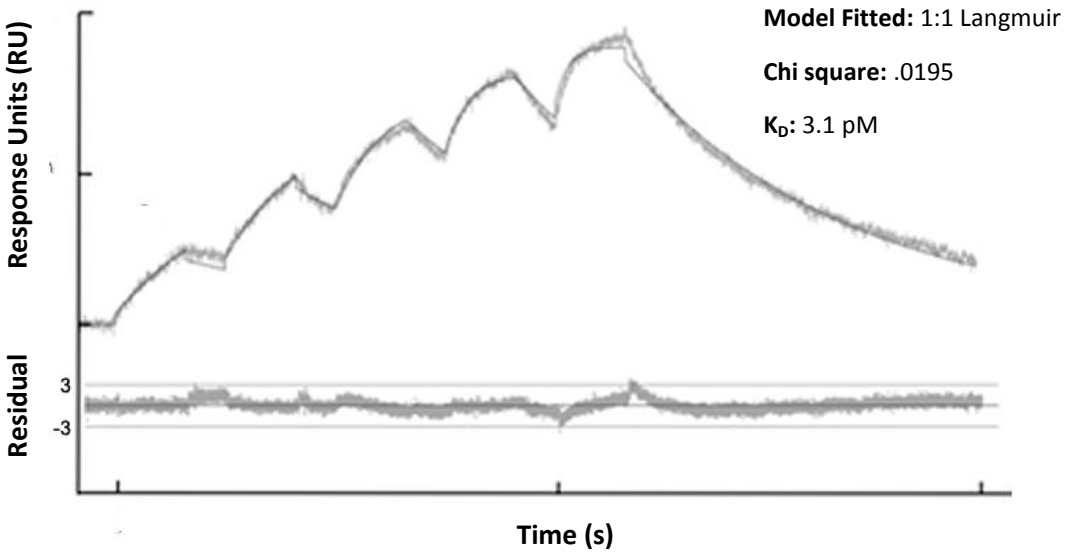

Figure 72. Single-cycle surface plasmon resonance analysis of prokaryote expressed human HMGB1 - DNA kinetics of interaction.

Prokaryote expressed human HMGB1 was immobilised on a CM5 chip (GE) using a T200 Biacore as described in section 2.7.4, with increasing concentrations of pBluescript II KS(–) cloning vector passed across the chip surface at 30 µL/min. The kinetics of interaction was measured using a T200 Biacore applying a single-cycle kinetics method, with the response file analysed using Biaevaluate 4.0 (GE) (collaboration with Wresti Anggayasti).

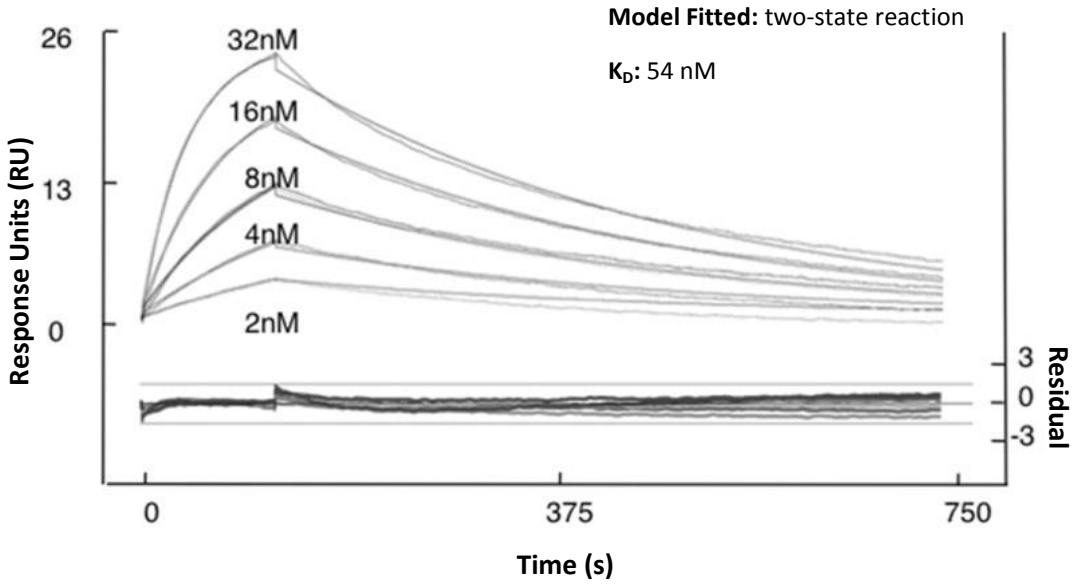

Figure 73. Multicycle kinetics of human HMGB1 interacting with prokaryote expressed RAGE VC_1C_2.

Prokaryote expressed human HMGB1 was immobilised on a CM5 chip (GE) using a Biacore T200 instrument (GE Healthcare) (section 2.7.4). Multiple cycles with different concentrations of prokaryote expressed RAGE VC_1C_2 were performed with the chip surface regenerated between cycles as outlined in section 2.7.5. Binding was measured as response units over time with the result file analysed using BIAevaluation 4.0 (GE). A 1:1 Langmuir binding model was fitted with the residuals indicating quality of fit.

4.0 DISCUSSION

4.1 Recombinant Protein Expression – The past, the present and the future

In 1978, somatostatin was the first recombinant protein to be manufactured through biotechnology (Itakura *et al.*, 1977). Since these early days of recombinant gene technology, broad leaps have been made in both our understanding of the microbial factories used and the underlying genetic and proteomic characteristics required for successful protein expression.

The post-genomic era has placed increasing demands on protein expression methodologies and techniques where little may be known about a protein targeted for heterologous expression. Traditional approaches become onerous where a large number of alternate constructs, vectors, hosts and tags need to be developed and evaluated. This has seen the development of rational approaches that leverage the emerging field of biostatistics and systems based analysis of likely outcomes (Papaneophytou and Kontopidis, 2014; Carinhas *et al.*, 2012). Multi-parallel protein expression is a high throughput empirical method for the evaluation of two or more host types, gene assemblies, expression conditions and platforms such as TOPO, Gateway™ or whole-gene synthesis (Hunt, 2005).

Bacterial systems are still considered the work horse organism of recombinant protein expression due to its unparalleled growth kinetics, with a doubling time of about 20 minutes in optimal environmental conditions (Rosano and Ceccarelli, 2014; Sezonov *et al.*, 2007). Today, a wide selection of organisms, molecular tools and technologies are commercially available for the production of recombinant proteins in both prokaryote and eukaryote hosts, with the choice of system often defined by the protein of interest and its intended use (Sahdev *et al.*, 2008). *Escherichia coli* mediated protein expression is perhaps the host most commonly used for first expression screens due to low costs, simplicity of manipulation and speed of production (Rosano and Ceccarelli, 2014). Where the target protein is complex in its assembly or structure, multi-domained, post-translationally modified or if prokaryote yields are low or of poor quality, then eukaryotic systems such as baculoviral insect expression are frequently used.

Much of the early work investigating the role and function of the Receptor for Advanced Glycation End-products (RAGE) from 1996 through to 2005, utilised protein expressed in *Sf9* insect cells using a baculoviral system (Hofmann *et al.*, 1999; Park *et al.*, 1998; Valencia *et al.*, 2004). However, some groups preferred to purify RAGE from animal tissue including mouse and bovine lung due to questions as to the quality of

recombinantly expressed human RAGE, and the role of post-translational modifications such as N-linked glycans in RAGE biology (Srikrishna *et al.*, 2002; Hanford *et al.*, 2004). A myriad of RAGE ligands such as S100 and HMGB1 proteins were also produced in a range of hosts including various prokaryote and insect cell systems (Huttunen *et al.*, 2000; Fages *et al.*, 2000; Park *et al.*, 1998; Arumugam *et al.*, 2004). This heterogeneity of RAGE receptor/ligand combinations that have been used adds to the complexity of data interpretation and raises some concern as to whether or not some observations are truly reflective of the endogenous RAGE-ligand paradigm. Indeed, estimates of ligand/receptor affinity and pathophysiological outcomes vary significantly between studies (Srikrishna *et al.*, 2010; Hofmann *et al.*, 1999; Leclerc *et al.*, 2009; Xie *et al.*, 2007; Dattilo *et al.*, 2007; Valencia *et al.*, 2004). Further confounding the myriad of ligand/receptor combinations in use is the discovery that RAGE not only has a number of alternative splice variants, but polymorphisms and post translational modifications influencing its structure and function (Hudson *et al.*, 2008a). The efficacy and complexity of assays used to verify functionality of the recombinant RAGE isoforms is also broad and inconsistent across the field. Radiolabelled ligand/receptor competition and saturation binding assays, luminescence and fluorescence imaging, quenching and proximity based assays utilising chimeric RAGE alongside surface plasmon resonance are just some of the techniques reported (Srikrishna *et al.*, 2010; Hofmann *et al.*, 1999; Leclerc *et al.*, 2009; Xie *et al.*, 2007; Dattilo *et al.*, 2007; Valencia *et al.*, 2004). This added complexity to unravelling the intimate interactions of RAGE with its ligands means that 20 years after its discovery, our understanding of RAGE and the physiological consequence of its activation is far from complete.

This project set out to address this complexity by undertaking a multi-parallel protein expression pathway, evaluating the emergent method of stable insect cell expression against traditional prokaryote protein expression.

Since all insect expressed RAGE has been previously produced using lytic baculoviral systems, this project set out to address some fundamental questions:

1. Is a plasmid based insect expression system able to produce recombinant RAGE with a greater degree of protein homogeneity in terms of post-translational modifications than the published lytic systems?
2. Can a non-lytic, non-viral system produce suitable quantities of RAGE for future structural, functional or in vivo studies?

3. Are there differences in yields based upon insect cell types or culture methods and conditions?

A number of *E. coli* strains optimised for recombinant protein expression are commercially available, however, few have been used for the expression of RAGE. This is likely due to, in part, the challenges of expressing proteins containing complex immunoglobulin type domains such as those found in RAGE (Papaneophytou and Kontopidis, 2014; Rosano and Ceccarelli, 2014).

This project further investigated the suitability of prokaryote strains traditionally used to express RAGE and two additional strains with greater degrees of modification to support heterologous protein expression. The primary considerations around the prokaryote expression systems used include:

1. Whether functional forms of the RAGE V, VC_1 and VC_1C_2 extracellular domains are expressed by the prokaryotic host.
2. Which strain characteristics lead to the highest yields in terms of quality and quantity of protein produced.

4.2 A Monk and Two Peas | Construct Development

Gregor Johan Mendel is often claimed as the father of modern genetics, heralding in the era of hereditable traits and the concept of a genetic legacy possessed by all living things. Today, our knowledge of genetics is continuing to expand with an increasingly complex arsenal of technologies and molecular machinery that is enabling our ability to translate genes into proteins.

RAGE is located near the junction of the major histocompatibility complex classes II and III on chromosome 6 and possesses the high variability in alternate splice variants common to many genes within this region (Sugaya *et al.*, 1994; Park *et al.*, 2004a; Hudson *et al.*, 2008a). To study the protein outcomes of this variability, we require accurate, agile and dynamic strategies for the production of gene constructs that encode and express these alternate isoforms. Hudson *et al* (2008) characterised and expressed a number of these spliced variants in HEK293 cells using a recombinatorial topoisomerase (TOPO) system. Considerations surrounding the use of TOPO vectors included the cost of TOPO expression plasmid conversion, whether to use a blunt-end, TA overhang or directional insert, and the size of the gene insert, with poor

incorporation rates for inserts over 1500bp (Hunt, 2005). Other rapid recombinant technologies are available such as Gateway and Univector to name a few; however, the vast majority of RAGE constructs reportedly used over the last 20 years leverage traditional sub-cloning methodologies (Park *et al.*, 2004a; Park *et al.*, 2010; Xie *et al.*, 2008; Wilton *et al.*, 2006; Ostendorp *et al.*, 2007).

4.2.1 Insect expression vector development

In this project, an alternative system not previously reported for the expression of RAGE was used that leverages both a rapid recombinant clone-in mechanism (TOPO), and the non-lytic, non-viral stable insect expression plasmid pIB/V5-HIS TOPO (Invitrogen™).

The VC_1C_2 domains of an open reading frame (ORF) clone of human RAGE was amplified by PCR and ligated into Gateway pENTR-SD/D-TOPO and pIB/V5-HIS TOPO (Figure 12 - Figure 14). Although expensive to initially purchase, both TOPO based expression systems were fast and simple to use. The Gateway vector had good TOPO incorporation of RAGE V, VC_1 and VC_1C_2 PCR products, however, the inserts were not successfully recombined into the destination vector pYES2-DEST52 despite considerable troubleshooting and effort. Alternatively, RAGE V, VC_1 and VC_1C_2 were successfully recombined into the pIB/V5 expression plasmid which was selected as the preferred vector for RAGE expression.

It was expected that the smallest V RAGE domain construct would yield the highest rate of incorporation, with decreasing rates of success as inserts increased in size (Litterer, 2009). Although the transformation efficiency for RAGE V was high, only 7% of colonies screened contained the insert in the correct orientation (section 3.1.4). Although no secondary DNA structures, palindromic sequences or other gene elements were identified, there is clearly an unknown association or element promoting the unfavourable orientation of the insert to the vector (Reuter and Mathews, 2010). The VC_1 and VC_1C_2 DNA fragments did adhere to the established TOPO dogma of decreasing transformation efficiencies with increasing insert size. Interestingly, the frequency of correctly orientated inserts varied greatly between the VC_1 and VC_1C_2 construct - 42% and 4% respectively (3.1.4). This is potentially due to inserts forming non-linear structures that obscure either the 3' or 5' ends. In lieu of this observation, care should be taken in the future to utilise directional overhangs in similar rapid recombination systems to ensure efficiency of ligation and transformation. Despite these challenges, the amount of time from PCR amplification to the propagation of insect plasmid

expression vectors containing human RAGE V, VC_1 and VC_1C_2 ready for transfection, was a matter of days. Traditionally, baculoviral systems take weeks to complete homologous recombination and viral assembly, plaque selection, purification and production of viral progeny per construct (Kitts and Possee, 1993; Jarvis, 2009; Rosano and Ceccarelli, 2014).

With the exception of two research groups reporting the use of TOPO vector systems, there are no groups we are aware of that have expressed RAGE using a rapid TOPO recombinant expression vector for insect cells (Hudson *et al.*, 2008a; Monteiro *et al.*, 2006). In contrast to *Sf9*-baculoviral expression traditionally used in RAGE research, this study reports the successful production of multiple RAGE insect expression vectors in quick succession. The plasmid based TOPO insect expression system used here represents a simple, one-step means of generating multiple expression vectors for the production of recombinant RAGE.

4.2.2 Bacterial expression vector development

The use of prokaryotic systems to produce RAGE for functional and physiological investigations increased in popularity from 2004 onwards. Despite the significant body of research relating to RAGE since this time, there is no definitive methodology that defines which strains, vectors or residues are optimal for the expression of RAGE V, VC_1 and VC_1C_2 in *E. coli*. Wilton *et al* (2006) described the bacterial expression of recombinant VC_1C_2 RAGE (a.a 23-340) using pASK40, which traffics expressed protein to the periplasmic domain of gram-positive hosts by incorporating an *OmpA* signal peptide at the N-terminus of recombinant proteins. This vector has been used to successfully express other proteins with immunoglobulin type variable domains similar to those found in RAGE (Stevens *et al.*, 1995; Raffen *et al.*, 1998). Today, there are a number of techniques that enable the targeting of recombinant protein to a range of bacterial compartments. The oxidizing potential and chaperones of the bacterial periplasmic space were utilised by Wilton *et al* (2006) to ensure that the internal disulphide bonds of expressed RAGE were not reduced (Schmidt *et al.*, 1998). In contrast, we expressed RAGE using prokaryotic strains with favourable oxidising cytosolic environments through the elimination of native reductases (section 3.3.6) (discussed in section 4.3.2). This allowed for the selection of a generic vector from an enormous catalogue of plasmids without the need to alter either our inserts or vector to include a periplasmic signal peptide.

There are a dizzying number of vectors and vector modifications available to enhance expression, particularly in the 5' untranslated region where transcription and translation factors are located. Plasmid pGS-21a (GenScript) was chosen as our archetypal vector for cytosolic expression due to familiarity with its use, along with promoter and cleavable tag characteristics similar to RAGE expression vectors previously used (Dattilo *et al.*, 2007; Allmen *et al.*, 2008; Xue *et al.*, 2011). During the process of sub-cloning our RAGE, HMGB1 and calgranulin sequences, the N-terminus GST fusion protein was removed leaving only the carboxyl terminus 6xHis tag.

Not only is the transcription and translation of heterologous proteins heavily influenced by the vector carrying the insert, but the intrinsic genetic characteristics and structure of the gene itself.

4.2.3 Gene sequence optimisation for bacterial expression

With gene sequence information becoming increasingly accessible and the expansion of cost-effective commercial gene synthesis services, the use of synthetic genes for recombinant protein expression is increasing (Welch *et al.*, 2009; Fath *et al.*, 2011; Rosano and Ceccarelli, 2014). However, there has been no reported optimisation of the human RAGE gene sequence to enhance levels of protein expression, with only a few groups reporting the use of Rosetta/Codon Plus host cells to address potential codon bias (Park *et al.*, 2010; Penumutchu *et al.*, 2014; Xue *et al.*, 2011).

The human RAGE gene sequence returned a poor codon adaptation index (CAI) value of 0.58, with 11% of codons identified as low frequency (OptimumGene™, GenScript). Additionally, one negative cis-element, a number of low frequency tandem codons and two segments of high GC content were identified. All of these factors can potentiate pauses in translation and disengagement of encoding mRNA from the ribosome and thus, significantly reduce yields. As an alternative to onerous point mutation correction of these deficiencies, a gene synthesis service (GenScript™) was used for the production of optimised RAGE V, VC_1 and VC_1C_2 synthetic gene inserts. Optimisation of the gene sequence for *E. coli* expression increased CAI estimates to 0.90, 0.93 and 0.89 for V, VC_1 and VC_1C_2 respectively; eliminating all previously identified genetic traits with the potential to confound translation.

Side-by-side expression of optimised and canonical RAGE gene sequences in the *E. coli* strain T7 Shuffle® K12 led to 6-fold, 3-fold and 1.5-fold increases in the quantities of

RAGE VC_1C_2, VC_1 and V produced from the optimised sequence (Figure 37). Codon optimisation can improve the kinetics of translation and associated yields of recombinant protein. Expression of some membrane bound proteins following gene optimisation has, however, led to decreases in yield (Cortazzo *et al.*, 2002; Schlegel *et al.*, 2012). Translational pauses may in fact be required to allow the formation of intermediate structures essential for correct folding, with their removal significantly reducing recombinant protein activity and yields (Komar *et al.*, 1999). No distinguishable increases in the production of insoluble recombinant RAGE isoforms from optimised gene sequences were observed in this project (data not shown). If functionality of purified protein proves to be poor (discussed in section 4.4), evaluation of endogenous and optimised gene sequences may point to translational rates as a cause of mis-folding and associated lack of functionality.

A number of *E. coli* strains such as BL21 (DE3) Codonplus (Strategene), Rosetta (DE3) (Novagen) and Rosetta-gami™ B (Millipore) have been engineered to address codon bias associated with the expression of heterologous proteins. These systems often incorporate additional copies of low frequency tRNAs such as argU, ileY and leuW, which can become depleted during overexpression of recombinant protein. This project expressed the native human gene sequence for V, VC_1 and VC_1C_2 RAGE domains in both Rosetta-gami™ B and Origami™ B. Rosetta-gami™ B did indeed express V, VC_1 and VC_1C_2 at levels 2-fold 3-fold and 4.5-fold higher, respectively, than Origami™ B (Table 7).

Codon optimisation dogma of 'one amino acid - one codon' that utilises the most abundant tRNAs within a host is increasingly being displaced by more complex algorithms that consider codon context, harmonization, stable free energy of mRNA and RNA instability motifs (ARE), to name a few (Gao *et al.*, 2004; Angov, 2011). The efficacy of such codon optimisation services such as OptimumGene™ and GeneArt® for heterologous expression is highly variable and dependent on the host and protein in question. This project found that T7 Shuffle®K12 transformed with optimised gene inserts expressed V, VC_1 and VC_1C_2 at levels 4.6-fold, 2.8-fold and 1.4 fold higher, respectively, than those of canonical human RAGE gene inserts (Figure 37). Interestingly, the levels of expression from insert optimisation or through the use of a rare codon optimised host was consistently $VC_1C_2 > VC_1 > V$ (Table 7). Speculation as to the cause of this reduction in yields with the removal of C-domains focused on possible mRNA instability or secondary structure formation (discussed in section 4.3.1), or mis-folding and aggregation of recombinant protein (discussed in section 4.4).

The prokaryotic hosts and vectors used in the development of RAGE domain constructs were similarly applied to the production of expression vectors containing HMGB1, ΔHMGB1 (C-terminus acidic tail truncated), S100B, S100P and S100A6. By utilizing common strategies for the production of both insect and bacterial forms of RAGE and its ligands, this study was able to generate 14 vectors for expression in eight hosts quickly, reliably and cost effectively (Table 8).

Table 8. Matrix of organisms transformed/transfected by expression vector and quantity expressed post-purification (bacterial) and pre-purification (insect) as determined by ELISA (mg/L).

Construct	BL21 (DE3)	Rosetta-gami™ B	Origami™ B	T7 Shuffle® B	T7 Shuffle® K12	*Sf9*	*Sf21*	*Tn5*
V – Native (pIB/V5)						.02	.03	.06
VC_1 – Native (pIB/V5)						.02	.07	.30
VC_1C_2 - Native (pIB/V5)						.06	.1	.42
V – Native (pGS-21a)		.04	.01		.18			
VC_1 – Native (pGS-21a)		.7	.21		.72			
VC_1C_2 - Native (pGS-21a)		4.1	.9		2.8			
V – Optimized (pGS-21a)	.08	.04	.09	.1	.27			
VC_1 – Optimized (pGS-21a)	.06	.72	.96	1.2	2.0			
VC_1C_2 – Optimized (pGS-21a)	.18	4.4	3.72	14.9	13.1			
HMGB1 – Optimized (pGS-21a)					1.8			
ΔHMGB1 – pGEX-6P-1					2.4			
S100B – Optimized (pGS-21a)					10.6			
S100P – Optimized (pGS-21a)					6.9			
S100A6 – Optimized (pGS-21a)					14.4			

This approach has provided a flexible, adaptive and systematic toolbox of methods, hosts and vectors, significantly reducing the complexities and nuances of expression vector development of RAGE and its ligands. This enables the research focus to be on the application of the expressed protein rather than the underlying molecular biology required for its production. Optimisation of the gene sequence for prokaryotic expression of RAGE did mitigate codon bias as predicted by the increased codon

adaptive index scores. Whether the quantities and functionality of the molecules produced are suitable for all possible research intents is clearly a consideration requiring further clarification.

4.3 From Gene to Protein

Despite RAGE being associated with multifarious disease states through its activation and interaction with a raft of ligands, it was nearly 16 years after its discovery that structural studies provided molecular insights into its modes of action (Xue *et al.*, 2011; Park *et al.*, 2010; Koch *et al.*, 2010; Neeper *et al.*, 1992). Due to its involvement in multiple chronic pathologies, it represents a significant therapeutic target for mitigating disease progression and the associated symptoms.

4.3.1 Insect cell expression of RAGE constructs

RAGE was almost exclusively expressed in insect cells for the first 10 years following its discovery. Over the last 10 years, RAGE is increasingly expressed in prokaryotic hosts (Hofmann *et al.*, 1999; de Arriba *et al.*, 2003; Srikrishna *et al.*, 2002; Xue *et al.*, 2011; Park *et al.*, 2010).

As discussed in section 4.2.1, the disadvantages of baculoviral systems lie in the complexity of constructing and packaging the expression vector for delivery through a baculoviral particle. This complexity in construct development hampers throughput in situations that require multi-parallel expression of many recombinant proteins such as RAGE isoforms. A number of alternatives to homologous recombination baculoviral systems exist, including Bac-to-Bac (bacmid), BaculoDirect and a raft of others. A non-viral transfection system for Lepidoptera cell lines such as *Spodoptera frugiperda 9* (*Sf9*), *Sf21* and *Trichoplusia ni* (High Five™ or *Tn5*) was chosen for this project.

The pIB/V5 TOPO plasmid (Invitrogen) used to construct the RAGE V, VC_1 and VC_1C_2 expression vectors in this study utilises a baculovirus immediate-early promoter OpIE2 which removes the requirement of complementary viral activation factors. Transient transfectants of all three RAGE constructs in *Sf9*, *Sf21* and *Tn5* cell lines were quick to generate using a lipid based transfection method (section 2.5.8). Jarvis *et al* (1990) reported a direct correlation between transfected copy number and expression levels. Optimisation of our transfection protocol confirmed this observation. Four micrograms of high pure plasmid maintained culture viability and passage rates whilst optimising

levels of protein expression (Figure 25). Transfection survival rates using 4 µg of plasmid were between 50-60% regardless of cell line, enabling the rapid expansion of transiently expressing cultures. By utilising the native human RAGE signal peptide (a.a 1-22), recombinant RAGE was successfully secreted without the need to customise the pIB/V5 vector itself. The presence of recombinant human V, VC_1 and VC_1C_2 was confirmed by Western blots of the P1 conditioned media of *Sf9*, *Sf21* and *Tn5* cultures only 48 hr post-transfection (Figure 22 to Figure 24).

Interestingly, there were two immunoreactive bands secreted by *Sf9* and *Sf21* for all three RAGE domain constructs, approximately 3 kDa apart (Figure 22, Figure 23). PNGaseF digestion of these proteins confirmed this variance was due to alternate forms of the N-linked glycans on the RAGE V domain (Figure 27). Heterogeneity of glycosylation is not uncommon in insect cells, with oligomannosidic and paucimannosidic structures being attached somewhat interchangeably (Cao *et al.*, 2005; de Arriba *et al.*, 2003). The V, VC_1 and VC_1C_2 RAGE constructs were each expressed as single protein bands in *Tn5* cells (Figure 24). This is likely due to the higher metabolic potential of *Tn5* cells and the significant down-regulation of paucimannosidic-type glycosylation of secreted proteins (only 5% of total glycospecies) compared to intracellular expressed proteins (56% of glycans attached) (Rendic *et al.,* 2008) . A number of research groups have discussed the significant role of N-linked glycans on ligand binding within the RAGE V domain (Park *et al.,* 2011; Srikrishna *et al.,* 2002). All of these studies utilise mammalian sources of RAGE due to the significantly more complex nature of glycosylation in mammalian cells (Srikrishna *et al.,* 2002; Srikrishna *et al.,* 2010). Interestingly, *Sf9*, *Sf21* and *Tn5* are ovary-derived in their origin and do not possess the entire glycomic potential of other insect cell lines (Rendic *et al.,* 2008; Kato *et al.,* 2005; Usami *et al.,* 2011). Although here we report the expression of homogeneously N-linked glycosylation of three recombinant forms of RAGE using the *Tn5* cell line (Figure 24), these glycans are not typical of those produced by mammalian cells; and as such, insect expressed RAGE is not a suitable source of protein for studying the role of these carbohydrate moieties. We have demonstrated that by using a *Tn5* cells in place of the traditionally used *Sf9* line in baculoviral production, alternate glycosylation can be minimised. This ensures that insect expressed extracellular RAGE domains V, VC_1 and VC_1C_2 are homogeneous in their composition and associated physical properties.

The initial transient expressing cultures were converted to stable cell lines in only two passages using Blasticidin, a potent peptidyl nucleoside antibiotic (Figure 26). Interestingly the levels of expression decreased dramatically across all cell lines with the removal of RAGE C-type domains (Figure 28). A common rate-limiting factor in protein synthesis is poor translation initiation as a result of mRNA secondary structures that impede the ability of ribosomal initiation factors to recruit and position the AUG initiation codon (Jackson *et al.*, 2010). Thermodynamic ensemble prediction of RAGE V, VC_1 and VC_1C_2 mRNA using the online tool RNAFold produced ensemble diversity estimates of 58 (ensemble ΔG -110 kcal/mol), 172.1 (ensemble ΔG -242 kcal/mol) and 209 (ensemble ΔG -388 kcal/mol) respectively (Gruber *et al.*, 2008). This data suggests that the V-domain is more likely to have a 'rigid' structure than the VC_1 and VC_1C_2 domains, and may thereby promote the formation of matched pair stems that have the potential to lower translation rates and increase mRNA degradation (Bollenbach and Stern, 2003; Paddison *et al.*, 2002). Indeed, the minimum free energy structure for RAGE V mRNA predicts the presence of two matched stems with a very high probability of forming in the first 50 base pairstem loop (Figure 74). No comparable matched pair stems were predicted with a high degree of likelihood in VC_1 or VC_1C_2 mRNA (Figure 74). The preference of the V domain gene to insert in the reverse orientation (3'-5' orientation) 95% of the time does suggest that the 5' end of the gene may not be readily accessible or occluded by secondary structures such as those predicted (Figure 74).

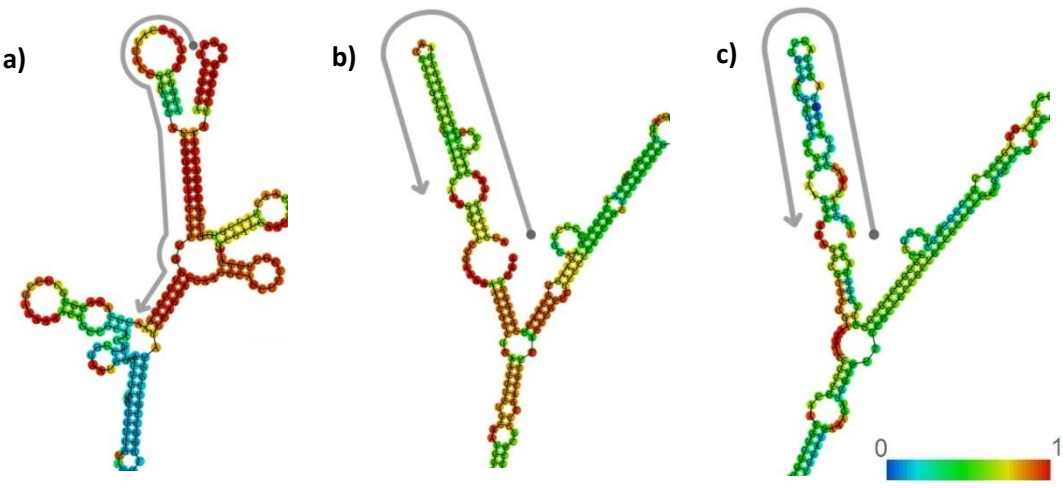

Figure 74. Predicted mRNA secondary structures of RAGE domain constructs. Putative minimum free energy structures of a) RAGE V mRNA b) RAGE VC_1 mRNA and c) RAGE VC_1C_2 with a grey line indicating the first 50 base pairs of the mRNA from the AUG initiation codon. Colour indicates the probability of the base pair being in that position (Lorenz *et al.*, 2011).

The importance of native and synthetic transcript leaders in the 5'-untranslated region (5'UTR) that modulate translation is discussed by Rojas-Duran and Gilbert (2012). They conclude that the transcription start site is greatly underappreciated as a quantitatively significant mechanism for regulating protein production. This is unlikely to be the cause of our observed decrease in translation as all constructs utilise the same 5' vector promoter and transcription initiation elements. Taken collectively, it is reasonable to speculate that the RAGE V domain mRNA may form secondary structures that are unfavourable to high rates of translation essential to overexpression of recombinant proteins.

A number of groups have previously incorporated cleavable tags such as glutathione S-transferase (GST) and maltose-binding protein (MBP) with the V-domain of RAGE expressed in prokaryote hosts that were used in purification (Ostendorp *et al.*, 2007; Zong *et al.*, 2010; Park *et al.*, 2010). Ling *et al* (2011) amino-terminally fused expressed MBP with the RAGE V domain and reported that the presence of this tag reduced the ability of HMGB1 to bind the V domain by 3-fold. Care must therefore be taken to ensure such fusion proteins do not alter the target proteins functional or structural characteristics. Whether these carrier proteins were incorporated solely for the purpose of purification, or to increase levels of expression, protein solubility or stabilisation of intermediate structures essential for correct folding was not reported. NMR studies of RAGE suggest that the C_1 domains play a key role in stabilising the structures of the V domain, with a loss of structure and increased random coils occurring in its absence (Dattilo *et al.*, 2007; Xie *et al.*, 2008). Minimal recombinant RAGE was detected by Western blot within the insoluble fractions of *Sf9*, *Sf21* or *Tn5* across all three domain constructs, suggesting expressed protein was not aggregating due to mis-folding (data not included). Whether the presence of a cleavable fusion protein is sufficient to disrupt the formation for mRNA secondary structures and increase translation of the V domain is sheer speculation. Unfortunately, due to limitations in time and resources, the effect of fusion proteins on protein production was not investigated.

There was no discernible difference in levels of expression of the V-domain between *Sf9* (20 µg/L) and *Sf21* (19 µg/L) cells, however, *Tn5* expression was 3-fold higher (62 µg/L of culture) (Table 8). Collectively, *Tn5* expressed all constructs at levels 4-10 fold greater than those seen in either *Sf9* or *Sf21* (Figure 28). Wickham *et al* (1992) similarly reported significant improvements in recombinant protein expression using *Tn5* with a baculoviral system compared with *Sf9*. Whilst the insect expression system in this study

offers advantages in speed, simplicity of construct production, cell maintenance and storage, yields were 10-100 fold less that that routinely reported for baculoviral expression (Figure 28) (Gomez-Sebastian *et al.*, 2014; Berger *et al.*, 2004; Kim *et al.*, 1993). Significant work to evaluate adherent and suspension culture techniques, optimised culture conditions and media, with the aim of enhancing cell growth rates delivered improvements in yield of approximately 20% for the VC_1C_2 construct in *Tn5* (Figure 33). Adapting all three cell lines to serum free suspension cultures provided higher cell densities and yields per litre of culture without compromising cell conditioning (3.3.5). This approach simplified protein production as it dramatically reduced contamination by other host cell proteins normally released by lytic baculoviral systems and protein contained in serum. However, despite optimisation, we were unable to produce the mg/L quantities, normally required for structural or in vivo studies, of any RAGE domain construct utilising the pIB/V5 expression vector in stably transfected Lepidoptera cells.

Insect cells are often considered a happy median between prokaryotic and mammalian expression hosts due to their capacity for high yields, relatively simple culture requirements, and robust nature and, most importantly, their capacity for post-translational modification. Where there is no need for these modifications or they can be provided alternately, bacterial expression is often the system of choice for its unparalleled growth kinetics, low cost, high cell densities and associated high yields.

4.3.2 Bacterial expression of RAGE constructs

Almost all *E. coli* strains used for recombinant protein expression today are derived from the B and K12 lines (Rosano and Ceccarelli, 2014; Studier and Moffatt, 1986). A number of significant modifications largely ubiquitous in expression strains today include the removal of various proteases (*OmpT* and *Ion*), improvements in plasmid retention and degradation, phage resistance, knockout of cytosolic reductases, and the addition of potent polymerases for high level mRNA transcription (Grodberg and Dunn, 1988; Rosano and Ceccarelli, 2014; de Marco, 2009; Brondyk, 2009).

RAGE has largely been expressed in BL21 (DE3), with a small number of groups using alternative strains such as M15p (REP4) and JM83 (Kumano-Kuramochi *et al.*, 2008; Srikrishna *et al.*, 2002; Ostendorp *et al.*, 2007; Park *et al.*, 2004a; Wilton *et al.*, 2006). A handful of publications report the use of Origami strains to mitigate poor disulphide bond formation, with only two publications describing the use of a Rosetta-gami™ B

strain to address codon bias (Kumano-Kuramochi *et al.*, 2008; Park *et al.*, 2010; Dattilo *et al.*, 2007; Xue *et al.*, 2011).

The correct formation of disulphide bonds has been identified as a significant limitation of *E. coli* expression systems since the late 1970's along with a lack of post-translational modifications (de Marco, 2009; Brondyk, 2009). In response to this and the ever-increasing demand for recombinant proteins, an extensive catalogue of commercially available bacterial hosts has been developed to address the myriad of factors influencing the quantity, quality and scope of application of expressed proteins. The scarcity of these strains within the field of RAGE research over the last 20 years, and the absence of a well-defined best practice for the bacterial expression of RAGE therefore warranted investigation.

This study utilised five bacterial strains to overexpress synonymous V, VC_1 and VC_1C_2 RAGE domains constructs to those expressed in the three Lepidoptera cell lines (section 4.2.1). In the last 5-10 years, a number of methods for the systematic multi-factorial analysis of host conditions influencing expression have gained favour (Papaneophytou and Kontopidis, 2014; Noguere *et al.*, 2012). These approaches offer significant enhancements to the classic empirical 'one-factor-at-a-time'. There are many elements of prokaryotic expression that can be tuned to enhance quantity or quality of yields, such as media, temperature, timing of induction, strength of induction, length of induction, to name a few. Although optimal recombinant protein expression is an exquisite entanglement of host, environmental conditions and the intrinsic nature of the recombinant protein, this project utilised conditions commonly reported for the prokaryotic expression of RAGE. Some preliminary investigations of the temperature of expression, strength and timing of induction did confirm that these conditions as outlined in method 2.6.1 produced relatively good yields (data not included). If additional time and resources were available, refinement of the many environmental conditions associated with this RAGE expression would almost certainly yield improved levels of expression.

In this study, BL21 (DE3), Rosetta-gami™ B and Origami™ B previously used for RAGE expression were evaluated alongside two strains optimised for enhanced disulphide bond formation – T7 Shuffle® B (rebranded as SHuffle® Express) (New England Biolabs), and T7 Shuffle® K12 (rebranded as SHuffle® T7) (New England Biolabs).

Expression in BL21 (DE3) of the optimised (synthetic) VC_1C_2 construct yielded 6.6 mg/L, however, less than 5% was present in the soluble fraction as determined by ELISA (Table 7). This is not surprising considering the presence of three cys-cys bridges (Figure 2) and the intrinsic reducing potential of the *E. coli* cytoplasm (de Marco, 2009; Brondyk, 2009). Wilton *et al* (2006) successfully expressed a similar VC_1C_2 form of RAGE into the periplasmic domain of *E. coli* utilising the native chaperones, foldases and isomerases that catalyse disulphide bond formation within this oxidising compartment (Kadokura *et al.*, 2003; Messens and Collet, 2006). Surprisingly, the yields reported were very good at 7.7 mg/g wet weight of pellet which is equivalent to the native RAGE VC_1C_2 construct expressed by T7 Shuffle® K, but only one third of the optimised RAGE VC_1C_2 construct expression in T7 Shuffle® B (Table 7) (Wilton *et al.,* 2006). It is not uncommon for periplasmic expression to be relatively low yielding due to limited availability of enzymes required for trafficking and refolding, as well as leakage of protein from the periplasm into the outer membrane and culture media (Figure 75) (Rinas and Hoffmann, 2004; de Marco, 2009). The additional complexity of tuning transcription, translation and translocation rates of periplasmic expression systems may also be required as trafficking machinery can become overwhelmed by recombinant protein at the expense of essential host periplasmic and outer membrane proteins (Wagner *et al.*, 2007).

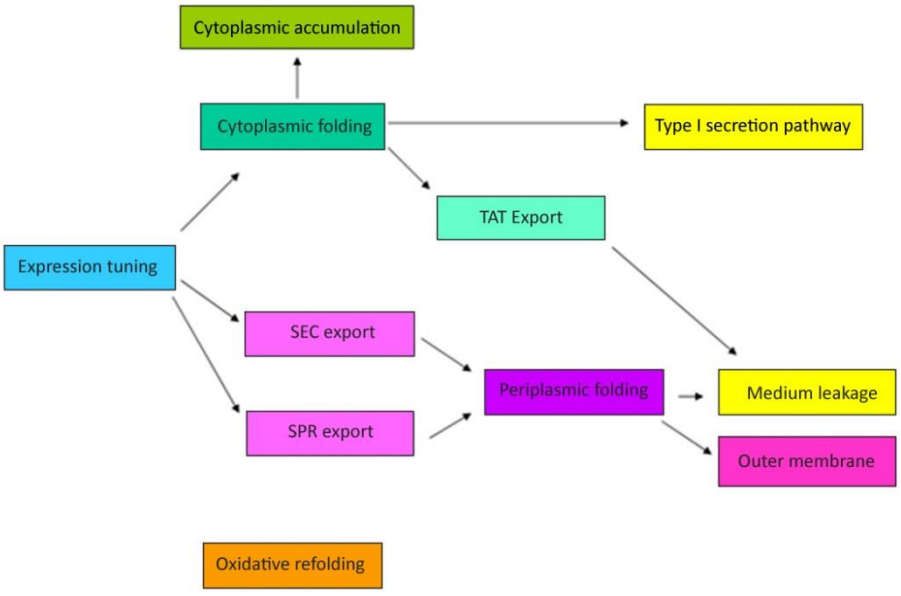

Figure 75. Periplasmic expression pathway of recombinant protein in *E. coli*. The pathway taken by recombinant protein expressed utilising the periplasmic compartment, demonstrating the complexity of *E. coli* periplasmic expression and tuning (adapted from de Marco, 2009).

As such, the exploration of hosts suitable for the cytoplasmic expression of soluble extracellular RAGE domains continued.

Origami strains were the first to be used for cytosolic expression of recombinant RAGE where the application involved functional or structural applications of the protein (Dattilo *et al.*, 2007; Xue *et al.*, 2011; Allmen *et al.*, 2008; Park *et al.*, 2010). Kumano-Kuramochi *et al* (2008) reported the expression of functional recombinant soluble RAGE using Origami (DE3), with yields of 2.2 mg/L. In this study, RAGE VC_1C_2, VC_1 and V was expressed in an Origami™ B strain with yields of 3.72 mg/L, 0.86 mg/L and 0.09 mg/L respectively (Table 8). It is interesting to note that our yields from Origami™ B were approximately half that reported by Wilton *et al* (2006). A comparison of methods revealed similar media, expression temperature and inducer concentrations, however, we induced mid-log phase at an OD^{600} of 0.6-0.8 AU. Wilton *et al* (2006) reported the use of baffled flasks with higher revolutions per minute that likely improved oxygenation of their cultures, with induction occurring at 2-3 AU $O.D^{600}$. Induction often occurs mid-log phase so as to maximise translation and associated yields (Rosano and Ceccarelli, 2014). It may be that by expressing in early stationary phase, Wilton *et al* (2008) reduced the rates of expression to prevent cytosolic accumulation of protein due to limitations in the number of gates available to transport recombinant protein into the periplasm (Galloway *et al.*, 2003; Ou *et al.*, 2004). This ensures that although rates of expression and production are slower, the cell density is significantly higher and as such, the total protein produced is greater.

In parallel with Origami™ B, this study expressed soluble forms of all three RAGE domains in Rosetta-gami™ B, T7 Shuffle® B and T7 Shuffle® K12. The Rosetta strain expressed all optimised constructs at levels approximating those of Origami, which was not unexpected as the synthetic gene effaces the advantage provided by the pRARE tRNA encoding plasmid (Table 7). Again, we observed the same decreasing levels of expression with the removal of the C domains as observed in the insect cell lines (Table 9). This phenomenon is clearly not confined to insect cell hosts, leading us to again speculate that it may be related to inefficient mRNA translation rather than the host organism inability to produce soluble, correctly folded recombinant RAGE. Investigation of mRNA transcription and accumulation within these various host cell lines by real-time PCR quantitative ananysis or mutagenic studies would have confirmed mRNA aggregation and supported the supposition that mRNA secondary structures impeded

translation; however, limitations in time and resources prevented these studies from being undertaken.

General comparison of the Shuffle®, Rosetta and Origami strain genotypes immediately identifies a notable difference, with the presence of disulphide bond isomerase C (DsbC) in the Shuffle® strains cytoplasm (Table 9). DsbC is a member of the thioredoxin superfamily which introduces disulphide bonds in target proteins through disulphide bond substitution from its active-site Cys30-Pro31-His32-Cys33; and generally assists in protein folding (Haebel *et al.*, 2002; Segatori *et al.*, 2004). Although *trxB*/*gor* knockout minimises the reduction of cystidine amino acids in the first instance, it does not prevent it entirely, with reduced thiol groups unable to form functional cys-cys bridges.

Table 9. The ratio of soluble recombinant RAGE V, VC1 and VC1C2 expressed by each host organism relative to the lowest expressing domain construct.

	Yield (ratio)					Yield (mg/L)		
Expression Host	V		VC_1		VC_1C_2	V	VC_1	VC_1C_2
BL21 (DE3)	1	:	1	:	2	.08	.06	.18
T7 Shuffle® B	1	:	7	:	142	.1	1.1	14.9
T7 Shuffle® K12	1	:	7	:	47	.27	2.0	13.1
Origami™ B	1	:	11	:	42	.09	.96	3.7
Rosetta-gami™ B	1	:	17	:	103	.04	.71	4.4
Sf9	1	:	1.5	:	3	.02	.03	.06
Sf21	1	:	3.7	:	15	.02	.07	.3
Tn5	1	:	1.6	:	6.8	.06	.1	.4

In this study, the presence of DsbC and use of optimised gene sequences resulted in RAGE expression 7-fold greater than Origami (DE3) yields reported by Kumano-Kuramochi *et al* (2008). Although T7 Shuffle® K12 expression of RAGE VC_1C_2 was 12% lower than that of Shuffle® B, this strain produced approximately 2-3 fold more VC_1 and V (Table 7). A comparison of the B and K-12 genomes demonstrates a significant degree of similarity, with less than 2% nucleotide sequence divergence between B and K-12

adjacent to insertion sequence elements (Schneider *et al.*, 2002). This study found no difference in growth rates between B and K12 strains under inducing conditions (section 2.6.1) (data not shown), to explain differences in yield as has been reported previously (Lobstein *et al.*, 2012). Lobstein *et al.* (2012), observed higher yields of recombinant protein expressed by Shuffle® B relative to the Shuffle® K12 strain and concluded this was due to subtle genetic difference between strains rather than engineered or environmental phenotypical factors. Interestingly, the T7 Shuffle® K12 genome does not indicate the deletion of *lon* and *OmpT* proteases that are native to K12 strains, where as the T7 Shuffle® B genome is devoid of both. It is therefore possible that the lower yields in T7 Shuffle® K12 may be a result of proteolytic degradation of recombinant protein, even in the presence of protease inhibitors. Despite the slightly lower yields of the VC_1C_2 and VC_1 constructs, the overall performance of T7 Shuffle® K12 led to its selection as our preferred prokaryotic host for heterologous expression of RAGE and its ligands. The suitability of T7 Shuffle® K12 and pGS-21a as a common 'toolbox' for the expression of various RAGE domain constructs, as well as its ligands, namely HMGB1, ΔHMGB1, S100B, S100P and S100A6 was subsequently investigated.

High-Mobility Group 1 Box (HMGB1) has been heavily implicated in the progression of multiple pathologies through the binding and activation of RAGE (Sims *et al.,* 2010). It is an interesting molecule comprising an internal disulphide bond in Box A and a free thiol (Cys^{106}) group in Box B, and is soluble in 6% perchloric acid with no subsequent loss of functionality. Surprisingly, despite the presence of these three cys residues, the vast majority of recombinant HMGB1 used in RAGE binding studies have been expressed in *Escherichia coli* strains such as BL21 that don't carry the *trxB*/*gor* reductase mutations (Rouhiainen *et al.*, 2007; Venereau *et al.*, 2012; Huttunen *et al.*, 1999; Yang *et al.*, 2010). Recently, the reversible redox potential of Cys^{106} was shown to modulate the ability of HMGB1 to bind and activate RAGE (Venereau *et al.*, 2012). Preliminary findings within our lab similarly identify a role for this free thiol group in HMGB1 self-association through the formation of a novel zinc clasp bridge (Figure 76).

Human HMGB1 sub-cloned into pGS-21a and using the T7 Shuffle® K12 strain was successfully expressed at 1.8 mg/L, however, surprisingly it was observed that HMGB1 was bactericidal, with cell death evident three hours post-induction (Figure 38). By inducing late log phase ($O.D^{600} \approx 1$), expression was optimised with an induction period of 2.5 hr. Toxic protein expression commonly utilises hosts that have tight regulation

over the T7 RNA polymerase through the LacI repressor to suppress basal level expression pre-induction.

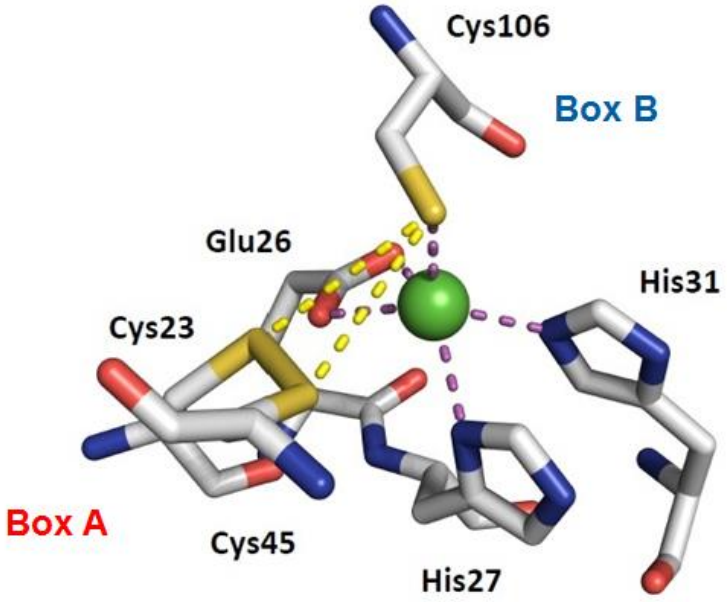

Figure 76. Modelling of HMGB1 self-association. Modelling of HMGB1 homodimers formed by a novel 'zinc clasp' structure involving the free thiol group on Cys^{106} (Anggayasti, Agostino, Mancera and Helmerhorst, Lorne Conference on Protein Structure and Function (2013)).

No reduction in pre-induction culture growth rates of T7 Shuffle® K12 was observed in this study, almost certainly due to the presence of the *lacI*^{q} repressor (Figure 38). A truncated form of HMGB1 (ΔHMGB1) was kindly provided by Dr Rouhiainen (University of Helsinki, Finland) and expressed as provided in T7 Shuffle® K12, largely for use in other projects within our group. Delta HMGB1 was expressed at approximately 2.4 mg/L under the same conditions as full length HMGB1 (Figure 58). Whether the slightly higher level of ΔHMGB1 in comparison with HMGB1 expression is due to the presence of a carboxy-terminal fusion tag (GST) is difficult to determine in lieu of differences in both vector and gene insert. Interestingly, it is reported that HMGB1 may undergo a number of post-translational modifications that include phosphorylation, methylation and ADP-ribosylation (Bonaldi *et al.,* 2003; Harris and Andersson, 2004). In addition, acetylation has been heavily implicated in its DNA binding avidity (Elenkov *et al.*, 2011). We discuss

the capacity of HMGB1 expressed in T7 Shuffle® K12 to bind DNA as an indication of functionality in section 4.4.2.

S100B, S100P and S100A6 are members of the calgranulin subfamily of calcium binding proteins that progress a number of pathophysiologies through RAGE (Ostendorp *et al.*, 2007; Bianchi *et al.*, 2007). The heterologous expression of S100's is well established in prokaryotic hosts, most notably BL21 strains, with some RAGE researchers using baculoviral systems as well (Hofmann *et al.*, 2002; Huttunen *et al.*, 2000; Srikrishna *et al.*, 2010). Human S100P, S100B and S100A6 were sub-cloned into pGS-21a and used to transform T7 Shuffle® K12. Using this host, 10.6 mg/L, 14.4 mg/L and 6.9 mg/L of soluble S100B, S100A6 and S100P was produced, respectively (Figure 44). The formation of inclusion bodies by recombinantly expressed S100s in *E. coli* is rare, most likely due to the structural simplicity of these proteins (Leclerc *et al.*, 2007; Gribenko *et al.*, 1998; Marlatt *et al.*, 2010). Interestingly, Western blot analysis of the soluble fractions from all three induced T7 Shuffle® K12 calgranulin cultures revealed a major band that correlated with the expected size of the recombinant proteins and a faint second immunoreactive band approximately twice the size of the majorative species (Figure 41-Figure 43). It is speculated that the larger band represents homodimers formed in response to conformational changes associated with the binding of intracellular bacterial calcium and other divalent metal cations. Despite these yields being less than the 20 mg/L reported for BL21 (DE3) strains by He *et al.* (2013), the levels of expression achieved with the pGS-21a vector and T7 Shuffle® K12 strain are certainly adequate for a wide range of applications, including structural studies (He *et al.*, 2013).

The T7 Shuffle® K12 recombinant soluble RAGE constructs and various S100 and HMGB1 ligands were purified following optimisation of their expression. As each protein is unique in the physical characteristics that can be exploited for the purpose of purification, different technologies and methodologies were utilised. The objective in each case was to minimise the number of steps needed to achieve an appropriate level of purity whilst considering the speed, cost and yields of each method. The RAGE proteins were purified utilising their affinity for heparin, with approximately 80% of starting material recovered (Figure 45 to Figure 47 respectively). All RAGE domain constructs were penta-his tagged at their C-terminus. Polyhistidine tags are one of the most versatile and widely used strategies for purifying recombinant proteins largely due to their small size and ease of elution with imidazole, however, efficacy of purification is on a protein-by-protein basis (Cao and Lin, 2009). All three recombinant RAGE domain

isoforms demonstrated excellent affinity for a nickel- nitrilotriacetic (Ni-NTA) acid resin, with approximately 65-70% of starting material recovered (Figure 48 to Figure 50). Interestingly, when the eluates were dialysed to remove the eluting imidazole, a white flocculate appeared that correlated with a significant loss in soluble RAGE. The addition of EDTA to the dialysis buffer prevented the appearance of this particulate, confirming our suspicion that it was associated with leaching nickel coordinating the polyhistidine tags of RAGE to promote aggregation. Full length HMGB1 was purified based on its remarkable solubility under acidic conditions and with the aid of a molecular sieve polishing step (Figure 52 and Figure 53 respectively). Truncated HMGB1 was purified utilising a GST tag attached at the C-terminus (Figure 55). A number of GST purification approaches were tried, with on-column cleavage delivering the highest degree of purification as determined by Coomassie staining (Figure 57). The addition of a HisTrap column in series with the GST column ensured that the polyhistidine tagged PreScission Protease used to cleave the GST fusion protein was removed. The intrinsic calcium binding characteristics of S100s is associated with a conformational shift that exposes a broad hydrophobic patch involved in S100 dimerization (Santamaria-Kisiel *et al.*, 2006). This characteristic was exploited by passing bacterial cell lysates containing recombinant S100s across phenyl Sepharose® in the presence of 5 mM calcium. Elution of bound protein was done using a wash buffer containing 2.5 mM EGTA, producing a single peak that was confirmed by Coomassie to consist of single S100B, S100P and S100A6 molecules at >95% purity (Figure 59 to Figure 61). Only S100A6 was detected in the column flow through by Coomassie, indicating that the column was overloaded, with an estimated capacity of approximately 14 mg/mL of S100 per millilitre of phenyl Sepharose® resin.

Given the oligomeric propensity of many of these ligands and the likely multivalent nature of their interactions with RAGE, a molecular sieve step immediately prior to the use of any of the proteins expressed and purified in this study was used to ensure they were aggregate free prior to commencing functional studies.

4.4 Functional Evaluation of Recombinant Proteins

The ability of RAGE to bind a plethora of ligands has been investigated through the use of various techniques that include fluorescence, radiolabel based saturation assays, surface plasmon resonance and a handful of colorimetric assays (Hori *et al.*, 1995; Xie *et al.*, 2008; Kislinger *et al.*, 1999; Schmidt *et al.*, 1992). It is difficult to interpret the many

affinities of interaction reported for RAGE due to the interchange of receptor sources, the varying methodologies applied and innate complexities of interaction.

4.4.1 Binding of RAGE constructs to ribose AGEs

This study developed a novel colorimetric binding assay (section 2.7.1), that enabled us to quickly evaluate the binding of RAGE to its ligands without the need to radiolabel RAGE, modify RAGE with fusion enzymes for use in measuring activity, or requiring expensive instrumentation. Specificity of RAGE binding was demonstrated by two negative controls that included wells coated with unmodified BSA and a triplicate set of wells containing binding buffer without RAGE. A very similar assay for the high throughput screening of compounds modulating RAGE binding, was patented in the US 18 months post development of the method developed in this study, validating the suitability of this approach (US 2006/0078956 A1, Shahbaz (2006). Both insect and prokaryote expressed VC_1C_2 and VC_1 RAGE bound ribose-AGE with comparable affinities in the range of K_D ≈ 58-79 nM and K_D ≈ 71-89 nM, respectively (Figure 63, Figure 64). This correlates well with estimates of affinity published for insect expressed forms of VC_1C_2 (IC_{50} ≈ 73 nM) and endogenous bovine RAGE (K_D ≈ 47 ± 23 nM) binding of AGEs (Valencia *et al.*, 2004; Schmidt *et al.*, 1992). Srikrishna *et al* (2002) reported that N-glycans present on endogenous RAGE influenced the affinity of interaction between RAGE and HMGB1. Whether this is also the case for AGE-RAGE interactions requires further investigation, with current NMR explanations of AGE-RAGE mechanisms of binding not considering N-linked glycan involvement.

The V domain expressed by insect cells bound ribose-AGE (K_D ≈ 1600 ± 5 nM) with approximately 2-fold higher affinity than the prokaryote equivalent (K_D ≈ 4300 ± 64 nM), yet 27 to 48-fold less than recombinant RAGE isoforms containing the C_1 domain in prokaryote and insect cells, respectively (Figure 63 and Figure 64) (Valencia *et al.*, 2004; Xie *et al.*, 2008; Schmidt *et al.*, 1992; Xue *et al.*, 2011; Xue *et al.*, 2014). It is tempting to speculate that the dramatic difference in the strength of binding of AGEs to RAGE isoforms with, and without, C-type domains is related to mis-folding of the V domain, or a loss of oligomeric RAGE quarternary structure that is C_1 domain dependent. Xie *et al* (2008) were the first to propose that residues in the C-terminus of the C_1 domain drive self-self association and the resultant multimeric forms of RAGE. Sitkiewicz *et al* (2013) recently demonstrated the involvement of the interlinking loop between the C_1 and C_2 domains in the formation of dimer-tetramers of extracellular RAGE, which is now know

to be its constitutive form (Xie *et al.*, 2007; Koch *et al.*, 2010). However, the extent to which this loop affects oligomerisation and potentially ligand binding has not been demonstrated. Closer inspection of both the prokaryote and insect VC_1C_2 and VC_1 estimates of affinity does show a consistently higher K_D for the VC_1C_2 (bacterial $K_D \approx 80 \pm 14$ nM; insect $K_D \approx 58 \pm 12$ nM), relative to VC_1 (bacterial $K_D \approx 89 \pm 29$ nM; insect $K_D \approx 72 \pm 14$ nM) in the order of 12% and 22%, respectively. These differences, however, are not statistically significant (p= 0.9575) applying a two-tailed t-test.

Surface plasmon resonance analysis of both insect and prokaryotic VC_1 forms of RAGE demonstrated a many-to-one ratio of receptor to ribose-AGEs (Figure 70, Figure 71). The interaction of free ribose-AGE passed over RAGE VC_1 captured on the surface of a CM5 chip was best described by a tetrameric model of binding with a $K_D \approx 1.8$ µM for the initial encounter complex (Figure 70, Figure 71). Immobilising RAGE to the chip surface only enabled measurement of the initial encounter interaction between the first immobilised RAGE molecule to bind free ribose-AGE, with subsequent interactions not contributing additional response units (). If the arrangement of the SPR experimental conditions was reversed, so that ribose-AGE is immobilised and RAGE passed across the chip surface as analyte, the binding kinetics of all RAGE oligomer components with ribose-AGE could be described, along with the stoichiometry of multimeric RAGE. It is enticing to speculate that the nanomolar affinity demonstrated in the plate based assay between VC_1, VC_1C_2 and ribose-AGE is the high affinity multimeric RAGE-ribose AGE interaction as opposed to the low affinity monomeric VC_1 binding demonstrated by SPR. The disparity in the binding affinities of RAGE constructs with and without a C_1 domain expressed in both prokaryotic and eukaryotic hosts provides further support for the proposition that the dramatic differences in binding strength reported here are associated with a loss of oligomeric quarternary structure as opposed to mis-folding of the V domain.

This study has demonstrated that the novel plate based assay developed within this laboratory is a simple, accurate, consistent and quick means of evaluating the binding of RAGE constructs with AGE molecules. This is in stark contrast to the many assays previously reported that require either radiolabelling, enzymatic tagging of RAGE or complex instrumentation. Collectively, the data produced using this assay in combination with SPR, support the likelihood that oligomerisation modulates the strength of binding between RAGE and AGE molecules as opposed to mis-folding of discrete V domain RAGE constructs by the heterologous host. The bacterial and insect

RAGE isoforms expressed in this study bound ribose-AGE with comparable affinities and approximated the micromolar affinities reported for V-domain binding and nanomolar affinities for VC_1 and VC_1C_2 forms of the receptor.

4.4.2 HMGB1 functionality

In 1995, Hori *et al* demonstrated the specific binding of RAGE with HMGB1 using both recombinant baculoviral expressed HMGB1 and endogenous rat RAGE and HMGB1. They reported binding in the range of $K_D \approx$ 6–10 nM dependent on the combination of receptor-ligand combination used (Hori *et al.,* 1995). In stark contrast, Liu *et al* (2009) reported affinities of $K_D \approx$ 710 nM using recombinant human RAGE (equivalent to VC_1C_2) and HMGB1 expressed in BL21 (DE3) using a plate based assay similar to that described in section 2.7.1. Ling *et al* (2010) were the first to publish the kinetics of interaction between human RAGE and HMGB1 (commercially purchased - bacterially expressed), using surface plasmon resonance, with an estimate of $K_D \approx$ 98nM. Interestingly, the 1:1 Langmuir fit applied by Ling *et al* (2010) to their data does not appear to be a good fit (Chi^2 values or residuals not reported), leading us to speculate whether a multimeric model would have been more appropriate. This broad set of binding affinity estimates for RAGE and HMGB1, spanning an order of magnitude is difficult to reconcile. In part, the use of RAGE without N-linked glycans has been shown to reduce binding to HMGB1 two-fold (Srikrishna *et al.,* 2002). Utilising a plate based assay, this study demonstrated no statistically significant difference (p=0.9425 two-tailed t-test) between estimates of binding between insect ($K_D \approx$ 64 ± 14 nM) and bacterial ($K_D \approx$ 58 ± 19 nM) expressed VC_1C_2 and HMGB1 (Figure 66). The reported importance of post-translational modification of HMGB1 in relation to its ability to bind DNA and the sensitivity of these to purification strategies was investigated in this study (Bonaldi *et al.,* 2003; Harris and Andersson, 2004) . Circular dichroism analysis confirmed the presence of secondary structures in proportions commonly associated with functional HMGB1, suggesting the molecule is correctly folded (Figure 68) (Belgrano *et al.*, 2013). Using SPR, this study found that prokaryote expressed HMGB1 purified through the use of a classical acid precipitation step, did not lose its ability to bind DNA, demonstrating a very high affinity interaction in the order of $K_D \approx$ 0.3 pM with pBluescript II SK- cloning vector (Figure 72). Additionally, multicycle SPR analysis of the strength of binding between free VC_1C_2 RAGE and immobilised HMGB1 was $K_D \approx$ 6 nM, strongly correlating with the plate based assay estimates of affinity (Figure 73). Notably, our SPR estimate of affinity are 2-fold higher than that reported by Ling *et al* (2011), possibly due to differences in experimental

design such as the presence of a background reducing agent to preserve the integrity of the free Cys^{106} in Box B of HMGB1. This study immobilised HMGB1 to the chip surface as opposed to RAGE, and subsequently passed RAGE across the surface to allow free oligomerisation of RAGE to occur. This approach also avoided exposing RAGE to harsh regeneration conditions of 10 mM NaOH between cycles used by Ling *et al* (2010). Although speculative, it is possible that the lower strength of binding reported by Ling *et al* (2011) may possibly be due to reduced levels of functional RAGE following immobilisation and subsequent regeneration cycles, or limitations in the freedom of RAGE to oligomerise when immobilised on the chip surface. Further studies are required to clarify this speculation.

It is reasonable to assume that the large disparity in binding estimates of the RAGE-HMGB1 interaction is in part a result of the myriad of receptor and HMGB1 sources utilised as well as variations in methodology. Of significance was the recent findings that the redox state of the free thiol of HMGB1 (Cys^{106}) modulates it ability to bind toll-like receptor 4 (TLR4) (Yang *et al.*, 2012; Venereau *et al.*, 2012). Tang *et al* (2010) reported that the pluripotent outcomes of RAGE-HMGB1 binding were in part regulated by the redox status of HMGB1. Janko *et al* (2014) postulated that this may be due to dimerization of HMGB1 mediated by the free Cys^{106} thiol. Ongoing work within this laboratory using HMGB1 produced in this study has, in fact, demonstrated the role of this thiol in the formation of a novel 'zinc clasp' structure that drives self-self association (Figure 76). This correlates with our observation that the V domain binds HMGB1 with an 8-fold lower affinity ($K_D \approx 5$ nM) than VC_1C_2 ($K_D \approx 58$ nM) (Figure 66). From these observations, it is reasonable to speculate that just as RAGE-AGE binding is influenced by the oligomeric state of the receptor, it is likely that RAGE-HMGB1 binding is even more complex, influenced by the multimeric form of HMGB1 driven by its redox state, the presence of zinc dications, as well as the quarternary structure of RAGE. These early observations provide tantalising preliminary insights into the possible mechanism by which the pluripotent outcomes of RAGE-HMGB1 binding are progressed, demanding active ongoing investigation.

4.4.3 Functionality of calgranulin (S100) molecules.

As previously discussed in section 1.3.3, calgranulins are a sub-family of calcium binding proteins ubiquitously expressed in vertebrates. They are associated with progression of a diverse array of pathophysiological outcomes in an autocrine or paracrine

manner through the activation of RAGE. Hofmann *et al* (1999) were the first to describe RAGE as a cell surface receptor for S100A12 and S100B, with a number of subsequent studies identifying RAGE-S100B as an axis of inflammation in microglia, neuronal and neuroblastoma cell lines (Huttunen *et al.*, 2000; Kogel *et al.*, 2004; Leclerc *et al.*, 2007; Adami *et al.*, 2004). Interestingly, a number of calgranulins elicit differential outcomes dependent of their physiological concentrations, with nanomolar concentrations promoting cell survival and micromolar triggering apoptosis (Schmidt *et al.*, 2007; Vincent *et al.*, 2007; Huttunen *et al.*, 2000). Datillo *et al* (2007) demonstrated by SPR that immobilised VC_1 RAGE binding to free S100B was best described by a heterogeneous analyte model. This implies that S100B was either not purely dimeric in form, or that immobilised RAGE consisted of various monomeric/multimeric forms that bound analyte with differing affinities estimated to be $K_D \approx 289$ nM and $K_D \approx 11$ nM. The partial flexibility of the dextran matrix to which VC_1 is coupled has been shown in some instances to allow receptor dimerization, however, this is highly dependent on the chip used, intrinsic characteristics of the receptor and the density of protein immobilised (Raghavan *et al.,* 1995). RAGE has been shown to form much more complex quarternary structures than homodimers, as described in this study by the tetrameric model of interaction between VC_1 RAGE to ribose-AGE (Figure 70). Datillo *et al* (2007) acknowledged that the heterogeneous model was not a particularly good fit to the experimental data, raising the possibility that a tetrameric model of binding may have better described their observed data. Others have provided estimates of S100B that range from 2.2 nM to 3.6 μM, with this variation partly described by the oligomeric form of S100B and its multimeric arrangement with RAGE (Ostendorp *et al.,* 2007; LeClerc *et al.,* 2007; Datillo *et al.,* 2007).

In all published SPR studies of the interaction between RAGE and S100, RAGE was immobilised to the surface of a CM5 chip with the assumption that the partially flexible nature of the chip surface allows receptor oligomerisation. By inverting the arrangement of molecules, not only could the immobilisation of dimer/tetramers of S100B be controlled and measured, but both the stoichiometry of the RAGE complexes and their associated kinetics of interaction with surface bound S100B could described in detail. Utilising the plate based assay developed in this project, we confirmed that S100B and S100A6 bound prokaryotic VC_1C_2 RAGE with $K_D \approx 36 \pm 22$ nM and $K_D \approx 19 \pm 6$ nM, respectively. This is in in general agreement with the nanomolar affinities of interaction for these calgranulins reported by Ostendorp *et al* (2007) ($K_D \approx 42$ nM) and

S100A6 binding to the C2 domain reported by LeClerc *et al* (2007) ($K_D \approx 28$ nM). RAGE-S100P binding is poorly described in the literature, with estimates for V domain binding in the micromolar range (Penumutchu *et al.*, 2014). Penumutchu *et al* (2014) reported the binding of two V domains of RAGE to an S100P homodimer, which is not surprising considering the importance of oligomerisation in high affinity RAGE-ligand binding demonstrated in this and other studies. Here, we described for the first time the nanomolar binding of S100P to RAGE VC_1C_2 with a $K_D \approx 154 \pm 41$ nM as determined by plate assay (section 2.7.1). This almost certainly represents the interaction of multimeric RAGE with immobilised S100P in comparison to the interactions of monomeric V domains of RAGE reported by Penumutchu *et al* (2014). A more detailed SPR analysis of the interaction of RAGE with S100P (and other molecules expressed and purified as part of this study) is needed to improve our understanding of the molecular mechanisms that potentiate the pathophysiological outcomes of S100P-RAGE ligation.

In Addition to SPR and the plate based binding assay, functionality of the calgranulins expressed by T7 Shuffle® K12 was also confirmed by their ability to undergo conformational rearrangement in the presence of calcium and bind phenyl Sepharose® (Figure 59 to Figure 61).

In summary, milligram quantities of functional calgranulins S100B, S100P and S100A6 were expressed in a vector and host common to the expression of RAGE, with a one-step purification strategy, and without the need for recombinant tags. As with all RAGE ligands, published estimates of binding strength between calgranulins and RAGE are broad, ranging from 2-2000 nM (Ostendorp *et al.*, 2007; Leclerc *et al.*, 2007; Dattilo *et al.*, 2007). It is reasonable to surmise that this variation is a reflection of the complexities of both RAGE and ligand oligomerisation, redox status, the RAGE source utilised and the method used to measure binding. There is a significant opportunity to use the molecules generated in this study to further investigate the precise nature of these interactions. By inverting the SPR experimental design of LeClerc *et al* (2007) so that calgranulins rather than RAGE are immobilised on the chip surface, greater detail surrounding the kinetics of interaction and stoichiometry of the associated RAGE complex could be described.

4.4.4 Binding of RAGE to beta-amyloid.

Beta amyloid (Aβ) is a potent progressor of pathophysiologies such as Alzheimer's disease and its interaction with RAGE is implicated in the activation of apoptotic

pathways in microglia, endothelia and neurons (Lue *et al.*, 2001a; Yan *et al.*, 1996; Wilson *et al.*, 2009; Sturchler *et al.*, 2008; Origlia *et al.*, 2008). The precise means by which Aβ ligands bind RAGE to promote signal transduction is yet to be clearly delineated. Complexities in intracellular signal crosstalk, activation of alternate Aβ receptors, the presence of differing RAGE isoforms, and the ability of Aβ to oligomerise are all complicating factors (section 1.3.2). Yan *et al* (1998) have reported cell based affinities of interaction in the order of 25 ± 9 nM to 57 ± 14 nM between the more soluble form Aβ1-40 and RAGE. Ding and Keller (2005) postulated that RAGE primarily bound aggregated Aβ, implicating the V domain as the RAGE domain mediating ligation. The Aβ1-42 form is notoriously difficult to work with due to its propensity to form insoluble hydrophobic assemblies (Broersen *et al.*, 2010; Mucke and Selkoe, 2012). Preliminary SPR analysis undertaken in this study of RAGE VC_1 and anti-Aβ monoclonal antibody binding to largely monomeric Aβ1-42 produced estimates of affinity of $K_D \approx 0.9$ nM (two-state reaction, Chi^2 0.016) and $K_D \approx 0.5$ nM (1:1 Langmuir model, Chi^2= 0.016) respectively (Figure 69). The propensity of Aβ1-42 to aggregate was minimised using a method that promotes the preparation of monomeric Aβ1-42 (section 2.7.3), and extremely diffuse (low) loading of amyloid on the chip surface at 10 pg/mm2. Although only preliminary, it is exciting to demonstrate for the first time, bacterial expressed RAGE VC_1 binding to monomeric Aβ1-42 by SPR with a high affinity. The complexities of this interaction, as with all RAGE-ligand interactions discussed here, require significantly greater degrees of investigation than that undertaken in this study. However, it is clear that these opportunities for investigating the interactions between RAGE and its ligands are possible through the use of the functional recombinant proteins produced in this study. By using a common vector and host to express synthetic gene inserts, we have significantly simplified the process of production while providing the assurance that the recombinant proteins expressed are functional and a reflection of their endogenous forms.

4.5 Conclusions and Future Direction

This project set out to address fundamental questions surrounding the optimal method of producing functional RAGE and its ligands for use in a range of research contexts. Traditionally, eukaryotic expression of RAGE has been conducted using a baculoviral system and a *Sf9* Lepidoptera host. This project investigated the use of rapid recombinant technologies such as TOPO™, as a means of producing insect expression vectors quickly and simply. Here it is reported that three RAGE extracellular domain

constructs using the pIB/V5 expression vector were produced in a matter of days. The benefits of speed in construct development are clearly evident where a large number of alternate target isoforms is required, as is the case for the multiple alternate spliced variants of RAGE. Optimisation of culture and media conditions yielded a 20% increase in yields of sRAGE (VC_1C_2) through the use of the Lepidoptera cell line *Tn5*. RAGE VC_1C_2 was expressed in this cell line at levels 7-fold greater than *Sf9.* In addition, sRAGE was homogeneously glycosylated by the *Tn5* cells in contrast to the heterogeneous glycosylation observed in *Sf9* and *Sf21* cell cultures. Whilst the use of a TOPO™ expression vector for stable expression of RAGE in a Lepidoptera host offers advantages of speed, simplicity of construct production and cell maintenance and storage, the relatively low yields made it unsuitable for our laboratory, where milligram quantities are required for functional and structural studies.

Where there is no need for post-translational modifications, or this can be provided alternately, bacterial expression is often the system of choice for delivering a high yield of protein at a low cost. In this project, five prokaryotic strains were successfully transformed with six RAGE constructs comprising synonymous canonical and optimised gene sequences. Additionally, five archetypal RAGE ligands were expressed in milligram quantities using pGS-21a expression vector and T7 Shuffle® K12 host. This combination of vector and host yielded optimal levels of expression across all three RAGE domain constructs and represents a common 'toolbox' that can be used to express both RAGE and its ligands in milligram quantities. The success of this host appears to be associated with its ability to facilitate the correct formation of disulphide bonds through disulphide bond isomerase C (DsbC), resulting in a 3.5-fold increase in levels of expression relative to Origami B transformed with the same optimised synthetic construct. Optimisation of the native human gene sequence for prokaryotic expression resulted in a 4.6-fold increase in VC_1C_2 expression in T7 Shuffle® K12. When both codon bias and disulphide bond formation are accounted for, this study demonstrated the ability of T7 Shuffle® K12 to express RAGE VC_1C_2 using the optimised gene sequence at levels 13-fold higher than Origami™ B transformed with canonical RAGE gene inserts. This study, therefore, confirms that both disulphide bond formation and sequence heterology are significant rate limiters in the expression of RAGE that are mitigated through the use of optimised gene sequences and the prokaryote host T7 Shuffle® K12.

It is speculated that the correlation between diminishing returns with the deletion of the C-type lectin domains in both eukaryotic and prokaryotic hosts, is a consequence of

mRNA secondary structures that are unfavourable to translation. It is tantalising to speculate that with the addition of a fusion protein, the predicted mRNA matched stem loops potentially impeding translation may be disrupted, particularly where those matched pairs occur in the first 50 base pair from the ribosomal binding site (RBS). Further investigation is required to determine if this is indeed the case.

There was no significant difference in the ability of insect and bacterial forms of RAGE produced in this study, to preferentially bind ribose-AGEs, HMGB1, Aβ1-42, S100B, S100P or S100A6. This suggests that the recombinant RAGE produced in either host system is functionally indistinguishable. It is reported here that HMGB1 recombinantly expressed in T7 Shuffle® K12 binds RAGE domain constructs with sub-micromolar affinities. Although it is difficult to compare the estimates of affinity from this study with those previously reported for RAGE-HMGB1 due to the variations in ligand/receptor source and methodologies, the majority of published data indicates nanomolar affinities. Similarly, the S100s expressed and purified in this study had comparable affinities to a number of published estimates as discussed in section 4.4.3. Collectively, we conclude that recombinant RAGE and its ligands expressed and purified here are functionally analogous to their endogenous counterparts. This leads us to conclude that the glycosylation and post-translational capabilities of insect cells are not a compelling reason for their use over bacterial hosts for studies on RAGE.

The novel plate based assay developed within this study produced comparable estimates of affinity between RAGE and its ligands, to those reported using a raft of complex, hazardous or bespoke methodologies. The plate assay was of low cost, simple to perform and did not require a high level of expertise. Notably, the results of the assay were in excellent agreement with surface plasmon resonance (SPR) studies which, whilst providing information in real time, were expensive and demanded considerable "built expertise".

Irrespective of the assay used, RAGE and ligand oligomerisation clearly complicates our understanding of the ligand-receptor interactions in question, which may explain why there is such diversity in reported affinities of interaction from nanomolar to micromolar. The multivalent nature of the interactions may especially complicate the interpretation of assays where one partner is immobilised to a surface, as is indeed the case with both the plate binding and SPR approaches used in this study. In such studies, care will need to be taken to characterise interactions in both orientations, with RAGE

treated as either the ligand or analyte. For example, in all published SPR studies of S100-RAGE interaction (Leclerc *et al.*, 2009; Ostendorp *et al.*, 2007), RAGE was immobilised on the chip surface and S100 was passed over the sensor chip surface as the analyte. Much greater detail surrounding the kinetics and stoichiometry of the interaction could be gained by comparing these results to those obtained with S100 immobilised to the chip surface and with RAGE used as the analyte. Alternatively, a microthermal isocolorimetry approach may be used, which does not rely on the immobilisation of one of the binding partners. However, this method does have its own pitfalls; in particular, it requires significant quantities of protein for general functional studies.

A significant body of work is now progressing in our laboratory as to the complex and intricate mechanisms of the oligomerisation of HMGB1 and its interaction with RAGE, leveraging the molecules and observations that have come from this study. It is apparent from these studies that HMGB1 specifically self associates in solution and that this affects the way it binds and bends DNA. Future studies should now focus on the effect of HMGB1 self association on its binding to and activation of RAGE. In particular, attention should be focused on the role of the redox state of HMGB1 in these studies. Given the reported zinc clasp structure discussed within the body of this thesis (Figure 76), the role of zinc and the redox state on HMGB1 and RAGE interactions, should also be investigated.

In conclusion, this study has demonstrated that the bacterial expression of RAGE and its ligands using the T7 Shuffle® K12 is a superior platform to insect expression due to the speed, simplicity and low cost of construct development and culturing. The system reported here represents a common 'toolbox' approach to the rapid production of milligram quantities of RAGE and its ligands. This achievement is now enabling the progress of several functional and structural studies on RAGE and its plethora of ligands, which in future may lead to new opportunities for pharmaceutical interventions for diseases, such as diabetes, dementias, inflammatory diseases and cancer.

5.0 REFERENCES

ABEL, M., RITTHALER, U., ZHANG, Y., DENG, Y., SCHMIDT, A. M., GRETEN, J., SERNAU, T., WAHL, P., ANDRASSY, K., RITZ, E. & ET AL. 1995. Expression of receptors for advanced glycosylated end-products in renal disease. *Nephrol Dial Transplant,* 10**,** 1662-7.

ADAMI, C., BIANCHI, R., PULA, G. & DONATO, R. 2004. S100B-stimulated NO production by BV-2 microglia is independent of RAGE transducing activity but dependent on RAGE extracellular domain. *Biochim Biophys Acta,* 1742**,** 169-77.

ALGHASHAM, A. & RASHEED, Z. 2014. Therapeutic targets for rheumatoid arthritis: Progress and promises. *Autoimmunity,* 47**,** 77-94.

ALLMEN, E. U., KOCH, M., FRITZ, G. & LEGLER, D. F. 2008. V domain of RAGE interacts with AGEs on prostate carcinoma cells. *Prostate,* 68**,** 748-58.

ANDRAS, I. E., EUM, S. Y. & TOBOREK, M. 2012. Lipid rafts and functional caveolae regulate HIV-induced amyloid beta accumulation in brain endothelial cells. *Biochem Biophys Res Commun,* 421**,** 177-83.

ANDRASSY, M., IGWE, J., AUTSCHBACH, F., VOLZ, C., REMPPIS, A., NEURATH, M. F., SCHLEICHER, E., HUMPERT, P. M., WENDT, T., LILIENSIEK, B., MORCOS, M., SCHIEKOFER, S., THIELE, K., CHEN, J., KIENTSCH-ENGEL, R., SCHMIDT, A. M., STREMMEL, W., STERN, D. M., KATUS, H. A., NAWROTH, P. P. & BIERHAUS, A. 2006. Posttranslationally modified proteins as mediators of sustained intestinal inflammation. *Am J Pathol,* 169**,** 1223-37.

ANGOV, E. 2011. Codon usage: nature's roadmap to expression and folding of proteins. *Biotechnol J,* 6**,** 650-9.

ARUMUGAM, T., SIMEONE, D. M., SCHMIDT, A. M. & LOGSDON, C. D. 2004. S100P stimulates cell proliferation and survival via receptor for activated glycation end products (RAGE). *J Biol Chem,* 279**,** 5059-65.

ARUMUGAM, T., SIMEONE, D. M., VAN GOLEN, K. & LOGSDON, C. D. 2005. S100P promotes pancreatic cancer growth, survival, and invasion. *Clin Cancer Res,* 11**,** 5356-64.

BALLEZA-TAPIA, H. & PENA, F. 2009. Pharmacology of the intracellular pathways activated by amyloid Beta protein. *Mini Rev Med Chem,* 9**,** 724-40.

BAO, W. J., ZHANG, W. J. & XU, S. Q. 2014. [The role of AGE and RAGE in diabetic neuropathy]. *Sheng Li Ke Xue Jin Zhan,* 45**,** 137-9.

BASSI, R., GIUSSANI, P., ANELLI, V., COLLEONI, T., PEDRAZZI, M., PATRONE, M., VIANI, P., SPARATORE, B., MELLONI, E. & RIBONI, L. 2008. HMGB1 as an autocrine stimulus in human T98G glioblastoma cells: role in cell growth and migration. *J Neurooncol,* 87**,** 23-33.

BASTA, G. 2008. Receptor for advanced glycation endproducts and atherosclerosis: From basic mechanisms to clinical implications. *Atherosclerosis,* 196**,** 9-21.

BELGRANO, F. S., DE ABREU DA SILVA, I. C., BASTOS DE OLIVEIRA, F. M., FANTAPPIE, M. R. & MOHANA-BORGES, R. 2013. Role of the acidic tail of high mobility group protein B1 (HMGB1) in protein stability and DNA bending. *PLoS One,* 8**,** e79572.

BERGER, I., FITZGERALD, D. J. & RICHMOND, T. J. 2004. Baculovirus expression system for heterologous multiprotein complexes. *Nat Biotechnol,* 22**,** 1583-7.

BHAWAL, U. K., OZAKI, Y., NISHIMURA, M., SUGIYAMA, M., SASAHIRA, T., NOMURA, Y., SATO, F., FUJIMOTO, K., SASAKI, N., IKEDA, M. A., TSUJI, K., KUNIYASU, H. & KATO, Y. 2005. Association of expression of receptor for advanced glycation end products and invasive activity of oral squamous cell carcinoma. *Oncology,* 69**,** 246-55.

BIANCHI, R., ADAMI, C., GIAMBANCO, I. & DONATO, R. 2007. S100B binding to RAGE in microglia stimulates COX-2 expression. *J Leukoc Biol,* 81**,** 108-18.

BIERHAUS, A., ILLMER, T., KASPER, M., LUTHER, T., QUEHENBERGER, P., TRITSCHLER, H., WAHL, P., ZIEGLER, R., MULLER, M. & NAWROTH, P. P. 1997. Advanced glycation end product (AGE)-mediated induction of tissue factor in cultured endothelial cells is dependent on RAGE. *Circulation,* 96**,** 2262-71.

BOLLENBACH, T. J. & STERN, D. B. 2003. Secondary structures common to chloroplast mRNA 3'-untranslated regions direct cleavage by CSP41, an endoribonuclease belonging to the short chain dehydrogenase/reductase superfamily. *J Biol Chem,* 278**,** 25832-8.

BONALDI, T., TALAMO, F., SCAFFIDI, P., FERRERA, D., PORTO, A., BACHI, A., RUBARTELLI, A., AGRESTI, A. & BIANCHI, M. E. 2003. Monocytic cells hyperacetylate chromatin protein HMGB1 to redirect it towards secretion. *Embo j,* 22**,** 5551-60.

BOOM, A., POCHET, R., AUTHELET, M., PRADIER, L., BORGHGRAEF, P., VAN LEUVEN, F., HEIZMANN, C. W. & BRION, J. P. 2004. Astrocytic calcium/zinc binding protein S100A6 over expression in Alzheimer's disease and in PS1/APP transgenic mice models. *Biochim Biophys Acta,* 1742**,** 161-8.

BRESLAUER, K. J., FRANK, R., BLOCKER, H. & MARKY, L. A. 1986. Predicting DNA duplex stability from the base sequence. *Proc Natl Acad Sci U S A,* 83**,** 3746-50.

BRETT, J., SCHMIDT, A. M., YAN, S. D., ZOU, Y. S., WEIDMAN, E., PINSKY, D., NOWYGROD, R., NEEPER, M., PRZYSIECKI, C., SHAW, A. & ET AL. 1993. Survey of the distribution of a newly characterized receptor for advanced glycation end products in tissues. *Am J Pathol,* 143**,** 1699-712.

BROERSEN, K., ROUSSEAU, F. & SCHYMKOWITZ, J. 2010. The culprit behind amyloid beta peptide related neurotoxicity in Alzheimer's disease: oligomer size or conformation? *Alzheimers Res Ther,* 2**,** 12.

BRONDYK, W. H. 2009. Selecting an appropriate method for expressing a recombinant protein. *Methods Enzymol,* 463**,** 131-47.

BROWNLEE, M. 1995. Advanced protein glycosylation in diabetes and aging. *Annu Rev Med,* 46**,** 223-34.

BROWNLEE, M., CERAMI, A. & VLASSARA, H. 1988. Advanced glycosylation end products in tissue and the biochemical basis of diabetic complications. *N Engl J Med,* 318**,** 1315-21.

BUCALA, R., TRACEY, K. J. & CERAMI, A. 1991. Advanced glycosylation products quench nitric oxide and mediate defective endothelium-dependent vasodilatation in experimental diabetes. *J Clin Invest,* 87**,** 432-8.

BURKE, A. P., KOLODGIE, F. D., ZIESKE, A., FOWLER, D. R., WEBER, D. K., VARGHESE, P. J., FARB, A. & VIRMANI, R. 2004. Morphologic findings of coronary atherosclerotic plaques in diabetics: a postmortem study. *Arterioscler Thromb Vasc Biol,* 24**,** 1266-71.

BURSTEIN, A. H., GRIMES, I., GALASKO, D. R., AISEN, P. S., SABBAGH, M. & MJALLI, A. M. 2014. Effect of TTP488 in patients with mild to moderate Alzheimer's disease. *BMC Neurol,* 14**,** 12.

CAO, H. & LIN, R. 2009. Quantitative evaluation of His-tag purification and immunoprecipitation of tristetraprolin and its mutant proteins from transfected human cells. *Biotechnol Prog,* 25**,** 461-7.

CAO, M. J., WU, G. P., GUO, C. & SU, W. J. 2005. Expression of chicken interleukin-2 in insect cells. *Biochemistry (Mosc),* 70**,** 1223-6.

CARINHAS, N., OLIVEIRA, R., ALVES, P. M., CARRONDO, M. J. & TEIXEIRA, A. P. 2012. Systems biotechnology of animal cells: the road to prediction. *Trends Biotechnol,* 30**,** 377-85.

CHANEY, M. O., STINE, W. B., KOKJOHN, T. A., KUO, Y.-M., ESH, C., RAHMAN, A., LUEHRS, D. C., SCHMIDT, A. M., STERN, D., YAN, S. D. & ROHER, A. E. 2005. RAGE and amyloid beta interactions: Atomic force microscopy and molecular modeling. *Biochimica et Biophysica Acta (BBA) - Molecular Basis of Disease,* 1741**,** 199-205.

CHARDIN, P. 2003. GTPase regulation: getting aRnd Rock and Rho inhibition. *Curr Biol,* 13**,** R702-4.

CHAVAKIS, T., BIERHAUS, A., AL-FAKHRI, N., SCHNEIDER, D., WITTE, S., LINN, T., NAGASHIMA, M., MORSER, J., ARNOLD, B., PREISSNER, K. T. & NAWROTH, P. P. 2003. The pattern recognition receptor (RAGE) is a counterreceptor for leukocyte integrins: a novel pathway for inflammatory cell recruitment. *J Exp Med,* 198**,** 1507-15.

CHEN, H., WU, L., LI, Y., MENG, J., LIN, N., YANG, D., ZHU, Y., LI, X., LI, M., XU, Y., WU, Y., TONG, X. & SU, Q. 2014a. Advanced glycation end products increase carbohydrate responsive element binding protein expression and promote cancer cell proliferation. *Mol Cell Endocrinol,* 395**,** 69-78.

CHEN, H., XU, C., JIN, Q. & LIU, Z. 2014b. S100 protein family in human cancer. *Am J Cancer Res,* 4**,** 89-115.

CHEN, Q., DONG, L., WANG, L., KANG, L. & XU, B. 2009a. Advanced glycation end products impair function of late endothelial progenitor cells through effects on protein kinase Akt and cyclooxygenase-2. *Biochem Biophys Res Commun,* 381**,** 192-7.

CHEN, X., WALKER, D. G., SCHMIDT, A. M., ARANCIO, O., LUE, L. F. & YAN, S. D. 2007. RAGE: a potential target for Abeta-mediated cellular perturbation in Alzheimer's disease. *Curr Mol Med,* 7**,** 735-42.

CHEN, Y., SUN, W., GAO, R., SU, Y., UMEHARA, H., DONG, L. & GONG, F. 2013. The role of high mobility group box chromosomal protein 1 in rheumatoid arthritis. *Rheumatology (Oxford),* 52**,** 1739-47.

CHEN, Y., YAN, S. S., COLGAN, J., ZHANG, H. P., LUBAN, J., SCHMIDT, A. M., STERN, D. & HEROLD, K. C. 2004. Blockade of late stages of autoimmune diabetes by inhibition of the receptor for advanced glycation end products. *J Immunol,* 173**,** 1399-405.

CHEN, Y. S., YAN, W., GECZY, C. L., BROWN, M. A. & THOMAS, R. 2009b. Serum levels of soluble receptor for advanced glycation end products and of S100 proteins are associated with inflammatory, autoantibody, and classical risk markers of joint and vascular damage in rheumatoid arthritis. *Arthritis Res Ther,* 11**,** R39.

CHO, S. Y. & KLEMKE, R. L. 2000. Extracellular-regulated kinase activation and CAS/Crk coupling regulate cell migration and suppress apoptosis during invasion of the extracellular matrix. *J Cell Biol,* 149**,** 223-36.

CHONG, Y. H., SHIN, Y. J., LEE, E. O., KAYED, R., GLABE, C. G. & TENNER, A. J. 2006. ERK1/2 activation mediates Abeta oligomer-induced neurotoxicity via caspase-3 activation and tau cleavage in rat organotypic hippocampal slice cultures. *J Biol Chem,* 281**,** 20315-25.

CHOU, D. K., ZHANG, J., SMITH, F. I., MCCAFFERY, P. & JUNGALWALA, F. B. 2004. Developmental expression of receptor for advanced glycation end products (RAGE), amphoterin and sulfoglucuronyl (HNK-1) carbohydrate in mouse cerebellum and their role in neurite outgrowth and cell migration. *J Neurochem,* 90**,** 1389-401.

CHRISTIANSEN, S. P., CHANDLER, D. L., HOLMES, J. M., BACAL, D. A., BIRCH, E., DONAHUE, S. P., MOHNEY, B. G., REPKA, M. X. & VERDERBER, L. C. 2009. The relationship between preoperative alignment stability and postoperative motor outcomes in children with esotropia. *J AAPOS,* 13**,** 335-8.

CHUAH, Y. K., BASIR, R., TALIB, H., TIE, T. H. & NORDIN, N. 2013. Receptor for advanced glycation end products and its involvement in inflammatory diseases. *Int J Inflam,* 2013**,** 403460.

CLYNES, R., MOSER, B., YAN, S. F., RAMASAMY, R., HEROLD, K. & SCHMIDT, A. M. 2007. Receptor for AGE (RAGE): weaving tangled webs within the inflammatory response. *Curr Mol Med,* 7**,** 743-51.

CORTAZZO, P., CERVENANSKY, C., MARIN, M., REISS, C., EHRLICH, R. & DEANA, A. 2002. Silent mutations affect in vivo protein folding in Escherichia coli. *Biochem Biophys Res Commun,* 293**,** 537-41.

DAFFU, G., DEL POZO, C. H., O'SHEA, K. M., ANANTHAKRISHNAN, R., RAMASAMY, R. & SCHMIDT, A. M. 2013. Radical roles for RAGE in the pathogenesis of oxidative stress in cardiovascular diseases and beyond. *Int J Mol Sci,* 14**,** 19891-910.

DATTILO, B. M., FRITZ, G., LECLERC, E., KOOI, C. W., HEIZMANN, C. W. & CHAZIN, W. J. 2007. The extracellular region of the receptor for advanced glycation end products is composed of two independent structural units. *Biochemistry,* 46**,** 6957-70.

DE ARRIBA, S. G., LOSKE, C., MEINERS, I., FLEISCHER, G., LOBISCH, M., WESSEL, K., TRITSCHLER, H., SCHINZEL, R. & MUNCH, G. 2003. Advanced glycation endproducts induce changes in glucose consumption, lactate production, and ATP levels in SH-SY5Y neuroblastoma cells by a redox-sensitive mechanism. *J Cereb Blood Flow Metab,* 23**,** 1307-13.

DE MARCO, A. 2009. Strategies for successful recombinant expression of disulfide bond-dependent proteins in Escherichia coli. *Microb Cell Fact,* 8**,** 26.

DEANE, R. J. 2012. Is RAGE still a therapeutic target for Alzheimer's disease? *Future Med Chem,* 4**,** 915-25.

DEMALI, K. A. & BURRIDGE, K. 2003. Coupling membrane protrusion and cell adhesion. *J Cell Sci,* 116**,** 2389-97.

DING, Q. & KELLER, J. N. 2005. Evaluation of rage isoforms, ligands, and signaling in the brain. *Biochim Biophys Acta,* 1746**,** 18-27.

DING, Y., KANTARCI, A., BADWEY, J. A., HASTURK, H., MALABANAN, A. & VAN DYKE, T. E. 2007. Phosphorylation of pleckstrin increases proinflammatory cytokine secretion by mononuclear phagocytes in diabetes mellitus. *J Immunol,* 179**,** 647-54.

DONATO, R. 1986. S-100 proteins. *Cell Calcium,* 7**,** 123-45.

DONATO, R. 2001. S100: a multigenic family of calcium-modulated proteins of the EF-hand type with intracellular and extracellular functional roles. *Int J Biochem Cell Biol,* 33**,** 637-68.

DONATO, R. 2007. RAGE: a single receptor for several ligands and different cellular responses: the case of certain S100 proteins. *Curr Mol Med,* 7**,** 711-24.

DUKIC-STEFANOVIC, S., GASIC-MILENKOVIC, J., DEUTHER-CONRAD, W. & MUNCH, G. 2003. Signal transduction pathways in mouse microglia N-11 cells activated by advanced glycation endproducts (AGEs). *J Neurochem,* 87**,** 44-55.

EL KHOURY, J., THOMAS, C. A., LOIKE, J. D., HICKMAN, S. E., CAO, L. & SILVERSTEIN, S. C. 1994. Macrophages adhere to glucose-modified basement membrane collagen IV via their scavenger receptors. *J Biol Chem,* 269**,** 10197-200.

ELENKOV, I., PELOVSKY, P., UGRINOVA, I., TAKAHASHI, M. & PASHEVA, E. 2011. The DNA binding and bending activities of truncated tail-less HMGB1 protein are differentially affected by Lys-2 and Lys-81 residues and their acetylation. *Int J Biol Sci,* 7**,** 691-9.

ELLIS, E. N. & GOOD, B. H. 1991. Prevention of glomerular basement membrane thickening by aminoguanidine in experimental diabetes mellitus. *Metabolism,* 40**,** 1016-9.

EMANUELE, E., D'ANGELO, A., TOMAINO, C., BINETTI, G., GHIDONI, R., POLITI, P., BERNARDI, L., MALETTA, R., BRUNI, A. C. & GEROLDI, D. 2005. Circulating levels of soluble receptor for advanced glycation end products in Alzheimer disease and vascular dementia. *Arch Neurol,* 62**,** 1734-6.

ERLANDSSON HARRIS, H. & ANDERSSON, U. 2004. Mini-review: The nuclear protein HMGB1 as a proinflammatory mediator. *Eur J Immunol,* 34**,** 1503-12.

ESPOSITO, C., GERLACH, H., BRETT, J., STERN, D. & VLASSARA, H. 1989. Endothelial receptor-mediated binding of glucose-modified albumin is associated with increased monolayer permeability and modulation of cell surface coagulant properties. *J Exp Med,* 170**,** 1387-407.

FAGES, C., NOLO, R., HUTTUNEN, H. J., ESKELINEN, E. & RAUVALA, H. 2000. Regulation of cell migration by amphoterin. *J Cell Sci,* 113 (Pt 4)**,** 611-20.

FALCONE, C., CAMPO, I., EMANUELE, E., BUZZI, M. P., GEROLDI, D., BELVITO, C., ZORZETTO, M., SBARSI, I. & CUCCIA, M. 2005. -374T/A polymorphism of the RAGE gene promoter in relation to severity of coronary atherosclerosis. *Clin Chim Acta,* 354**,** 111-6.

FALCONE, C., GEROLDI, D., BUZZI, M. P., EMANUELE, E., YILMAZ, Y., FONTANA, J. M., VIGNALI, L., BOIOCCHI, C., SBARSI, I. & CUCCIA, M. 2008. The -374T/A RAGE polymorphism protects against future cardiac events in nondiabetic patients with coronary artery disease. *Arch Med Res,* 39**,** 320-5.

FATH, S., BAUER, A. P., LISS, M., SPRIESTERSBACH, A., MAERTENS, B., HAHN, P., LUDWIG, C., SCHAFER, F., GRAF, M. & WAGNER, R. 2011. Multiparameter RNA and codon optimization: a standardized tool to assess and enhance autologous mammalian gene expression. *PLoS One,* 6**,** e17596.

FERNANDEZ, F. J. & VEGA, M. C. 2013. Technologies to keep an eye on: alternative hosts for protein production in structural biology. *Curr Opin Struct Biol,* 23**,** 365-73.

FERRER-MIRALLES, N. & VILLAVERDE, A. 2013. Bacterial cell factories for recombinant protein production; expanding the catalogue. *Microb Cell Fact,* 12**,** 113.

FIUZA, C., BUSTIN, M., TALWAR, S., TROPEA, M., GERSTENBERGER, E., SHELHAMER, J. H. & SUFFREDINI, A. F. 2003. Inflammation-promoting activity of HMGB1 on human microvascular endothelial cells. *Blood,* 101**,** 2652-60.

FOELL, D., WITTKOWSKI, H., VOGL, T. & ROTH, J. 2007. S100 proteins expressed in phagocytes: a novel group of damage-associated molecular pattern molecules. *J Leukoc Biol,* 81**,** 28-37.

FRYE, E. B., DEGENHARDT, T. P., THORPE, S. R. & BAYNES, J. W. 1998. Role of the Maillard reaction in aging of tissue proteins. Advanced glycation end product-dependent increase in imidazolium cross-links in human lens proteins. *J Biol Chem,* 273**,** 18714-9.

FUENTES, M. K., NIGAVEKAR, S. S., ARUMUGAM, T., LOGSDON, C. D., SCHMIDT, A. M., PARK, J. C. & HUANG, E. H. 2007. RAGE activation by S100P in colon cancer

stimulates growth, migration, and cell signaling pathways. *Dis Colon Rectum,* 50**,** 1230-40.

GALKINA, E. & LEY, K. 2009. Immune and inflammatory mechanisms of atherosclerosis (*). *Annu Rev Immunol,* 27**,** 165-97.

GALLOWAY, C. A., SOWDEN, M. P. & SMITH, H. C. 2003. Increasing the yield of soluble recombinant protein expressed in E. coli by induction during late log phase. *Biotechniques,* 34**,** 524-6, 528, 530.

GAO, W., RZEWSKI, A., SUN, H., ROBBINS, P. D. & GAMBOTTO, A. 2004. UpGene: Application of a web-based DNA codon optimization algorithm. *Biotechnol Prog,* 20**,** 443-8.

GARDELLA, S., ANDREI, C., FERRERA, D., LOTTI, L. V., TORRISI, M. R., BIANCHI, M. E. & RUBARTELLI, A. 2002. The nuclear protein HMGB1 is secreted by monocytes via a non-classical, vesicle-mediated secretory pathway. *EMBO Rep,* 3**,** 995-1001.

GERRARD, J. A. 2002. New Aspects of an AGEing Chemistry - Recent Developments Concerning the Maillard Reaction. *Australian Journal of Chemistry,* 55**,** 299-310.

GOLDBERG, T., CAI, W., PEPPA, M., DARDAINE, V., BALIGA, B. S., URIBARRI, J. & VLASSARA, H. 2004. Advanced Glycoxidation End Products in Commonly Consumed Foods. *Journal of the American Dietic Association,* 104**,** 1287 - 1291.

GOMEZ-SEBASTIAN, S., LOPEZ-VIDAL, J. & ESCRIBANO, J. M. 2014. Significant productivity improvement of the baculovirus expression vector system by engineering a novel expression cassette. *PLoS One,* 9**,** e96562.

GREENHALGH, D. G., SPRUGEL, K. H., MURRAY, M. J. & ROSS, R. 1990. PDGF and FGF stimulate wound healing in the genetically diabetic mouse. *Am J Pathol,* 136**,** 1235-46.

GRIBENKO, A., LOPEZ, M. M., RICHARDSON, J. M., 3RD & MAKHATADZE, G. I. 1998. Cloning, overexpression, purification, and spectroscopic characterization of human S100P. *Protein Sci,* 7**,** 211-5.

GRODBERG, J. & DUNN, J. J. 1988. ompT encodes the Escherichia coli outer membrane protease that cleaves T7 RNA polymerase during purification. *J Bacteriol,* 170**,** 1245-53.

GROSS, S. R., SIN, C. G., BARRACLOUGH, R. & RUDLAND, P. S. 2014. Joining S100 proteins and migration: for better or for worse, in sickness and in health. *Cell Mol Life Sci,* 71**,** 1551-79.

GRUBER, A. R., LORENZ, R., BERNHART, S. H., NEUBOCK, R. & HOFACKER, I. L. 2008. The Vienna RNA websuite. *Nucleic Acids Res,* 36**,** W70-4.

GUGLIUCCI, A. & MENINI, T. 2014. The Axis AGE-RAGE-Soluble RAGE and Oxidative Stress in Chronic Kidney Disease. *Adv Exp Med Biol,* 824**,** 191-208.

GUO, Z. J., NIU, H. X., HOU, F. F., ZHANG, L., FU, N., NAGAI, R., LU, X., CHEN, B. H., SHAN, Y. X., TIAN, J. W., NAGARAJ, R. H., XIE, D. & ZHANG, X. 2008. Advanced oxidation

protein products activate vascular endothelial cells via a RAGE-mediated signaling pathway. *Antioxid Redox Signal,* 10**,** 1699-712.

HAEBEL, P. W., GOLDSTONE, D., KATZEN, F., BECKWITH, J. & METCALF, P. 2002. The disulfide bond isomerase DsbC is activated by an immunoglobulin-fold thiol oxidoreductase: crystal structure of the DsbC-DsbDalpha complex. *Embo j,* 21**,** 4774-84.

HAMMES, H. P., BROWNLEE, M., EDELSTEIN, D., SALECK, M., MARTIN, S. & FEDERLIN, K. 1994. Aminoguanidine inhibits the development of accelerated diabetic retinopathy in the spontaneous hypertensive rat. *Diabetologia,* 37**,** 32-5.

HANFORD, L. E., ENGHILD, J. J., VALNICKOVA, Z., PETERSEN, S. V., SCHAEFER, L. M., SCHAEFER, T. M., REINHART, T. A. & OURY, T. D. 2004. Purification and characterization of mouse soluble receptor for advanced glycation end products (sRAGE). *J Biol Chem,* 279**,** 50019-24.

HARDY, J. 1997. Amyloid, the presenilins and Alzheimer's disease. *Trends Neurosci,* 20**,** 154-9.

HASSID, B. G., NAIR, M. N., DUCRUET, A. F., OTTEN, M. L., KOMOTAR, R. J., PINSKY, D. J., SCHMIDT, A. M., YAN, S. F. & CONNOLLY, E. S. 2009. Neuronal RAGE expression modulates severity of injury following transient focal cerebral ischemia. *J Clin Neurosci,* 16**,** 302-6.

HE, H., HAN, L., GUAN, W., LI, J., HAN, W. & YU, Y. 2013. An efficient expression and purification strategy for the production of S100 proteins in Escherichia coli. *Bioengineered,* 4**,** 55-8.

HELFMAN, D. M., KIM, E. J., LUKANIDIN, E. & GRIGORIAN, M. 2005. The metastasis associated protein S100A4: role in tumour progression and metastasis. *Br J Cancer,* 92**,** 1955-8.

HIGASHI, T., SANO, H., SAISHOJI, T., IKEDA, K., JINNOUCHI, Y., KANZAKI, T., MORISAKI, N., RAUVALA, H., SHICHIRI, M. & HORIUCHI, S. 1997. The receptor for advanced glycation end products mediates the chemotaxis of rabbit smooth muscle cells. *Diabetes,* 46**,** 463-72.

HOFMANN, M. A., DRURY, S., FU, C., QU, W., TAGUCHI, A., LU, Y., AVILA, C., KAMBHAM, N., BIERHAUS, A., NAWROTH, P., NEURATH, M. F., SLATTERY, T., BEACH, D., MCCLARY, J., NAGASHIMA, M., MORSER, J., STERN, D. & SCHMIDT, A. M. 1999. RAGE mediates a novel proinflammatory axis: a central cell surface receptor for S100/calgranulin polypeptides. *Cell,* 97**,** 889-901.

HOFMANN, M. A., DRURY, S., HUDSON, B. I., GLEASON, M. R., QU, W., LU, Y., LALLA, E., CHITNIS, S., MONTEIRO, J., STICKLAND, M. H., BUCCIARELLI, L. G., MOSER, B., MOXLEY, G., ITESCU, S., GRANT, P. J., GREGERSEN, P. K., STERN, D. M. & SCHMIDT, A. M. 2002. RAGE and arthritis: the G82S polymorphism amplifies the inflammatory response. *Genes Immun,* 3**,** 123-35.

HOGAN, M., CERAMI, A. & BUCALA, R. 1992. Advanced glycosylation endproducts block the antiproliferative effect of nitric oxide. Role in the vascular and renal complications of diabetes mellitus. *J Clin Invest,* 90**,** 1110-5.

HORI, O., BRETT, J., SLATTERY, T., CAO, R., ZHANG, J., CHEN, J. X., NAGASHIMA, M., LUNDH, E. R., VIJAY, S., NITECKI, D. & ET AL. 1995. The receptor for advanced glycation end products (RAGE) is a cellular binding site for amphoterin. Mediation of neurite outgrowth and co-expression of rage and amphoterin in the developing nervous system. *J Biol Chem,* 270**,** 25752-61.

HOULE, F., POIRIER, A., DUMARESQ, J. & HUOT, J. 2007. DAP kinase mediates the phosphorylation of tropomyosin-1 downstream of the ERK pathway, which regulates the formation of stress fibers in response to oxidative stress. *J Cell Sci,* 120**,** 3666-77.

HSIN, J., CHANDLER, D. E., GUMBART, J., HARRISON, C. B., SENER, M., STRUMPFER, J. & SCHULTEN, K. 2010. Self-Assembly of Photosynthetic Membranes. *Chemphyschem*.

HUDSON, B. I., CARTER, A. M., HARJA, E., KALEA, A. Z., ARRIERO, M., YANG, H., GRANT, P. J. & SCHMIDT, A. M. 2008a. Identification, classification, and expression of RAGE gene splice variants. *FASEB J,* 22**,** 1572-80.

HUDSON, B. I., KALEA, A. Z., DEL MAR ARRIERO, M., HARJA, E., BOULANGER, E., D'AGATI, V. & SCHMIDT, A. M. 2008b. Interaction of the RAGE cytoplasmic domain with diaphanous-1 is required for ligand-stimulated cellular migration through activation of Rac1 and Cdc42. *J Biol Chem,* 283**,** 34457-68.

HUDSON, B. I., STICKLAND, M. H., FUTERS, T. S. & GRANT, P. J. 2001. Effects of novel polymorphisms in the RAGE gene on transcriptional regulation and their association with diabetic retinopathy. *Diabetes,* 50**,** 1505-11.

HUIJBERTS, M. S., WOLFFENBUTTEL, B. H., BOUDIER, H. A., CRIJNS, F. R., KRUSEMAN, A. C., POITEVIN, P. & LEVY, B. I. 1993. Aminoguanidine treatment increases elasticity and decreases fluid filtration of large arteries from diabetic rats. *J Clin Invest,* 92**,** 1407-11.

HUNT, I. 2005. From gene to protein: a review of new and enabling technologies for multi-parallel protein expression. *Protein Expr Purif,* 40**,** 1-22.

HUNTER, M. J. & CHAZIN, W. J. 1998. High level expression and dimer characterization of the S100 EF-hand proteins, migration inhibitory factor-related proteins 8 and 14. *J Biol Chem,* 273**,** 12427-35.

HUTTUNEN, H. J., FAGES, C., KUJA-PANULA, J., RIDLEY, A. J. & RAUVALA, H. 2002. Receptor for advanced glycation end products-binding COOH-terminal motif of amphoterin inhibits invasive migration and metastasis. *Cancer Res,* 62**,** 4805-11.

HUTTUNEN, H. J., FAGES, C. & RAUVALA, H. 1999. Receptor for advanced glycation end products (RAGE)-mediated neurite outgrowth and activation of NF-kappaB require the cytoplasmic domain of the receptor but different downstream signaling pathways. *J Biol Chem,* 274**,** 19919-24.

HUTTUNEN, H. J., KUJA-PANULA, J., SORCI, G., AGNELETTI, A. L., DONATO, R. & RAUVALA, H. 2000. Coregulation of neurite outgrowth and cell survival by amphoterin and S100 proteins through receptor for advanced glycation end products (RAGE) activation. *J Biol Chem,* 275**,** 40096-105.

HUTTUNEN, H. J. & RAUVALA, H. 2004. Amphoterin as an extracellular regulator of cell motility: from discovery to disease. *J Intern Med,* 255**,** 351-66.

HUVENEERS, S. & DANEN, E. H. 2009. Adhesion signaling - crosstalk between integrins, Src and Rho. *J Cell Sci,* 122**,** 1059-69.

IBRAHIM, Z. A., ARMOUR, C. L., PHIPPS, S. & SUKKAR, M. B. 2013. RAGE and TLRs: relatives, friends or neighbours? *Mol Immunol,* 56**,** 739-44.

IKEDA, K., HIGASHI, T., SANO, H., JINNOUCHI, Y., YOSHIDA, M., ARAKI, T., UEDA, S. & HORIUCHI, S. 1996. N (epsilon)-(carboxymethyl)lysine protein adduct is a major immunological epitope in proteins modified with advanced glycation end products of the Maillard reaction. *Biochemistry,* 35**,** 8075-83.

INOUE, K., KAWAHARA, K., BISWAS, K. K., ANDO, K., MITSUDO, K., NOBUYOSHI, M. & MARUYAMA, I. 2007. HMGB1 expression by activated vascular smooth muscle cells in advanced human atherosclerosis plaques. *Cardiovasc Pathol,* 16**,** 136-43.

ISHIHARA, K., TSUTSUMI, K., KAWANE, S., NAKAJIMA, M. & KASAOKA, T. 2003. The receptor for advanced glycation end-products (RAGE) directly binds to ERK by a D-domain-like docking site. *FEBS Lett,* 550**,** 107-13.

ITAKURA, K., HIROSE, T., CREA, R., RIGGS, A. D., HEYNEKER, H. L., BOLIVAR, F. & BOYER, H. W. 1977. Expression in Escherichia coli of a chemically synthesized gene for the hormone somatostatin. *Science,* 198**,** 1056-63.

JACKSON, R. J., HELLEN, C. U. & PESTOVA, T. V. 2010. The mechanism of eukaryotic translation initiation and principles of its regulation. *Nat Rev Mol Cell Biol,* 11**,** 113-27.

JANG, Y., KIM, J. Y., KANG, S. M., KIM, J. S., CHAE, J. S., KIM, O. Y., KOH, S. J., LEE, H. C., AHN, C. W., SONG, Y. D. & LEE, J. H. 2007. Association of the Gly82Ser polymorphism in the receptor for advanced glycation end products (RAGE) gene with circulating levels of soluble RAGE and inflammatory markers in nondiabetic and nonobese Koreans. *Metabolism,* 56**,** 199-205.

JANKO, C., FILIPOVIC, M., MUNOZ, L. E., SCHORN, C., SCHETT, G., IVANOVIC-BURMAZOVIC, I. & HERRMANN, M. 2014. Redox modulation of HMGB1-related signaling. *Antioxid Redox Signal,* 20**,** 1075-85.

JARVIS, D. L. 2009. Baculovirus-insect cell expression systems. *Methods Enzymol,* 463**,** 191-222.

JARVIS, D. L., FLEMING, J. A., KOVACS, G. R., SUMMERS, M. D. & GUARINO, L. A. 1990. Use of early baculovirus promoters for continuous expression and efficient processing of foreign gene products in stably transformed lepidopteran cells. *Biotechnology (N Y),* 8**,** 950-5.

KADOKURA, H., KATZEN, F. & BECKWITH, J. 2003. Protein disulfide bond formation in prokaryotes. *Annu Rev Biochem,* 72**,** 111-35.

KALEA, A. Z., REINIGER, N., YANG, H., ARRIERO, M., SCHMIDT, A. M. & HUDSON, B. I. 2009a. Alternative splicing of the murine receptor for advanced glycation end-products (RAGE) gene. *FASEB J,* 23**,** 1766-74.

KALEA, A. Z., SCHMIDT, A. M. & HUDSON, B. I. 2009b. RAGE: a novel biological and genetic marker for vascular disease. *Clin Sci (Lond),* 116**,** 621-37.

KATO, T., SUZUKI, M., MURATA, T. & PARK, E. Y. 2005. The effects of N-glycosylation sites and the N-terminal region on the biological function of beta1,3-N-acetylglucosaminyltransferase 2 and its secretion. *Biochem Biophys Res Commun,* 329**,** 699-705.

KAY, J. J., VAN DE MEERAKKER, S. Y., STRECKER, K. E. & CHANDLER, D. W. 2009. Production of cold ND3 by kinematic cooling. *Faraday Discuss,* 142**,** 143-53; discussion 221-55.

KIM, C. M., DION, S. B., ONORATO, J. J. & BENOVIC, J. L. 1993. Expression and characterization of two beta-adrenergic receptor kinase isoforms using the baculovirus expression system. *Receptor,* 3**,** 39-55.

KIM, O. Y., JO, S. H., JANG, Y., CHAE, J. S., KIM, J. Y., HYUN, Y. J. & LEE, J. H. 2009. G allele at RAGE SNP82 is associated with proinflammatory markers in obese subjects. *Nutr Res,* 29**,** 106-13.

KIMBERLY, W. T., LAVOIE, M. J., OSTASZEWSKI, B. L., YE, W., WOLFE, M. S. & SELKOE, D. J. 2003. Gamma-secretase is a membrane protein complex comprised of presenilin, nicastrin, Aph-1, and Pen-2. *Proc Natl Acad Sci U S A,* 100**,** 6382-7.

KIRSTEIN, M., ASTON, C., HINTZ, R. & VLASSARA, H. 1992. Receptor-specific induction of insulin-like growth factor I in human monocytes by advanced glycosylation end product-modified proteins. *J Clin Invest,* 90**,** 439-46.

KIRSTEIN, M., BRETT, J., RADOFF, S., OGAWA, S., STERN, D. & VLASSARA, H. 1990. Advanced protein glycosylation induces transendothelial human monocyte chemotaxis and secretion of platelet-derived growth factor: role in vascular disease of diabetes and aging. *Proc Natl Acad Sci U S A,* 87**,** 9010-4.

KISLINGER, T., FU, C., HUBER, B., QU, W., TAGUCHI, A., DU YAN, S., HOFMANN, M., YAN, S. F., PISCHETSRIEDER, M., STERN, D. & SCHMIDT, A. M. 1999. N(epsilon)-(carboxymethyl)lysine adducts of proteins are ligands for receptor for advanced glycation end products that activate cell signaling pathways and modulate gene expression. *J Biol Chem,* 274**,** 31740-9.

KITTS, P. A. & POSSEE, R. D. 1993. A method for producing recombinant baculovirus expression vectors at high frequency. *Biotechniques,* 14**,** 810-7.

KOCH, M., CHITAYAT, S., DATTILO, B. M., SCHIEFNER, A., DIEZ, J., CHAZIN, W. J. & FRITZ, G. 2010. Structural basis for ligand recognition and activation of RAGE. *Structure,* 18**,** 1342-52.

KOGEL, D., PETERS, M., KONIG, H. G., HASHEMI, S. M., BUI, N. T., AROLT, V., ROTHERMUNDT, M. & PREHN, J. H. 2004. S100B potently activates p65/c-Rel transcriptional complexes in hippocampal neurons: Clinical implications for the role of S100B in excitotoxic brain injury. *Neuroscience,* 127**,** 913-20.

KOHN, R. R. 1982. *Testing the Theories of Aging,* Boca Raton, Florida, CRC Press Inc.

KOKKOLA, R., ANDERSSON, A., MULLINS, G., OSTBERG, T., TREUTIGER, C. J., ARNOLD, B., NAWROTH, P., ANDERSSON, U., HARRIS, R. A. & HARRIS, H. E. 2005. RAGE is the major receptor for the proinflammatory activity of HMGB1 in rodent macrophages. *Scand J Immunol,* 61**,** 1-9.

KOMAR, A. A., LESNIK, T. & REISS, C. 1999. Synonymous codon substitutions affect ribosome traffic and protein folding during in vitro translation. *FEBS Lett,* 462**,** 387-91.

KOOK, S. Y., HONG, H. S., MOON, M., HA, C. M., CHANG, S. & MOOK-JUNG, I. 2012. Abeta(1)(-)(4)(2)-RAGE interaction disrupts tight junctions of the blood-brain barrier via Ca(2)(+)-calcineurin signaling. *J Neurosci,* 32**,** 8845-54.

KUMANO-KURAMOCHI, M., XIE, Q., SAKAKIBARA, Y., NIIMI, S., SEKIZAWA, K., KOMBA, S. & MACHIDA, S. 2008. Expression and characterization of recombinant C-terminal biotinylated extracellular domain of human receptor for advanced glycation end products (hsRAGE) in Escherichia coli. *J Biochem,* 143**,** 229-36.

LECLERC, E., FRITZ, G., VETTER, S. W. & HEIZMANN, C. W. 2009. Binding of S100 proteins to RAGE: An update. *Biochim Biophys Acta,* 1793**,** 993-1007.

LECLERC, E., FRITZ, G., WEIBEL, M., HEIZMANN, C. W. & GALICHET, A. 2007. S100B and S100A6 differentially modulate cell survival by interacting with distinct RAGE (receptor for advanced glycation end products) immunoglobulin domains. *J Biol Chem,* 282**,** 31317-31.

LEE, E. J. & PARK, J. H. 2013. Receptor for Advanced Glycation Endproducts (RAGE), Its Ligands, and Soluble RAGE: Potential Biomarkers for Diagnosis and Therapeutic Targets for Human Renal Diseases. *Genomics Inform,* 11**,** 224-9.

LEIBOVICH, S. J. & ROSS, R. 1975. The role of the macrophage in wound repair. A study with hydrocortisone and antimacrophage serum. *Am J Pathol,* 78**,** 71-100.

LI, J. & SCHMIDT, A. M. 1997. Characterization and functional analysis of the promoter of RAGE, the receptor for advanced glycation end products. *J Biol Chem,* 272**,** 16498-506.

LI, Y. M., MITSUHASHI, T., WOJCIECHOWICZ, D., SHIMIZU, N., LI, J., STITT, A., HE, C., BANERJEE, D. & VLASSARA, H. 1996. Molecular identity and cellular distribution of advanced glycation endproduct receptors: relationship of p60 to OST-48 and p90 to 80K-H membrane proteins. *Proc Natl Acad Sci U S A,* 93**,** 11047-52.

LING, Y., YANG, Z. Y., YIN, T., LI, L., YUAN, W. W., WU, H. S. & WANG, C. Y. 2011. Heparin changes the conformation of high-mobility group protein 1 and decreases its affinity toward receptor for advanced glycation endproducts in vitro. *Int Immunopharmacol,* 11**,** 187-93.

LIU, R., MORI, S., WAKE, H., ZHANG, J., LIU, K., IZUSHI, Y., TAKAHASHI, H. K., PENG, B. & NISHIBORI, M. 2009. Establishment of in vitro binding assay of high mobility group box-1 and S100A12 to receptor for advanced glycation endproducts: heparin's effect on binding. *Acta Med Okayama,* 63**,** 203-11.

LOBSTEIN, J., EMRICH, C. A., JEANS, C., FAULKNER, M., RIGGS, P. & BERKMEN, M. 2012. SHuffle, a novel Escherichia coli protein expression strain capable of correctly folding disulfide bonded proteins in its cytoplasm. *Microb Cell Fact,* 11**,** 56.

LORENZ, R., BERNHART, S. H., HONER ZU SIEDERDISSEN, C., TAFER, H., FLAMM, C., STADLER, P. F. & HOFACKER, I. L. 2011. ViennaRNA Package 2.0. *Algorithms Mol Biol,* 6**,** 26.

LOS, M., MADDIKA, S., ERB, B. & SCHULZE-OSTHOFF, K. 2009. Switching Akt: from survival signaling to deadly response. *Bioessays,* 31**,** 492-5.

LUE, L.-F., WALKER, D. G., BRACHOVA, L., BEACH, T. G., ROGERS, J., SCHMIDT, A. M., STERN, D. M. & YAN, S. D. 2001a. Involvement of Microglial Receptor for Advanced Glycation Endproducts (RAGE) in Alzheimer's Disease: Identification of a Cellular Activation Mechanism. *Experimental Neurology,* 171**,** 29-45.

LUE, L. F., WALKER, D. G., BRACHOVA, L., BEACH, T. G., ROGERS, J., SCHMIDT, A. M., STERN, D. M. & YAN, S. D. 2001b. Involvement of microglial receptor for advanced glycation endproducts (RAGE) in Alzheimer's disease: identification of a cellular activation mechanism. *Exp Neurol,* 171**,** 29-45.

LUE, L. F., YAN, S. D., STERN, D. M. & WALKER, D. G. 2005. Preventing activation of receptor for advanced glycation endproducts in Alzheimer's disease. *Curr Drug Targets CNS Neurol Disord,* 4**,** 249-66.

MAEDA, S., HIKIBA, Y., SHIBATA, W., OHMAE, T., YANAI, A., OGURA, K., YAMADA, S. & OMATA, M. 2007. Essential roles of high-mobility group box 1 in the development of murine colitis and colitis-associated cancer. *Biochem Biophys Res Commun,* 360**,** 394-400.

MAILLARD, L. C. 1912. Action des acides amines sur les sucres: Formation des melanoidines par voie methodique. . *C R Acad Sci.,* 154**,** 66.

MALLE, E., SODIN-SEMRL, S. & KOVACEVIC, A. 2009. Serum amyloid A: an acute-phase protein involved in tumour pathogenesis. *Cell Mol Life Sci,* 66**,** 9-26.

MALLIPATTU, S. K. & URIBARRI, J. 2014. Advanced glycation end product accumulation: a new enemy to target in chronic kidney disease? *Curr Opin Nephrol Hypertens*.

MANIGRASSO, M. B., JURANEK, J., RAMASAMY, R. & SCHMIDT, A. M. 2014. Unlocking the biology of RAGE in diabetic microvascular complications. *Trends Endocrinol Metab,* 25**,** 15-22.

MARIGNANI, P. A. & CARPENTER, C. L. 2001. Vav2 is required for cell spreading. *J Cell Biol,* 154**,** 177-86.

MARLATT, N. M., SPRATT, D. E. & SHAW, G. S. 2010. Codon optimization for enhanced Escherichia coli expression of human S100A11 and S100A1 proteins. *Protein Expr Purif,* 73**,** 58-64.

MARUYAMA, Y., NUMATA, M., NAKAYAMA, M., MATSUO, N., NORDFORS, L., HOSOYA, T. & LINDHOLM, B. 2007. Relationship between the -374T/A receptor of advanced glycation end products gene polymorphism and peritoneal solute transport status at the initiation of peritoneal dialysis. *Ther Apher Dial,* 11**,** 301-5.

MATRONE, C., DJELLOUL, M., TAGLIALATELA, G. & PERRONE, L. 2014. Inflammatory risk factors and pathologies promoting Alzheimer`s disease progression: is RAGE the key? *Histol Histopathol*.

MATSUMOTO, S., YOSHIDA, T., MURATA, H., HARADA, S., FUJITA, N., NAKAMURA, S., YAMAMOTO, Y., WATANABE, T., YONEKURA, H., YAMAMOTO, H., OHKUBO, T. & KOBAYASHI, Y. 2008. Solution structure of the variable-type domain of the receptor for advanced glycation end products: new insight into AGE-RAGE interaction. *Biochemistry,* 47**,** 12299-311.

MATSUNAGA, N., ANAN, I., ROSENBERG, P., NAGAI, R., LUNDSTROM, O., HORIUCHI, S., ANDO, Y. & SUHR, O. B. 2005. Advanced glycation end product is implicated in amyloid-related kidney complications. *Scand J Clin Lab Invest,* 65**,** 263-71.

MCCORMICK, M. M., RAHIMI, F., BOBRYSHEV, Y. V., GAUS, K., ZREIQAT, H., CAI, H., LORD, R. S. & GECZY, C. L. 2005. S100A8 and S100A9 in human arterial wall. Implications for atherogenesis. *J Biol Chem,* 280**,** 41521-9.

MCKINSEY, T. A., BROCKMAN, J. A., SCHERER, D. C., AL-MURRANI, S. W., GREEN, P. L. & BALLARD, D. W. 1996. Inactivation of IkappaBbeta by the tax protein of human T-cell leukemia virus type 1: a potential mechanism for constitutive induction of NF-kappaB. *Mol Cell Biol,* 16**,** 2083-90.

MEBRATU, Y. & TESFAIGZI, Y. 2009. How ERK1/2 activation controls cell proliferation and cell death: Is subcellular localization the answer? *Cell Cycle,* 8**,** 1168-75.

MERHI, Z., MCGEE, E. A. & BUYUK, E. 2014. Role of advanced glycation end-products in obesity-related ovarian dysfunction. *Minerva Endocrinol,* 39**,** 167-74.

MESSENS, J. & COLLET, J. F. 2006. Pathways of disulfide bond formation in Escherichia coli. *Int J Biochem Cell Biol,* 38**,** 1050-62.

MIKI, S., KASAYAMA, S., MIKI, Y., NAKAMURA, Y., YAMAMOTO, M., SATO, B. & KISHIMOTO, T. 1993. Expression of receptors for advanced glycosylation end products on renal cell carcinoma cells in vitro. *Biochem Biophys Res Commun,* 196**,** 984-9.

MONNIER, V. M., BAUTISTA, O., KENNY, D., SELL, D. R., FOGARTY, J., DAHMS, W., CLEARY, P. A., LACHIN, J. & GENUTH, S. 1999. Skin collagen glycation, glycoxidation, and crosslinking are lower in subjects with long-term intensive versus conventional therapy of type 1 diabetes: relevance of glycated collagen products versus HbA1c as markers of diabetic complications. DCCT Skin Collagen Ancillary Study Group. Diabetes Control and Complications Trial. *Diabetes,* 48**,** 870-80.

MONTEIRO, F. A., CARDOSO, I., SOUSA, M. M. & SARAIVA, M. J. 2006. In vitro inhibition of transthyretin aggregate-induced cytotoxicity by full and peptide derived forms of the soluble receptor for advanced glycation end products (RAGE). *FEBS Lett,* 580**,** 3451-6.

MOORE, B. W. 1965. A soluble protein characteristic of the nervous system. *Biochem Biophys Res Commun,* 19**,** 739-44.

MUCKE, L. & SELKOE, D. J. 2012. Neurotoxicity of amyloid beta-protein: synaptic and network dysfunction. *Cold Spring Harb Perspect Med,* 2**,** a006338.

MULLARKEY, C. J., EDELSTEIN, D. & BROWNLEE, M. 1990. Free radical generation by early glycation products: a mechanism for accelerated atherogenesis in diabetes. *Biochem Biophys Res Commun,* 173**,** 932-9.

MULLOKANDOV, E. A., FRANKLIN, W. A. & BROWNLEE, M. 1994. DNA damage by the glycation products of glyceraldehyde 3-phosphate and lysine. *Diabetologia,* 37**,** 145-9.

NAGARAJ, R. H. & SADY, C. 1996. The presence of a glucose-derived Maillard reaction product in the human lens. *FEBS Lett,* 382**,** 234-8.

NAH, S. S., CHOI, I. Y., LEE, C. K., OH, J. S., KIM, Y. G., MOON, H. B. & YOO, B. 2008. Effects of advanced glycation end products on the expression of COX-2, PGE2 and NO in human osteoarthritic chondrocytes. *Rheumatology (Oxford),* 47**,** 425-31.

NAKA, Y., BUCCIARELLI, L. G., WENDT, T., LEE, L. K., RONG, L. L., RAMASAMY, R., YAN, S. F. & SCHMIDT, A. M. 2004. RAGE axis: Animal models and novel insights into the vascular complications of diabetes. *Arterioscler Thromb Vasc Biol,* 24**,** 1342-9.

NAKAMURA, K., YAMAGISHI, S., ADACHI, H., MATSUI, T., KURITA-NAKAMURA, Y., TAKEUCHI, M., INOUE, H. & IMAIZUMI, T. 2008. Serum levels of soluble form of receptor for advanced glycation end products (sRAGE) are positively associated with circulating AGEs and soluble form of VCAM-1 in patients with type 2 diabetes. *Microvasc Res,* 76**,** 52-6.

NEEPER, M., SCHMIDT, A. M., BRETT, J., YAN, S. D., WANG, F., PAN, Y. C., ELLISTON, K., STERN, D. & SHAW, A. 1992. Cloning and expression of a cell surface receptor for advanced glycosylation end products of proteins. *J Biol Chem,* 267**,** 14998-5004.

NEUMANN, A., SCHINZEL, R., PALM, D., RIEDERER, P. & MUNCH, G. 1999. High molecular weight hyaluronic acid inhibits advanced glycation endproduct-induced NF-kappaB activation and cytokine expression. *FEBS Lett,* 453**,** 283-7.

NITTI, M., FURFARO, A. L., TRAVERSO, N., ODETTI, P., STORACE, D., COTTALASSO, D., PRONZATO, M. A., MARINARI, U. M. & DOMENICOTTI, C. 2007. PKC delta and NADPH oxidase in AGE-induced neuronal death. *Neurosci Lett,* 416**,** 261-5.

NOGUEIRA-MACHADO, J. A. & DE OLIVEIRA VOLPE, C. M. 2012. HMGB-1 as a target for inflammation controlling. *Recent Pat Endocr Metab Immune Drug Discov,* 6**,** 201-9.

NOGUERE, C., LARSSON, A. M., GUYOT, J. C. & BIGNON, C. 2012. Fractional factorial approach combining 4 Escherichia coli strains, 3 culture media, 3 expression temperatures and 5 N-terminal fusion tags for screening the soluble expression of recombinant proteins. *Protein Expr Purif,* 84**,** 204-13.

OIMOMI, M., IGAKI, N., HATA, F., KITAMURA, Y., NISHIMOTO, S., BABA, S. & MAEDA, S. 1989. Age- and diabetes-accelerated glycation in the human aorta. *Arch Gerontol Geriatr,* 8**,** 123-7.

OKAMOTO, H., KATAGIRI, Y., KIIRE, A., MOMOHARA, S. & KAMATANI, N. 2008. Serum amyloid A activates nuclear factor-kappaB in rheumatoid synovial fibroblasts through binding to receptor of advanced glycation end-products. *J Rheumatol,* 35**,** 752-6.

ORIGLIA, N., CRISCUOLO, C., ARANCIO, O., YAN, S. S. & DOMENICI, L. 2014. RAGE inhibition in microglia prevents ischemia-dependent synaptic dysfunction in an amyloid-enriched environment. *J Neurosci,* 34**,** 8749-60.

ORIGLIA, N., RIGHI, M., CAPSONI, S., CATTANEO, A., FANG, F., STERN, D. M., CHEN, J. X., SCHMIDT, A. M., ARANCIO, O., YAN, S. D. & DOMENICI, L. 2008. Receptor for advanced glycation end product-dependent activation of p38 mitogen-activated protein kinase contributes to amyloid-beta-mediated cortical synaptic dysfunction. *J Neurosci,* 28**,** 3521-30.

ORLOVA, V. V., CHOI, E. Y., XIE, C., CHAVAKIS, E., BIERHAUS, A., IHANUS, E., BALLANTYNE, C. M., GAHMBERG, C. G., BIANCHI, M. E., NAWROTH, P. P. & CHAVAKIS, T. 2007. A novel pathway of HMGB1-mediated inflammatory cell recruitment that requires Mac-1-integrin. *Embo j,* 26**,** 1129-39.

OSAWA, M., YAMAMOTO, Y., MUNESUE, S., MURAKAMI, N., SAKURAI, S., WATANABE, T., YONEKURA, H., UCHIGATA, Y., IWAMOTO, Y. & YAMAMOTO, H. 2007. De-N-glycosylation or G82S mutation of RAGE sensitizes its interaction with advanced glycation endproducts. *Biochim Biophys Acta,* 1770**,** 1468-74.

OSTENDORP, T., LECLERC, E., GALICHET, A., KOCH, M., DEMLING, N., WEIGLE, B., HEIZMANN, C. W., KRONECK, P. M. & FRITZ, G. 2007. Structural and functional insights into RAGE activation by multimeric S100B. *EMBO J,* 26**,** 3868-78.

OU, J., WANG, L., DING, X., DU, J., ZHANG, Y., CHEN, H. & XU, A. 2004. Stationary phase protein overproduction is a fundamental capability of Escherichia coli. *Biochem Biophys Res Commun,* 314**,** 174-80.

PADDISON, P. J., CAUDY, A. A., BERNSTEIN, E., HANNON, G. J. & CONKLIN, D. S. 2002. Short hairpin RNAs (shRNAs) induce sequence-specific silencing in mammalian cells. *Genes Dev,* 16**,** 948-58.

PALL, M. E., LAO, M. C., PATEL, S. S., LEE, M. L., GHODS, D. E., CHANDLER, D. W. & FRIEDMAN, T. C. 2008. Testosterone and bioavailable testosterone help to distinguish between mild Cushing's syndrome and polycystic ovarian syndrome. *Horm Metab Res,* 40**,** 813-8.

PAPANEOPHYTOU, C. P. & KONTOPIDIS, G. 2014. Statistical approaches to maximize recombinant protein expression in Escherichia coli: a general review. *Protein Expr Purif,* 94**,** 22-32.

PARK, H., ADSIT, F. G. & BOYINGTON, J. C. 2010. The 1.5 A crystal structure of human receptor for advanced glycation endproducts (RAGE) ectodomains reveals unique features determining ligand binding. *J Biol Chem,* 285**,** 40762-70.

PARK, I. H., YEON, S. I., YOUN, J. H., CHOI, J. E., SASAKI, N., CHOI, I. H. & SHIN, J. S. 2004a. Expression of a novel secreted splice variant of the receptor for advanced

glycation end products (RAGE) in human brain astrocytes and peripheral blood mononuclear cells. *Mol Immunol,* 40**,** 1203-11.

PARK, J. S., SVETKAUSKAITE, D., HE, Q., KIM, J. Y., STRASSHEIM, D., ISHIZAKA, A. & ABRAHAM, E. 2004b. Involvement of toll-like receptors 2 and 4 in cellular activation by high mobility group box 1 protein. *J Biol Chem,* 279**,** 7370-7.

PARK, L., RAMAN, K. G., LEE, K. J., LU, Y., FERRAN, L. J., JR., CHOW, W. S., STERN, D. & SCHMIDT, A. M. 1998. Suppression of accelerated diabetic atherosclerosis by the soluble receptor for advanced glycation endproducts. *Nat Med,* 4**,** 1025-31.

PATEL, A. J., VARILLY, P. & CHANDLER, D. 2010. Fluctuations of water near extended hydrophobic and hydrophilic surfaces. *J Phys Chem B,* 114**,** 1632-7.

PATEL, H., FELLOWES, R., COADE, S. & WOO, P. 1998. Human serum amyloid A has cytokine-like properties. *Scand J Immunol,* 48**,** 410-8.

PENUMUTCHU, S. R., CHOU, R. H. & YU, C. 2014. Structural Insights into Calcium-Bound S100P and the V Domain of the RAGE Complex. *PLoS One,* 9**,** e103947.

PETERS, K., WILTSHIRE, S., HENDERS, A. K., DRAGOVIC, M., BADCOCK, J. C., CHANDLER, D., HOWELL, S., ELLIS, C., BOUWER, S., MONTGOMERY, G. W., PALMER, L. J., KALAYDJIEVA, L. & JABLENSKY, A. 2008. Comprehensive analysis of tagging sequence variants in DTNBP1 shows no association with schizophrenia or with its composite neurocognitive endophenotypes. *Am J Med Genet B Neuropsychiatr Genet,* 147B**,** 1159-66.

PETTERSSON-FERNHOLM, K., FORSBLOM, C., HUDSON, B. I., PEROLA, M., GRANT, P. J. & GROOP, P. H. 2003. The functional -374 T/A RAGE gene polymorphism is associated with proteinuria and cardiovascular disease in type 1 diabetic patients. *Diabetes,* 52**,** 891-4.

PONATH, G., SCHETTLER, C., KAESTNER, F., VOIGT, B., WENTKER, D., AROLT, V. & ROTHERMUNDT, M. 2007. Autocrine S100B effects on astrocytes are mediated via RAGE. *J Neuroimmunol,* 184**,** 214-22.

PORRO, D., GASSER, B., FOSSATI, T., MAURER, M., BRANDUARDI, P., SAUER, M. & MATTANOVICH, D. 2011. Production of recombinant proteins and metabolites in yeasts: when are these systems better than bacterial production systems? *Appl Microbiol Biotechnol,* 89**,** 939-48.

QOSA, H., LEVINE, H., 3RD, KELLER, J. N. & KADDOUMI, A. 2014. Mixed oligomers and monomeric amyloid-beta disrupts endothelial cells integrity and reduces monomeric amyloid-beta transport across hCMEC/D3 cell line as an in vitro blood-brain barrier model. *Biochim Biophys Acta,* 1842**,** 1806-15.

QUINN, M. T., PARTHASARATHY, S., FONG, L. G. & STEINBERG, D. 1987. Oxidatively modified low density lipoproteins: a potential role in recruitment and retention of monocyte/macrophages during atherogenesis. *Proc Natl Acad Sci U S A,* 84**,** 2995-8.

RAFFEN, R., STEVENS, P. W., BOOGAARD, C., SCHIFFER, M. & STEVENS, F. J. 1998. Reengineering immunoglobulin domain interactions by introduction of charged residues. *Protein Eng,* 11**,** 303-9.

RAGHAVAN, M., WANG, Y. & BJORKMAN, P. J. 1995. Effects of receptor dimerization on the interaction between the class I major histocompatibility complex-related Fc receptor and IgG. *Proc Natl Acad Sci U S A,* 92**,** 11200-4.

RAMASAMY, R., YAN, S. F. & SCHMIDT, A. M. 2009. RAGE: therapeutic target and biomarker of the inflammatory response--the evidence mounts. *J Leukoc Biol*.

RAMASAMY, R., YAN, S. F. & SCHMIDT, A. M. 2012. The diverse ligand repertoire of the receptor for advanced glycation endproducts and pathways to the complications of diabetes. *Vascul Pharmacol,* 57**,** 160-7.

RAMPRASAD, S., RADHA, V., MATHIAS, R. A., MAJUMDER, P. P., RAO, M. R. & REMA, M. 2007. Rage gene promoter polymorphisms and diabetic retinopathy in a clinic-based population from South India. *Eye,* 21**,** 395-401.

RAUVALA, H. & ROUHIAINEN, A. 2007. RAGE as a receptor of HMGB1 (Amphoterin): roles in health and disease. *Curr Mol Med,* 7**,** 725-34.

RAUVALA, H. & ROUHIAINEN, A. 2010. Physiological and pathophysiological outcomes of the interactions of HMGB1 with cell surface receptors. *Biochim Biophys Acta,* 1799**,** 164-70.

READ, C. M., CARY, P. D., CRANE-ROBINSON, C., DRISCOLL, P. C. & NORMAN, D. G. 1993. Solution structure of a DNA-binding domain from HMG1. *Nucleic Acids Res,* 21**,** 3427-36.

REDDY, M. A., LI, S. L., SAHAR, S., KIM, Y. S., XU, Z. G., LANTING, L. & NATARAJAN, R. 2006. Key role of Src kinase in S100B-induced activation of the receptor for advanced glycation end products in vascular smooth muscle cells. *J Biol Chem,* 281**,** 13685-93.

REEVES, R. H., YAO, J., CROWLEY, M. R., BUCK, S., ZHANG, X., YAROWSKY, P., GEARHART, J. D. & HILT, D. C. 1994. Astrocytosis and axonal proliferation in the hippocampus of S100b transgenic mice. *Proc Natl Acad Sci U S A,* 91**,** 5359-63.

RENDIC, D. W., I.; PASCHINGER, K 2008. The Glycosylation Capacity of Insect Cells. *CROATICA CHEMICA ACTA,* 81**,** 14.

REUTER, J. S. & MATHEWS, D. H. 2010. RNAstructure: software for RNA secondary structure prediction and analysis. *BMC Bioinformatics,* 11**,** 129.

RINAS, U. & HOFFMANN, F. 2004. Selective leakage of host-cell proteins during high-cell-density cultivation of recombinant and non-recombinant Escherichia coli. *Biotechnol Prog,* 20**,** 679-87.

ROJAS-DURAN, M. F. & GILBERT, W. V. 2012. Alternative transcription start site selection leads to large differences in translation activity in yeast. *Rna,* 18**,** 2299-305.

ROSANO, G. L. & CECCARELLI, E. A. 2014. Recombinant protein expression in Escherichia coli: advances and challenges. *Front Microbiol,* 5**,** 172.

ROSS, R. 1986. The pathogenesis of atherosclerosis--an update. *N Engl J Med,* 314**,** 488-500.

ROTH, J., VOGL, T., SORG, C. & SUNDERKOTTER, C. 2003. Phagocyte-specific S100 proteins: a novel group of proinflammatory molecules. *Trends Immunol,* 24**,** 155-8.

ROUHIAINEN, A., TUMOVA, S., VALMU, L., KALKKINEN, N. & RAUVALA, H. 2007. Pivotal advance: analysis of proinflammatory activity of highly purified eukaryotic recombinant HMGB1 (amphoterin). *J Leukoc Biol,* 81**,** 49-58.

ROULEAU, P., VANDAL, K., RYCKMAN, C., POUBELLE, P. E., BOIVIN, A., TALBOT, M. & TESSIER, P. A. 2003. The calcium-binding protein S100A12 induces neutrophil adhesion, migration, and release from bone marrow in mouse at concentrations similar to those found in human inflammatory arthritis. *Clin Immunol,* 107**,** 46-54.

SAHDEV, S., KHATTAR, S. K. & SAINI, K. S. 2008. Production of active eukaryotic proteins through bacterial expression systems: a review of the existing biotechnology strategies. *Mol Cell Biochem,* 307**,** 249-64.

SAKAGUCHI, T., YAN, S. F., YAN, S. D., BELOV, D., RONG, L. L., SOUSA, M., ANDRASSY, M., MARSO, S. P., DUDA, S., ARNOLD, B., LILIENSIEK, B., NAWROTH, P. P., STERN, D. M., SCHMIDT, A. M. & NAKA, Y. 2003. Central role of RAGE-dependent neointimal expansion in arterial restenosis. *J Clin Invest,* 111**,** 959-72.

SAKURAI, T., SUGIOKA, K. & NAKANO, M. 1990. O2- generation and lipid peroxidation during the oxidation of a glycated polypeptide, glycated polylysine, in the presence of iron-ADP. *Biochim Biophys Acta,* 1043**,** 27-33.

SALAHUDDIN, P., RABBANI, G. & KHAN, R. H. 2014. The role of advanced glycation end products in various types of neurodegenerative disease: a therapeutic approach. *Cell Mol Biol Lett,* 19**,** 407-37.

SALMIVIRTA, M., RAUVALA, H., ELENIUS, K. & JALKANEN, M. 1992. Neurite growth-promoting protein (amphoterin, p30) binds syndecan. *Exp Cell Res,* 200**,** 444-51.

SANTAMARIA-KISIEL, L., RINTALA-DEMPSEY, A. C. & SHAW, G. S. 2006. Calcium-dependent and -independent interactions of the S100 protein family. *Biochem J,* 396**,** 201-14.

SASAHIRA, T., KIRITA, T., BHAWAL, U. K., IKEDA, M., NAGASAWA, A., YAMAMOTO, K. & KUNIYASU, H. 2007. The expression of receptor for advanced glycation end products is associated with angiogenesis in human oral squamous cell carcinoma. *Virchows Arch,* 450**,** 287-95.

SCHAFER, B. W., WICKI, R., ENGELKAMP, D., MATTEI, M. G. & HEIZMANN, C. W. 1995. Isolation of a YAC clone covering a cluster of nine S100 genes on human chromosome 1q21: rationale for a new nomenclature of the S100 calcium-binding protein family. *Genomics,* 25**,** 638-43.

SCHLEGEL, S., LOFBLOM, J., LEE, C., HJELM, A., KLEPSCH, M., STROUS, M., DREW, D., SLOTBOOM, D. J. & DE GIER, J. W. 2012. Optimizing membrane protein

overexpression in the Escherichia coli strain Lemo21(DE3). *J Mol Biol,* 423**,** 648-59.

SCHMIDT, A., KUHLA, B., BIGL, K., MUNCH, G. & ARENDT, T. 2007. Cell cycle related signaling in Neuro2a cells proceeds via the receptor for advanced glycation end products. *J Neural Transm,* 114**,** 1413-24.

SCHMIDT, A. M., BLOSS, I. & SKERRA, A. 1998. Improved folding of apo-retinol-binding protein in the periplasm of Escherichia coli: positive influences of dsbC coexpression and of an amino acid exchange in the vitamin A binding site. *Protein Eng,* 11**,** 601-7.

SCHMIDT, A. M., HORI, O., CAO, R., YAN, S. D., BRETT, J., WAUTIER, J. L., OGAWA, S., KUWABARA, K., MATSUMOTO, M. & STERN, D. 1996. RAGE: a novel cellular receptor for advanced glycation end products. *Diabetes,* 45 Suppl 3**,** S77-80.

SCHMIDT, A. M., MORA, R., CAO, R., YAN, S. D., BRETT, J., RAMAKRISHNAN, R., TSANG, T. C., SIMIONESCU, M. & STERN, D. 1994. The endothelial cell binding site for advanced glycation end products consists of a complex: an integral membrane protein and a lactoferrin-like polypeptide. *J Biol Chem,* 269**,** 9882-8.

SCHMIDT, A. M. & STERN, D. M. 2000. RAGE: a new target for the prevention and treatment of the vascular and inflammatory complications of diabetes. *Trends Endocrinol Metab,* 11**,** 368-75.

SCHMIDT, A. M., VIANNA, M., GERLACH, M., BRETT, J., RYAN, J., KAO, J., ESPOSITO, C., HEGARTY, H., HURLEY, W., CLAUSS, M. & ET AL. 1992. Isolation and characterization of two binding proteins for advanced glycosylation end products from bovine lung which are present on the endothelial cell surface. *J Biol Chem,* 267**,** 14987-97.

SCHMIDT, A. M., YAN, S. D., BRETT, J., MORA, R., NOWYGROD, R. & STERN, D. 1993. Regulation of human mononuclear phagocyte migration by cell surface-binding proteins for advanced glycation end products. *J Clin Invest,* 91**,** 2155-68.

SCHMIDT, A. M., YAN, S. D., YAN, S. F. & STERN, D. M. 2001. The multiligand receptor RAGE as a progression factor amplifying immune and inflammatory responses. *J Clin Invest,* 108**,** 949-55.

SCHNEIDER, D., DUPERCHY, E., DEPEYROT, J., COURSANGE, E., LENSKI, R. E. & BLOT, M. 2002. Genomic comparisons among Escherichia coli strains B, K-12, and O157:H7 using IS elements as molecular markers. *BMC Microbiol,* 2**,** 18.

SEGATORI, L., PAUKSTELIS, P. J., GILBERT, H. F. & GEORGIOU, G. 2004. Engineered DsbC chimeras catalyze both protein oxidation and disulfide-bond isomerization in Escherichia coli: Reconciling two competing pathways. *Proc Natl Acad Sci U S A,* 101**,** 10018-23.

SELKOE, D. J. 2001. Alzheimer's disease: genes, proteins, and therapy. *Physiol Rev,* 81**,** 741-66.

SELL, D. R. & MONNIER, V. M. 1989. Structure elucidation of a senescence cross-link from human extracellular matrix. Implication of pentoses in the aging process. *J Biol Chem,* 264**,** 21597-602.

SENOLT, L., GRIGORIAN, M., LUKANIDIN, E., MICHEL, B. A., GAY, R. E., GAY, S., PAVELKA, K. & NEIDHART, M. 2006. S100A4 (Mts1): is there any relation to the pathogenesis of rheumatoid arthritis? *Autoimmun Rev,* 5**,** 129-31.

SEZONOV, G., JOSELEAU-PETIT, D. & D'ARI, R. 2007. Escherichia coli physiology in Luria-Bertani broth. *J Bacteriol,* 189**,** 8746-9.

SHAHBAZ, M. 2006. Methods to identify compounds that modulate rage. Google Patents.

SHANMUGAM, N., KIM, Y. S., LANTING, L. & NATARAJAN, R. 2003. Regulation of cyclooxygenase-2 expression in monocytes by ligation of the receptor for advanced glycation end products. *J Biol Chem,* 278**,** 34834-44.

SHARMA, H. S., CASTELLANI, R. J., SMITH, M. A. & SHARMA, A. 2012. The blood-brain barrier in Alzheimer's disease: novel therapeutic targets and nanodrug delivery. *Int Rev Neurobiol,* 102**,** 47-90.

SHAW, S. S., SCHMIDT, A. M., BANES, A. K., WANG, X., STERN, D. M. & MARRERO, M. B. 2003. S100B-RAGE-mediated augmentation of angiotensin II-induced activation of JAK2 in vascular smooth muscle cells is dependent on PLD2. *Diabetes,* 52**,** 2381-8.

SINGH, V. P., BALI, A., SINGH, N. & JAGGI, A. S. 2014. Advanced glycation end products and diabetic complications. *Korean J Physiol Pharmacol,* 18**,** 1-14.

SITKIEWICZ, E., TARNOWSKI, K., POZNANSKI, J., KULMA, M. & DADLEZ, M. 2013. Oligomerization interface of RAGE receptor revealed by MS-monitored hydrogen deuterium exchange. *PLoS One,* 8**,** e76353.

SKELTON, N. J., KORDEL, J., AKKE, M., FORSEN, S. & CHAZIN, W. J. 1994. Signal transduction versus buffering activity in Ca(2+)-binding proteins. *Nat Struct Biol,* 1**,** 239-45.

SOUSA, M. M., DU YAN, S., FERNANDES, R., GUIMARAES, A., STERN, D. & SARAIVA, M. J. 2001. Familial amyloid polyneuropathy: receptor for advanced glycation end products-dependent triggering of neuronal inflammatory and apoptotic pathways. *J Neurosci,* 21**,** 7576-86.

SPARROW, C. P., PARTHASARATHY, S. & STEINBERG, D. 1989. A macrophage receptor that recognizes oxidized low density lipoprotein but not acetylated low density lipoprotein. *J Biol Chem,* 264**,** 2599-604.

SRIKRISHNA, G., HUTTUNEN, H. J., JOHANSSON, L., WEIGLE, B., YAMAGUCHI, Y., RAUVALA, H. & FREEZE, H. H. 2002. N -Glycans on the receptor for advanced glycation end products influence amphoterin binding and neurite outgrowth. *J Neurochem,* 80**,** 998-1008.

SRIKRISHNA, G., NAYAK, J., WEIGLE, B., TEMME, A., FOELL, D., HAZELWOOD, L., OLSSON, A., VOLKMANN, N., HANEIN, D. & FREEZE, H. H. 2010. Carboxylated N-glycans on RAGE promote S100A12 binding and signaling. *J Cell Biochem,* 110**,** 645-59.

STEPHENSON, M. R., BYRNE, D. C., OHLIN, D. W., MURPHY, W. J., CHANDLER, D. W., DAVIS, R. R., ALLEN, J. R. & DANIELSON, R. W. 2010. Perspectives on "Efficacy of the U.S. Army policy on hearing conservation programs". *Mil Med,* 175**,** xii-xvi.

STERENCZAK, K. A., WILLENBROCK, S., BARANN, M., KLEMKE, M., SOLLER, J. T., EBERLE, N., NOLTE, I., BULLERDIEK, J. & MURUA ESCOBAR, H. 2009. Cloning, characterisation, and comparative quantitative expression analyses of receptor for advanced glycation end products (RAGE) transcript forms. *Gene,* 434**,** 35-42.

STEVENS, P. W., RAFFEN, R., HANSON, D. K., DENG, Y. L., BERRIOS-HAMMOND, M., WESTHOLM, F. A., MURPHY, C., EULITZ, M., WETZEL, R., SOLOMON, A. & ET AL. 1995. Recombinant immunoglobulin variable domains generated from synthetic genes provide a system for in vitro characterization of light-chain amyloid proteins. *Protein Sci,* 4**,** 421-32.

STITES, D. P., TERR, A. I., & PARSLOW, T. G. 1997. *Medical immunology,* Stamford, Connecticut, Appleton & Lange.

STUDIER, F. W. & MOFFATT, B. A. 1986. Use of bacteriophage T7 RNA polymerase to direct selective high-level expression of cloned genes. *J Mol Biol,* 189**,** 113-30.

STURCHLER, E., GALICHET, A., WEIBEL, M., LECLERC, E. & HEIZMANN, C. W. 2008. Site-specific blockade of RAGE-Vd prevents amyloid-beta oligomer neurotoxicity. *J Neurosci,* 28**,** 5149-58.

SUGAYA, K., FUKAGAWA, T., MATSUMOTO, K., MITA, K., TAKAHASHI, E., ANDO, A., INOKO, H. & IKEMURA, T. 1994. Three genes in the human MHC class III region near the junction with the class II: gene for receptor of advanced glycosylation end products, PBX2 homeobox gene and a notch homolog, human counterpart of mouse mammary tumor gene int-3. *Genomics,* 23**,** 408-19.

TAGUCHI, A., BLOOD, D. C., DEL TORO, G., CANET, A., LEE, D. C., QU, W., TANJI, N., LU, Y., LALLA, E., FU, C., HOFMANN, M. A., KISLINGER, T., INGRAM, M., LU, A., TANAKA, H., HORI, O., OGAWA, S., STERN, D. M. & SCHMIDT, A. M. 2000. Blockade of RAGE-amphoterin signalling suppresses tumour growth and metastases. *Nature,* 405**,** 354-60.

TANG, D., LOZE, M. T., ZEH, H. J. & KANG, R. 2010. The redox protein HMGB1 regulates cell death and survival in cancer treatment. *Autophagy,* 6**,** 1181-3.

TANOUE, T. & NISHIDA, E. 2002. Docking interactions in the mitogen-activated protein kinase cascades. *Pharmacol Ther,* 93**,** 193-202.

TESAROVA, P., KALOUSOVA, M., JACHYMOVA, M., MESTEK, O., PETRUZELKA, L. & ZIMA, T. 2007. Receptor for advanced glycation end products (RAGE)--soluble form (sRAGE) and gene polymorphisms in patients with breast cancer. *Cancer Invest,* 25**,** 720-5.

TOMINAGA, T., SAHAI, E., CHARDIN, P., MCCORMICK, F., COURTNEIDGE, S. A. & ALBERTS, A. S. 2000. Diaphanous-related formins bridge Rho GTPase and Src tyrosine kinase signaling. *Mol Cell,* 5**,** 13-25.

TOTHOVA, V. & GIBADULINOVA, A. 2013. S100P, a peculiar member of S100 family of calcium-binding proteins implicated in cancer. *Acta Virol,* 57**,** 238-46.

TOURE, F., ZAHM, J. M., GARNOTEL, R., LAMBERT, E., BONNET, N., SCHMIDT, A. M., VITRY, F., CHANARD, J., GILLERY, P. & RIEU, P. 2008. Receptor for advanced glycation end-products (RAGE) modulates neutrophil adhesion and migration on glycoxidated extracellular matrix. *Biochem J,* 416**,** 255-61.

TRAHERNE, J. A. 2008. Human MHC architecture and evolution: implications for disease association studies. *Int J Immunogenet,* 35**,** 179-92.

URBONAVICIUTE, V., FURNROHR, B. G., MEISTER, S., MUNOZ, L., HEYDER, P., DE MARCHIS, F., BIANCHI, M. E., KIRSCHNING, C., WAGNER, H., MANFREDI, A. A., KALDEN, J. R., SCHETT, G., ROVERE-QUERINI, P., HERRMANN, M. & VOLL, R. E. 2008. Induction of inflammatory and immune responses by HMGB1-nucleosome complexes: implications for the pathogenesis of SLE. *J Exp Med,* 205**,** 3007-18.

USAMI, A., ISHIYAMA, S., ENOMOTO, C., OKAZAKI, H., HIGUCHI, K., IKEDA, M., YAMAMOTO, T., SUGAI, M., ISHIKAWA, Y., HOSAKA, Y., KOYAMA, T., TOBITA, Y., EBIHARA, S., MOCHIZUKI, T., ASANO, Y. & NAGAYA, H. 2011. Comparison of recombinant protein expression in a baculovirus system in insect cells (Sf9) and silkworm. *J Biochem,* 149**,** 219-27.

VALENCIA, J. V., WELDON, S. C., QUINN, D., KIERS, G. H., DEGROOT, J., TEKOPPELE, J. M. & HUGHES, T. E. 2004. Advanced glycation end product ligands for the receptor for advanced glycation end products: biochemical characterization and formation kinetics. *Anal Biochem,* 324**,** 68-78.

VAN DIECK, J., FERNANDEZ-FERNANDEZ, M. R., VEPRINTSEV, D. B. & FERSHT, A. R. 2009. Modulation of the oligomerization state of p53 by differential binding of proteins of the S100family to p53 monomers and tetramers. *J Biol Chem*.

VAN ELDIK, L. J. & WAINWRIGHT, M. S. 2003. The Janus face of glial-derived S100B: beneficial and detrimental functions in the brain. *Restor Neurol Neurosci,* 21**,** 97-108.

VAN ZOELEN, M. A., ACHOUITI, A. & VAN DER POLL, T. 2011. RAGE during infectious diseases. *Front Biosci (Schol Ed),* 3**,** 1119-32.

VENEREAU, E., CASALGRANDI, M., SCHIRALDI, M., ANTOINE, D. J., CATTANEO, A., DE MARCHIS, F., LIU, J., ANTONELLI, A., PRETI, A., RAELI, L., SHAMS, S. S., YANG, H., VARANI, L., ANDERSSON, U., TRACEY, K. J., BACHI, A., UGUCCIONI, M. & BIANCHI, M. E. 2012. Mutually exclusive redox forms of HMGB1 promote cell recruitment or proinflammatory cytokine release. *J Exp Med,* 209**,** 1519-28.

VINCENT, A. M., PERRONE, L., SULLIVAN, K. A., BACKUS, C., SASTRY, A. M., LASTOSKIE, C. & FELDMAN, E. L. 2007. Receptor for advanced glycation end products activation injures primary sensory neurons via oxidative stress. *Endocrinology,* 148**,** 548-58.

VIRCHOW R 1854. Ueber eine im Gehirn und Ruckenmark des Menschen aufgefunde Substanz mit der chemishen Reaction der Cellulose. *Virchows Arch Path Anat,* 6**,** 135-138.

VLASSARA, H., FUH, H., MAKITA, Z., KRUNGKRAI, S., CERAMI, A. & BUCALA, R. 1992. Exogenous advanced glycosylation end products induce complex vascular dysfunction in normal animals: a model for diabetic and aging complications. *Proc Natl Acad Sci U S A,* 89**,** 12043-7.

VLASSARA, H., LI, Y. M., IMANI, F., WOJCIECHOWICZ, D., YANG, Z., LIU, F. T. & CERAMI, A. 1995. Identification of galectin-3 as a high-affinity binding protein for advanced glycation end products (AGE): a new member of the AGE-receptor complex. *Mol Med,* 1**,** 634-46.

WAGNER, S., BAARS, L., YTTERBERG, A. J., KLUSSMEIER, A., WAGNER, C. S., NORD, O., NYGREN, P. A., VAN WIJK, K. J. & DE GIER, J. W. 2007. Consequences of membrane protein overexpression in Escherichia coli. *Mol Cell Proteomics,* 6**,** 1527-50.

WANG, H., BLOOM, O., ZHANG, M., VISHNUBHAKAT, J. M., OMBRELLINO, M., CHE, J., FRAZIER, A., YANG, H., IVANOVA, S., BOROVIKOVA, L., MANOGUE, K. R., FAIST, E., ABRAHAM, E., ANDERSSON, J., ANDERSSON, U., MOLINA, P. E., ABUMRAD, N. N., SAMA, A. & TRACEY, K. J. 1999. HMG-1 as a late mediator of endotoxin lethality in mice. *Science,* 285**,** 248-51.

WARBOYS, C. M., TOH, H. B. & FRASER, P. A. 2009. Role of NADPH oxidase in retinal microvascular permeability increase by RAGE activation. *Invest Ophthalmol Vis Sci,* 50**,** 1319-28.

WAUTIER, J. L., PATON, R. C., WAUTIER, M. P., PINTIGNY, D., ABADIE, E., PASSA, P. & CAEN, J. P. 1981. Increased adhesion of erythrocytes to endothelial cells in diabetes mellitus and its relation to vascular complications. *N Engl J Med,* 305**,** 237-42.

WAUTIER, J. L., WAUTIER, M. P., SCHMIDT, A. M., ANDERSON, G. M., HORI, O., ZOUKOURIAN, C., CAPRON, L., CHAPPEY, O., YAN, S. D., BRETT, J. & ET AL. 1994. Advanced glycation end products (AGEs) on the surface of diabetic erythrocytes bind to the vessel wall via a specific receptor inducing oxidant stress in the vasculature: a link between surface-associated AGEs and diabetic complications. *Proc Natl Acad Sci U S A,* 91**,** 7742-6.

WAUTIER, M. P., CHAPPEY, O., CORDA, S., STERN, D. M., SCHMIDT, A. M. & WAUTIER, J. L. 2001. Activation of NADPH oxidase by AGE links oxidant stress to altered gene expression via RAGE. *Am J Physiol Endocrinol Metab,* 280**,** E685-94.

WELCH, M., GOVINDARAJAN, S., NESS, J. E., VILLALOBOS, A., GURNEY, A., MINSHULL, J. & GUSTAFSSON, C. 2009. Design parameters to control synthetic gene expression in Escherichia coli. *PLoS One,* 4**,** e7002.

WESTERMARK, P., BENSON, M. D., BUXBAUM, J. N., COHEN, A. S., FRANGIONE, B., IKEDA, S., MASTERS, C. L., MERLINI, G., SARAIVA, M. J. & SIPE, J. D. 2005. Amyloid: toward terminology clarification. Report from the Nomenclature Committee of the International Society of Amyloidosis. *Amyloid,* 12**,** 1-4.

WESTWOOD, M. E., MCLELLAN, A. C. & THORNALLEY, P. J. 1994. Receptor-mediated endocytic uptake of methylglyoxal-modified serum albumin. Competition with advanced glycation end product-modified serum albumin at the advanced glycation end product receptor. *J Biol Chem,* 269**,** 32293-8.

WICKHAM, T. J., DAVIS, T., GRANADOS, R. R., SHULER, M. L. & WOOD, H. A. 1992. Screening of insect cell lines for the production of recombinant proteins and infectious virus in the baculovirus expression system. *Biotechnol Prog,* 8**,** 391-6.

WILDENBERG, G. A., DOHN, M. R., CARNAHAN, R. H., DAVIS, M. A., LOBDELL, N. A., SETTLEMAN, J. & REYNOLDS, A. B. 2006. p120-catenin and p190RhoGAP regulate cell-cell adhesion by coordinating antagonism between Rac and Rho. *Cell,* 127**,** 1027-39.

WILSON, J. S., MRUTHINTI, S., BUCCAFUSCO, J. J., SCHADE, R. F., MITCHELL, M. B., HARRELL, D. U., GULATI, N. K. & STEPHEN MILLER, L. 2009. Anti-RAGE and A{beta} Immunoglobulin Levels Are Related to Dementia Level and Cognitive Performance. *J Gerontol A Biol Sci Med Sci*.

WILSON, P. W., KANNEL, W. B. & ANDERSON, K. M. 1985. Lipids, glucose intolerance and vascular disease: the Framingham Study. *Monogr Atheroscler,* 13**,** 1-11.

WILTON, R., YOUSEF, M. A., SAXENA, P., SZPUNAR, M. & STEVENS, F. J. 2006. Expression and purification of recombinant human receptor for advanced glycation endproducts in Escherichia coli. *Protein Expr Purif,* 47**,** 25-35.

WITTKOWSKI, H., STURROCK, A., VAN ZOELEN, M. A., VIEMANN, D., VAN DER POLL, T., HOIDAL, J. R., ROTH, J. & FOELL, D. 2007. Neutrophil-derived S100A12 in acute lung injury and respiratory distress syndrome. *Crit Care Med,* 35**,** 1369-75.

WOLFF, S. P. & DEAN, R. T. 1987. Glucose autoxidation and protein modification. The potential role of 'autoxidative glycosylation' in diabetes. *Biochem J,* 245**,** 243-50.

XIE, J., BURZ, D. S., HE, W., BRONSTEIN, I. B., LEDNEV, I. & SHEKHTMAN, A. 2007. Hexameric calgranulin C (S100A12) binds to the receptor for advanced glycated end products (RAGE) using symmetric hydrophobic target-binding patches. *J Biol Chem,* 282**,** 4218-31.

XIE, J., MENDEZ, J. D., MENDEZ-VALENZUELA, V. & AGUILAR-HERNANDEZ, M. M. 2013. Cellular signalling of the receptor for advanced glycation end products (RAGE). *Cell Signal,* 25**,** 2185-97.

XIE, J., REVERDATTO, S., FROLOV, A., HOFFMANN, R., BURZ, D. S. & SHEKHTMAN, A. 2008. Structural basis for pattern recognition by the receptor for advanced glycation end products (RAGE). *J Biol Chem,* 283**,** 27255-69.

XU, Y. D., YIN, L. M., WANG, Y., WEI, Y. & YANG, Y. Q. 2012. [S100A8 protein in inflammation]. *Sheng Li Xue Bao,* 64**,** 231-7.

XUE, J., RAI, V., SINGER, D., CHABIERSKI, S., XIE, J., REVERDATTO, S., BURZ, D. S., SCHMIDT, A. M., HOFFMANN, R. & SHEKHTMAN, A. 2011. Advanced glycation end product recognition by the receptor for AGEs. *Structure,* 19**,** 722-32.

XUE, J., RAY, R., SINGER, D., BOHME, D., BURZ, D. S., RAI, V., HOFFMANN, R. & SHEKHTMAN, A. 2014. The receptor for advanced glycation end products (RAGE) specifically recognizes methylglyoxal-derived AGEs. *Biochemistry,* 53**,** 3327-35.

YAMANA, N., ARAKAWA, Y., NISHINO, T., KUROKAWA, K., TANJI, M., ITOH, R. E., MONYPENNY, J., ISHIZAKI, T., BITO, H., NOZAKI, K., HASHIMOTO, N., MATSUDA, M. & NARUMIYA, S. 2006. The Rho-mDia1 pathway regulates cell polarity and focal adhesion turnover in migrating cells through mobilizing Apc and c-Src. *Mol Cell Biol,* 26**,** 6844-58.

YAN, F. L., ZHENG, Y. & ZHAO, F. D. 2008. Effects of ginkgo biloba extract EGb761 on expression of RAGE and LRP-1 in cerebral microvascular endothelial cells under chronic hypoxia and hypoglycemia. *Acta Neuropathol,* 116**,** 529-35.

YAN, S. D., CHEN, X., FU, J., CHEN, M., ZHU, H., ROHER, A., SLATTERY, T., ZHAO, L., NAGASHIMA, M., MORSER, J., MIGHELI, A., NAWROTH, P., STERN, D. & SCHMIDT, A. M. 1996. RAGE and amyloid-beta peptide neurotoxicity in Alzheimer's disease. *Nature,* 382**,** 685-91.

YAN, S. D., SCHMIDT, A. M., ANDERSON, G. M., ZHANG, J., BRETT, J., ZOU, Y. S., PINSKY, D. & STERN, D. 1994. Enhanced cellular oxidant stress by the interaction of advanced glycation end products with their receptors/binding proteins. *J Biol Chem,* 269**,** 9889-97.

YAN, S. D., ZHU, H., ZHU, A., GOLABEK, A., DU, H., ROHER, A., YU, J., SOTO, C., SCHMIDT, A. M., STERN, D. & KINDY, M. 2000. Receptor-dependent cell stress and amyloid accumulation in systemic amyloidosis. *Nat Med,* 6**,** 643-51.

YAN, S. F., DU YAN, S., RAMASAMY, R. & SCHMIDT, A. M. 2009. Tempering the wrath of RAGE: An emerging therapeutic strategy against diabetic complications, neurodegeneration, and inflammation. *Ann Med***,** 1-15.

YANEZ, M., GIL-LONGO, J. & CAMPOS-TOIMIL, M. 2012. Calcium binding proteins. *Adv Exp Med Biol,* 740**,** 461-82.

YANG, H., HREGGVIDSDOTTIR, H. S., PALMBLAD, K., WANG, H., OCHANI, M., LI, J., LU, B., CHAVAN, S., ROSAS-BALLINA, M., AL-ABED, Y., AKIRA, S., BIERHAUS, A., ERLANDSSON-HARRIS, H., ANDERSSON, U. & TRACEY, K. J. 2010. A critical cysteine is required for HMGB1 binding to Toll-like receptor 4 and activation of macrophage cytokine release. *Proc Natl Acad Sci U S A,* 107**,** 11942-7.

YANG, H., LUNDBACK, P., OTTOSSON, L., ERLANDSSON-HARRIS, H., VENEREAU, E., BIANCHI, M. E., AL-ABED, Y., ANDERSSON, U., TRACEY, K. J. & ANTOINE, D. J. 2012. Redox modification of cysteine residues regulates the cytokine activity of high mobility group box-1 (HMGB1). *Mol Med,* 18**,** 250-9.

YANG, Z., YAN, W. X., CAI, H., TEDLA, N., ARMISHAW, C., DI GIROLAMO, N., WANG, H. W., HAMPARTZOUMIAN, T., SIMPSON, J. L., GIBSON, P. G., HUNT, J., HART, P., HUGHES, J. M., PERRY, M. A., ALEWOOD, P. F. & GECZY, C. L. 2007. S100A12 provokes mast cell activation: a potential amplification pathway in asthma and innate immunity. *J Allergy Clin Immunol,* 119**,** 106-14.

YU, Y. & YE, R. D. 2014. Microglial Abeta Receptors in Alzheimer's Disease. *Cell Mol Neurobiol*.

ZHANG, Y. H., LIN, J. X. & VILCEK, J. 1990. Interleukin-6 induction by tumor necrosis factor and interleukin-1 in human fibroblasts involves activation of a nuclear factor binding to a kappa B-like sequence. *Mol Cell Biol,* 10**,** 3818-23.

ZHAO, C. B., BAO, J. M., LU, Y. J., ZHAO, T., ZHOU, X. H., ZHENG, D. Y. & ZHAO, S. C. 2014. Co-expression of RAGE and HMGB1 is associated with cancer progression and poor patient outcome of prostate cancer. *Am J Cancer Res,* 4**,** 369-77.

ZONG, H., MADDEN, A., WARD, M., MOONEY, M. H., ELLIOTT, C. T. & STITT, A. W. 2010. Homodimerization is essential for the receptor for advanced glycation end products (RAGE)-mediated signal transduction. *J Biol Chem,* 285**,** 23137-46.

6.0 APPENDICES

Appendix A. Genotypes of bacterial expression hosts used in this study.

Table 10. List of bacterial expression hosts and their genotypes.

Strain Name	Genotype
Origami B	F^- ompT $hsdS_B(r_B^- m_B^-)$ gal dcm lacY1 aphC gor522::Tn*10* trxB (Kan^R, Tet^R)
BL21 (DE3)	F^- ompT $hsdS_B(r_B^- m_B^-)$ gal dcm (DE3)
Rosetta-gami™ 2	Δ(ara–leu)7697 ΔlacX74 ΔphoA PvuII phoR araD139 ahpC galE galK rpsL F'[lac^+ $lacI^q$ pro] gor522::Tn10 trxB pRARE2[3] (Cam^R, Str^R, Tet^R)[4]
Rosetta-gami™ 2(DE3)	Δ(ara–leu)7697 ΔlacX74 ΔphoA PvuII phoR araD139 ahpC galE galK rpsL (DE3) F'[lac^+ $lacI^q$ pro] gor522::Tn10 trxB pRARE2[3] (Cam^R, Str^R, Tet^R)[4]
T7 Shuffle® K12	F´ lac, pro, $lacI^Q$ / Δ(ara-leu)7697 araD139 fhuA2 lacZ::T7 gene1 Δ(phoA) PvuII phoR ahpC* galE (or U) galK λatt::pNEB3-r1-cDsbC ($Spec^R$, $lacI^q$) ΔtrxB rpsL150(Str^R) Δgor Δ(malF)3
T7 Shuffle® B	fhuA2 lacZ::T7 gene1 [lon] ompT ahpC gal λatt::pNEB3-r1-cDsbC ($Spec^R$, $lacI^q$) ΔtrxB sulA11 R(mcr-73::miniTn10--Tet^S)2 [dcm] R(zgb-210::Tn10 --Tet^S) endA1 Δgor Δ(mcrC-mrr)114::IS10

Appendix B. Expression vector maps

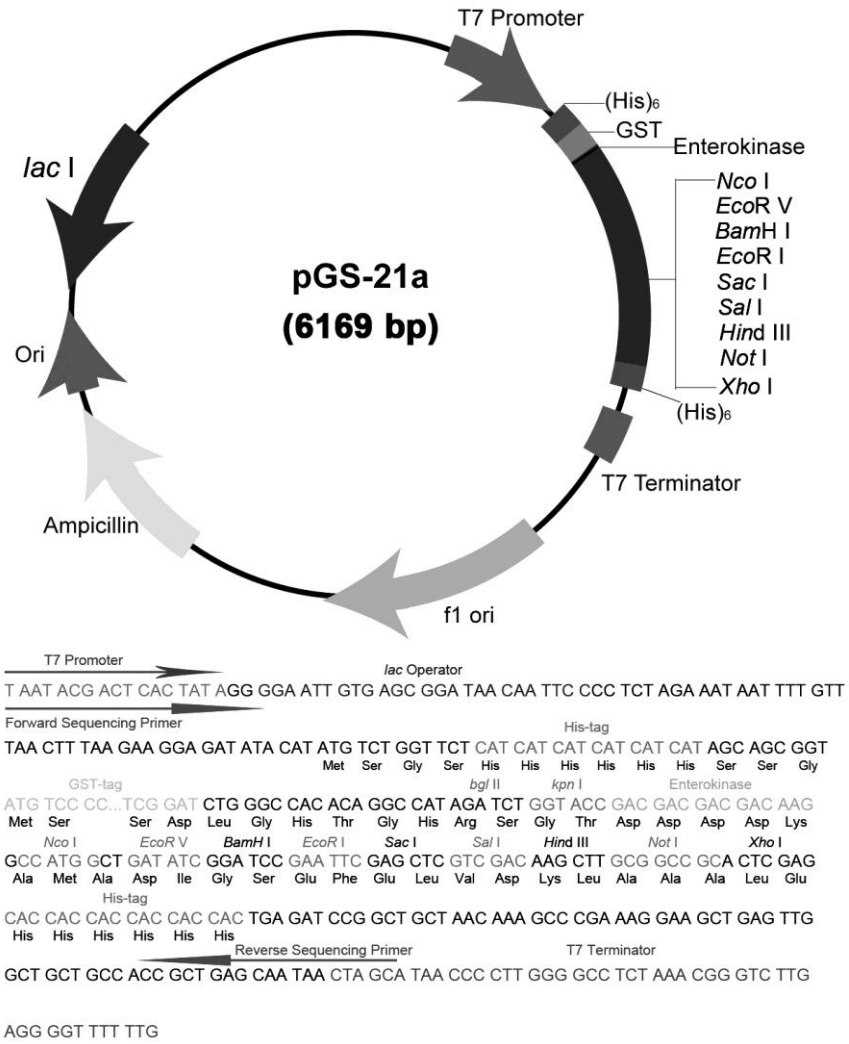

Figure 77. Vector map of pGS-21a with the multiple cloning site sequence. (*pGS-21a – Genscript – Making Research Easy, vector sequence and map*, 2015. Available from http://www.genscript.com/vector/SD0121-pGS_21a.html. [01 May 2015]).

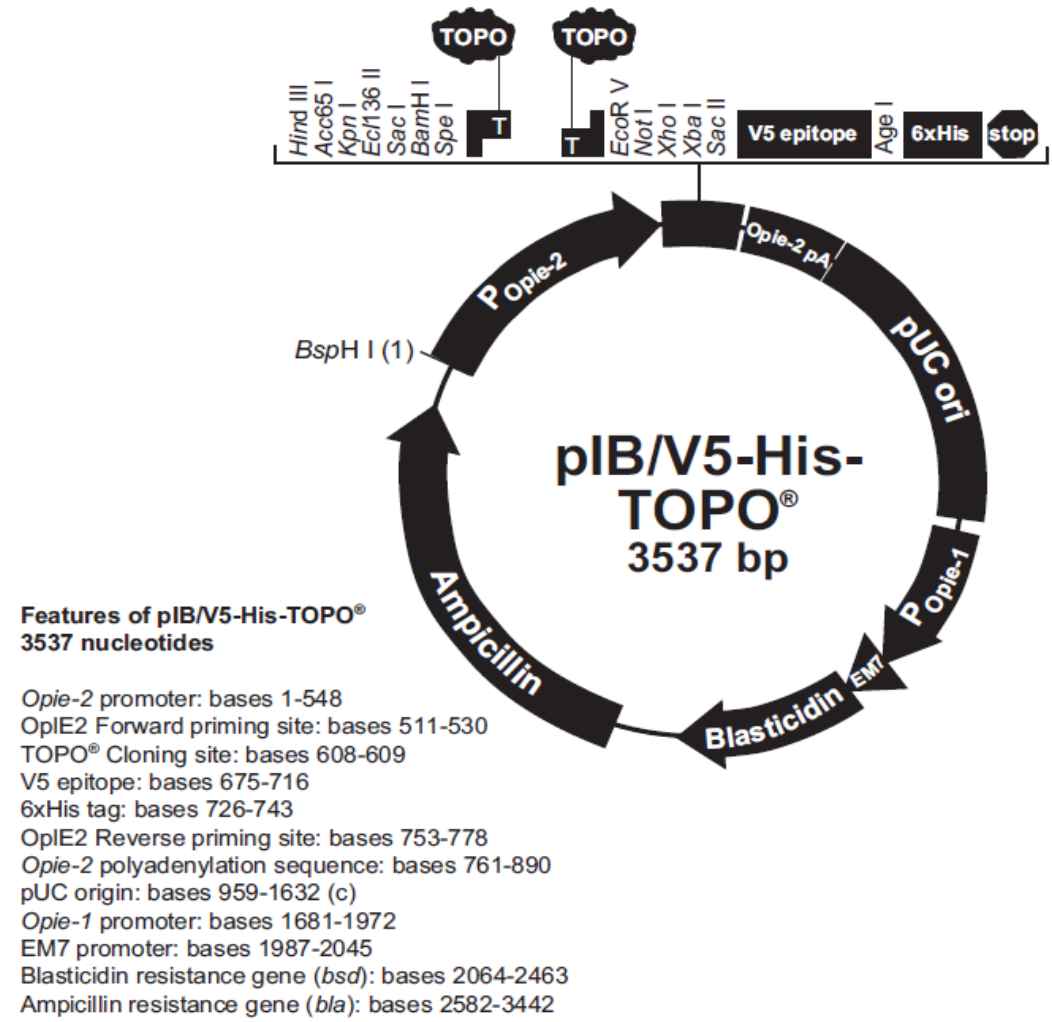

Figure 78. Vector map of pIB/V5-His-TOPO with the multiple cloning site sequence. (*pIB/V5-His TOPO® TA Expression Kit - Life Technologies*, 2004. Available from http://tools.lifetechnologies.com/content/sfs/manuals/insectselectpibtopo_man.pdf. [01 May 2015]).

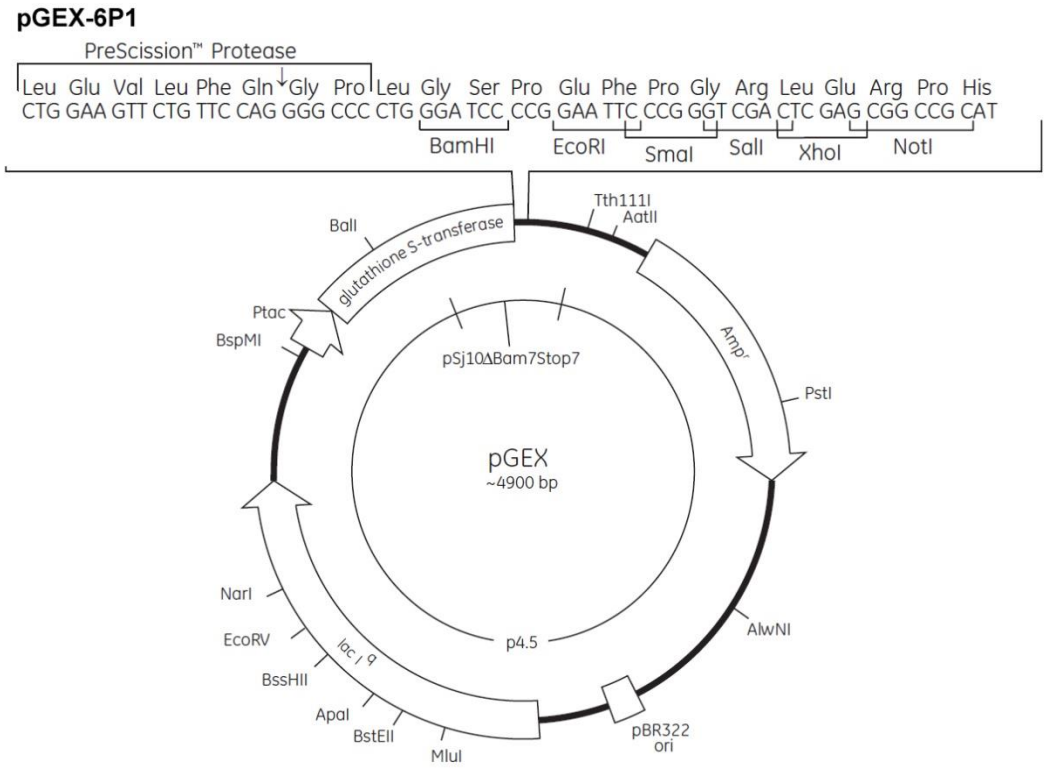

Figure 79. Vector map of pGEX-6P-1 with the multiple cloning site sequence and PreScission Protease cleavage site. (*GE Healthcare Life Sciences "pGEX-6P-1"-* , 2015. Available from https://www.gelifesciences.com/gehcls_images/GELS/Related%20Content/Files/1314774443672/litdoc28919162AC_20110831100927.pdf. [01 May 2015]).